UNIVERSITÀ DEGLI STUDI DI MILANO

Department of Pharmacological and Biomolecular Sciences

PhD in Pharmacological Biomolecular Sciences, Experimental and Clinical

XXXV Cycle – SSD: BIO/13

The interplay between the protein quality control system and extracellular vesicles in the disposal of disease-associated proteins and miRNAs in ALS and FTD models

Elena Casarotto

R12613

PhD Tutor: Prof.ssa Valeria Crippa

PhD co-Tutor: Prof. Angelo Poletti

PhD School Coordinator: Prof. Giuseppe Danilo Norata

Academic Year 2021-2022

ABSTRACT

Amyotrophic Lateral Sclerosis (ALS) and Frontotemporal dementia (FTD) are two neurodegenerative diseases characterized by the presence within neurons of toxic cytoplasmic inclusions containing the insoluble forms of the TAR DNA-binding protein of 43 KDa (TDP-43) and its C-terminal fragments (CTFs) of 35 (TDP-35) and 25 KDa (TDP-25).

The accumulation of TDP-43 into insoluble cytoplasmic aggregates is toxic for cells that prevent their formation and/or promote their degradation through the protein quality control (PQC) system (i.e. chaperone and co-chaperone proteins, the ubiquitin proteasome system (UPS) and the autophagy). However, TDP-43 has been also found into extracellular vesicles (EVs), both large (LEVs) and small (SEVs), suggesting that EVs could cooperate with the PQC system for the disposal of TDP species.

Moreover, TDP-43 is an RNA-binding protein that plays several functions in RNA metabolism, including miRNAs biogenesis. Its accumulation within the ALS/FTD-associated cytoplasmic aggregates prevents it from performing these functions causing an alteration in miRNAs biogenesis and possibly a deregulation of miRNAs secreted by the affected cells respect to the control condition.

In my PhD project I investigated the crosstalk between EVs and PQC i) in the disposal of ALS and FTD-associated TDP species both in neuron and in muscle cells, and ii) in the secretion of miRNAs, both in physiological and in pathological (when the UPS and autophagy are blocked) conditions.

By analyzing EVs obtained from neuronal (NSC34) and muscle (C2C12) cells and plasma of FTD patients and healthy controls, I demonstrated that both neurons and muscles cells secrete TDP-43, TDP-35 and TDP-25 (mainly in their insoluble form in LEVs) and that the Chaperone assisted selective autophagy (CASA) complex and/or the chaperone HSPB8 alone may assist TDP species secretion in EVs. I also found that the targeting of TDP species to EVs in neurons and muscle cells is increased mainly following the UPS and the autophagy blockade, respectively. This suggests that neurons degrade TDP species mainly via UPS, while muscle cells via autophagy and that the re-routing of TDP species into EVs may represent a protective compensatory mechanism for their disposal when the intracellular degradation is blocked. However, I demonstrated that these EVs were toxic to recipient

cells, therefore they may contribute to the spreading of the disease. In line with this observation, I specifically detected the pro-aggregating TDP species TDP-35 in EVs derived from plasma of FTD patients.

Finally, the analysis of EVs miRNA content demonstrated that LEVs and SEVs contain different miRNAs and that UPS and autophagy inhibition similarly deregulated the secretion of several miRNAs in SEVs. Interestingly, a number of SEVs deregulated miRNAs targets the prion disease pathway and thus probably affects cell survival.

Taken together these data suggest that the secretion of TDP species and potentially harmful miRNAs into EVs normally happens in cell in basal condition, but the PQC inhibition, a typical ALS and FTD condition, increases the secretion of the TDP species and causes the deregulation of specific EVs miRNAs, contributing to the spreading of the disease to neighboring and/or more distant cells.

RIASSUNTO

La sclerosi laterale amiotrofica (SLA) e la demenza frontotemporale (FTD) sono due malattie neurodegenerative caratterizzate dalla presenza all'interno dei neuroni di inclusioni citoplasmatiche tossiche contenenti le forme insolubili della proteina TAR DNA-binding protein di 43 KDa (TDP-43) e dei suoi frammenti C-terminali (CTF) di 35 (TDP-35) e 25 KDa (TDP-25).

L'accumulo di TDP-43 in aggregati citoplasmatici insolubili è tossico per le cellule che, pertanto, ne impediscono la formazione e/o ne promuovono la degradazione attraverso il sistema di controllo di qualità delle proteine (PQC) (formato da proteine chaperone e co-chaperone, il sistema dell'ubiquitina proteasoma (UPS) e l'autofagia). Tuttavia, il TDP-43 è stato trovato anche nelle vescicole extracellulari (EVs), sia grandi (LEVs) che piccole (SEVs), suggerendo che le EVs potrebbero cooperare con il PQC per lo smaltimento delle specie di TDP.

Inoltre, il TDP-43 è una proteina legante l'RNA che svolge diverse funzioni nel metabolismo dell'RNA, inclusa la biogenesi dei miRNA. Il suo accumulo all'interno degli aggregati citoplasmatici associati alla SLA/FTD gli impedisce di svolgere queste funzioni causando un'alterazione nella biogenesi dei miRNA e una possibile deregolazione dei miRNA secreti dalle cellule malate rispetto a quelli secreti dalle cellule sane.

Nel mio progetto di dottorato ho studiato il rapporto tra le EVs e il PQC i) nello smaltimento delle specie di TDP associate a SLA e FTD sia nei neuroni che nelle cellule muscolari, e ii) nella secrezione di miRNA, sia in condizioni fisiologiche che patologiche (quando l'UPS e l'autofagia sono bloccati).

Analizzando le EVs ottenute da cellule neuronali (NSC34) e muscolari (C2C12) e da plasma di pazienti FTD e controlli sani, ho dimostrato che sia i neuroni che le cellule muscolari secernono TDP-43, TDP-35 e TDP-25 (principalmente nelle LEVs nella loro forma insolubile) e che il complesso CASA (Chaperone Assisted Selective Autophagy) e/o la sola proteina chaperone HSPB8 possono favorire la secrezione delle specie di TDP nelle EVs. Ho anche scoperto che il targeting delle specie di TDP verso le EVs nei neuroni e nelle cellule muscolari è aumentato principalmente in seguito, rispettivamente, al blocco dell'UPS e dell'autofagia. Ciò suggerisce che i neuroni degradano le specie di TDP principalmente

tramite UPS, mentre le cellule muscolari tramite l'autofagia e che il reindirizzamento delle specie di TDP alle EVs può rappresentare un meccanismo compensatorio protettivo per il loro smaltimento quando la degradazione intracellulare è bloccata. Tuttavia, ho dimostrato che queste EVs sono tossiche per le cellule riceventi, e che possono contribuire alla diffusione della malattia. In linea con questa osservazione, ho osservato la presenza principalmente della specie pro-aggregante di TDP-43, TDP-35, nelle EVs derivanti da plasma di pazienti FTD.

Infine, l'analisi del contenuto di miRNA delle EVs ha dimostrato che le LEVs e le SEVs contengono miRNA diversi e che l'inibizione del proteasoma e dell'autofagia causano una deregolazione simile di diversi miRNA secreti nelle SEVs. È stato inoltre interessante osservare come un certo numero di miRNA deregolati nelle SEVs abbiano come target geni che appartengono al pathway della prion disease che probabilmente influenzano la sopravvivenza cellulare.

Presi insieme questi dati suggeriscono che la secrezione nelle EVs delle specie di TDP e di miRNA potenzialmente dannosi avviene normalmente nelle cellule in condizioni basali, ma che l'inibizione del PQC, una condizione tipica della SLA e dell'FTD, aumenta la secrezione delle specie TDP e causa la deregolazione di specifici miRNA secreti nelle EVs, contribuendo alla diffusione della malattia alle cellule vicine e/o a quelle più distanti.

INTRODUCTION

NEURODEGENERATIVE DISEASES AND THE SPREADING OF THE DISEASE

Neurodegenerative diseases (NDs) are one of the major causes of dementia and death in adulthood. They are a heterogeneous group of disorders characterized by a gradual degeneration and loss of neurons within various regions of the brain and/or of the spinal cord (Dugger & Dickson, 2017).

Despite these diseases differ in their clinical phenotype, they share one important pathological feature: the accumulation of specific proteins in insoluble aggregates inside or outside the affected neurons and glial cells. Due to this common feature some NDs such as Alzheimer's disease (AD), frontotemporal lobar degeneration (FTD), Lewy body disease (LBD), Parkinson's disease (PD), and amyotrophic lateral sclerosis (ALS) are also known as proteinopathies (Bayer, 2015; Chopra et al., 2022).

Amyloid β-protein, Tau protein, α-synuclein, Superoxide dismutase 1 (SOD1) protein and the human transactive responsive (TAR) DNA-binding protein 43 (TDP-43) are the most frequently aggregated proteins in these disorders (Fig. 1) (Kovacs, 2018). Although they are not similar in size, sequence, structure or function, they all undergo protein misfolding and aggregation (Soto, 2001). Misfolding may result from a stressed environment, a defective folding mechanism, a malfunctioning protein quality control mechanism and/or gene mutation, that directly cause the production of proteins unable to fold properly (Hartl, 2017; Labbadia & Morimoto, 2015). Once misfolded, proteins become more prone to aggregation. Indeed, they expose their hydrophobic amino acid side chains (which in native conditions are confined within the protein), thus increasing their ability to form oligomers that are able to bind other proteins, leading to the formation of insoluble protein aggregates (Candelise et al., 2021).

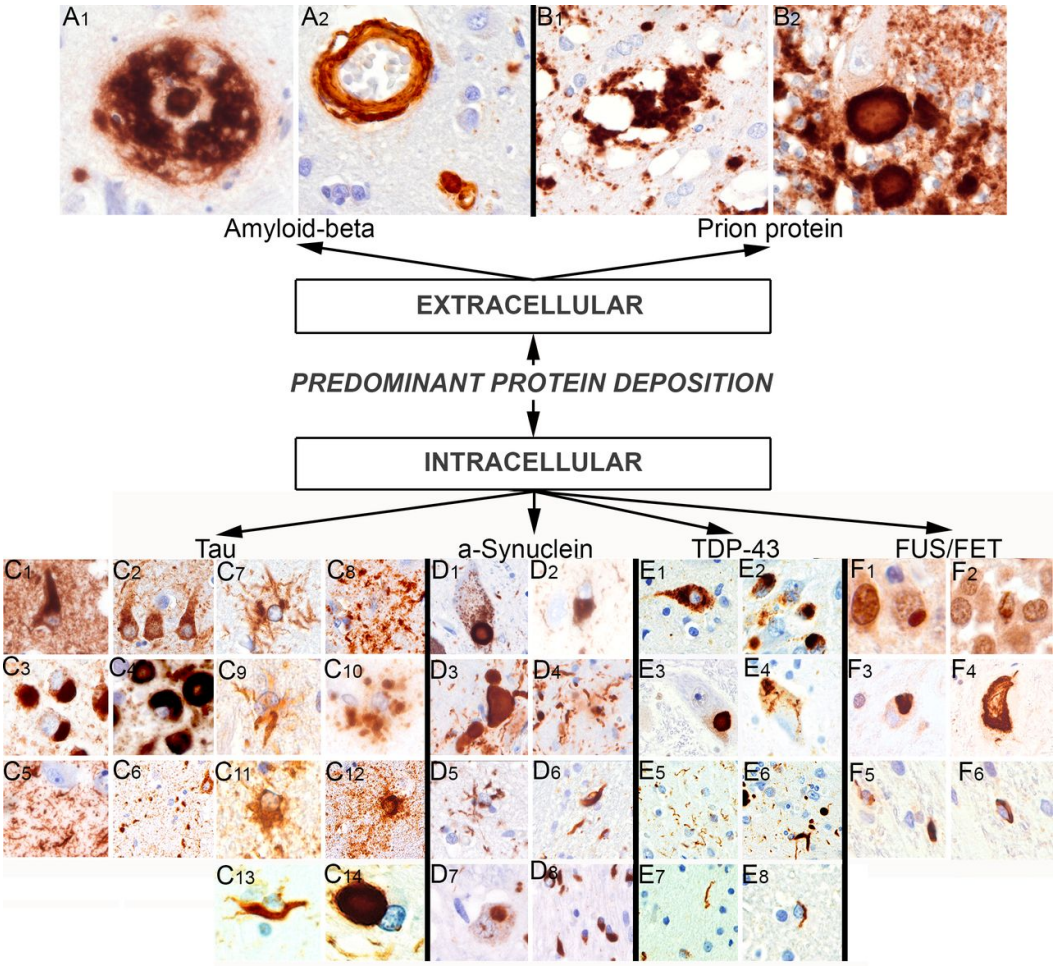

Figure 1. Intracellular and extracellular protein aggregates commonly present in NDs (Kovacs, 2019)

The insoluble protein aggregates are toxic for cells because they can directly (i.e. by physically interfering with physiological processes, such as transport within the cell) and/or indirectly (i.e. by sequestering other proteins) alter the cellular homeostasis or they can be released and deposit in the extracellular environment affecting the organ integrity (J. P. Taylor et al., 2002). In particular, aggregates can stress neurons and lead to the development of subsequent cytotoxic events, such as increased production of reactive oxygen species (ROS), excitotoxicity, synaptic dysfunction, impaired degradation protein systems, endoplasmic reticulum (ER) stress, DNA damage, mitochondrial dysfunction, inflammation and cell cycle re-entry that can, if not effectively counteracted, cause neurons death. However, also protein misfolding itself contribute to cell death as it prevents proteins from performing their functions that could be essential for cells (Chi et al., 2018; Chiti & Dobson, 2017; McAlary et al., 2019) (Fig. 2).

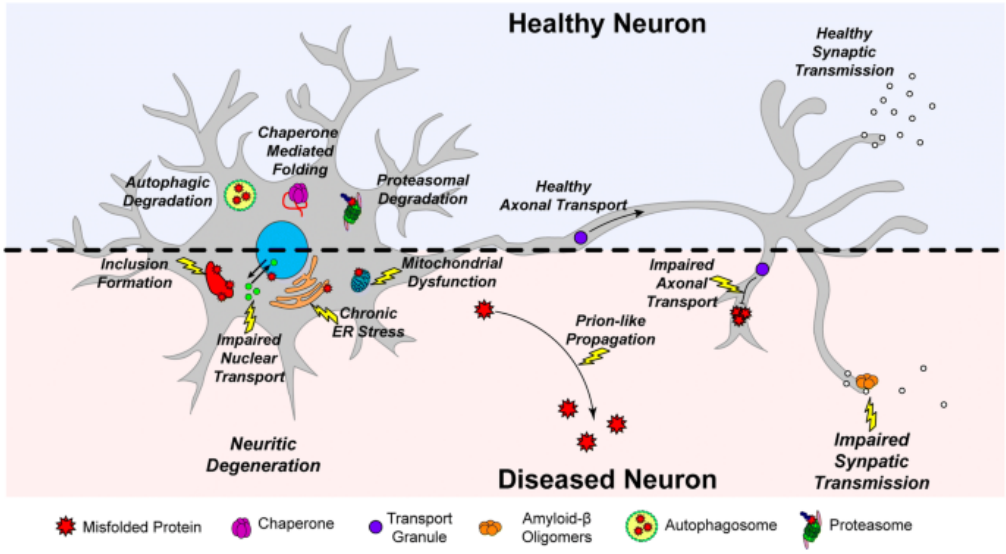

Figure 2. Toxicity of misfolded and aggregated proteins (McAlary et al., 2019)

For many years it was thought that insoluble protein aggregates found in different portions of the brain and spinal cord of patients affected by NDs formed within the cells as a result of various insults to which the cell itself was subjected. However, in the past two decades it has been observed that misfolded proteins are able to spread, starting from a specific region of the nervous system to a larger area, through a prion-like mechanism (S.-J. Lee et al., 2010). In particular, it has been proposed a mechanism according to which these pathological misfolded proteins accumulate over a potential threshold in a small number of cells, thus constituting a primordial seed that is capable of growing larger and larger by recruiting physiological soluble proteins around it, leading to the formation of plaques and fibers. However, portions of this primordial seed can detach from it and spread in the extracellular space where they can be recaptured by healthy cells, thus acting as new seeds for protein aggregation in these latter (Polymenidou & Cleveland, 2011; Soto & Pritzkow, 2018; Vaquer-Alicea & Diamond, 2019) (Fig. 3).

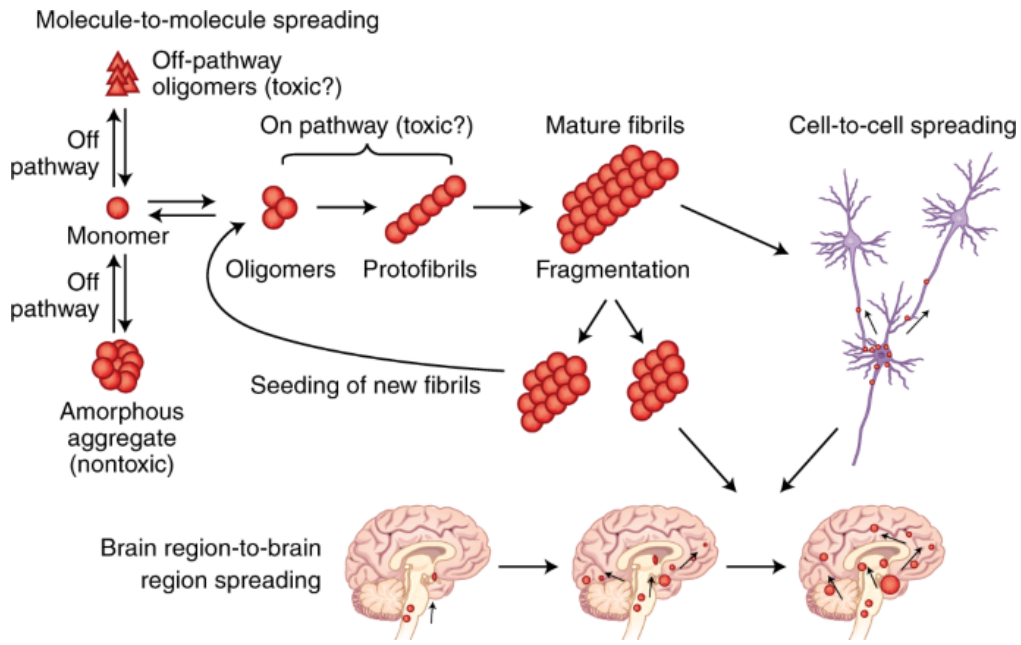

Figure 3. The prion-like mechanism of transmission of the aggregated proteins (Soto & Pritzkow, 2018)

Several mechanisms have been proposed to explain how misfolded proteins are transmitted from cell to cell, including the use of tunnelling nanotubules, the membrane disruption, the secretion of soluble material, the cell death and the release through extracellular vesicles (EVs) (Gosset et al., 2022; Lim & Lee, 2017; Vilette et al., 2018).

EVs and their role in the spreading of misfolded proteins in NDs have been extensively analysed in the last decade (Fevrier et al., 2004; Rajendran et al., 2006; Saman et al., 2012; Sproviero et al., 2018). Interestingly, most of the proteins listed above have been found enriched within EVs released form several NDs cell and animal models and patients, therefore EVs could represent a good source of NDs biomarkers, more reliable than conventional specimens, such as pure CSF, blood and urine (Hill, 2019; Rastogi et al., 2021).

Despite the identification of misfolded proteins within EVs, there are still many aspects that need to be clarified. First of all, which is the mechanism of secretion of misfolded proteins within the different types of vesicles. Is it a random addressing mechanism or is it mediated by specific proteins? Then, why misfolded proteins are secreted within EVs. Do EVs have a protective function and play an active role in cellular proteostasis? Or do they simply contribute to the spreading of misfolded proteins and to the progression of the disease to a more extended area? Finally, what is EVs role as cellular messengers? Since it is known

that, in addition to proteins, EVs also contain a rich repertoire of RNA transcripts (in particular miRNAs), is it possible that they have a role in the propagation of the disease by modulating the expression of specific target genes?

During my PhD I try to answer to some of these open question by studying EVs secretion in cell models of ALS and FTD.

AMYOTROPHIC LATERAL SCLEROSIS

ALS is a fatal ND described for the first time by the French neurologist Jean-Martin Charcot in 1869 (A. Verma, 2021). ALS is also known as motor neuron disease since it is characterized by a progressive degeneration of both upper and lower motor neurons in the primary motor cortex, corticospinal tracts, brainstem and spinal cord. The onset of the disease occurs most frequently in the limbs, where loss of dexterity in the fingers or slight lameness is generally observed. However, it can also be bulbar (20-25% of cases), characterized by confusing language (dysarthria) or difficulty swallowing (dysphagia), or respiratory (less than 3% of cases), characterized by shortness of breath (dyspnea) (Wijesekera & Nigel Leigh, 2009) (Fig. 4).

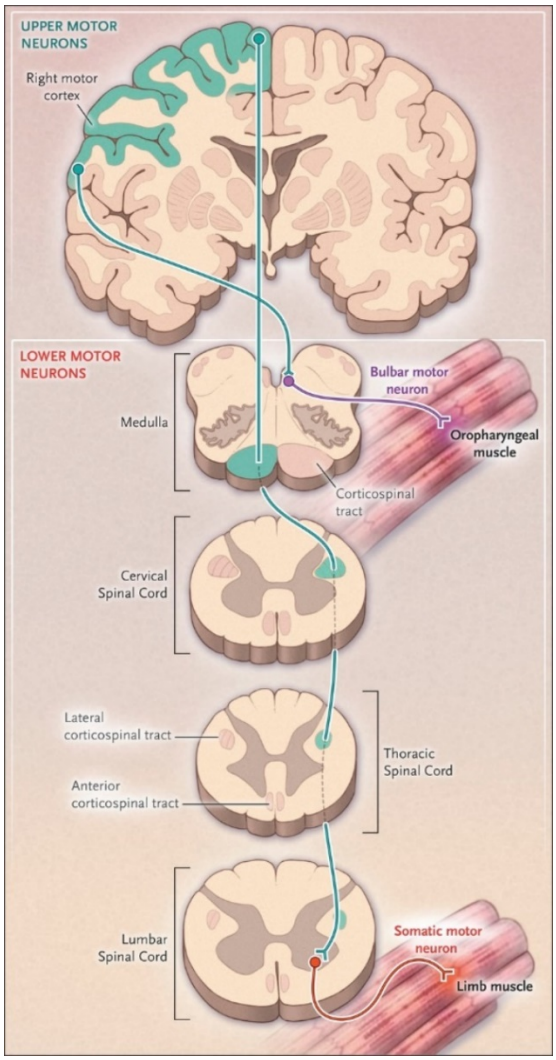

Figure 4. Upper and lower motor neuron affected in ALS (Brown & Al-Chalabi, 2017)

ALS is a rapidly progressing disease that leads to the development of symptoms ranging from muscle wasting and muscular atrophy to paralysis that then lead to death by respiratory failure (Gordon, 2013; Versluys et al., 2022; Wijesekera & Nigel Leigh, 2009).

ALS is an age-associated ND characterized by a disease onset which is around 55 years old, with a peak around 70 years of age. It is considered a rare disease with a prevalence estimated around 5 individuals out of 100 000 each year worldwide. However, these data are intended to change because of the increase in the size of the world population and in the life expectancy. ALS is rapidly fatal indeed usually patients die after 3-5 years from the onset of the first symptoms, usually for respiratory failure (Al-Chalabi & Hardiman, 2013; Logroscino et al., 2022; Prasad et al., 2019; Versluys et al., 2022; M.-D. Wang et al., 2017).

ALS cases can be divided into familial (fALS) and sporadic (sALS) forms. Most of them, about 90-95% of ALS cases, are considered sporadic (i.e., of unknown origin, probably determined by both genetic and environmental factors), while the remaining 5-10% have a family history. fALS are characterized by a Mendelian inheritance and a high penetrance. The vast majority of fALS cases have an autosomal dominant pattern of inheritance, although cases with an autosomal recessive pattern have also been highlighted (Prasad et al., 2019; Versluys et al., 2022; Wijesekera & Nigel Leigh, 2009). In particular, ALS is considered familial if at least one first- or second-degree relative is reported to have ALS (Boylan, 2015).

60-70% of the genes involved in fALS are known. Most of fALS cases can be associated with mutations in genes for *chromosome 9 open reading frame 72 (C9ORF72), SOD1, TDP-43* and *fused in sarcoma/translocated in liposarcoma (FUS)*. However, mutations in these genes have also been found in some cases of sALS (Boylan, 2015; Karagiannis & Inoue, 2020) (Fig. 5).

Both fALS and sALS are characterized by the presence in motor neurons (but not exclusively) of cytoplasmic protein aggregates that, in about 97% of ALS cases, are positive for the TDP-43 protein, and for this reason ALS is also known as TDP-43 proteinopathy (Brown & Al-Chalabi, 2017; Ojaimi et al., 2022).

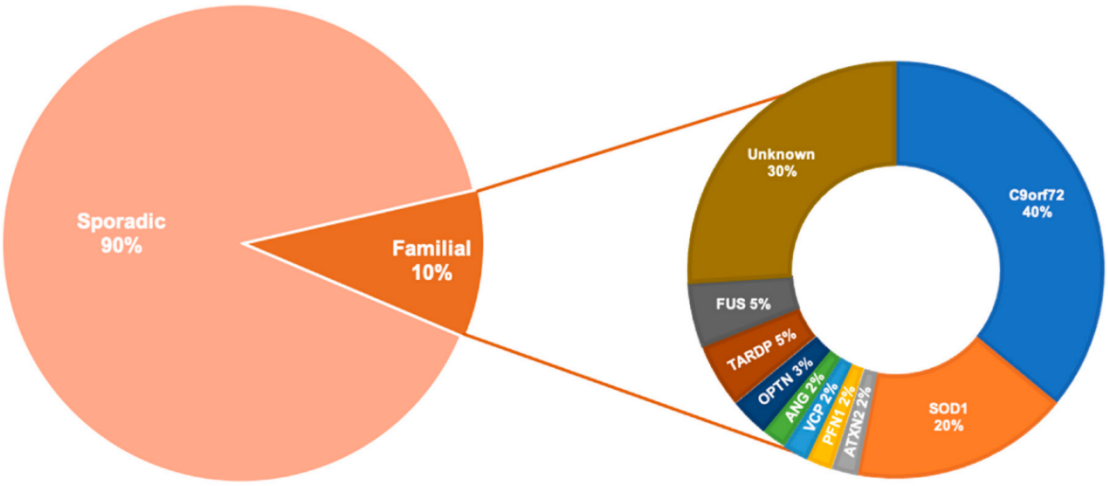

Figure 5. The most commonly known genetic causes of Amyotrophic Lateral Sclerosis (ALS) and their relative percentage (Amin et al., 2020)

FRONTOTEMPORAL DEMENTIA

FTD is the second most common cause of dementia after Alzheimer's disease that occurs in people under the age of 65. It is a ND characterized by a progressive neuronal atrophy of the frontal and anterior temporal lobes that leads to personality and behavioural changes and gradual impairment of language skills. Clinically, FTD is divided into three main variants: i) the behavioural variant FTD, in which changes in behaviour, personality, emotions and executive control are mainly observed, ii) the semantic variant primary progressive aphasia, in which language is compromised, especially in the first two years after the onset of the disease iii) and nonfluent variant primary progressive aphasia, characterized by difficulties in speeches and word-finding problems. Among these, the behavioural variant FTD is the most common form accounting for nearly 60% of FTD patients (Gao et al., 2018; Mancuso & Navarro, 2015; Olney et al., 2017).

FTD prevalence is estimated around 15-22 individuals per 100 000. Life expectancy is short and survival is similar to that of the AD. Although many FTD cases are sporadic, about 30-50% of the cases are familial. They are inherited in an autosomal dominant fashion, with 100% of penetrance. Familial FTD cases are mainly associated with genetic mutations in *C9ORF72, progranulin (GRN)* and *microtubule-associated protein tau.* However, although rarer, mutations in *VCP, Chromatin-modifying protein 2B, TDP-43, FUS, p62/SQSTM1,* and *ubiquilin 2 (UBQLN2)* have also been observed (Galimberti et al., 2015; Gao et al., 2018; Onyike & Diehl-Schmid, 2013).

FTD, like many other NDs, is also characterized by the presence of protein aggregates in the brain. These aggregates are mainly formed by the microtubule-associated protein tau, TDP-43 and FUS proteins. Thus, depending on the type of protein involved, FTLD can be classified into 3 main groups: FTLD with tau-positive inclusions (FTLD-tau), FTLD with tau and alpha-synuclein-negative but TDP-43 and ubiquitin-positive inclusions (FTLD-TDP) and FTLD with FUS-positive inclusions (FTLD-FUS). Among these three groups FTLD-TDP is the most widespread form, regardless of the presence of mutations in the gene encoding TDP-43 which, as mentioned above, are among the rarest. Therefore, since about 50% of FTD cases have cytoplasmic aggregates of TDP-43, such as ALS, FTD can be considered a TDP-43 proteinopathy too (Carlos & Josephs, 2022; Gao et al., 2018) (Fig. 6).

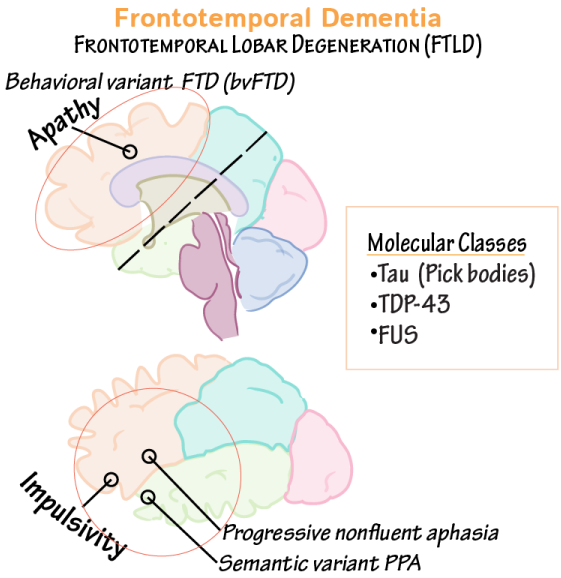

Figure 6. Frontotemporal Dementia: different brain areas affected and principal aggregated proteins (Frontotemporal Dementia - Pathology Flashcards | Draw it to Know it)

ALS/FTD

For years, ALS and FTD have been considered two distinct and unrelated diseases, but recently it has been shown that they represent the extremes of a disease spectrum. Indeed, they are NDs characterized by a sometimes-overlapping clinical picture (A. Verma, 2014). In particular, it has been observed that about 15% of FTD patients, in addition to cognitive and behavioural deficits (typical of this type of dementia) manifests motor symptoms, typical of ALS and vice versa. About 50% of ALS patients manifest not only motor neuronal defects but also cognitive impairment and abnormalities in behaviour.

In addition to their overlapping clinical spectrum, the identification of TDP-43 as the major ubiquitinate protein found both in sALS and fALS and in the more frequent pathological form of FTD allowed to suppose the existence of a common disease mechanism between these two NDs (Arai et al., 2006; Neumann et al., 2006). In fact, in over 90% of ALS and over 50% of FTD patients, TDP-43 represents the main protein component of the cytoplasmic aggregates found in affected cells. For this reason, as already mentioned above, they are both considered as TDP-43 proteinopathies (Ling et al., 2013). Further support to the hypothesis that ALS and FTD are part of a single disease spectrum has been provided by the identification of several genetic mutations common to both diseases. The most frequent mutation detected in families with ALS and/or FTD was the hexanucleotide repeat

expansion in intron 1 of *C9orf72* gene, observed in approximately 25% of fALS patients and 40% of fFTD patients (DeJesus-Hernandez et al., 2011; Renton et al., 2011). However, other ALS/FTD causing mutations were identified in several genes such as *TARDBP* (Benajiba et al., 2009; Borroni et al., 2009), *FUS* (Kwiatkowski et al., 2009; Vance et al., 2009), *VCP* (Scarian et al., 2022; Watts et al., 2004), *SQSTM1* (Rubino et al., 2012), *UBQLN2* (Deng et al., 2011), *CHCHD10* (Bannwarth et al., 2014), *OPTN* (Feng et al., 2019), *TBK1* (Freischmidt et al., 2015), *CCNF* (Williams et al., 2016), *CHMP2B* (Parkinson et al., 2006), *TIA1* (Mackenzie et al., 2017) (Fig. 7).

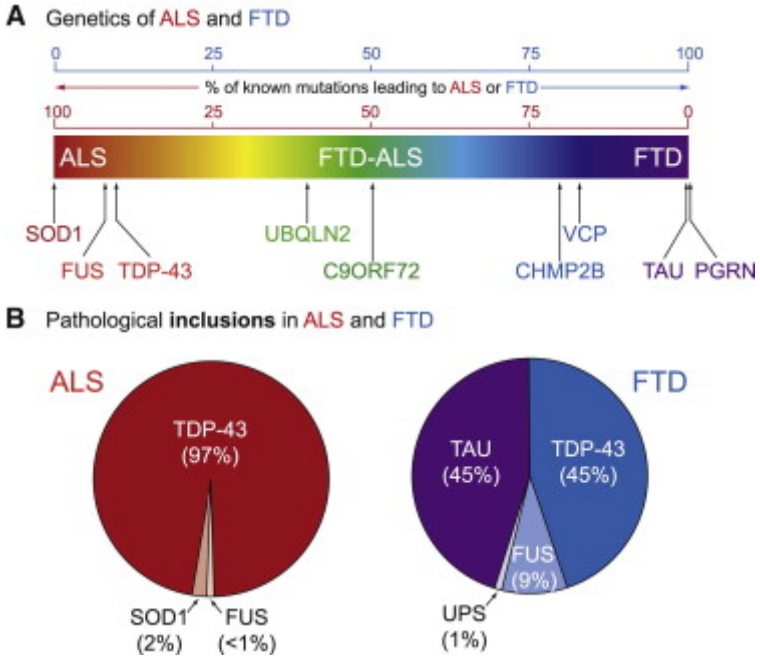

Figure 7. Clinical, Genetic, and Pathological Overlap of ALS and FTD (Ling et al., 2013)

Interestingly, many of these genes such as *VCP, CHMP2B, SQSTM1/p62, TBK1, UBQLN2, OPTN* and *CCNF* are involved in the protein clearance pathway and therefore play a role in the regulation of protein homeostasis (proteostasis). This suggests that mutations in them and the resulting malfunction of cellular proteostasis, together with the cytoplasmic aggregates of TDP-43, are the major pathological hallmarks that characterize the ALS/FTD spectrum (Lattante et al., 2015).

TDP-43

TDP-43, encoded by the *TARDBP* gene on chromosome 1p36.2, is a highly conserved and ubiquitously expressed protein of 414 amino acids belonging to the family of heteronuclear ribonucleotide binding protein (hnRNP). It is a protein located mainly in the nucleus but

also able to move into the cytoplasm, in which it is present at low levels (Prasad et al., 2019).

TDP-43 is involved in almost all the aspects of the RNA metabolism and is thought to be associated with more than 6000 species of RNA (François-Moutal et al., 2019). In particular, via DNA/RNA binding, it plays a crucial role in expression regulation of thousands of genes, RNA transcription and splicing, mRNA maturation and stability, mRNA transport, mRNA translation and miRNAs biogenesis (Ratti & Buratti, 2016). However, TDP-43 is also able to shuttle from the nucleus to the cytoplasm (Tziortzouda et al., 2021). In the cytoplasm, it can undergo several post-translational modifications (PTMs), including cleavage, aggregation, acetylation, ubiquitination, SUMOylation and phosphorylation (Suk & Rousseaux, 2020; Wood et al., 2021).

In neuronal cells of ALS/FTD patients, the abnormal accumulation of TDP-43 at the cytoplasmic level is accompanied by a reduction of its content at the nuclear level. Therefore TDP-43 aggregation exerts toxicity via both a loss of function mechanism in the nucleus and a gain of toxic mechanism exerted by the aggregates in the cytoplasm (Fig. 8).

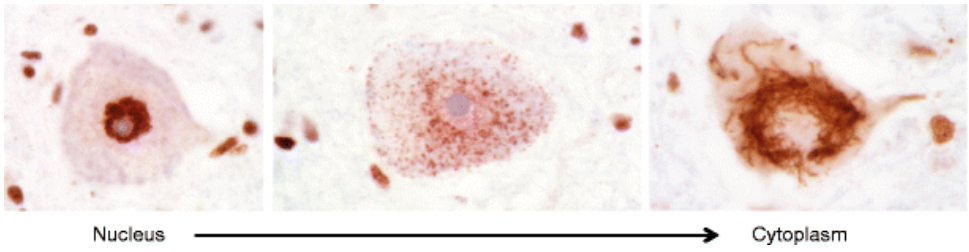

Figure 8. TDP-43 mis localization from the nucleus to the cytoplasm (Feneberg et al., 2018)

TDP-43 aggregates are usually rich of PTMs (in particular cleavage, phosphorylation and ubiquitination) (Buratti, 2018). PTMs (mainly the cleavage) would give to TDP-43 the tendency to accumulate at the cytoplasmic level, forming insoluble aggregates capable of sequestering other functional endogenous proteins (including the wild type TDP-43) or other factors, such as TDP-43 binding partners or RNA, thus causing toxicity and cell death and contributing to the pathogenesis of ALS and FTD (Wood et al., 2021).

However, in some cases, also mutations in the *TARDBP* gene are responsible for the pathogenesis of these diseases. The mutated TDP-43s, in fact, sometime lose the ability to interact with their molecular partners and to perform their physiological functions. They may also change their conformation (i.e., they can misfold), relocate in the cytoplasm and accumulate, inducing the formation of pathological TDP-43 inclusions (Lattante et al., 2013; Prasad et al., 2019).

Finally, a further aspect possibly involved in ALS/FTD pathogenesis is the presence of alterations in the intracellular system responsible for protein homeostasis: the protein quality control (PQC) system. As we will observe in detail in the following paragraphs, in ALS/FTD, the PQC system may not work properly (due to mutations in some of its components or simply due to cellular aging). It could, in fact, prevent the clearance of the full length TDP-43 and of its C-terminal fragments, promoting its aggregation within the cells. Thus, also PQC impairment could contribute to ALS/FTD pathogenesis through a mechanism of both loss and gain of toxic function (Cascella et al., 2019).

To better understand the role of TDP-43 in the pathogenesis of ALS and FTD, in the next paragraph we will better analyse its structure, its functions and the main post-translational modifications that it can undergo. Then we will describe how TDP-43 homeostasis is maintained within the cell.

TDP-43 STRUCTURE

TDP-43 consists of an N-terminal domain (NTD) (aa 1-106) that contain a nuclear localization sequence (NLS) (aa 82-98), two highly conserved RNA recognition motifs (RRM1 (aa 106-176) and RRM2 (aa 191-262)), a nuclear export signal (NES) (aa 239-250) and a Glycine-rich C-terminal domain (aa 274-414) (François-Moutal et al., 2019) (Fig. 9).

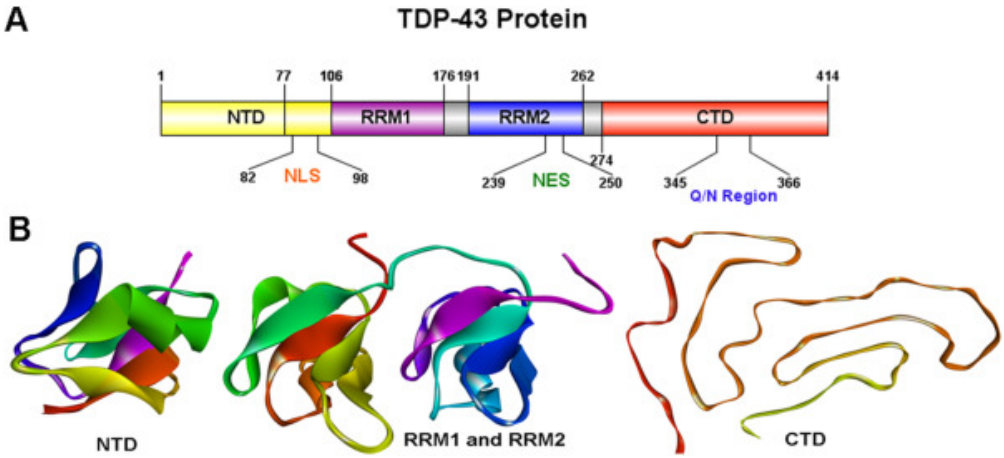

Figure 9. TDP-43 structures (Rao et al., 2021)

TDP-43 is a natively dimeric protein or, at least, in physiological conditions, it exists in a monomer-dimer equilibrium (Prasad et al., 2019). The dimerization of TDP-43 occurs through its NTD and allows TDP-43 to perform its main functions (particularly its mRNA splicing activity) (Jiang et al., 2017).

The TDP-43 NTD is well-folded. It is composed of six β-strands and a single α-helix organized in a Ubiquitin-like fold (β1-β2-α1-β3-β4-β5-β6), that facilitate the dimer formation and the further TDP-43 oligomerisation by a head-to-tail disposition of the individual subunits (Mompeán et al., 2016; Qin et al., 2014).

The involvement of the TDP-43 NTD in the formation of dimers/oligomers and in the mRNA splicing activity of TDP-43 has been demonstrated in several studies. In particular, Zhang et al., showed that the deletion of the TDP-43 NTD and in particular of its first 10 amino acid residues is sufficient to abolish TDP-43 homodimer formation and thus the TDP-43–mediated RNA splicing activity (Y.-J. Zhang et al., 2013).

However, the TDP-43 oligomerization through its NTD is necessary not only for the TDP-43 proper function but also because it counteracts the tendency of TDP-43 to aggregate. This was demonstrated in a study of Tariq Afroz et al., in which the ability of the oligomerization-deficient TDP-43 to be recruited into cytoplasmic phosphorylated TDP-43 inclusion, was compared to the wild-type TDP-43 (Afroz et al., 2017). These observations therefore underline the importance of the NTD for the maintenance of the correct TDP-43 conformation and for its activity. They also explain why the TDP-43 species that lose or partially lose the NTD, known as TDP-43 C-terminal fragments, are highly aggregation-

prone and unable to perform their mRNA splicing activity. These C-terminal fragments are often present in ALS/FTD-associated TDP-43 cytoplasmic aggregate.

The NTD also contains the nuclear localization signal (NLS), which is responsible for maintaining the TDP-43 balance between nucleus and cytoplasm. It is recognized by the α-importin that allows the active transport of TDP-43 within the nucleus (Doll et al., 2022). The loss of this domain, because of mutations or following PTMs (such as cleavage) causes the translocation of TDP-43 from the nucleus to the cytoplasm where it accumulates forming the ALS/FTD-associated insoluble pathological aggregates (Winton et al., 2008).

Since TDP-43 is an RNA binding protein, it also contains in its structure two RNA recognition motifs (RRM1 and RRM2), responsible for the TDP-43 binding to the DNA/RNA sequences. Both RRM1 and RRM2 fold into a 5-stranded β-sheet stacked against two α-helices (β1-α1-β2-β3-α2-β4-β5). They also contain two highly conserved short sequence motifs known as RNP-1 (octameric sequence: KGFGFVRF in RRM1 and RAFAFVTF in RRM2) and RNP-2 (hexameric sequence: LIVLGL in RRM1 and VFVGRC in RRM2) at which level, TDP-43 binds the nucleic acids (François-Moutal et al., 2019).

TDP-43 binds preferentially to the TG-repeated single-stranded DNA (ssDNA) and UG-repeated/enriched RNA. Indeed, one of the physiological functions of TDP-43 is to bind UG-repeats near the splicing site of pre-mRNA transcripts and promote exon skipping or inclusion. It has been observed by Kuo et al. that RRM1 plays a more dominant role than RRM2 in binding TDP-43 to the UG- and TG-rich nucleic acids. It seems, in fact, that RRM2 plays a more supportive role (probably it helps RRM1 to bind these repeated sequences) (Kuo et al., 2014).

Recently, several studies have also highlighted the presence of amyloidogenic cores in both RRM1 and RRM2. Interestingly, it has been observed that these regions are targets of some post translational modifications, such as caspase cleavage and ubiquitination, that can induce their misfolding contributing to the TDP-43 aggregation. In particular, it has been observed the presence of two regions prone to misfold and therefore possibly responsible for the TDP-43 aggregation: the one consisting of residues 166–173 in RRM1 and that consisting of residues 246–255 in RRM2 (François-Moutal et al., 2019).

Within the second of two tandem RNA Recognition Motifs (RRMs) there is the NES. Until recently, it was thought that the NES was the binding site for the export protein XPO1 and therefore was responsible for the active export of TDP-43 from the nucleus to the cytoplasm (Ayala et al., 2008). However, today it is thought that TDP-43 nuclear export is not dependent on the binding of XPO1 to the NES but it is the result of a passive diffusion (Pinarbasi et al., 2018).

Finally, there is the CTD, that is the domain that has been most studied since is where are located most of the ALS/FTD-associated *TARDBP* mutations (about 50 disease-linked mutations) and phosphorylation sites (François-Moutal et al., 2019). It consists of an intrinsically disordered structure formed by a low complexity domain (LCD) containing a glycine-rich region and a segment enriched in uncharged polar amino acids (glutamine and asparagine (Q/N)) that resembles the yeast prion sequence (the so-called prion-like domain (PrLD)) (Prasad et al., 2019).

TDP-43 LCD has several functions. It has been proposed to mediate interactions with DNA, RNA, and other proteins to regulate mRNA stability, splicing and translation and mRNA and ribonucleoprotein transport. It may also contribute to the binding of TDP-43 to other proteins, to the homo-oligomerisation of TDP-43 and to the formation of pathological cytosolic aggregates (Ayala et al., 2005; D'Ambrogio et al., 2009).

The TDP-43 LCD is highly aggregation prone. In physiological conditions, the hydrophilic and hydrophobic residues that constitute it undergo a process called liquid-liquid phase separation (LLPS) (Prasad et al., 2019). They form transient intermolecular interactions that lead to a phase-separation of the TDP-43 within membranelles liquid droplet-like organelles (H.-R. Li et al., 2018). These membranelles liquid droplet-like organelles, also called biomolecular condensates, are intracellular dynamic and reversible structures that assemble to perform certain biological functions. In particular, TDP-43, through its LCD, is mainly involved in the formation of the stress granules (Dewey et al., 2012). Stress granules are protective biomolecular condensate that form in neurons in response to heat, osmotic and oxidative stress. They sequester untranslated mRNAs and associated proteins in order to decrease energy demands and safeguard cell survival until the stressor removal from the system. For their protective function, stress granules are critical for cell survival. Therefore, mutations and/or PTMs in the TDP-43 LCD, which could alter stress granules structure

and/or prevent their formation, are harmful to the cell (Protter & Parker, 2016). Interestingly, it has been observed that the stress granules formation is often altered also in ALS/FTD patients. The increased pathological cytoplasmic localization of TDP-43 (due, for example, to mutations in the NLS or to particular PTMs) can, in fact, alter the propensity of neuronal cells to form stress granules and prevent their disassembly by transforming them into irreversible insoluble aggregates toxic to the cell. The transformation of stress granules into insoluble aggregates can therefore represent the nucleation step in the formation of ALS/FTD-associated cytoplasmic aggregates (Carey & Guo, 2022; Prasad et al., 2019) (Fig. 10). Therefore, the structure of the TDP-43 CTD, together with its localization are fundamental for the correct assembly and disassembly of stress granules and for cell survival.

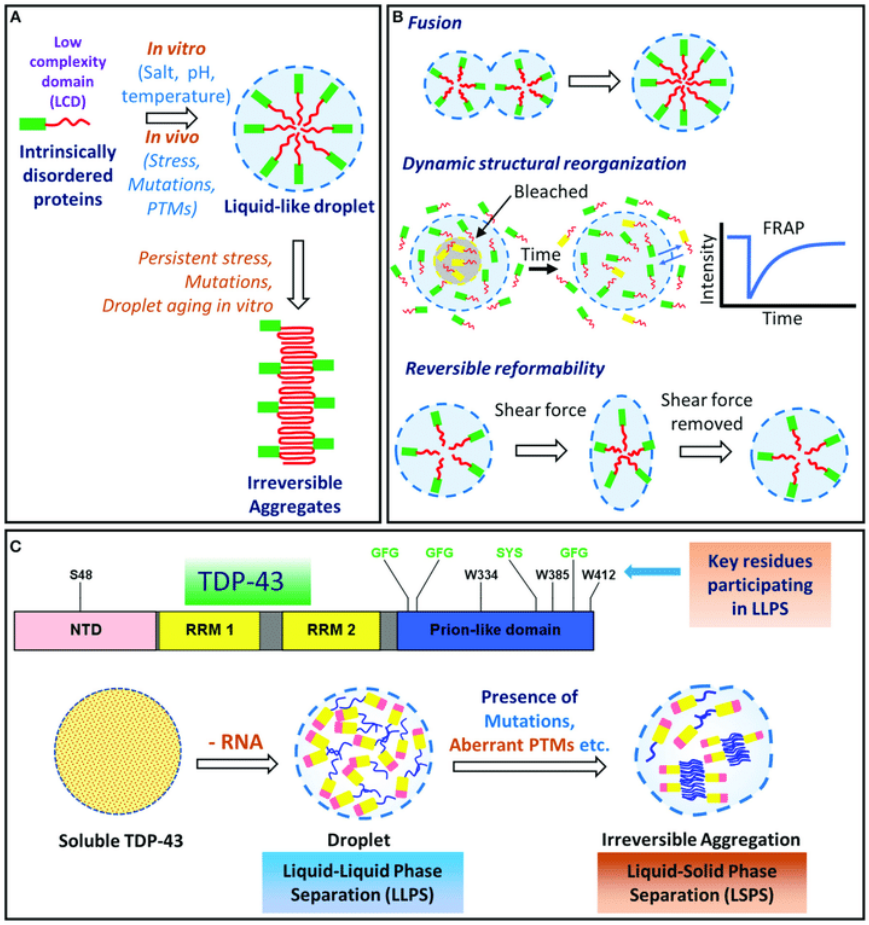

Figure 10. Process of LLPS of TDP-43 (Prasad et al., 2019)

TDP-43 FUNCTIONS AND PATHOLOGICAL IMPLICATIONS

At the physiological level, TDP-43 performs several functions. It is involved in many steps concerning RNA metabolism such as mRNA splicing, transcription, translation, mRNA transport and stabilization and microRNAs (miRNAs) and long non-coding RNAs (lncRNAs) processing (Prasad et al., 2019). Since the loss of functional TDP-43 is one of the main aspects of the ALS/FTD pathogenesis, below we will analyse in detail all these functions and we will try to understand their possible implications at the pathological level (Fig. 11).

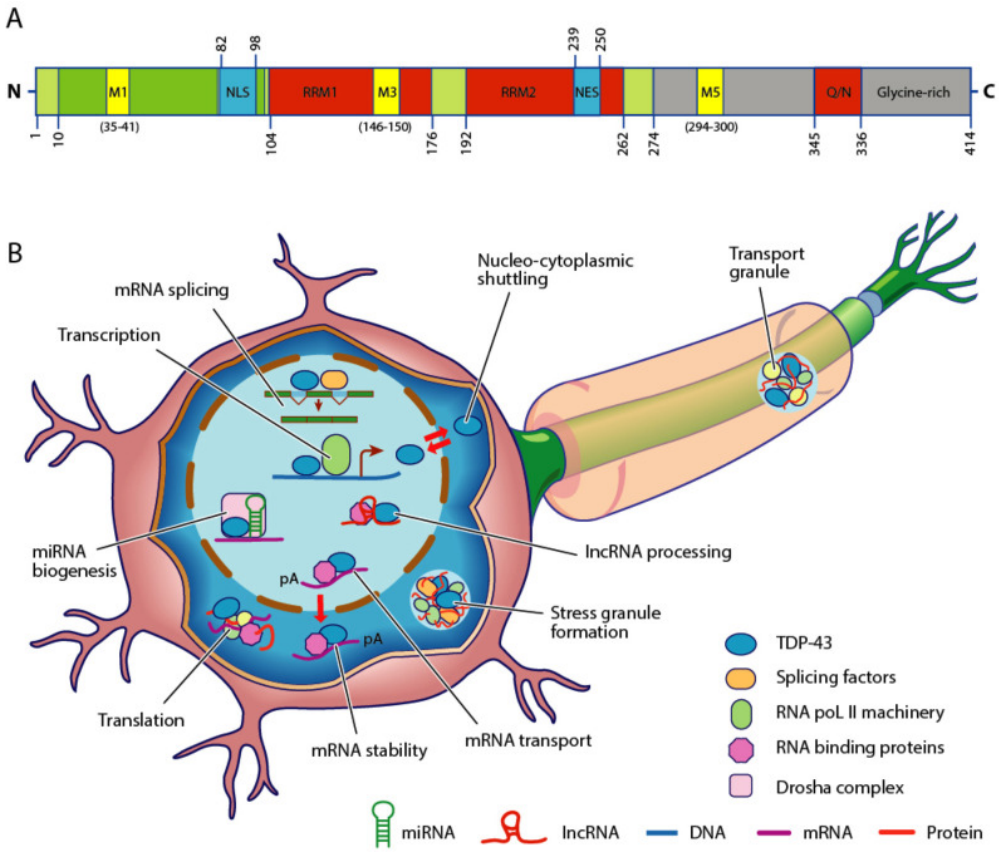

Figure 11. The main cellular functions of TDP-43 (de Boer et al., 2021)

mRNA TRANSCRIPTION AND SPLICING

The role of TDP-43 in the regulation of pre-mRNA splicing was described for the first time in 2001 by Buratti and Baralle, that observed its involvement in the splicing of exon 9 of the cystic fibrosis transmembrane conductance regulator (*CFTR*) gene (Buratti & Baralle, 2001). However, today it is known that TDP-43 regulates both directly and indirectly the splicing pattern of several important genes such as *POLDIP3/SKAR* (DNA polymerase delta interacting protein 3/S6K1 Aly/REF-like target), *SORT1* (Sortilin 1), *STAG2* (Cohesin subunit

SA-2), *MADD* (MAPK-activating death domain protein), *TNIK* (Traf2- and Nck- interacting kinase), *FUS*, *SNCA* (α-synuclein), *HTT* (Huntingtin), *APP* (Amyloid precursor protein) (Ratti & Buratti, 2016).

Interestingly, TDP-43 also regulates its own transcript that undergoes splicing in its 3'-UTR region. In particular, this splicing event regulates the differential use of the TARDBP alternative polyadenylation sites, and thus allows self-regulation of the *TARDBP* gene expression within cells to maintain TDP-43 protein levels within a physiological range (Ayala et al., 2011) (Fig. 12).

In ALS/FTD pathological conditions, the aggregation of TDP-43 in the cytosol and its consequent reduction in the nucleus, can alter these splicing mechanisms that are fundamental for proper cellular functioning, thus leading to an increase in stress within the cells and consequently to their death.

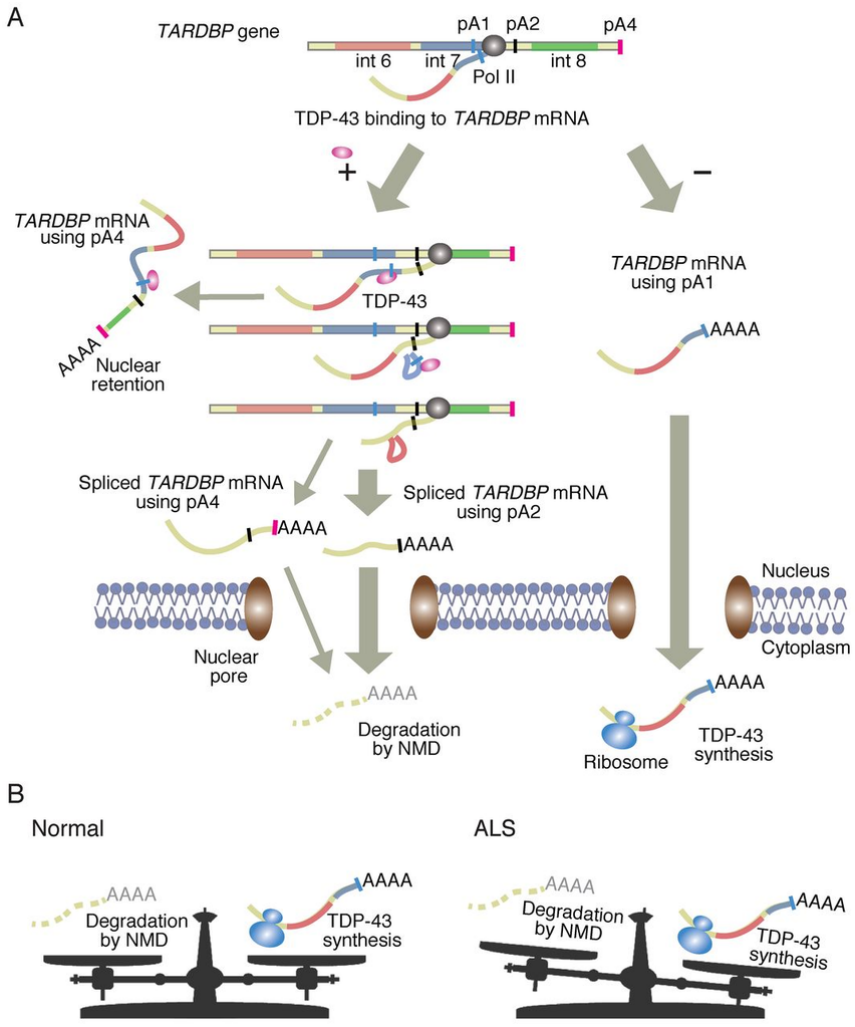

Figure 11. Mechanism of autoregulation of TDP-43 (Koyama et al., 2016)

mRNA TRANSLATION

TDP-43 also plays an important role in mRNA translation (I.-F. Wang et al., 2008). Indeed, it can interact with several proteins to form complexes involved in the translation machinery (Prasad et al., 2019). Interestingly, it has been observed by Russo et al. that TDP-43 binds the translational machinery by interacting with a specific ribosomal protein, RACK1. They also observed that an excess of cytoplasmic TDP-43 (usually observed in neurons of ALS/FTD patients) reduces the global protein synthesis through the interaction with RACK1 on polyribosomes (Russo et al., 2019).

TDP-43 can mediate the synthesis of several proteins. Recently, two have been identified: futsch/Map1b and Rac1. Both these proteins play an important role in the architecture of muscle junctions, in the axonal and dendritic development, in the organization of microtubules at the synapse and in spinogenesis (Coyne et al., 2014; Majumder et al., 2012). Therefore, they are fundamental for the correct neuronal functioning. A reduction in their expression levels as a consequence of TDP-43 aggregation in the cytoplasm could have important consequences at the pathological level.

Finally, the involvement of TDP-43 in the formation of stress granules also contributes to regulate the translation of several mRNAs (Freibaum et al., 2010). In fact, as said before, stress granules are protective biomolecular condensate that form in neurons in response to heat, osmotic and oxidative stress to facilitate cell survival by prioritizing the synthesis of stress-protective proteins, such as heat shock proteins and chaperones, and preventing the translation of non-essential mRNA transcripts till the end of the stress exposure (Protter & Parker, 2016; Wood et al., 2021). However, in pathological condition the increase of cytoplasmic TDP-43 it has been observed that is able to promote the stress granules assembly and reduce the rate of their disassembly, inhibiting the transcription of several proteins even in the absence of exposure of cells to stress (Khalfallah et al., 2018).

mRNA STABILITY AND TRANSPORT

Cytoplasmic TDP-43 is able to bind mRNA molecules, mainly at the level of their regulatory 3'-UTR sequence, and to regulate their stability and transport (Prasad et al., 2019). The binding of TDP-43 to mRNA molecules can regulate their stability in a positive way, by increasing it, as it does, for example, with the transcript encoding for the human low

molecular weight neurofilament, or in a negative way, by reducing it, as it does for the vascular endothelial growth factor a (Vegfa) and GRN mRNAs (Colombrita et al., 2012). Therefore, the decrease of soluble TDP-43 in the cytoplasm, due to its accumulation within the pathological aggregates, can alter the stability of those mRNA usually bound to TDP-43, thus negatively affecting cell viability.

In addition to stability, TDP-43 also regulates mRNA transport. In fact, it forms, together with RNA molecules, the ribonucleoproteins (RNPs) granules that allow the transport of mRNA molecules from the nucleus to the periphery of the cell (Vishal et al., 2022). This TDP-43 function is particularly important in polarized cells, such as neurons, where mRNA transport into axon and dendrites represents a fundamental process to maintain neuronal activity and synaptic plasticity (Swanger & Bassell, 2011). Also in this case, any alteration of TDP-43 levels can reduce TDP-43-mediated RNA axonal transport and thus affect cell viability.

miRNAs AND lncRNAs PROCESSING

Another important function of TDP-43 is its ability to promote the miRNAs biogenesis and processing, and the expression of long non-coding RNAs (lncRNAs) (Prasad et al., 2019; Ratti & Buratti, 2016).

MiRNAs are small noncoding RNAs composed of about 20–22 nucleotides that act as regulatory factors of gene expression. They couple with the mRNAs of their target protein-coding genes and induce their post-transcriptional repression.

MiRNAs originate from long primary transcripts, called pri-miRNAs, characterized by a short dsRNA region and a loop. The pri-miRNAs are then cleaved by the nuclear Drosha complex to produce the intermediate precursors, called pre-miRNAs. Pre-miRNAs, in turn, are transported into the cytoplasm by the esportin 5 and are cleaved by the Dicer complex thus generating mature miRNAs. MiRNAs, by following incorporation into the RNA-induced silencing complex (RISC), bind to the 3’-untranslated region (UTR) of their target mRNAs repressing their translation or inducing their degradation (Xue et al., 2017).

TDP-43, as mentioned above, performs several functions in the biogenesis and maturation of miRNAs. At the nuclear level, it facilitates the binding of the Drosha complex to a subset

of pri-miRNAs, inducing the cleavage of these pri-miRNAs into pre-miRNAs. Instead, at the cytoplasmic level, it associates with the cytoplasmic Dicer complex and facilitates the processing of the specific pre-miRNAs (in particular of those miRNAs whose production in the nucleus is regulated by TDP-43), via a direct binding to their terminal loops (Kawahara & Mieda-Sato, 2012) (Fig. 13).

Given the important role of TDP-43 in the biogenesis of some miRNAs (including let-7b, miR663, miR-9, miR1 / miR206, miR-520, miR-132, miR-143, miR-574 and miR-NID1), its reduction in the nucleus and its accumulation at the cytoplasmic level can cause the dysregulation of these miRNA, with very harmful consequences for cell survival (Ratti & Buratti, 2016).

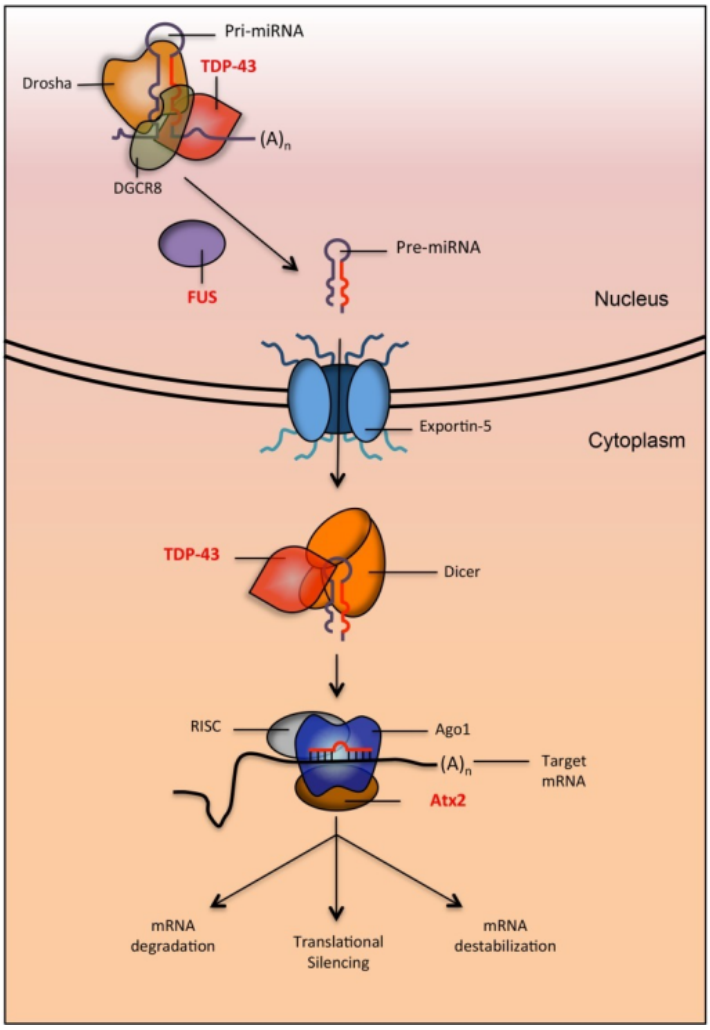

Figure 13. Involvement of TDP-43 in miRNAs biogenesis (Szafranski, 2015)

As mentioned above, TDP-43 also regulates the expression of the long non-coding RNAs (lncRNAs): a class of transcripts, consisting of more than 200 nucleotides without any protein-coding potential (Ratti & Buratti, 2016).

The main function of lncRNAs is gene regulation, in which they intervene at different points. At the epigenetic level, they act as scaffolds for the chromatin-modifying protein complexes and/or influence the epigenetic regulation by modulating the DNA methylation at the CpG nucleotide level (Kung et al., 2013; Law & Jacobsen, 2010). At the transcriptional level, lncRNAs can: i) sequester the transcription factors by competing with them, ii) alter the cellular localization of the transcription factors, iii) act as transcriptional coregulators or corepressors, iv) prevent the formation of preinitiation complexes, acting as inhibitors of pol II. Finally, at the post-transcriptional level, lncRNAs collaborate in mRNA processing. They can influence alternative splicing and polyadenylation of mRNAs, stabilize or destabilize mRNAs in the cytoplasm and disrupt translational regulation (Lourenco et al., 2015).

TDP-43 binds several lncRNAs including gadd7, MALAT1, NEAT1_2 and lncLSTR (F. Guo et al., 2015; Liu et al., 2012; Tollervey et al., 2011). Interestingly, Tollervey et al. showed that, the binding of TDP-43 with NEAT1_2 (essential for paraspeckle assembly) and with MALAT1 (localized at distinct nuclear sub-domains, the speckles, in association to different splicing factors) is increased in human FTD brains compared to healthy controls, and that the NEAT1_2 expression and localization in paraspeckels, in which it has been observed also the presence of TDP-43, are increased in spinal motoneurons of sporadic ALS patients at early stages of the disease (Tollervey et al., 2011). These observations suggest a possible role of TDP-43 in the regulation of these lncRNAs. However, it is still unclear how it regulates them and how they can affect lncRNA-based mechanisms in ALS/FTLD. Probably, the unavailability of TDP-43 in the nucleus following its aggregation within the cytoplasm could affect the lncRNAs transcriptional or post-transcriptional regulation, altering their cellular levels. Alternatively, the lack of functional TDP-43 could affect not the expression levels but the function of lncRNAs.

TDP-43 POST-TRANSLATIONAL MODIFICATIONS

TDP-43, at the cytoplasmic level, can undergo a series of post-translational modifications (PTMs) such as phosphorylation, ubiquitination, SUMOylation, acetylation and cleavage. These PTMs can confer a toxic gain of function to TDP-43. They can induce its aggregation (indeed, often the TDP-43 found within the cytoplasmic aggregates is phosphorylated, ubiquitinated and/or cleaved) or they can reduce the ability of the protein to perform some of its main physiological functions (for example the mRNA splicing activity) (Prasad et al., 2019; Wood et al., 2021) (Fig. 14).

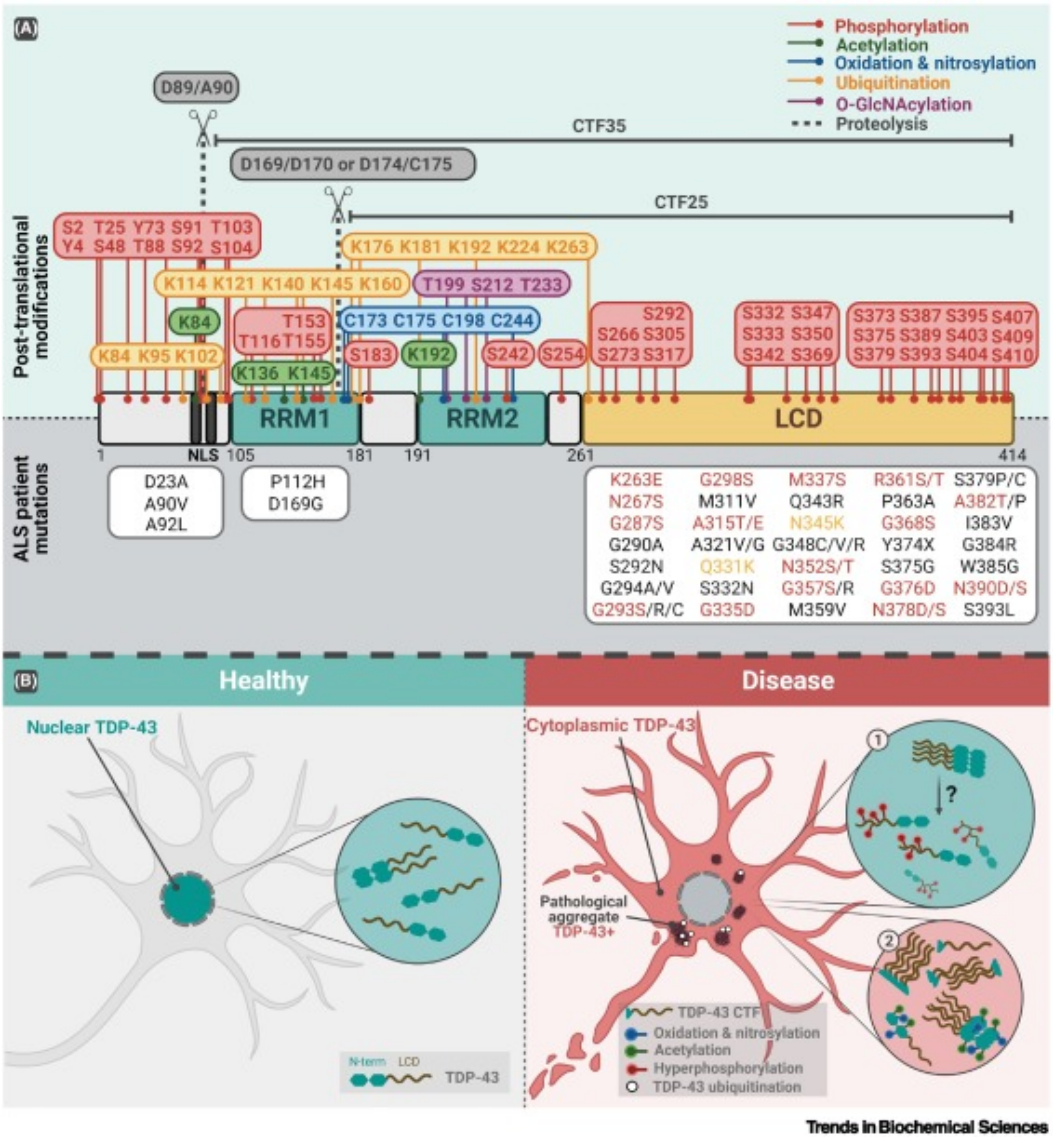

Figure 14. Principal disease-associated TDP-43 PTMs (Sternburg et al., 2022)

PHOSPHORYLATION

The phosphorylation is a type of post-translational modification that TDP-43 easily undergo and that is often observed in ALS/FTD-associated cytoplasmic aggregates (Prasad et al., 2019).

TDP-43 has 64 potential phosphorylation sites: 41 serines (Ser), 15 threonins (Thr) and 8 tyrosines (Tyr). However, the phosphorylation that consistently occurs in the context of disease are those at the level of serine residues 369, 379, 403/404 and/or 409/410. These phosphorylations are used as diagnostic markers to identify TDP-43 positive inclusions in brain and spinal cord of ALS/FTD patients (Hasegawa et al., 2008; Neumann et al., 2009, 2021) (Fig. 15).

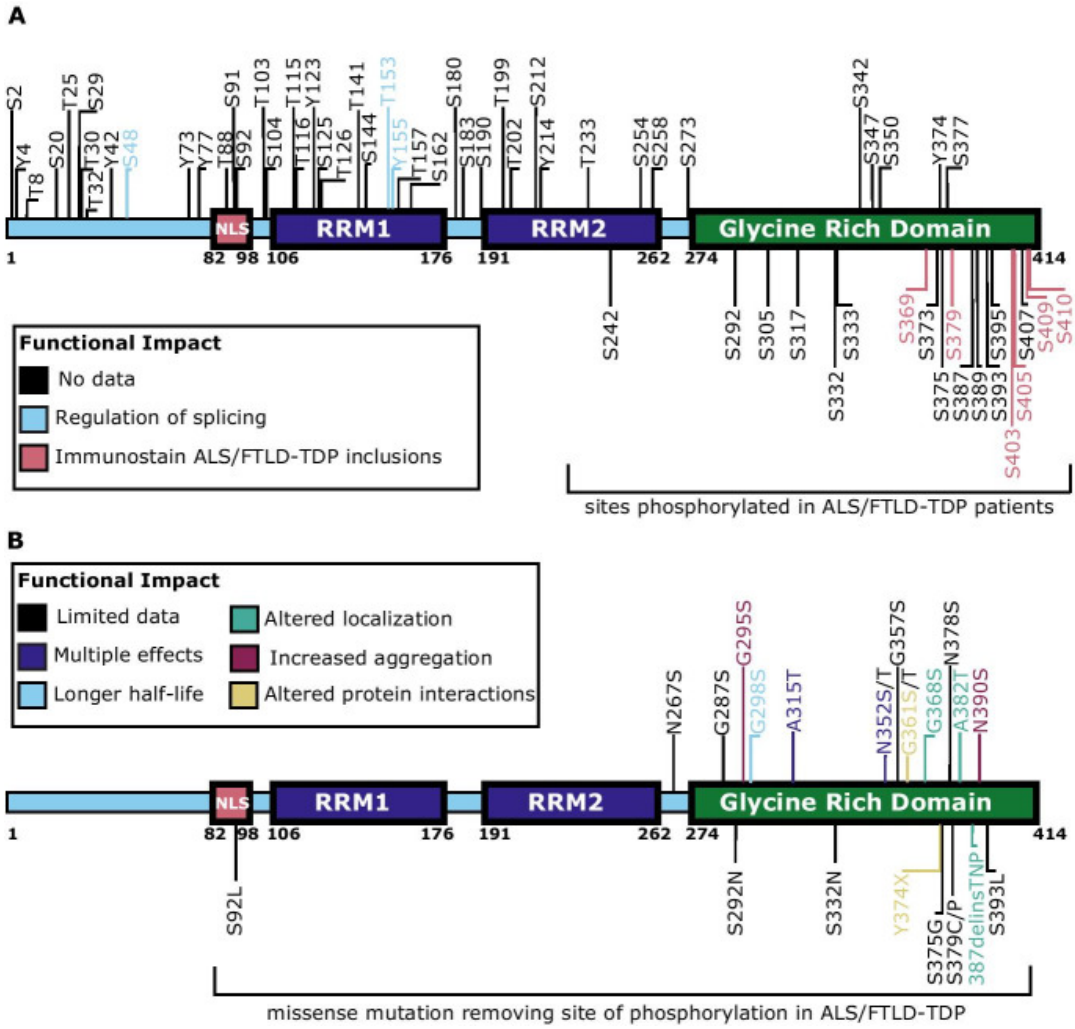

Figure 15. TDP-43 phosphorylation sites (Eck et al., 2021)

The increased phosphorylation of TDP-43 may be due to alterations in the activity of certain kinases and phosphatases that often occurs in old age (when NDs generally occur). 5 kinases (casein kinases 1 and 2 (CK1 and CK2), cell division cycle 7 (CDC7), and tau tubulin kinases 1 and 2 (TTBK1 and TTBK2), and 3 phosphatases (phosphatases PP1, PP2, and calcineurin) responsible for regulating the phosphorylation level of TDP-43 have been identified (Gu et al., 2018; Hasegawa et al., 2008; Kametani et al., 2009; Liachko et al., 2013, 2016).

It has been observed that the inhibition of the kinases CK1 and CDC7 prevents accumulation of phosphorylated TDP-43 and protect against neuron loss, while overexpression of CDC7, TTBK1, or TTBK2 (that usually co-localize with aggregated and phosphorylated TDP-43) promotes TDP-43 phosphorylation (Martínez-González et al., 2020; Rojas-Prats et al., 2021; Salado et al., 2014; L. M. Taylor et al., 2018). Moreover, it has been observed that the overexpression of the Casein kinase I isoform epsilon (CSNK1E), a serine/threonine protein kinase member of the casein kinase I protein family (whose mRNA levels in ALS patients correlate with phosphorylated TDP-43 present in affected cells) promotes the TDP-43 cytoplasmic accumulation in iPSC-derived motor neuron lines (Krach et al., 2018).

About TDP-43 dephosphorylation, it has been observed that PP1 is responsible for the dephosphorylation of TDP-43 at pathological sites S379, S403, S404, S409, and S410 (Gu et al., 2018). While calcineurin has been shown to dephosphorylate TDP-43 at S409 and S410. Interestingly, a reduction in Calcineurin activity was observed in both sporadic and familial ALS patients, suggesting that calcineurin dysregulation could contribute to the disease (Ferri et al., 2004; Liachko et al., 2016; Wagey et al., 1997) (Fig. 16).

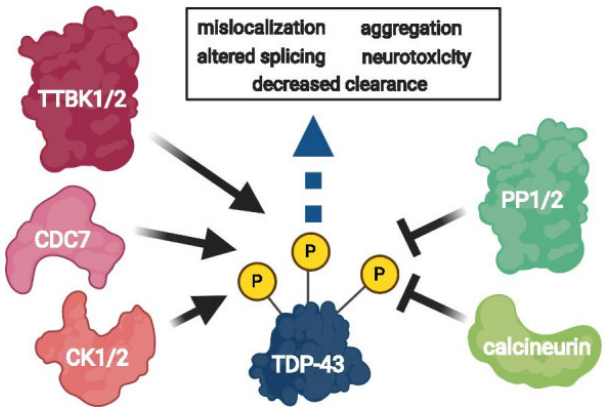

Figure 16. kinases and Phosphatase that regulate TDP-43 phosphorylation (Eck et al., 2021)

In the last years, several studies have been conducted to understand the effect of this PTMs on TDP-43. These studies tried to understand if and which TDP-43 functions can be altered following its phosphorylation and if phosphorylation may play a role in the TDP-43 cytoplasmic localization and aggregation (Eck et al., 2021).

Although the role of TDP-43 phosphorylation in the ALS/FTD pathogenesis is still unclear, these studies showed that it often gives TDP-43 a greater tendency to accumulate at the cytoplasmic level (Hicks et al., 2020; Newell et al., 2019). Phosphorylation, in fact, can alter the solubility of TDP-43, making it more resistant to the proteasomal degradation and consequently also more prone to aggregation. In addition, it can increase the TDP-43 cytoplasmic localization (Y.-J. Zhang et al., 2010). Therefore, phosphorylation, by conferring these features to TDP-43, could contribute to the pathogenesis of ALS/FTD through a mechanism of gain of toxic function (Liachko et al., 2013).

However, these studies also showed that the abnormal TDP-43 phosphorylation can also determine an alteration of its splicing activity and a reduction in its ability to bind nucleic acids (both functions that are fundamental for cell survival) suggesting that it could also contribute to the ALS/FTD pathogenesis through a loss of function mechanism (W. Li et al., 2017; A. Wang et al., 2018).

Finally, in addition to the 64 potential phosphorylation sites present in the TDP-43 protein, 20 disease-linked TDP-43 missense mutations have been identified, able to introduce or eliminate some phosphorylation sites and therefore potentially capable of altering TDP-43 localization, aggregation tendency and functions (Buratti, 2015) (Fig. 15).

UBIQUITINATION

Ubiquitination is a type of post-translational modification that results in the binding of one or more ubiquitin molecules (a highly conserved protein of 8.6 kDa) at the level of the Lys residues of a target protein, through an ATP-dependent conjugation reaction.

There are different forms of ubiquitination. Proteins can undergo i) monoubiquitination (i.e. a single molecule of ubiquitin attaches to the protein), ii) multiubiquitination (i.e. multiple ubiquitin molecules can bind to the protein), iii) polyubiquitination (i.e. a ubiquitin chain formed by several ubiquitin molecules joined together through a link between the C-

terminal glycine residue of a ubiquitin unit and a specific internal Lysine residue of the ubiquitin unit previously attached to the protein) (Grumati & Dikic, 2018; Sadowski et al., 2012).

These different forms of ubiquitination confer different fates to the target protein. Monoubiquitination and multiubiquitination often target proteins towards the secretory/endocytic pathway, while polyubiquitination is mainly associated with degradation of target proteins via proteasome. However, polyubiquitination does not always direct the target proteins to degradation via proteasome but can also lead it to a different fate, which depends on the type of polyubiquitin chain attached to it (Sadowski et al., 2012).

The ubiquitin protein, in fact, having 7 Lysine residues (K6, K11, K27, K29, K33, K48 and K63), allows the formation of 7 different types of links between two adjacent ubiquitin molecules. These different types of links, in turn, can lead to the formation of different polyubiquitinated chains (formed by ubiquitin units connected each other through the same link or through links that occur at the level of different Lysine residues) (Tracz & Bialek, 2021).

Among the various existing polyubiquitin chains, the most studied and abundant types are those formed by links through the Lysine residues 48 (K48) and 63 (K63). In particular, it has been observed that the linkage through K48 directs proteins to the degradation via proteasome, while linkage through K63, seem to have a role in the endocytic pathway and the degradation of target protein via autophagy (Grumati & Dikic, 2018) (Fig. 17).

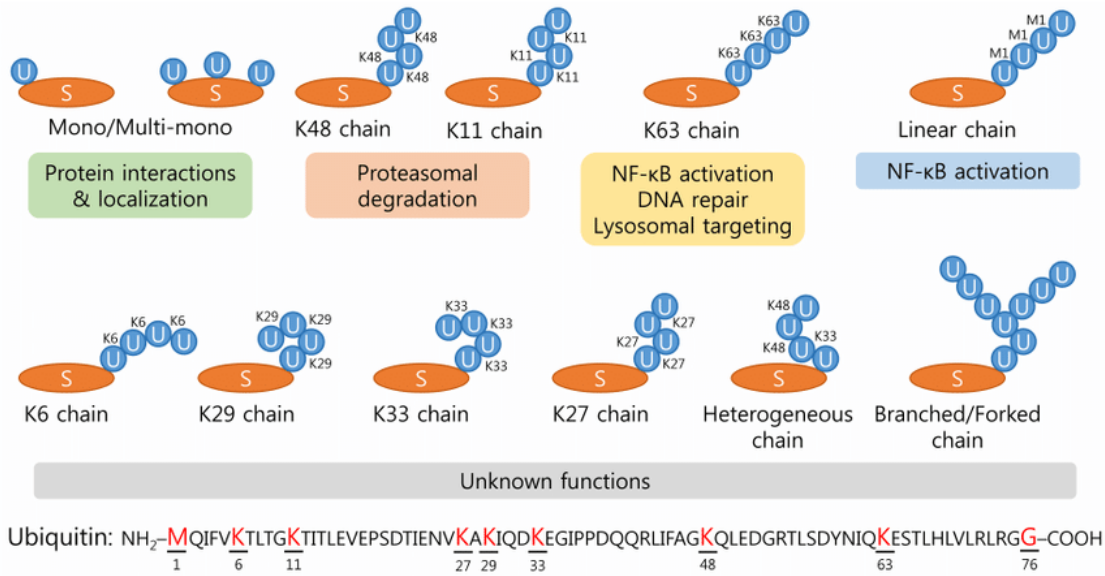

Figure 17. Different types of ubiquitination and their fate (Park & Ryu, 2014)

Ubiquitination is a PTM that TDP-43 often undergoes. Moreover, the presence of polyubiquitinated TDP-43 within the insoluble cytoplasmic inclusions is a characteristic pathological aspect of ALS and FTD (Arai et al., 2006; Neumann et al., 2006). For this reason, in recent years, many studies have been conducted in order to better understand, through which mechanism this PTM can contribute to the development and progression of these two diseases (Hans et al., 2014; Hebron et al., 2013; Y.-C. Lee et al., 2018; Uchida et al., 2016; Watabe et al., 2020).

These studies showed that TDP-43 is normally poly-ubiquitinated, both by K48- and K63-linked polyubiquitin chains, in order to be degraded, respectively, by the proteasome and autophagy (that, as we will see later, constitute the PQC system) (Hans et al., 2018). However, in ALS/FTD pathological conditions, these protein degradation systems are often altered and do not function properly. Therefore, the polyubiquintated TDP-43 that cannot be removed remains in the cytoplasm where it accumulates within the insoluble cytoplasmic aggregates, thus becoming toxic for the cell (Fig. 18). Moreover, the cytoplasmic accumulation of the poly-ubiquitinated TDP-43, by reducing the pool of ubiquitin available for the cell, can also damage the proteostasis system (Farrawell et al., 2020; Riemenschneider et al., 2022). Usually, in fact, following the degradation of the target proteins, ubiquitin is recovered by the cell that uses it to ubiquitinate other proteins (Komander et al., 2009; Tran & Lee, 2022). Therefore, the reduction of ubiquitin induces

the cytoplasmic accumulation of damaged proteins (which would be ubiquitinated and degraded) further reducing cell survival (Fig. 19).

Finally, it has been observed that the accumulation of polyubiquitinated TDP-43 within the pathological inclusions or the cytoplasmic aggregates could have an additional cytotoxic effect. It may act as avid and irreversible absorbent chamber to sequester many important proteolysis components such as the ubiquitin binding proteins and the proteasome, thus preventing cell to perform some of its essential biological functions (Tran & Lee, 2022).

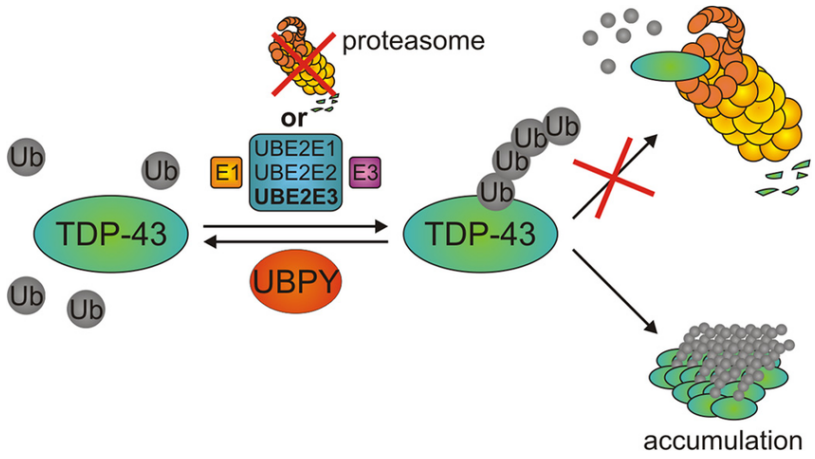

Figure 18. Proteasome inhibition and Ub-TDP-43 aggregation (Hans et al., 2014)

SUMOYLATION

SUMOylation is another type of PTM that TDP-43 contained in ALS/FTD-associated pathological aggregates can undergo. It consists in the covalent binding of different small ubiquitin-related modifiers (SUMO-1, 2/3 and 4) to specific Lysines residues of the target protein (Maraschi et al., 2021).

SUMOylation is known to regulate several cellular processes by modifying the structure, the stability, the solubility and the localization of target proteins and also their interaction with partner proteins (Celen & Sahin, 2020). In addition, it plays an important role in the cellular response to oxidative stress, hypoxia, glutamate excitotoxicity and proteasomal impairment (Vertegaal, 2022).

TDP-43 contains a single consensus site in which SUMOylation can occur: the Lysine 136. This consensus site was first identified by Maurel et al. that also highlighted the effect of

SUMOylation on TDP-43 localization. They showed that SUMOylation induces the delocalization of TDP-43 from the nucleus to the cytoplasm and stimulates its aggregation (Maurel et al., 2020).

The 12KDa SUMO protein may also interact non-covalently with several target proteins containing the SUMO-Interaction Motif (SIM). Interestingly, the ability to form this type of interaction allows SUMO to act as a scaffold to promote the formation of multiprotein complexes (Song et al., 2004). It is therefore important for the organization and compartmentalization of sub-cellular domains, especially in the nucleus, where it has been observed that several spliceosome components are SUMOylated. SUMO conjugation to the spliceosomal proteins favours the proper assembly of the spliceosome machinery and, consequently, an efficient control of the splicing activity (Pozzi et al., 2017; Sahin et al., 2014). This aspect has also been analysed for TDP-43. It has been observed that the SUMO scaffold proteins favour the TDP-43 spatial organization within the nucleus and regulate its splicing activity which, in turn, can be further partially modulated by SUMOylation at its RRM1 domain (Maraschi et al., 2021).

Thus, the SUMOylation of TDP-43 can modify its exon skipping activity and its RNA-binding capacity. It can also alter its localization, favouring its translocation from the nucleus to the cytoplasm, and its aggregation (Maraschi et al., 2021). For this reason, it can be considered a PTM capable of conferring a toxic function to the TDP-43, therefore contributing to the pathogenesis of ALS/FTD.

ACETYLATION

Acetylation is an enzyme-mediated process whereby an acetyl group is moved from one molecule to another to alter intracellular localization, protein–protein interactions or tag proteins for degradation (Wood et al., 2021). It is a type or PTM, usually promoted by the cell exposure to oxidative stress, which generally occurs at the level of the Lysine residues of TDP-43, within the RNA-binding domains (RRMs) (Cohen et al., 2015).

Since TDP-43 can be acetylated, several studies have recently been conducted in order to evaluate the possible effect of this PTM on the TDP-43 functionality. These studies showed that the acetylation of the Lysine residues of TDP-43 can modulate its functions and aggregation. The acetylation of TDP-43 Lysine residues, in fact, generally occurs at the level

of the RRMs. Thus, it can damage the RNA-binding capacity of TDP-43 and promotes accumulation of insoluble, hyper-phosphorylated TDP-43 species. This observation therefore suggests that aberrant acetylation of TDP-43, in association also with mutations and/or other PTMs (for example those able to stimulate the translocation of TDP-43 from the nucleus to the cytoplasm) may have a role in the formation of insoluble aggregates. In addition, it can promote the transformation of reversible membranelles organelles, which are formed in the cell because of the LLPS process, into insoluble aggregates (Cohen et al., 2015) (Fig. 19).

For these reasons also TDP-43 acetylation may contribute to the ALS/FTD pathogenesis through a gain of toxic function mechanism.

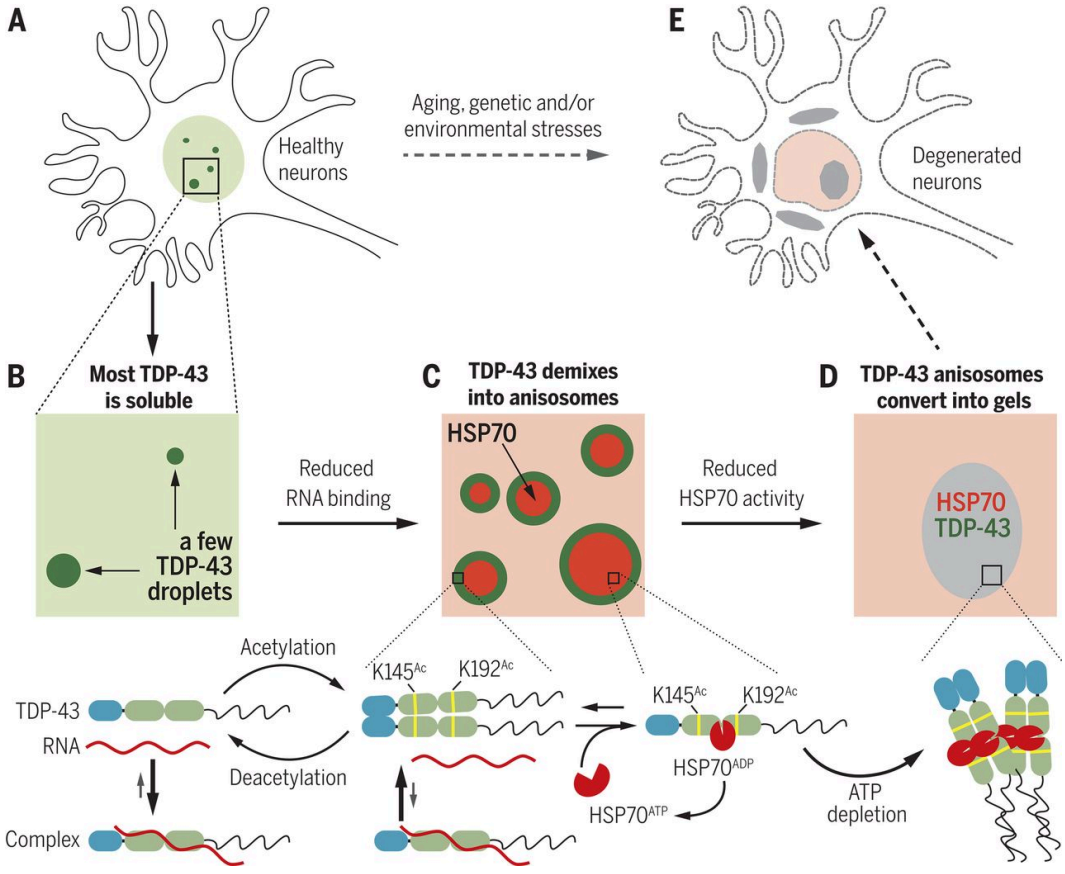

Figure 19. Acetylation-induced aggregation of TDP-43 (Yu et al., 2021)

CLEAVAGE

The cleavage has been identified, together with the phosphorylation, the major PTMs of TDP-43 (Berning & Walker, 2019; Y.-J. Zhang et al., 2007). It generally occurs by the activity of caspase-3 and calpains that cut TDP-43 at the level of certain potential cleavage consensus sites and give rise to several TDP-43 C-terminal fragments (CTFs), of different sizes (Dormann et al., 2009; Y.-J. Zhang et al., 2007). Among the CTFs, those of 35 kDa and 25 kDa, called respectively TDP-35 and TDP-25, are the most produced and studied.

TDP-43 cleavage is a type of PTMs that occurs physiologically at the cellular level. The production of CTFs, in fact, represents a prerequisite for the proteolytic degradation of TDP-43 by the PQC system (fundamental, together with transcriptional autoregulation, for the maintenance of the correct amount of TDP-43 at the intracellular level and therefore for cell survival) (Huang et al., 2014). However, CTFs are not always degraded by the PQC. In fact, in patients with ALS/FTD, they often accumulate at the cytoplasmic level together with the full length TDP-43 (Nonaka et al., 2009).

The presence of these CTFs within the ALS/FTD associated inclusions suggested that cleavage may play a role in the pathogenesis of these diseases. It is thought that CTFs may be responsible, along with other factors, for the formation of toxic cytoplasmic aggregates (Walker et al., 2015). Indeed, it has been observed that when CTFs are expressed in cultured neuronal cells, they are able to form toxic ubiquitinated, phosphorylated inclusions that closely resemble aggregated species found in human ALS and FTD-TDP brain (Y.-J. Zhang et al., 2009) (Fig. 20).

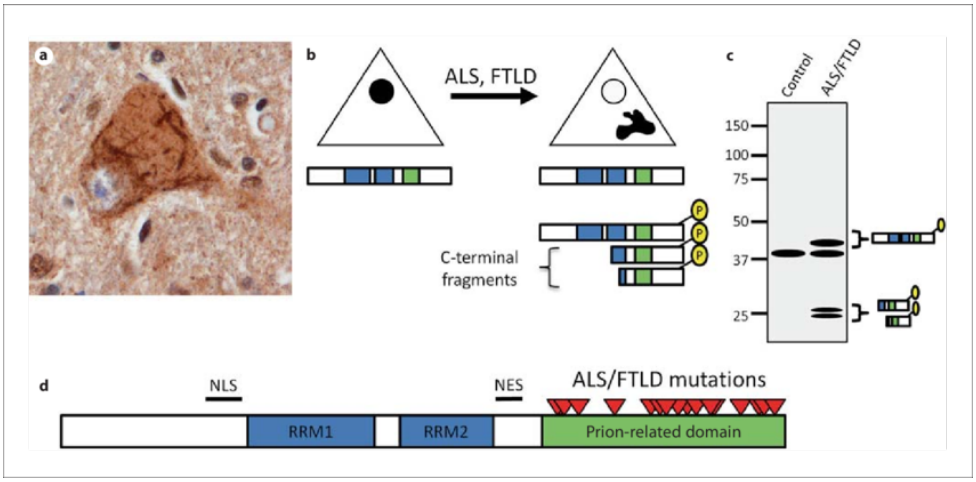

Figure 20. The principal TDP-43 C-terminal fragments TDP-25 and TDP-35 (Wegorzewska & Baloh, 2011)

In particular, TDP-25 fragment is the TDP species characterized by the highest aggregation propensity. It forms large rounded aggregates localized almost exclusively in the cell cytoplasm. While TDP-35, instead, is more soluble than TDP-25 and accumulates both in the nucleus, where it is characterized by a diffuse pattern and in the cytoplasm, where it forms aggregates. Moreover, it has been observed that TDP-25 aggregates are characterized by an irregular shape and are much bigger than those generated by TDP-35. (Cicardi et al., 2018; Crippa, Cicardi, et al., 2016) (Fig. 21).

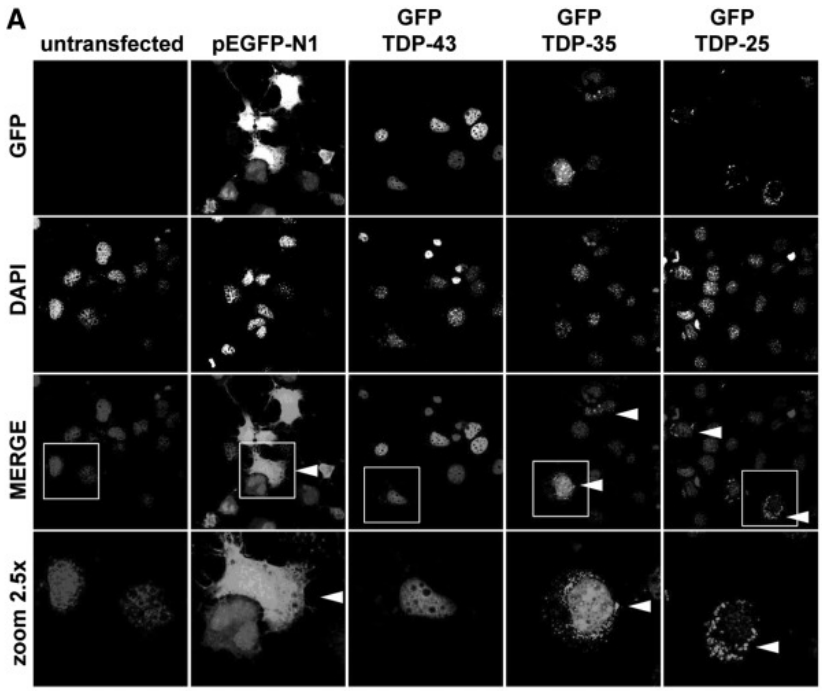

Figure 21. CTFs aggregates localization (Modified from Crippa, Cicardi, et al., 2016)

The TDP-43 CTFs accumulate in the cytoplasm of the cell, likely due to the removal of the NLS during proteolytic cleavage. The propensity of TDP-43 to aggregate appears to be mediated by its highly disordered C-terminal domain (CTD) (Y.-J. Zhang et al., 2007). The loss of the NLS and the maintenance of the CTD, inducing its cytoplasmic aggregation, give TDP-43 a toxic function. Therefore, CTFs contribute to the pathogenesis of ALS/FTD through a gain of toxic function mechanism.

It has been observed that the CTFs TDP-35 and TDP-25 are also able to sequester the full length TDP-43 from the nucleus, thus reducing its activity in the nucleus and contributing to the pathogenesis of ALS/FTD also through a loss of function mechanism (Y.-J. Zhang et al., 2009).

MAINTENANCE OF TDP-43 PROTEIN HOMEOSTASIS

Since intracellular TDP-43 accumulation and aggregation are toxic for cells, maintaining intracellular TDP-43 levels is critical for cell survival. TDP-43 homeostasis is maintained by the self-regulation of its expression and an integrated action of chaperones, co-chaperones and degradative systems, that together represent the PQC system.

First, TDP-43 is known to undergo self-regulation through a negative-feedback loop (Huang et al., 2014). Indeed, it binds to the 3'UTR of its transcript to prevent the translation, thus maintaining a TDP-43 stable intracellular protein concentration (Ayala et al., 2011). Often, mutations in the gene encoding TDP-43 improve the half-life of TDP-43 and the propensity to aggregate. However, other cellular machineries are involved in maintaining TDP-43 protein homeostasis. In particular, cells try to inhibit the aggregation of TDP-43 in the cytoplasm, by degrading the cytosolic misfolded TDP-43 through the PQC system that is composed by the chaperones and co-chaperones proteins, the ubiquitin proteasome system (UPS) and the autophagic pathway (Cascella et al., 2017; Ciechanover & Kwon, 2017) (Fig. 22).

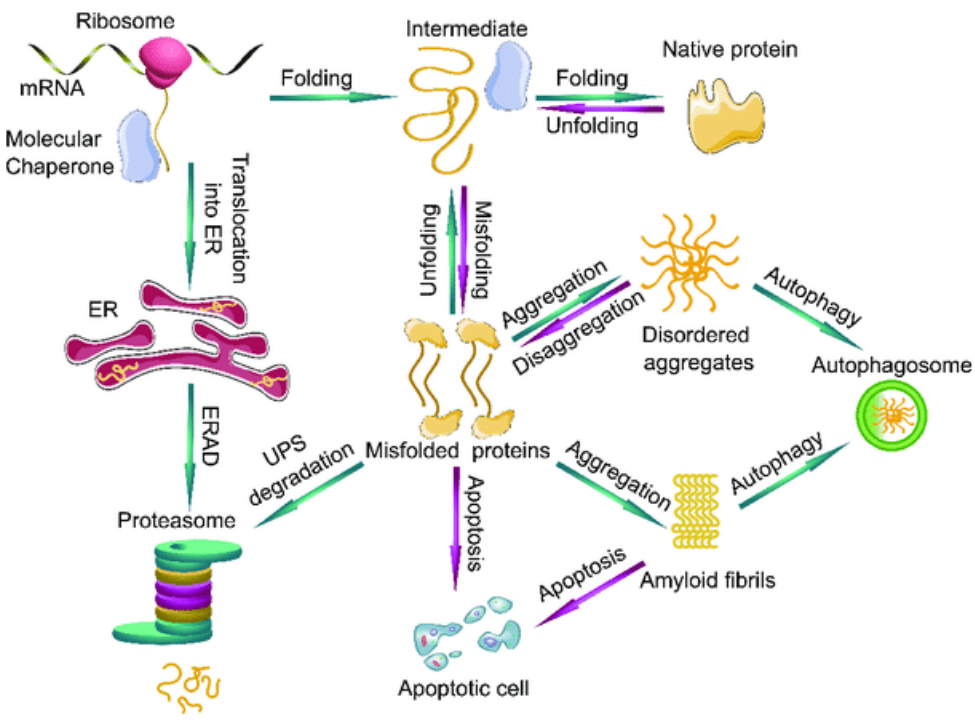

Figure 22. Regulation of protein homeostasis by the PQC system (Kulka et al., 2020)

THE CHAPERONE SYSTEM

Chaperones are ubiquitously expressed proteins which has the primary role of assisting misfolded or unfolded proteins in regaining or acquiring their normal fold, thus counteracting their aggregation (Y. E. Kim et al., 2013). Misfolded proteins are recognized by the chaperone proteins because of the exposure of hydrophobic residues normally localized inside the protein structure (Hartl et al., 2011). Chaperone proteins play important functions under normal conditions, but their role is even more relevant during cellular stress responses, in which the Heat Shock Factor 1 (HSF-1) (the main transcription factor responsible for stress-induced genes expression) induces their expression to prevent or correct the protein denaturation caused by heat shock, oxidative, toxic chemical, and inflammation stresses (Anckar & Sistonen, 2011). Given this feature, the majority of them are called heat-shock proteins (HSPs) (Garrido et al., 2001).

The HSPs are classified according to their molecular weights in several subgroups, such as Hsp40, Hsp60, Hsp70, Hsp90, Hsp100 and small HSPs (Ciechanover & Kwon, 2017). Some of them, like HSP60, HSP70, HSP90 and HSP100 have an ATP dependent activity (in

particular, they assist protein folding or refolding through the ATP hydrolysis) while other, like HSP40s and sHSPs, do not use ATP for their activity, and they just bind substrates protecting them during their assembly and favouring substrates recognition and interaction with an ATP-dependent HSP.

HSP70

HSP70 is involved in several cellular processes. It functions in newly synthesised protein folding, in misfolded and aggregated protein refolding, in the transport of proteins across membranes, and in driving misfolded proteins to degradation (Fontaine et al., 2016).

HSP70 usually interacts with its client proteins through a stretch of four or five hydrophobic amino acid residues exposed on their surface (Rudiger, 1997) and performs its functions by means of an ATP-dependent cycle of substrate binding and release (Kampinga & Craig, 2010).

It is composed by an N-terminal ATPase domain (NBD) and a C-terminal substrate binding domain (SBD). The SBD, in turn, is divided into two subdomains that form a hydrophobic binding pocket and a lid that can pass from an open to a closed conformation depending on whether the NBD is linked respectively to ATP or ADP. When the NBD is bound to ATP, SBD is open and HSP70 has a low affinity for the client substrate. When NBD is bound to ADP, SBD is closed and HSP70 can associate to the misfolding substrate and facilitate its proper folding. When the HSP70 client substrate reaches its correct folding, no longer has the exposed hydrophobic patches and, thus, is released from Hsp70 (Lackie et al., 2017).

To facilitate the reaction cycle between ATP and ADP bound states and perform its functions, Hsp70 requires the assistance of two type of co-chaperones: the members of the DnaJ (Hsp40) family, that stimulate the ATP hydrolysis promoting the substrate entry into the Hsp70 binding cleft, and the nucleotide exchange factors (NEFs), that promote ADP release and subsequent ATP rebinding, allowing substrate leaving the cleft (Aragonès Pedrola & Rüdiger, 2021) (Fig.23).

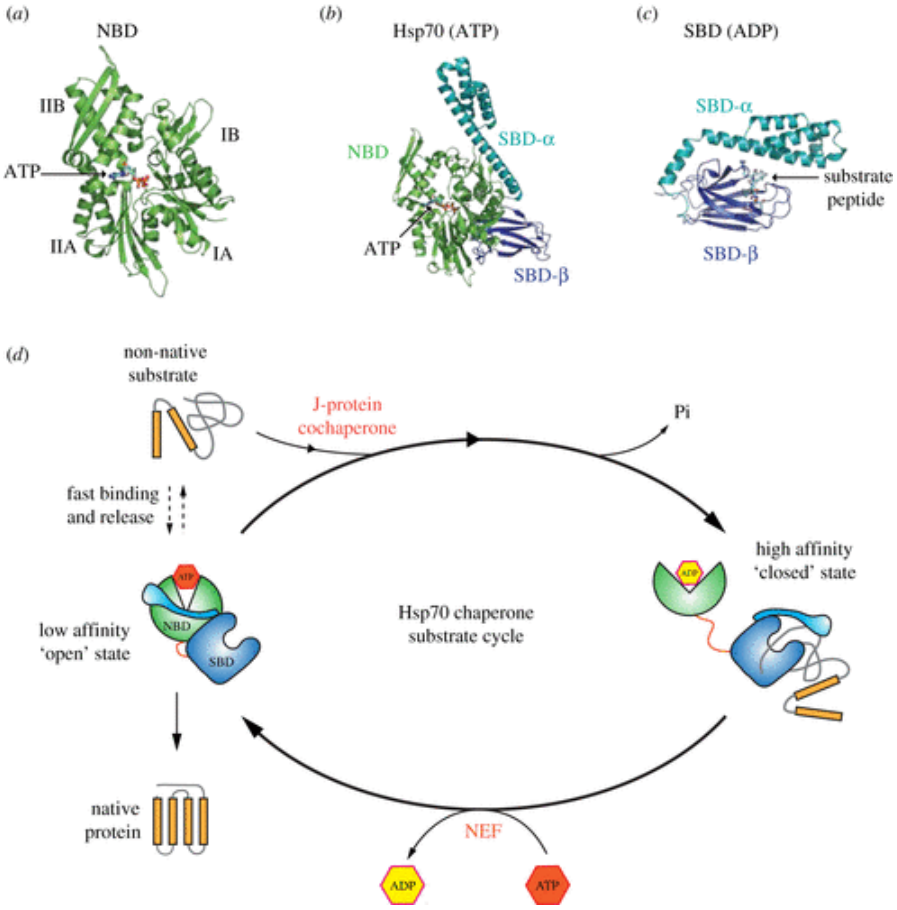

Figure 23 HSP70 structure and mechanism of function (Larburu et al., 2020)

HSP40

The HSP40 proteins, are a group of 49 co-chaperone proteins that, as said before, regulate the HSP70 activity by stimulating the ATP hydrolysis. They are also called J-proteins because contain the J domain, that is responsible for the interaction with HSP70. However, in addition to the J domain, they contain other domains that can give them specialized functions. For example, they contain domains that enable them to deliver clients to the SBD of HSP70 and also domains that can facilitate the targeting of clients for degradation (Smith et al., 2015) (Fig. 24).

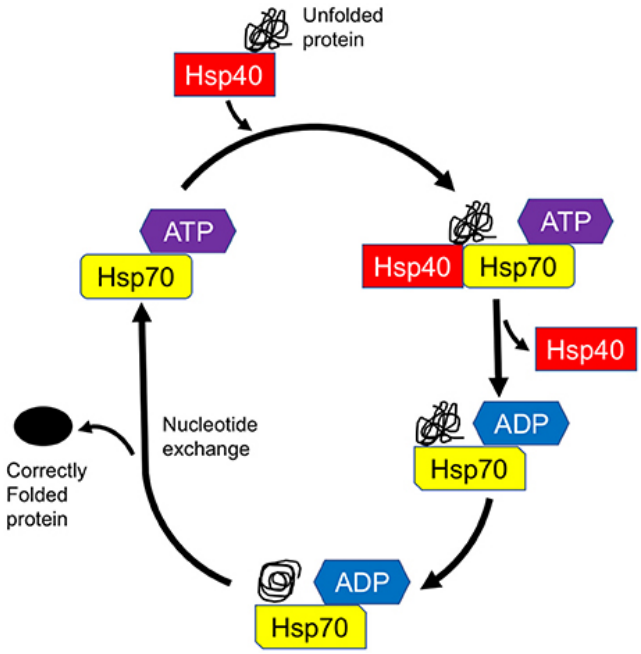

Figure 24. HSP40 recognizes and target protein to HSP70 and also assists HSP70 in refolding process (K. Zhang et al., 2022)

HSP90

HSP90 is another abundant and ubiquitous chaperone protein that, like the other HSPs can bind unfolded proteins and prevent their aggregation. HSP90, differently from the other HSPs, seems to act at the late stages of substrate folding. In particular, it is important for the maturation of the signalling proteins involved in development and cell division, indeed its substrates include steroid hormone receptors, kinases and key oncogenic proteins such as the tumour suppressor p53 (Saibil, 2013). As like as for the HSP70 clients, the folding cycle of HSP90 clients is ATP-dependent. Also in this case, in fact, the hydrolysis of ATP guides the transition of HSP40 from a closed conformation to an open one, thus making it more or less affine to the substrate. HSP90 usually exists in the form of a homodimer in which each subunit consists of i) an N-terminal ATP-binding domain (ND), ii) a middle domain that binds the substrate (MD) and iii) a C-terminal dimerization domain (CD). In the absence of ATP, HSP90 homodimer adopts a V-shaped open conformation, in which the NDs of the two subunits are separated. The binding of the ATP to the ND induces the NDs dimerization, that causes the transition of the HSP90 homodimer from an open to a closed conformation (affine to the client substrates). In the closed conformation the ATP molecule is hydrolysed to ADP. This promotes the separation of the NDs and the return of Hsp90 to the open conformation, with the release of the substrate. This cycle of reactions is

regulated by various co-chaperones such as HOP, p23/Sba1, and Cdc37, that usually co-operate in a sequential cycle to facilitate the maturation of HSP90 clients (Ciechanover & Kwon, 2017; Lackie et al., 2017; Smith et al., 2015) (Fig. 25).

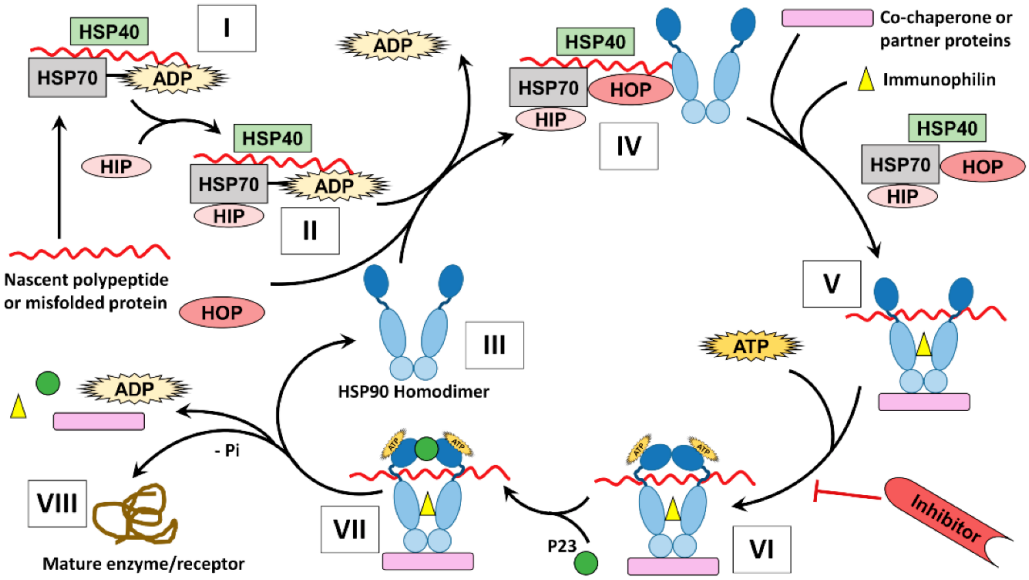

Figure 25. Protein folding by HSP90 (Hoter et al., 2018)

HSP60

The members of the HSP60 family, also called chaperonins, are large complexes composed by a double ring structure containing a central cavity in which the unfolded substrates (the most common HSP60 client substrates) are enclosed for refolding. These HSPs can be divided into two subgroups: the group I, that contains the chaperonins GroEL and HSP60, (present respectively in bacteria and in the mitochondrial matrix) that are composed by 7 subunits per ring and that require co-chaperones for their activity (GroES in bacteria and Hsp10 in mitochondria, that act as lids over the complex), and the Group II, containing the chaperonins that are usually present in archaea (thermosome) and in the cytosol of eukaryotes (CCT or TRiC). They, differently from the chaperonins of the group I, typically have 8 subunits per ring and do not require co-chaperones (Saibil, 2013).

HSP100

Members of the chaperone family HSP100 are unfoldase and disaggregase. They usually provide substrates to compartmentalized proteases and/or play a role in the disassembly of protein aggregates containing misfolded proteins. In addition, they are members of the AAA+ superfamily. They typically form oligomer ring structures that, exploiting the chemical energy resulting from the ATP hydrolysis and transforming it into mechanical energy, allow the threading of polypeptides or polynucleotides through their central channel to unfold them (Saibil, 2013).

sHSP

The members of the sHSPs family are ATP-independent. In human, there are 10 sHSPs, called HSPBs (B1-10), with a molecular weight between 12 and 42 kDa. Their structure is composed by a 100-residue α-crystallin domain flanked by variable N-terminal and C-terminal extensions that enable the formation dimer/oligomers and mediate the recognition of substrates. Like other HSPs, also sHSPs have the main function to maintain protein homeostasis (Carra et al., 2012; Ciechanover & Kwon, 2017; Smith et al., 2015). They do this through different mechanisms: i) they bind partially denatured and misfolded proteins and prevent their aggregation keeping them in a state maximally suitable for the interaction with other HSPs, such as Hsp70, that can renature these proteins; ii) they promote the targeting of denatured proteins to the degradation via proteasomes or autophagy; iii) they cooperate with HSP110, HSP70, and HSP40, for the disassembling of amyloid aggregates (Carra et al., 2012; Muranova et al., 2019).

Of the ten HSPBs present in human, six (B1, B2, B5, B6, B7 and B8) are ubiquitously expressed in all human tissues while the other 4 are expressed only in specific ones. However, also the expression level of the ubiquitously expressed HSPBs has been observed higher in certain cell types, such as neurons, skeletal and cardiac muscle cells, suggesting that in these cells the HSPBs activity is fundamental. In fact, mutations in HSPBs are usually associated to neuropathies, myopathies, and/or cardiomyopathies (Tedesco, Cristofani, et al., 2022).

In particular, it has been observed that some members of the HSPBs family are clearly implicated in NDs. Among these, those that have been most associated with NDs are HSPB1 and HSPB8 (Tedesco, Ferrari, et al., 2022).

HSPB1 is a 23 kDa protein constitutively expressed in human tissues that exerts several functions under physiological or stressed conditions. In particular, HSPB1: i) cooperates in refolding or degradation of substrates, ii) interacts with cytoskeletal elements, modulating their correct assembly and preventing their damage, iii) plays an anti-apoptotic activity both by interfering with the pro-apoptotic proteins Bax and Bid and by inhibiting the caspase cascade through the sequestration of the cytochrome c released from mitochondria (Tedesco, Cristofani, et al., 2022). Moreover, in the brain, HSPB1 is also involved in stress granule maintenance and liquid–liquid phase transition process. In this context, it has been observed that HSPB1 has a role in TDP-43 pathology, in fact HSPB1 regulates liquid–liquid phase separation and aggregation of TDP-43 (Lu et al., 2022).

HSPB8 is a 22 kDa protein ubiquitously expressed but mainly present in cardiac and skeletal muscle cells. HSPB8 is mainly localized in the cytoplasm and nucleus, however, it has been observed that it can associate with the inner surfaces of cell membranes (F. Li et al., 2018). As like as the other HSPBs, HSPB8 tend to form highly dynamic oligomeric complexes consisting of a variable number of identical or nonidentical subunits. In particular, HSPB8 interacts with HSPB1, HSPB2, HSPB3, HSPB5, HSPB6 and HSPB7. However, it has been found mainly as a monomer and homodimer associated to the co-chaperone BAG3 with whom it forms a 2:1 stoichiometric complex by means of two BAG3 Isoleucine-Proline-Valine (IPV) domains (Tedesco, Cristofani, et al., 2022; Tedesco, Ferrari, et al., 2022). The formation of this HSPB8/BAG3 complex takes part in the Chaperone-Assisted Selective Autophagy (CASA), a selective type of autophagy, particularly active in NDs, that favours the disposal of damaged and misfolded substrates (Carra et al., 2008; Rusmini et al., 2017). In this context HSPB8 recognizes the substrates, and, by interacting with BAG3 (which enhance HSPB8 protein stability), it helps HSP70 in the refolding of the substrate or in its degradation through autophagy. In addition, HSPB8 plays a role in graulostasis, which is the process that regulates the composition and dynamic structure of the stress granules. In fact, HSPB8 having an holdase activity, when it is recruited to stress granules prevents the irreversible aggregation of the misfolded proteins by recruiting BAG3-HSP70 machinery, for their

disposal (Tedesco, Cristofani, et al., 2022). Finally, HSPB8, upon proteotoxicity, by promoting the phosphorylation of the eukaryotic initiation factor-2α (eIF2α), shuts down translation of unnecessary proteins (Tedesco, Cristofani, et al., 2022).

CO-CHAPERONE PROTEINS

HSPs proteins, in particular HSP70 and HSP90, to perform their activity need the support of a group of proteins called co-chaperone proteins. These proteins usually regulate the refolding activity of HSPs and facilitate the interactions between chaperones and their client substrates (Altinok et al., 2021). The co-chaperone proteins can be divided in several families based on the domains that characterize them. Among these there are: i) the family containing the TPR motif, whose members are CHIP, HIP and HOP, ii) proteins containing the J domain, formed by the already described members of the HSP40 family, and finally iii) the Bcl-2-associated athanogene (BAG) containing family, that contains the BAG domain.

CHIP

CHIP, Carboxyl terminus of HSC70 Interacting Protein, is a co-chaperone protein usually present in cells as homodimer. Each monomer of CHIP can bind both HSP70 and HSP90, (although not simultaneously) and is composed by three functional domains: a tetratricopeptide repeat (TPR) domain, that mediates the interaction with the chaperones HSP70 and HSP90 through the binding of their EEVD motif, a coiled-coil domain, essential for dimerization, and a C-terminal U-box domain, necessary as a ubiquitin ligase domain. Since the presence of the U-box domain, CHIP acts as an E3 ubiquitin ligase and catalyzes the ubiquitination of HSP70 and HSP90-bound substrates. In particular, ubiquitin is transferred from an E2 ubiquitin conjugating enzyme bound to CHIP to an ε-amino group of a Lysine residue of the substrates. Therefore, CHIP tags substrates with ubiquitin and direct them to the proteasomal or lysosomal degradation pathway (Altinok et al., 2021; Karunanayake & Page, 2021).

HIP

The HSC70 interacting protein (HIP) binds the NBD of HSP70 and mainly exists as a dimer. It is composed by an N-terminal domain responsible for the dimerization, a TPR domain, a charged region composed by repeats of the GGMP peptide, and a C-terminal aspartic-

proline (DP) domain. The bind of HIP to the NBD of HSP70 stabilizes the ADP bound state of HSP70 delaying the release of substrate. Moreover, it competes with the co-chaperone BAG1 for the binding to the HSP70 NBD, inhibiting its nucleotide exchange activity. HIP alters the dynamic nature of the NBD. It locks HSP70 in the ADP-bound state, delaying the substrate release by HSP70. Given this, HIP appears important for avoiding premature substrate release and for facilitating the HSP70 foldase function (Karunanayake & Page, 2021).

HOP

The co-chaperone HSP70-HSP90 Organizing Protein (HOP) can mediate the transfer of client substrates from HSP70 to HSP90 for their folding and/or maturation. These co-chaperones allows HSP70 and HSP90 to cooperate in the maturation of transcription factors, kinases and nuclear receptors (Alvira et al., 2014). In particular, Hop is composed by three TPR domains (TPR1, TPR2A, and TPR2B), two DP domains (DP1 and DP2), and a linker region. To transfer substrate clients between HSP90 and HSP70, HOP binds simultaneously both the chaperone proteins (Altinok et al., 2021). It binds HSP70 through its TPR1 and TPR2B domains, while through the TPR2A domain, it binds HSP90 via its MEEVD motif. The refolding mediated by HSP70, HOP and HSP90 takes place through a four-step mechanism: i) the SBD of HSP70, with the help of HSP40, recognizes and binds the substrates while the TPR2A domain of Hop binds HSP90 that adopts a semi-closed substrate binding conformation; ii) the HOP/HSP90 complex binds to the HSP70/substrate complex through the TPR1 domain of HOP; iii) the DP2 domain of HOP activates and pass the substrates to HSP90, forming the HSP90/substrate complex; iv) the NBDs of HSP70 and HSP90 interact each other while the SBD of HSP70 interacts with the TPR2B domain of HOP, inducing lateral reengagements in HOP and facilitating a further folding of the substrates mediated by HSP90 (Karunanayake & Page, 2021).

BAG FAMILY

This family of co-chaperones is composed by six members (BAG1, BAG2, BAG3, BAG4, BAG5, ad BAG6) named BAG (Bcl-2-associated Athanogenes) proteins because of the presence in their structure of at least one BAG domain. They, interact with the ATPase

domain of HSP70 and act as nucleotide exchange factors (NEF), favouring the ATP-ADP cycle of HSP70 and the release of the substrate (Altinok et al., 2021).

Between the different type of BAG proteins, the first to be identified was BAG1. BAG1, in humans, exists in four different isoforms (BAG1S of 52 kDa, BAG1M of 46 kDa, BAG1 of 34 kDa and BAG1L of 29 kDa) that are the result of an alternative initiation translation site. It acts as a NEF of HSP70 by binding its ATPase domain through its C-terminal BAG domain. However, since BAG1 contains, at its C-terminus, a ubiquitin-like (UBL) domain that can bind the proteasome, it can also promote the delivery of HSP70-bound misfolded substrates to the proteasome (Kermer et al., 2015).

BAG2 is characterized by a BAG domain that has a low homology with the other members of the family, however it is still able to interact with HSP70 and acts as NEF, although through a different binding mode (Z. Xu et al., 2008). In addition to the NEF activity, BAG2 acts also as an inhibitor of CHIP. In particular, it binds HSP70 through its ATPase domain and interferes with CHIP-mediated ubiquitylation of the HSP70-bound substrate by abrogating the cooperation between CHIP and the E2 enzyme (Arndt et al., 2005). Interestingly, BAG2 also promote protein degradation by the 20S proteasomal degradation pathway acting independent of ubiquitin (Behl, 2016).

BAG3 is a ubiquitously expressed protein with a higher expression level in heart and skeletal muscle but also in brain and in the peripheral nervous system. As like as the other BAG proteins, it contains the BAG domain in its structure, however it is formed also by a Tryptophan-Tryptophan (WW) domain, a PxxP repeat, and two conserved IPV (isoleucine–proline–valin) motifs – one located at the centre of the molecule and one closer to the N terminus, that allow BAG3 to interact with different proteins, regulating many major biological processes including apoptosis, development, cytoskeleton arrangement, and, as more recently discovered, autophagy. In particular, through the WW domain, it binds proline-rich ligands, for instance, the adenovirus penton base protein or the guanine nucleotide exchange factor 2, through the PxxP motif it binds the SH3 (Src homology 3) domains, present in proteins such as phospholipase Cγ (an important signal transduction enzyme), while, finally through the IPV motifs it binds to some sHSPs proteins, such as HSPB5, and HSPB6, although its favourite partner is HSPB8, with whom, as said before, takes part in the CASA-complex formation. Moreover, recently, it has been observed that

BAG3 can interact also with the transcription factor HSF1 through its BAG domain. This binding causes a co-translocation of BAG3 to the nucleus upon stress, increasing the BAG3 activity (Behl, 2016).

The most studied role of BAG4 is in regulating apoptosis in cancer cells. Indeed, given its ability to bind the death domains of the tumour necrosis factor (TNF) receptors preventing the apoptotic pathway activation, it is also named silencer of death domains (SODD). However, little is known about its role in neurodegenerative diseases (Annunziata et al., 2007)

BAG5, instead, is quite different from the other BAG proteins because it possesses not one but four BAG domains. However, only one of these domains seems important for the interaction of this protein with HSP70. Like BAG2, BAG5 inhibits CHIP activity (Gupta et al., 2022).

BAG6 is composed by 1229 amino acids, and it is the largest member of the BAG proteins family. It contains a BAG domain but, differently from the other BAG proteins, it seems that it has no interaction, and thus no action, on HSP70. However, BAG6 has a UBL domain at its N-terminus that, as already observed for BAG1, helps in driving substrates to proteasome (Behl, 2016).

THE INTRACELLULAR PROTEIN DEGRADATION PATHWAY

While, as we observed until now, molecular chaperones have the primary function of assist misfolded or unfolded proteins to regain or acquire the normal folding, when these proteins are no able to reach their correct folding, molecular chaperones can also promote their degradation collaborating with proteolytic machinery. The main proteolytic systems through with eukaryotic cells degrade these proteins, as mentioned before, are UPS and autophagy. In particular, substrates to be degraded are initially ubiquitinates by an E3 Ub ligase (for example CHIP) and then they are degraded by the proteasome. However, if these proteins are highly aggregated or if, for some other reasons, they escape the surveillance of the UPS, molecular chaperones direct them to the autophagic pathway, where, as we will see later, they will be degraded by lysosomal hydrolases (Ciechanover & Kwon, 2017) (Fig. 26).

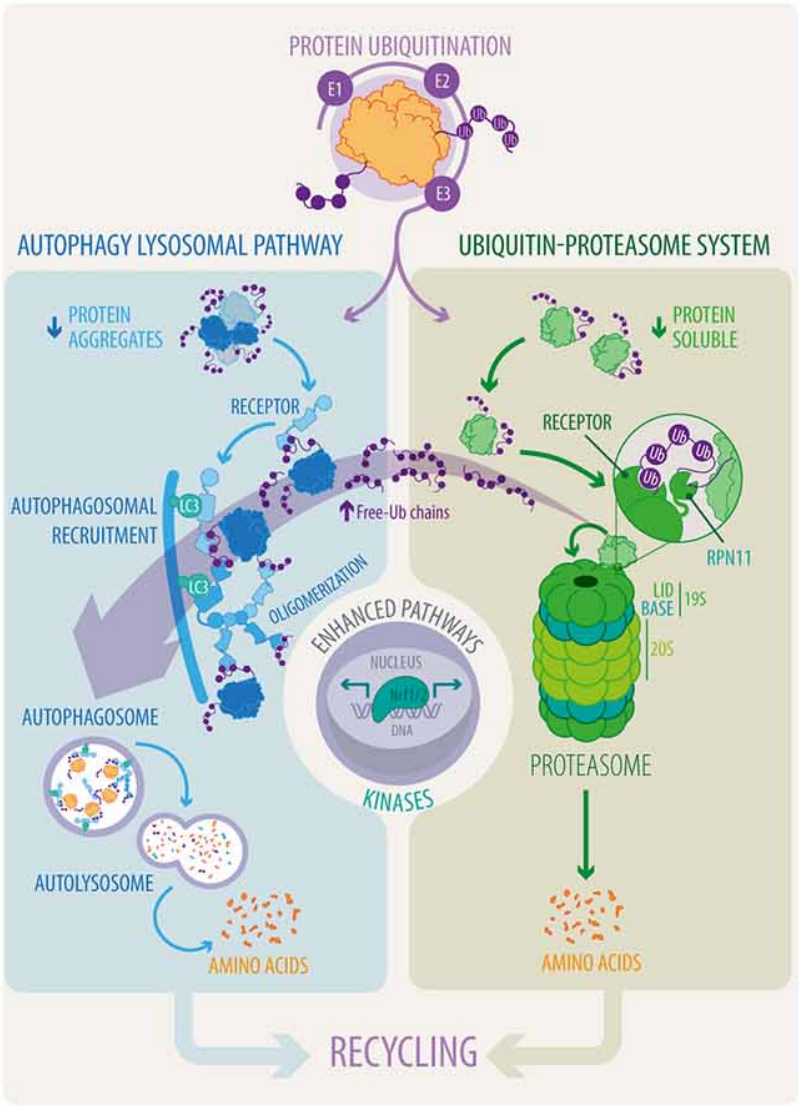

Figure 26. UPS and autophagy (adapted from Bustamante et al., 2018)

THE UBIQUITIN PROTEASOME SYSTEM

The ubiquitin-proteasome system (UPS) is an ATP-dependent, highly selective protein degradation system that is involved in the degradation of misfolded or damaged proteins in small peptides (Ciechanover & Stanhill, 2014).

Proteins degraded by UPS are first of all ubiquitinated and later proteolyzed by a multi-enzymatic complex known as the 26S proteasome. Proteasome degrades mainly proteins that are poly-ubiquitinated, particularly that linked to a K48 polyubiquitinated chain (Ciechanover & Stanhill, 2014).

The substrate ubiquitination process is carried out by an ATP-dependent enzymatic cascade, composed of three main steps, in which are involved three groups of enzymes: ubiquitin E1 (activating enzyme), ubiquitin E2 (conjugating enzyme), and ubiquitin E3 (ligase enzyme). For some substrates, it is involved also a fourth enzyme, ubiquitin E4 (the ubiquitin chain elongation factor), that catalyzes the elongation of the ubiquitin chains (Nandi et al., 2006).

During this process, E1, that is an ATP-dependent enzyme, activates ubiquitin forming a highly reactive thiol-ester bond between the Glycin76 in the ubiquitin C-terminal edge and a Cysteine residue in the active site of the E1 enzyme. After the activation, E1 transfers ubiquitin on the active-site cysteine residue of the ubiquitin E2 conjugating enzyme and then to the substrate directly by the E2 or via the ubiquitin ligases E3. E3 acts as a scaffold by binding to both the substrate and the E2-ubiquitin complex to facilitate substrate ubiquitination (Roos-Mattjus & Sistonen, 2004). Finally, E4 mediates the attachment of ubiquitin moieties mainly through K48 linkage.

After the ubiquitination, substrates are directed to the proteasome for the degradation. The 26S proteasome is a tubular organelle of proteolytic enzymes consisting approximately of 32 different subunits in two copies, which catalyzes protein degradation. It is composed by a proteolytic core complex (the 20S subunit) flanked at both ends by the 19S regulatory complexes that regulate the 20S subunit and prepare the substrates for the degradation. The 20S subunit it is characterized by a barrel-like structure consisting of four rings (two inner and two outer) each composed of seven subunits (seven β-subunits for the inner rings and seven α-subunits for the outer rings) (Roos-Mattjus & Sistonen, 2004). These rings form a cavity where three β-subunits (β5, β2 and β1), having a chymotryptic, tryptic and post-acidic action, perform the proteolytic activity (ADAMS, 2003). The α-subunits contained in the outer rings, instead, regulates the interaction between the 19S and 20S complexes and the entry of substrates in the inner active cavity (Glickman & Ciechanover, 2002). The 20S subunit is in an activate state when interacts with the 19S regulatory complex (Fig. 27). The 19S regulatory complex is responsible for the recognition, deubiquitylation, unfolding and translocation of the substrates to the proteolytic core complex of the 20S subunit to be degraded. It consists of at least 18 proteins that can be divided in two multisubunits complexes, the base and the lid, that respectively function in opening the central channel

and translocating the substrates to the 20S subunit for the degradation, and properly degrading polyubiquitinated proteins and deubiquitylating substrates (Glickman et al., 1998). The subunit of the 19S complex that seems to be responsible for the recognition of the substrate is the Rpn10, since it has been reported that it is able to bind polyubiquitin chains. Moreover, Rpn10 interacts both with the lid and the base stabilizing their interaction. Another 19S complex subunit that it resulted important for the function of the proteasome is the Rpn11, a metallodeubiquitylase that removes polyubiquitin chains from the substrates allowing their degradation (R. Verma et al., 2002). The substrates, in fact, are degraded only after being deubiquitinated. In particular, ubiquitin chains are released in the cytosol as long chains that are subsequently reduced into ubiquitin monomer by the deubiquitinating enzymes (DUBs). This step allows the ubiquitins to be recycled and used for other proteins degradation (Roos-Mattjus & Sistonen, 2004).

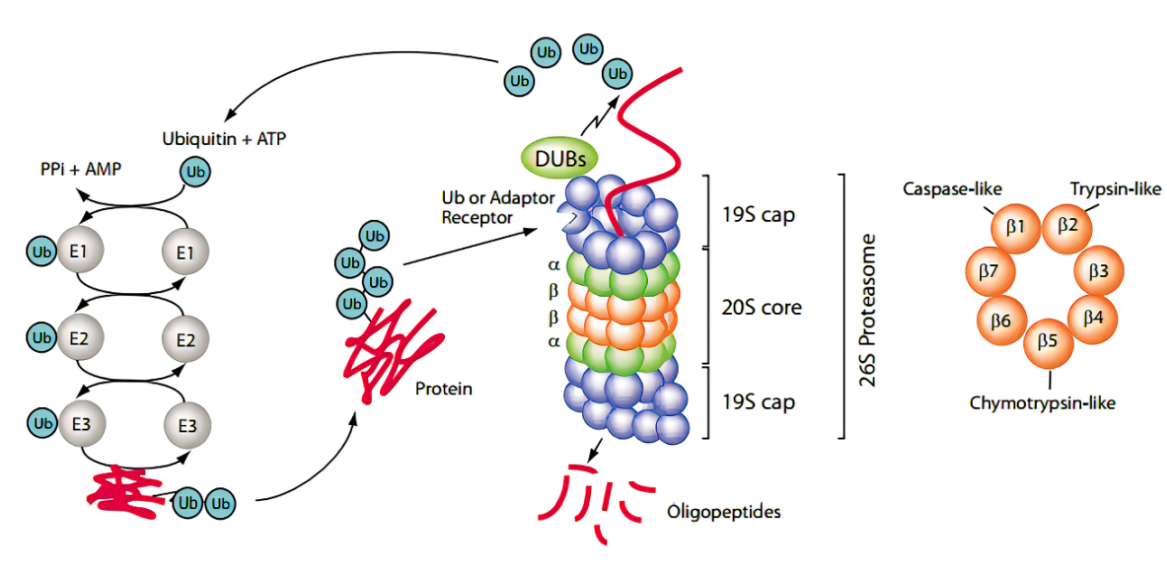

Figure 27. Substrate ubiquitination and degradation by the proteasome (https://www.caltagmedsystems.co.uk/information/the-ubiquitin-proteasome-system-2/)

As already mentioned above, the neurodegenerative diseases-associated proteinaceous inclusions, are usually rich in ubiquitinated proteins (Bendotti et al., 2012).

This is mainly due to the fact that in the vast majority of these diseases, including ALS and FTD, the UPS components are usually downregulated and ubiquitinated proteins are not properly degraded but accumulate in the cytosol, forming toxic aggregates (Ardley et al., 2005).

The downregulation of UPS components is mainly ascribable to the late onset of these diseases. Old neurons, in fact, are usually characterized by impaired UPS activity that prevents them from properly degrading ubiquitinated proteins (Goto et al., 2006).

However, UPS activity can also be inhibited by the aggregates themselves. The proteasome, in fact, is characterized by a narrow chamber of only 13 angstroms in diameter that is particularly vulnerable to protein aggregates. Not properly unfolded proteins, in fact, can block the opening of the 20S proteasome, further reducing its activity.

Notably, the UPS plays an important role in TDP-43 proteinopathies in which, interestingly, it represents the preferred route for the disposal of soluble TDP species (Scotter et al., 2014). However, since TDP-43 proteinopathies are characterize by an accumulation of highly ubiquitinated TDP species in cytoplasm of affected cells, it has been hypothesized that the impairment of the UPS could represent another important contribute, in addition to those described in the previous paragraph, to the pathogenesis of this proteinopathy and its associated diseases (in particular ALS and FTD) (Cascella et al., 2017).

AUTOPHAGY

Autophagy, that literally from the Greek means “self-eating”, is a catabolic process in which long-lived proteins, aggregates and organelles are delivered to the lysosomal compartment for degradation (Yin et al., 2016). The role of autophagy in proteostasis is particularly important for postmitotic neurons since they are terminally differentiated cells that cannot diluted cytotoxic proteins by cell division (Stavoe & Holzbaur, 2019).

Autophagy can be divided into three different branches depending on the mechanism by which cargo is directed to the lysosome. These branches are microautophagy, Chaperone mediated autophagy (CMA), and macroautophagy (Ciechanover & Kwon, 2017).

Microautophagy consists in the degradation of cytosolic material through its direct egulfment within the lysosome, which occurs thanks to the invagination of the lysosomal membrane itself (Parzych & Klionsky, 2014).

CMA is a selective type of autophagy involved in the lysosomal degradation of misfolded cytoplasmic proteins containing the KFERQ pentapeptide sequence or a KFERQ-like motifs (Fred Dice, 1990). In this type of autophagy, KFERQ-containing substrates are recognized

by the molecular chaperone HSP70 that subsequently routes them to the lysosome where they are degraded by lysosomal hydrolases. The substrate entrance within the lumen of the lysosome is mediated by the lysosomal-associated membrane protein 2A (LAMP2A) which, by binding the HSC70 chaperone, oligomerizes and forms a channel that allows the substrate to translocate (Ciechanover & Kwon, 2017).

Finally, macroautophagy (here referred to as "autophagy") is a type of autophagy in which the material to be degraded is initially engulfed in a double-membraned structure called phagophore, that rounds up and eventually fuses forming a structure called autophagosome that, in turn, fuses with the lysosome allowing lysosomal hydrolases to degrade its content (Parzych & Klionsky, 2014) (Fig. 28).

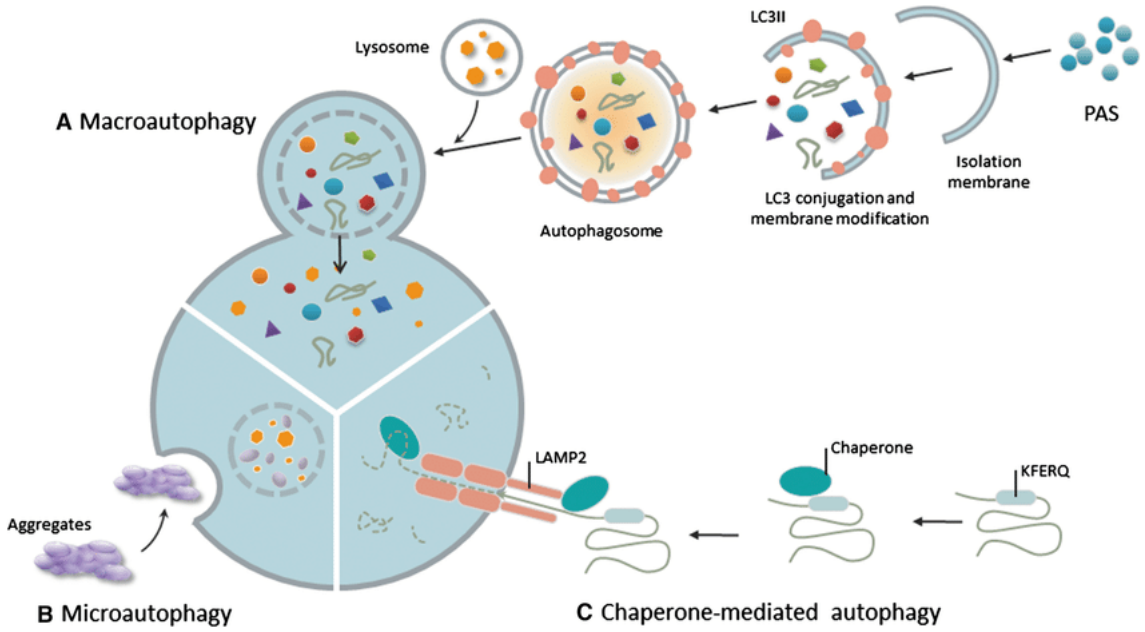

Figure 28. Different types of autophagy (W. Xu et al., 2021)

For years autophagy was considered a non-selective degradative pathway activated by cells to recycle nutrients during conditions of starvation and stress. However, recently, it has been observed the existence of different forms of selective autophagy that mediate the degradation of specific intracellular structures. Among these we can mention the mitophagy for mitochondria, the reticulophagy for the endoplasmic reticulum, the

nucleophagy for portions of the nucleus, the ribophagy for the ribosomes and the aggrephagy for protein aggregates (Shaid et al., 2013).

Interestingly, also misfolded proteins prone to aggregation can be directed to macroautophagy for lysosomal degradation. These substrates are usually conjugated to ubiquitin and are inserted into the autophagosomes following the linkage with specific proteins located in the autophagosomal membrane, such as the phosphatidylethanolamine (PE)-lipidated microtubule-associated proteins 1A/1B light chain 3B (MAP1LC3B or simply LC3). The linkage between the ubiquitinated substrates and the autophagosomes membrane is mediated by specialized autophagic receptor, like the sequestostome-1/p62 (SQSTM1/p62). In particular, p62 allows the formation of this linkage because it contains in its structure a ubiquitin-associated domain that can interact with the ubiquitinated targets and a LC3-interacting region (LIR) that, in turn, can recognize and bind the autophagosome membrane-inserted protein LC3 (Bjørkøy et al., 2005; Pankiv et al., 2007; Shvets et al., 2008) (Fig. 29).

In the context of ALS/FTD, it has been observed that exists a selective type of autophagy particularly important for the degradation of disease-associated TDP-43 species: the so-called Chaperone-Assisted Selective Autophagy (CASA) (Crippa, Cicardi, et al., 2016).

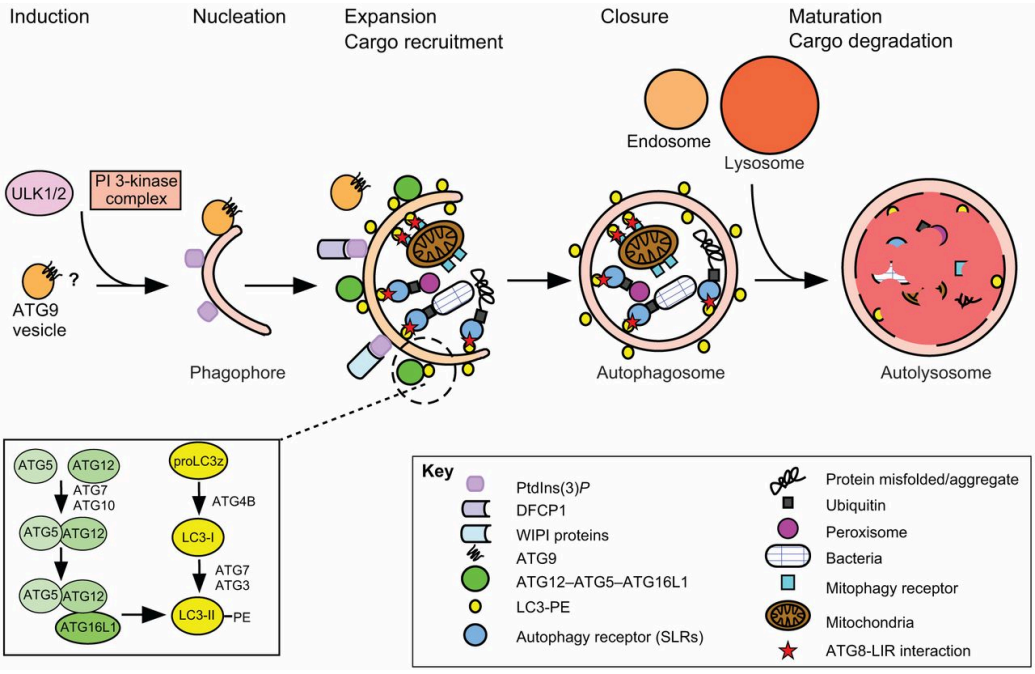

Figure 28. Selective autophagy of ubiquitinated misfolded proteins mediated by p62 (Birgisdottir et al., 2013)

CHAPERONE-ASSISTED SELECTIVE AUTOPHAGY

CASA is a type of autophagy in which substrates are directed to the autophagosome through the assistance of chaperone and co-chaperone proteins. Chaperone and co-chaperone proteins involved in this type of autophagy are HSP70, HSPB8, CHIP and BAG3. They assemble themselves together, through a series of passages, to form the so-called CASA-complex (Carra et al., 2008). Initially HSPB8 complexes with BAG3 and subsequently recruits HSP70 and CHIP (Crippa et al., 2010). HSP70 and HSPB8 recognize the substrate that need to be degraded. Then CHIP, that is associated to HSP70, ubiquitinates it and finally, BAG3 via its dynein interacting domain, drives the substrate-complex along microtubules to the microtubule organizing centre (MTOC), where it is usually localized p62 that binds them. Here, BAG3, by its NEF activity, allows the release of substrates by HSP70. Substrates, therefore aggregate in structures called aggresomes that are subsequently internalized in the forming autophagosomes, by means the interaction of p62 with the protein LC3 present on their membrane (Gamerdinger et al., 2011) (Fig. 29).

As said before CASA complex has a relevant role in the degradation of ALS/FTD-associated TDP species. Indeed, it has been observed the CASA-complex member HSPB8 is activated in response to the aberrant behavior of insoluble TDP species, in the attempt to counteract their neurotoxicity (Crippa et al., 2010). Moreover, it has been observed that HSPB8 is overexpressed also when the UPS is impaired suggesting that the two degradative pathway, UPS and autophagy, work together, to maintain the correct intracellular homeostasis of TDP species, through a finely orchestrated equilibrium, controlled by specific chaperones and co-chaperones (Crippa et al., 2010).

The role of HSPB8 in the degradation of TDP species has also been confirmed by studies conducted in both motor neurones and fly models expressing TDP-43 or its truncated forms. These studies showed that the overexpression of HSPB8 decreases the total accumulation and degree of aggregation of both TDP-25 and TDP-35 fragments, while its downregulation enhances them (Crippa, Cicardi, et al., 2016). It has also been shown that overexpression of BAG3 also reduces the accumulation of all three TDP species, suggesting an effective role of the CASA-complex in their degradation. However, they also showed that the overexpression of BAG3 is less effective on TDP-25 and the soluble species of TDP-43

and TDP-35, suggesting that a BAG3-independent activity of HSPB8 may exist (Cicardi et al., 2018).

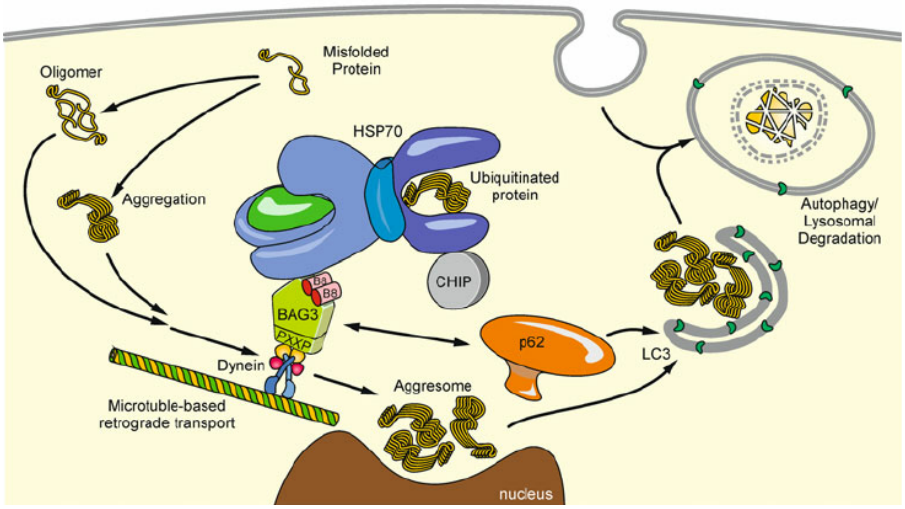

Figure 29. Schematic representation of the CASA-complex mechanism (Gamerdinger et al., 2011)

THE ROLE OF UPS AND AUTOPHAGY IN THE CLEARANCE OF TDP SPECIES

TDP-43 and its C-terminal fragments can be degraded by both the proteasome and the autophagy (Bose et al., 2011; Cicardi et al., 2018; Crippa et al., 2016; Huang et al., 2014; Urushitani et al., 2009). In particular, it has been observed that, in physiological conditions, they are preferentially degraded via the UPS (Scotter et al., 2014). Indeed, the impairment and/or the overloading of the proteasome (a common condition observed in ALS/FTD) is usually associated to an increase in the amount of TDP species present in the cytosol and also an increase in their aggregation (van Eersel et al., 2011). Autophagy (and particularly the CASA-complex), in turn, seems to have a relevant role in the degradation of the most insoluble and aggregated TDP species and particularly in pathological conditions (i.e., proteasome blockade and subsequent increase in aggregated TDP species), where it seems to be activated (Cascella et al., 2017; Crippa, Cicardi, et al., 2016; Scotter et al., 2014). It has been observed, in fact, that proteasome and autophagy work together, in a compensatory manner to avoid the aberrant intracellular aggregation of TDP species that could lead to the cell death (Cicardi et al., 2018; X. Wang et al., 2010). Moreover, the presence within the ALS/FTD-associated TDP aggregates of TDP-43 labelled by both K48- and K63-linked

polyubiquitin chains is an aspect that further confirms the existence of a compensatory mechanism between UPS and autophagy. Indeed, as said before, these two different types of polyubiquitin chains have the role to direct proteins respectively towards UPS degradation and autophagic fate. Therefore, the presence of both types of chain in TDP aggregates is consistent with a model in which K48–ubiquitin-labelled substrates that escape the UPS degradation are subsequently labelled with K63–ubiquitin for the autophagic degradation or *vice versa* (Scotter et al., 2014; Urushitani et al., 2009).

From the molecular point of view, this compensatory mechanism is explained by the ability of the chaperone protein HSP70 to bind both BAG1 and BAG3. In particular, HSP70 binding to BAG1 directs the substrate to the proteasome for degradation, while BAG3 binding directs it to the autophagy. Interestingly, the autophagy-proteasome switch seems to depend on the ratio between HSP70 co-chaperones BAG1/BAG3. Indeed, it has been observed that in pathological conditions, when UPS is overwhelmed, this ration is shifted in favour of BAG3 and thus autophagy activity is increased and *vice versa*, when autophagy is blocked, the expression of BAG1 increases and the substrates are directed to proteasomal degradation (Stürner & Behl, 2017) (Fig. 30).

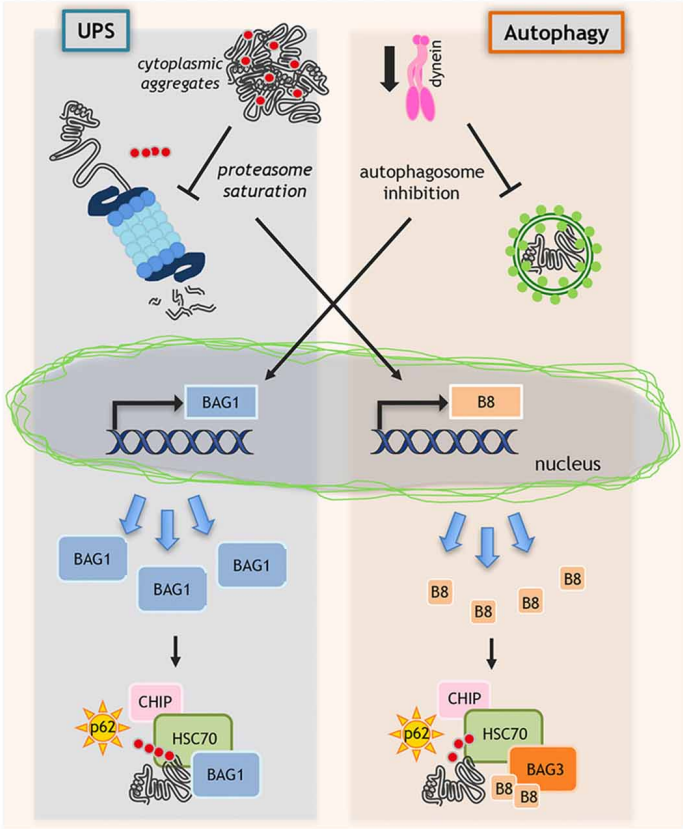

Figure 30. Compensatory mechanism between UPS and autophagy (Rusmini et al., 2017)

The increased expression of the CASA-complex members HSPB8 when the UPS is impaired or overwhelmed, confirms this hypothesis. HSPB8, in fact, to carry out its activity needs to interact with the co-chaperone protein BAG3. HSPB8 and BAG3, in particular, assemble themselves together (in a 2:1 ratio), forming a stable and stoichiometric complex. The increase of HSPB8, therefore, is always associated to an increase in BAG3 which, in turn, shifts the BAG1/BAG3 balance towards BAG3 increasing autophagic activity as a compensatory mechanism for proteasome inhibition (Crippa, Cicardi, et al., 2016; Crippa, D'Agostino, et al., 2016). This compensatory mechanism has been observed both in neuron and in muscle cells (Cicardi et al., 2018). In ALS, in fact, also non-neuronal cells (e.g., surrounding astrocytes or Schwann cells, chemotactically attracted microglial cells, and target muscle cells) are involved in disease onset and progression.

In particular, ALS can also occur following distal axonal degeneration, through a hypothetical mechanism defined "dying back" mechanism in which pathological changes, like for example proteins aggregation, appear in the axon distally, at the neuromuscular junctions or even in the skeletal muscle, and are transmitted into the soma prior to the

onset of clinical symptoms and MN death (Coleman, 2022; Pikatza-Menoio et al., 2021). According to this mechanism, an altered proteostasis at the level of muscle cells could therefore contribute to the pathogenesis of ALS. There are many evidences in favour of this mechanism. In particular, it has been observed that ALS mouse models are characterized by smaller and more atrophic muscles than control mouse (Fig. 31).

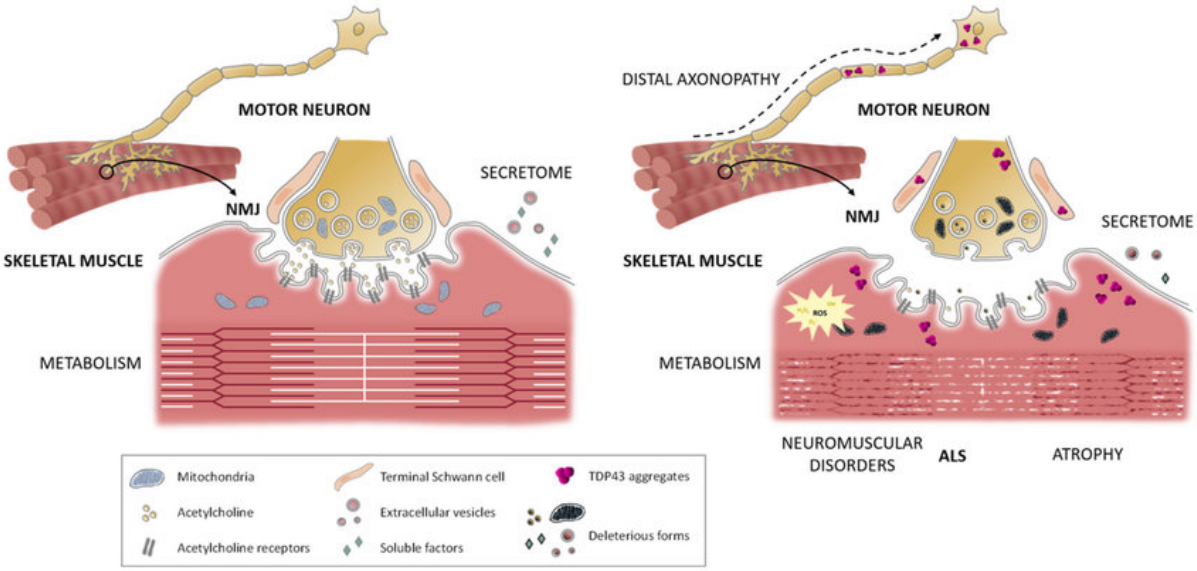

Figure 31. The "Dying Back" mechanism: from muscles to nerves (Pikatza-Menoio et al., 2021)

Interestingly, muscle cells seem to be characterized by a more efficient routing system between proteasome and autophagy than motoneurons (Cicardi et al., 2018; Crippa et al., 2013). Indeed, in muscle cells accumulated only TDP-25 fragment, that is the most aggregating TDP-43 fragment, while both TDP-43 and TDP-35 are cleared, mainly by the UPS. Interestingly, the routing of TDP-25 fragment to proteasome, by overexpressing BAG1, or to autophagy, by overexpressing HSPB8 or BAG3 decreased its accumulation in both cell types (Cicardi et al., 2018). Therefore, CASA-complex has a beneficial role not only in motoneurons but also in muscle cells.

Until now we have described the main degradative systems that cells can use to counteract the abnormal aggregation of TDP species. However, it has been observed that the aggregated forms of TDP can also be secreted from cells through different mechanisms.

SECRETION OF TDP SPECIES AND miRNAs AND SPREADING OF THE DISEASE

Several studies have shown that TDP species are also secreted into the extracellular space through mainly three different mechanisms: the unconventional secretion of free proteins, the transmission to adjacent cells through tunnelling nanotubes (thin tubes of about 50-200 nm in diameter that directly connect the cytoplasm of two distinct cells) and the secretion within EVs (Cicardi et al., 2021) (Fig. 32).

The secretion of TDP species, together with their intracellular disposal exerted by the PQC system, may contribute to TDP-43 intracellular proteostatis (Cicardi et al., 2021). However, TDP-43 secretion may also have a role in the spreading of TDP-43 pathology. Secreted TDP species, in fact, can be taken up by recipient cells and within them they can act as seeds for the formation of new toxic insoluble aggregates of TDP-43 (Ding et al., 2021; Feiler et al., 2015; R. Zhang et al., 2021).

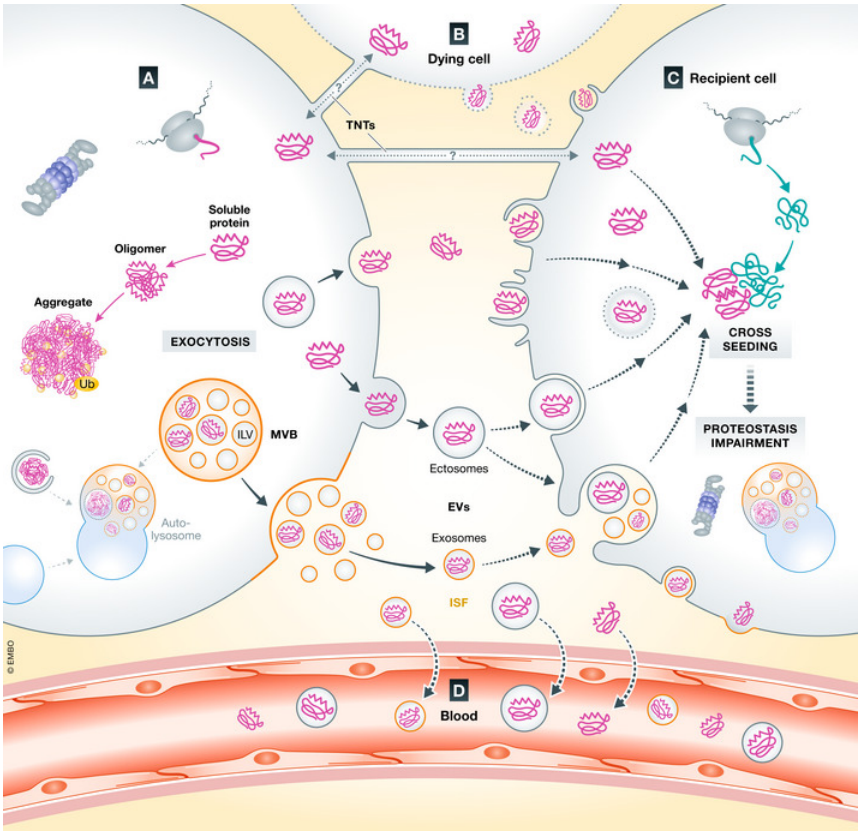

Figure 32. Different mechanism of protein secretion: unconventional secretion of free proteins, tunnelling nanotubes and EVs (Cicardi et al., 2021)

The ability of secreted TDP species to induce the formation of TDP-43 aggregates within the recipient cells depends mainly on the TDP-43 structure itself. TDP-43, in fact, as mentioned before, contains a prion-like domain in its C-terminal fraction that makes it prone to aggregate and able to sequester other soluble proteins, inducing their aggregation. Since this mechanism resembles the replication of infectious prions it is often termed “prion-like” (Maniecka & Polymenidou, 2015).

This mechanism was confirmed by several in vitro and in vivo studies in which it has been observed that i) the incubation of recipient cells with the conditioned medium obtained from cells transfected with a plasmid encoding for TDP-43, ii) the transfection of cells with TDP-43 insoluble species obtained from brain lysates or cerebrospinal fluid of ALS and FTD patients and iii) the injection of brain-derived FTD-TDP extracts into the neocortex, hippocampus, and thalamus of transgenic mice expressing human TDP-43, that are able to induce the mislocalization, aggregation, hyperphosphorylation of TDP-43 in the recipient cells (Jo et al., 2020).

However, in ALS and FTD, affected cells can also contribute to the spreading of the disease through the secretion of miRNAs (Q. Y. Chen et al., 2021). Secreted miRNAs, in fact, as like as proteins, are usually taken up by recipient cells within which can modulate specific intracellular pathway essential for cell survival. Aberrant RNA metabolism is a pathological feature of both ALS and FTD, therefore, it is not surprising that miRNAs secreted by affected cells are deregulated respect to those secreted by the cells of healthy controls (Sheinerman et al., 2017) and they may differently affect recipient cells, contributing to the disease.

Cells secrete miRNAs through the same mechanisms used for proteins secretion. However, since free miRNAs in the extracellular fluids are subject to the degradative action of several RNA enzyme and other environmental damage, studies have focused their attentions mainly on miRNAs secreted into EVs that, being encapsulated within a bilayer proteolipid membrane, are protected from the action of RNA enzyme (Zhao et al., 2017).

The analysis of miRNAs profile of EVs obtained from ALS patients revealed that it was different from that of EVs obtained from healthy controls (Sproviero et al., 2021). Moreover, it was shown that miRNAs secretion within EVs can be mediated by different RNA-binding proteins (such as hnRNPA2B1, the argonaute2 (Ago2) protein, the Y-Box

Binding Protein 1 (YBX-1), MEX3C, the Major vault protein (MVP) and the La protein) as well as by membranous proteins involved in EV biogenesis (such as the Caveolin-1 (Cav-1) protein and the Neural Sphingomyelinase 2 (nSMase2)) (Groot & Lee, 2020). The involvement of the RNA-binding proteins in miRNAs sorting within EVs is interesting especially in the context of the TDP-43 pathology in which, as said before, the TDP species are also present within EVs. This observation, in fact, suggests that the secretion of TDP-43 within EVs could also affect the secretion of specific miRNAs.

The mechanism of uptake of the extracellular TDP species and miRNAs by the recipient cells depends on whether they are secreted in a free manner of within EVs. Indeed, proteins and miRNAs secreted as free proteins/miRNAs are usually taken up by surrounding recipient cells, predominantly via micropinocytosis (Yerbury, 2016), while proteins secreted within EVs can be taken up by both neighbouring and more distant cells mainly following the formation of specific linkages between proteins that are enriched at the EVs surface and receptors located at the plasma membrane of the recipient cells. The main known mediators of these linkages are tetraspanins, integrins, lipids, lectins, heparan sulfate proteoglycans and extracellular matrix (ECM) components. After the formation of these interactions, cells uptake EVs through several mechanisms such as clathrin-mediated endocytosis, macropinocytosis, and phagocytosis that probably come in place simultaneously. Moreover, EVs can also fuse with the plasma membrane of the recipient cells and transfer their cargo directly into the cytoplasm (Cicardi et al., 2021; van Niel et al., 2018) (Fig. 33).

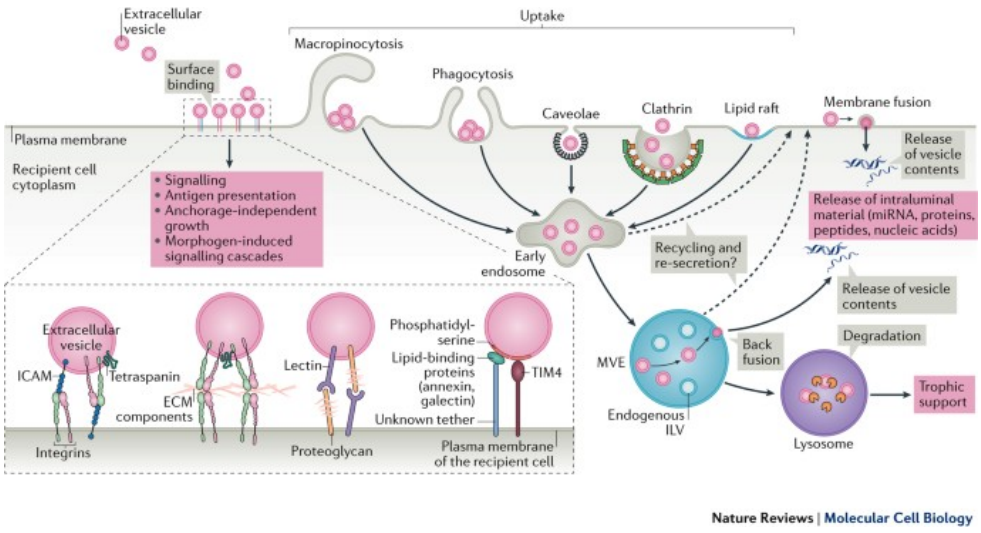

Figure 33. Mechanisms of EVs uptake (van Niel et al., 2018)

Finally, the propagation of ALS/FTD through the secretion of proteins and miRNAs from the affected cells and their uptake by healthy cells is also supported by the fact that neurodegenerative diseases, including ALS and FTD, typically start affecting a specific subset of neurons and then gradually progress to contiguous anatomical regions (in a spatiotemporal fashion), affecting a more extended area of the central nervous system and involving also different neural cell types (Cicardi et al., 2021) (Fig. 34).

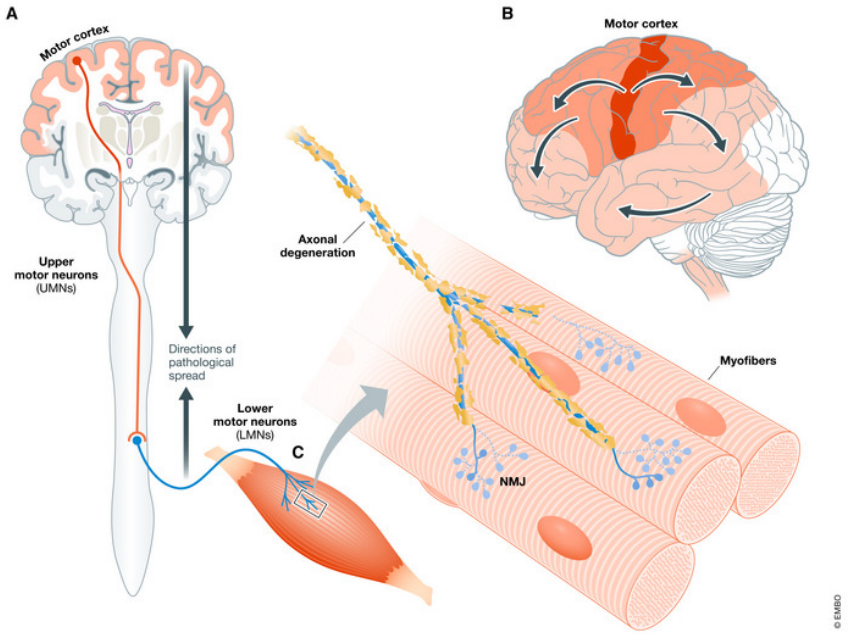

Figure 34. Illustration of the anatomical spreading of ALS/FTD (Cicardi et al., 2021)

EXTRACELLULAR VESICLES

EVs are a heterogeneous group of double-membrane enclosed particles secreted by all the eukaryotic cell types. EVs are characterized by a content, composed by lipid, proteins, mRNAs and ncRNAs (mostly miRNAs), that represents a "mirror" of the physiological as well as the pathological state of the donor cells. When they were first identified, EVs were thought to serve only as cell scavengers; however, it is now clear that they also play a fundamental role in the intercellular communication. Indeed, they can transfer their contents, through different mechanisms, to recipient cells in the neighborhood as well as in the periphery even passing through the blood-brain barrier (D'Anca et al., 2019).

EVs are present in different biological fluids such as serum, plasma, urine, cerebrospinal fluid (CSF) and others, and for this reason they are also considered as potential biological markers of disease (Boukouris & Mathivanan, 2015).

Cells produce many types of EVs, characterized by differ size, composition and biological functions, however, according to their mechanism of biogenesis, they are divided into two main group: the microvesicles and the exosomes (van Niel et al., 2018) (Fig. 35).

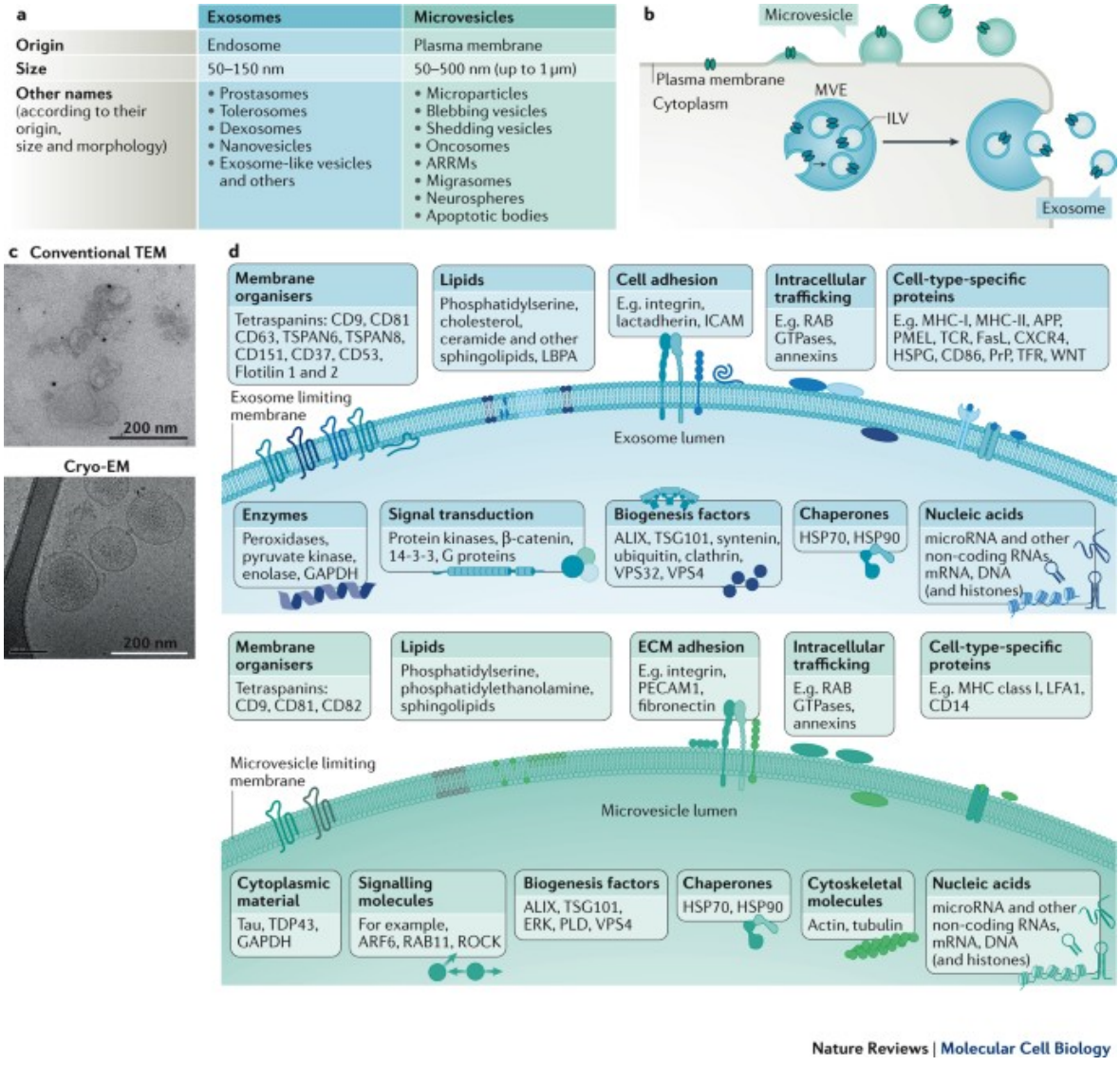

Figure 35. The two main types of vesicles: microvesicles and exosomes (van Niel et al., 2018)

MICROVESICLES

Microvesicles (MVs) originate by the outward budding and fission of the plasma membrane, and are characterized by a ranging size from 50 nm to 1–2 μm in diameter (Tricarico et al., 2017). Given their mechanism of biogenesis, these vesicles are usually

characterized by the presence on their surface of proteins that are commonly located on the plasma membrane of their original cells. For this reason, there are few proteins that have been found enriched in all MVs produced by different cell types. One of them is the Integrin β1 which is usually used as a marker to characterize them (Théry et al., 2018).

The biogenesis of MVs requires rearrangements of the plasma membrane, such as changes in lipid and protein composition and in Ca2+ levels. During this process, following the action of different Ca2+-dependent enzymatic machineries, including aminophospholipid translocases (flippases and floppases), scramblases and calpains, the plasma membrane undergoes a change in its normal asymmetry of membrane phospholipids that causes its flexion, and the rearrangement of the underlying cytoskeleton that, in turn, cause the membrane budding and the formation of MVs (Fig. 36).

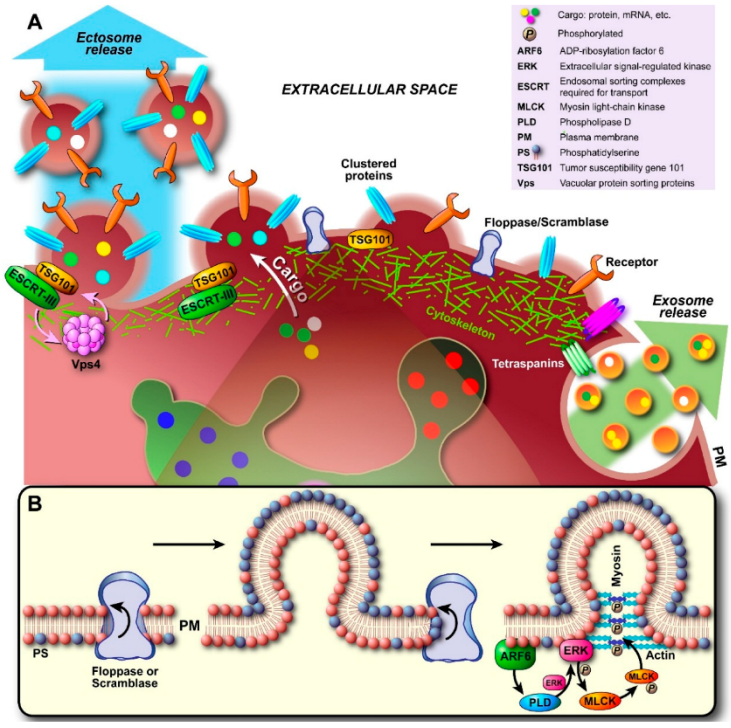

Figure 36. MVs biogenesis mechanisms (Kalra et al., 2016)

However, the biogenesis of MVs occurs also when the membrane lipid asymmetry is conserved, suggesting that other lipids, and the domains that they form, could contribute to this process. Cholesterol (that is one of the most abundant lipid components of the MVs

membrane) probably represents one of these lipids since it has been observed that its pharmacological depletion impairs the generation of MVs (van Niel et al., 2018).

Moreover, MVs biogenesis is also regulated by cytoskeletal elements and their regulators such as the RHO family of small GTPases and the RHO-associated protein kinase (ROCK), (important regulators of actin dynamics) that, as observed in different populations of tumour cells, are able to induce MVs biogenesis (B. Li et al., 2012).

The secretion of lipids and cytoplasmic proteins in MVs is mediated by their linkage to the inner leaflet of the plasma membrane. In particular, for lipids and other membrane-associated cargoes it occurs through their natural affinity for lipid rafts, while for the oligomeric cytoplasmic proteins it depends on their modifications with specific plasma membrane anchors such as palmitoylation, prenylation and myristoylation. Moreover, to be secreted they need to concentrate themselves in high-order complexes at the level of the membrane domains from which MVs will bud (Yang & Gould, 2013).

Interestingly, the sequestration of cytosolic proteins into MVs can also result from co-sorting with other proteins, such as the chaperones protein HSP70. Indeed, its presence has been observed in EVs derived from most cell types, suggesting a role of this chaperone in the selection and addressing of cargo to the vesicles (Kowal et al., 2016).

MVs also contain nucleic acids like mRNAs and miRNAs. However, it is still unclear how they are targeted to the cell surface for the secretion on MVs. One possible mechanism, revealed from studies of cancer cells, suggests that it could be mediated by conserved zipcode RNA sequence motifs in their 3‘ untranslated regions, but the details of this process remain to be discovered (van Niel et al., 2018).

EXOSOMES

Exosome (EXOs) are characterized by a size ranging from 30 to 100 nm. They correspond to the intraluminal vesicles (ILVs) contained in the multivesicular bodies (MVBs) (intermediates within the endosomal system) that are released in the extracellular space after the fusion of the MVBs with the plasma membrane. Therefore, EXOs originate as ILVs within the lumen of the endosomes during their maturation into MVBs. In particular, their formation is mediated by specific sorting machineries that first segregate cargoes on

microdomains of the MVBs membrane and then mediate the inward budding and fission of this membrane, forming EXOs that contain cytosolic components (van Niel et al., 2018).

One of these sorting machineries is the so-called endosomal sorting required for transport (ESCRT) machinery that is composed by four different sub-complex (ESCRT 0-I-II-III) that work together to promote the biogenesis of the ILVs. In particular, ESCRT-0 and ESCRT-I cluster ubiquitylated transmembrane cargoes on microdomains on the cytosolic side of the MVBs membrane; then the ESCRT-III sub-complex, via ESCRT-II, performs budding and fission of these microdomains. In this process also syntenin and the ESCRT accessory protein ALG-2 interacting protein X (ALIX) have a role. Both proteins are generally used as EXOs markers and act forming a bridge between cargoes and the vacuolar protein sorting-associated protein 32 (VPS32), a subunit of the ESCRT-III sub-complex (Hanson & Cashikar, 2012; Théry et al., 2018; van Niel et al., 2018; Wollert et al., 2009).

However, ILVs (featuring EXOs) biogenesis can also occur in an ESCRT-independent manner, through a mechanism that requires the formation of ceramide. Ceramide, produced following the hydrolysis of the sphingomyelin by the neutral type II sphingomyelinase, allows the generation of subdomains of the MVBs membrane that impose a spontaneous negative curvature of the membranes, favouring the formation of vesicles. Alternatively, ceramide could be metabolised to sphingosine 1-phosphate which, in turn, activates the G-protein-coupled sphingosine 1-phosphate (S1PR) receptor, essential for cargo sorting into EXOs (Trajkovic et al., 2008).

Moreover, it has been observed that the ESCRT-independent endosomal sorting is regulated by proteins of the tetraspanin family (for example CD63, CD9 and CD81, that are particularly enriched on the EXOs surface) that, by forming clusters and dynamic membrane platforms with different transmembrane and cytosolic proteins, probably act in the formation of the microdomains that will bud. Tetraspanins also regulate the cargo routing to MVBs (Fig. 37).

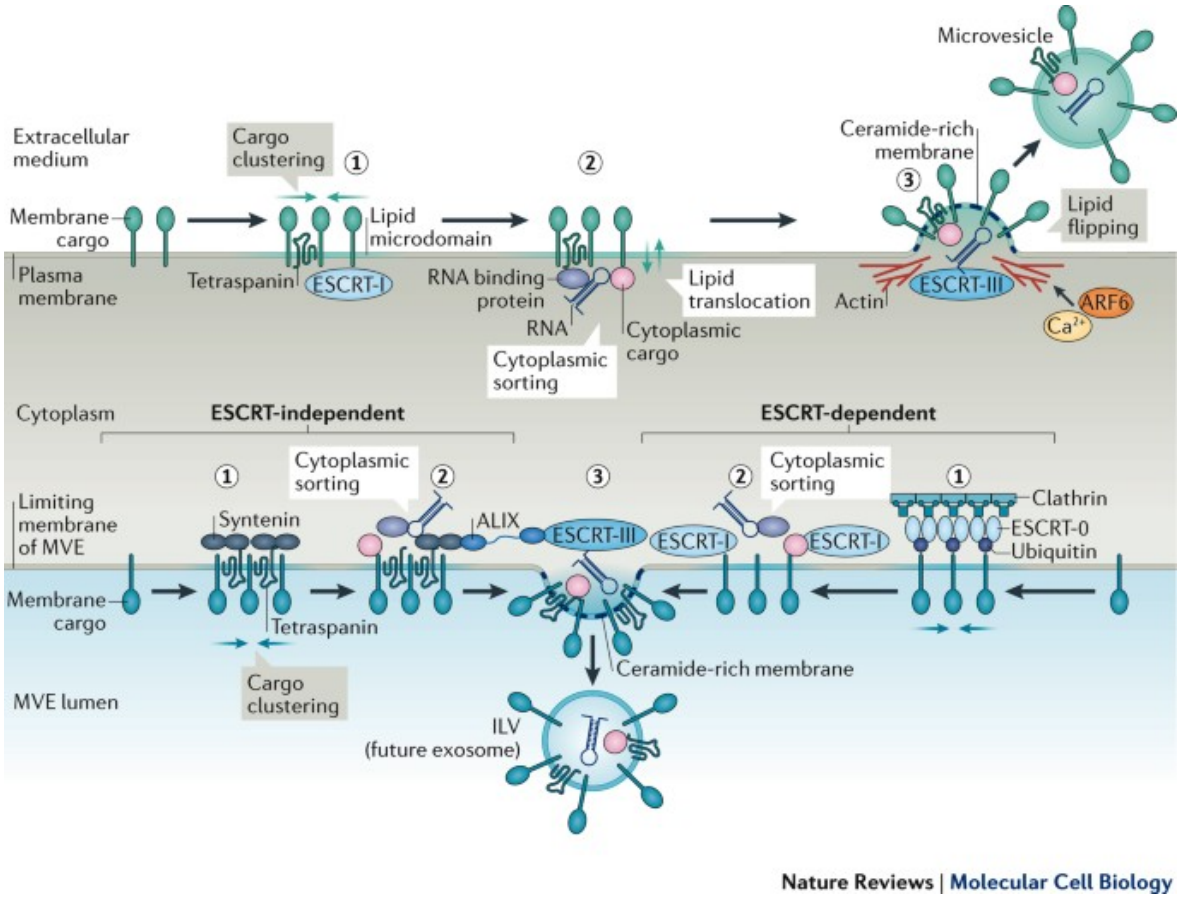

Figure 37. EXOs biogenesis through ESCRT-dependent and independent mechanisms (van Niel et al., 2018)

Cargo routing to MVBs could also be mediated by other mechanism: cytosolic proteins could be co-sorted to EXOs with the chaperone protein HSP70 (as observed also for the LEVs), while membrane cargoes, such as glycosylphosphatidylinositol (GPI)-anchored proteins, could be directed to SEVs because of their affinity for lipid domains and lipid rafts that are involved in vesicles generation (van Niel et al., 2018).

Moreover, recently, Leidal et al. identified a new mechanism of secretion, defined LC3 dependent EV loading and secretion (LDELS) that exploits the LC3-conjugation machinery for cargo selection and secretion of EVs. in particular, LC3-conjugation machinery allows the internalization of RBPs containing a LC3 interacting region (LIR) motif within the ILVs of the MVBs (Leidal et al., 2020) (Fig. 38).

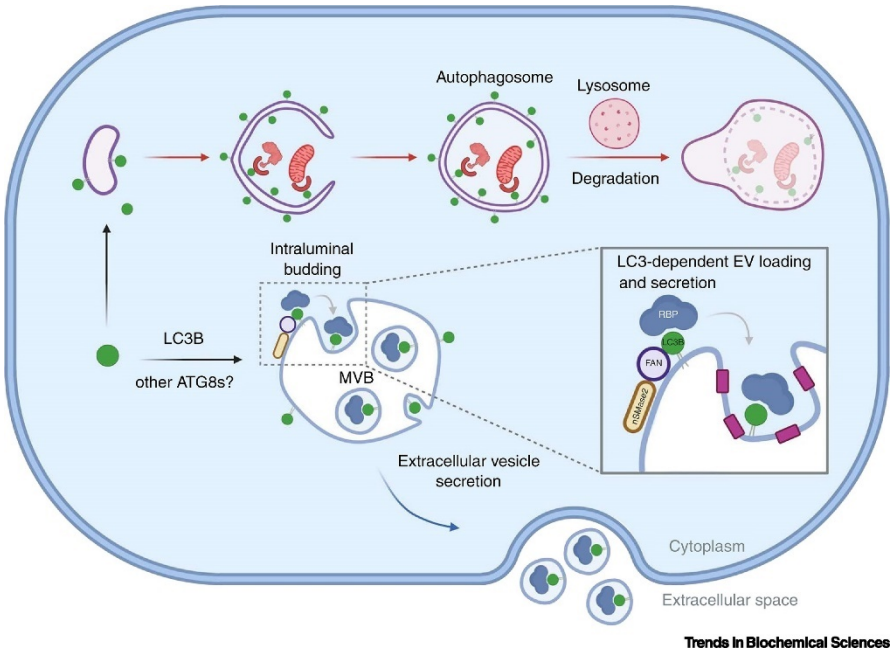

Figure 38. Schematic representation of the LDELS mechanism (Nieto-Torres et al., 2021)

As the MVs, EXOs carry also nucleic acids, including RNAs (mRNAs and miRNAs) and DNA that are differentially sorted to EXOs depending on their sequence. Indeed, usually, nucleic acids contained in EXOs are characterized by specific motifs that seem to regulate their incorporation into EXOs. The mechanisms involved in targeting nucleic acids to EXOs are still unclear. It has been proposed that it could be mediated by i) the ESCRT-II subcomplex that could act as an RNA-binding complex, ii) the tetraspanin-enriched microdomains that could sequester RNA binding proteins in the membrane subdomain and/or iii) the miRNA-induced silencing complex (miRISC) and protein argonaute 2 (AGO2), which mediate RNA-silencing processes (van Niel et al., 2018).

As mentioned before, EXOs originate from the fusion of MVBs with the plasma membrane. However, MVBs are primarily destined to fuse with lysosomes for degradation. This dual fate of MVBs suggests the existence of a mechanism that prevents their degradation and allows them to fuse with the plasma membrane releasing EXOs into the extracellular space. This mechanism was confirmed by several studies that showed that the inhibition of lysosome activity through different drugs such as Bafilomycin A1 and ammonium chloride (NH_4Cl) increases the numbers of SEVs secreted and also their protein content (Alvarez-Erviti et al., 2011; Miao et al., 2015).

The regulation between degradative and secretory fate of the MVBs is largely unexplored, however it could have a relevant role in neurodegenerative proteinopathies since, as observed in some studies, its modulation could contribute to the secretion of proteinaceous aggregates (Eitan et al., 2016).

Although MVs and EXOs are characterized by two different mechanisms of biogenesis, the currently existing isolation methods, including the differential ultracentrifugation method (that I used in my thesis), allow their separation mainly based on their size. However, MVs and EXOs usually contain vesicular subgroups of overlapping size which, therefore, may be isolated together. For this reason, MISEV guidelines have recently suggested to distinguish EVs on the basis of their size into large extracellular vesicles (LEVs) and small extracellular vesicles (SEVs), rather than on the basis of their biogenesis (Théry et al., 2018). Therefore, here after, I will talk about LEVs, for the EVs isolated by centrifuging the biological samples at 20,000 g and SEVs for those obtained by centrifuging them at 100,000 g.

MATERIALS AND METHODS

CHEMICALS

Z-Leu-Leu-Leu-al (MG132) (Sigma-Aldrich, St. Louis, MO, USA) was used for 16 hours to inhibit the proteasome, at the dose of 10 µM for the NSC34 cells and at the dose of 2,5 µM for the C2C12 cells;

Ammonium chloride (NH_4Cl) (Euroclone, Pero, Italy) was used to inhibit the autophagy, at the dose of 20 mM for 16hrs. This compound inhibits the autophagy neutralizing the lysosomal pH thus inhibiting the degradation of autophagosomes into lysosomes.

3-benzyl-2-((Z)-((E)-5-(6-chloro-3-methylbenzo[d]thiazol-2(3H)-ylidene)-3-ethyl-4 oxothiazolidin-2-ylidene)methyl)thiazol-3-ium chloride (JG-98) (MedChem express, Monmouth Junction, NJ, USA) is an allosteric inhibitor of HSP70, used to block the interaction between HSP70 and its co-chaperones BAG1 and BAG3. It was used at different doses (0,1, 1, 2, 3, 4, 5 µM) to the determine the optimal one that finally resulted to be the 2 µM dose.

siRNA

Following siRNA duplex were used for silencing the endogenous murine expression of HSPB8 (sense: 5'-CGGAAGAGCUGAUGGUAAAUU-3'; antisense: 5'-UUU ACCAUCAGCUCUUCCGUU-3') and BAG3. A custom non-targeting siRNA duplex was used as a negative control (sense: 5'-GGGUAAAGCUAGAGAGAAUUU-3'; antisense: 5'-AUUCUCU CUAGCUUUACCCUU-3'). All siRNAs were purchased from Dharmacon (Thermo Scientific Life Sciences Research, Waltham, MA, USA).

CELL CULTURES

NSC34 cells (routinely used in our lab) were used as motor neuronal model. These cells were grown in high glucose medium (Euroclone) supplemented with glutamine (Euroclone), penicillin (SERVA, Electrophoresis GmbH, Heidelberg, Germany), streptomycin (Sigma-Aldrich) and 5% fetal bovine serum (Sigma-Aldrich). Cells were maintained at 37°C in 5% CO2.

C2C12 cells were used as muscle model. Cells were maintained in high glucose medium completed with glutamine (Euroclone), penicillin (SERVA), streptomycin (Sigma-Aldrich)

and 10% of fetal bovine serum (GIBCO, Thermo Scientific Life Sciences Research, Waltham, MA, USA). Cells are growth at 37°C in 5% CO2.

To perform the different experiments cells were seeded at different cellular densities:

For the mRNA expression levels, protein expression levels and silencing experiments, cells were seeded at the concentration of 75,000 cells/ml in a 6-wells multiwell.

For the MTT and the LDH assay, cells were seeded at the concentration of 50 000 cells/ml in a 96-wells multiwell.

For the experiment of EVs isolation, cells were seeded in 10 Primo® TC dishes of 150 mm (Euroclone) at the concentration of 100,000 cells/ml (both for NSC34 and for C2C12 cells) using 15 ml of complete medium per dish.

For the LDH experiments to evaluate the citotoxicity caused by the treatment of the NSC34 cells with EVs obtained from untreated and DT-treated NSC34 cells, cells to be treated were seeded at the concentration of 70,000 cells/ml in a 48-wells multiwell, while cells used to isolate EVs were seeded at the concentration of 25,000 cells/ml in a 6-wells multiwell. LEVs and SEVs isolated from the culture medium contained in one well of the 6-wells multiwell were used, together, to treat one well of the 48-wells multiwell. EVs produced by treated and untreated NSC34 cells were isolated after changing the medium with 2 ml per well of exo-free medium, through the differential ultracentrifugation medium described below. LEVs and SEVs were resuspended together in 10 µl of 0,22 µm filter-filtered PBS (Sigma-Aldrich) and added directly into the well to treat cells.

SUBJECTS

FTD patients were recruited at the IRCCS Mondino Foundation of Pavia (Italy). The platelet-free plasma was obtained processing the blood sample of three FTD patients. Patients were screened for mutations (Sure Select QXT Target Enrichment, Agilent Technology, Santa Clara, CA, USA) and only sporadic patients negative to known mutations were chosen. Three age-matched healthy volunteers, free from any pharmacological treatment, were recruited at the Immunohematological and Transfusional Service IRCCS Foundation “San Matteo”, Pavia (Italy) and used as healthy controls (ctrl). Subjects participating in the study

signed, before being enrolled, an informed consent form approved by the Ethical Committee (Protocol n°20180049077).

EXO-FREE MEDIUM PREPARATION

The exo-free medium corresponds to culture medium deprived of serum derived EVs. It was obtained by subjecting the complete medium supplemented with 20% of serum, to ultracentrifugation at 40,000g for 16h at 4°C (in the ultracentrifuge LE-70 (Beckman Coulter, Brea, CA, USA) equipped with the 50.2 TI rotor (Beckman Coulter)) to eliminate the EVs.

The exo-free medium was used at 5% serum concentration. It was diluted using DMEM high glucose, added with 1 mM L-glutamine and penicillin-streptomycin.

DIFFERENTIAL ULTRACETRIFUGATION METHOD FOR THE ISOLATION OF LEVs AND SEVs FROM CELLS CULTURE MEDIUM

The isolation of the EVs from the culture medium of the cells (both the NSC34 and the C2C12) was performed on the culture medium collected 16 hours after changing the complete culture medium in which the cells were seeded with the exo-free medium (15 ml per dish for the 10 Primo® TC dishes and 2 ml per well for the 6-wells multiwell). Cells were changed upon the reachment of about 70% of confluence. Before the medium change, cells were washed with 0,22 µm filter-filtered PBS (5 ml per dish for the 10 Primo® TC dishes and 1 ml per well for the 6-wells multiwell) to eliminate residual of the complete medium in which they were initially seeded.

To perform the isolation, the collected media was centrifuged at 500 g for 10 min at 4°C to remove dead cells and cell debris. The containing EVs supernatant was collected and centrifuged at 2,000 g for 10 min at 4°C. The supernatant obtained from this centrifuge was collected and re-centrifuged at 20,000 g at 4°C for 2 hours (using the centrifuge Avanti J-25 (Beckman Coulter) and the rotor JA-20 (Beckman Coulter) for medium obtained from 10 Primo® TC dishes and using the ultracentrifuge Optima TL (Beckman Coulter) equipped with the rotor TLA 100.3 (Beckman Coulter) for medium obtained from 6-wells multiwell) to collect LEVs. Both for experiments conducted in 10 Primo® TC dishes and for those conducted in 6-wells multiwell, the obtained LEVs pellet was washed with 3 ml of filtered

PBS and centrifuged twice at 20,000 g at 4°C for 1 hour (with the ultracentrifuge Optima TL (Beckman Coulter) equipped with the rotor TLA 100.3 (Beckman Coulter)), to eliminate any traces of non-LEVs particles. While the supernatant that contained the SEVs was centrifuged at 100,000 g for 1 hour at 4°C (using the ultracentrifuge LE-70 (Beckman Coulter) with the rotor 50.2 TI (Beckman Coulter) for experiments conducted in 10 Primo® TC dishes and using the ultracentrifuge Optima TL (Beckman Coulter) equipped with the rotor TLA 100.3 (Beckman Coulter) for experiments conducted in 6-wells multiwell) to obtain a pellet of SEVs. The SEVs pellet, as for the LEVs, was subsequently resuspended in 3 ml of filtered PBS and was centrifuged twice at 100,000 g for 1 hour at 4°C (with the ultracentrifuge Optima TL and the rotor TLA 100.3), to eliminate any traces of non-SEVs particles.

LEVs and SEVs final pellets obtained from 10 Primo® TC dishes were resuspended in 20 µl of PBS added with a protease inhibitors cocktail (Sigma-Aldrich). 5 µl of the suspension obtained for both the LEVs and the SEVs were used to perform the NTA analysis. The remaining 15 µl were subjected to protein extraction through the RIPA buffer and subsequent analysis through the Western Blot (WB).

In parallel with the collecting of the culture medium for the isolation of the EVs, also the cells that produced the EVs contained in the medium were collected. In particular, they were harvested and centrifuged at 500 g for 5 min at 4°C and the pellet was collected for RNA and protein extraction analysis.

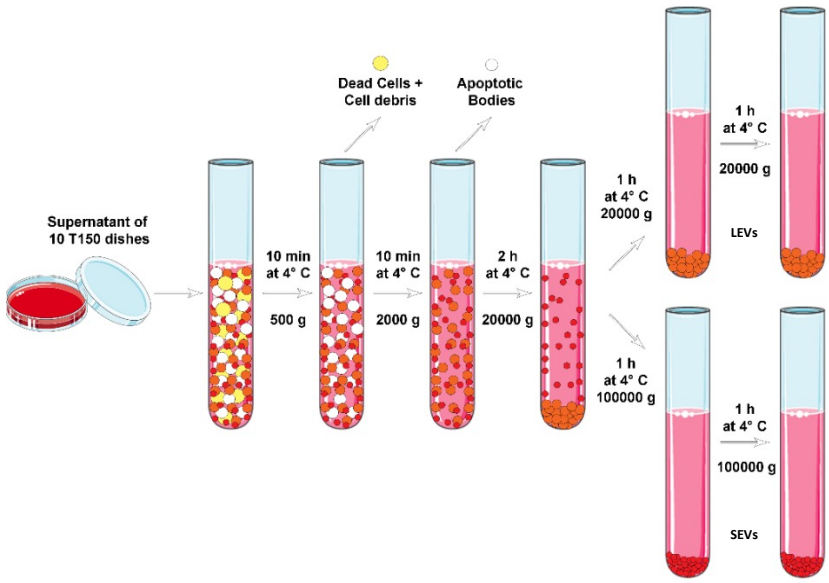

Figure 39. Schematic representation of the differential ultracentrifugation method used to isolate LEVs and SEVs from the culture medium of the cells.

DIFFERENTIAL ULTRACETRIFUGATION METHOD FOR THE ISOLATION OF EVs FROM HUMAN PLASMA

The isolation was performed starting from the platelet-free plasma (obtained processing, as described in (Sproviero et al., 2018), the venous blood collected in sodium citrate tubes). Plasma was centrifuged at 20,000 g for 1 hour to obtain the LEVs pellet, that was then washed with 0.22 µm filter-filtered PBS. The supernatant containing the SEVs was filtered through a 0.22 µm filter and centrifuge at 100,000 g for 1 hour at 4°C, using the MAX-TL Ultracentrifuge, to obtain the SEVs pellet, that was then washed with 1 mL of filtered PBS.

NANOPARTICLE TRACKING ANALYSIS

LEVs and SEVs analyzed were diluted to a concentration of approximately 107–109 particles/ml and analyzed for their size and concentration using a Nanosight NS300 (Malvern, UK), with a rate of about 30 frames/s. Particle movement videos (60 s/video) were recorded three times per test and size and mean concentration were analyzed by the NTA software (version 2.2, NanoSight). The results of NTA were presented as the mean of the three tests.

TRANSMISSION ELECTRON MICROSCOPY

The EVs pellets resulting from the last passage of the isolation with the ultracentrifugation method were resuspended in 20 µl PBS (pH 7.4) and fixed by adding an equal volume of 2% paraformaldehyde in 0.1 mol/L phosphate buffer (pH 7.4). EVs were then adsorbed for 20 min to formvar-carbon coated copper grids, by floating the grids on 5 µl drops on parafilm. Subsequently, grids were rinsed in PBS and negatively stained with 2% uranyl acetate for 5 min at RT. Stained grids were embedded in 2.5% methylcellulose for improved preservation and air dried before examination. Electron micrographs were obtained using the Hitachi TEM microscope (HT7800 series, Tokyo, Japan) equipped with Megaview G3 digital camera and Radius software (EMSIS, Muenster, Germany).

LDH ASSAY

The LDH assay allows to determine the cytotoxicity of the treatments by measuring the amount of Lactate dehydrogenase (LDH) that cells release in the culture supernatant. It was performed using the CyQUANTUM LDH Cytotoxicity Assay Kit (Thermo Fisher Scientific) according to the manufacturer's instructions. Cells lysed with the lysis buffer was used as positive control. The absorbance was measured at 490 nm using spectrophotometer Enspire (PerkinElmer, Waltham, MA, USA). Results were expressed as the mean ± SD of 3 independent replicates for the experiments conducted to evaluate the cytotoxicity induced by the EVs and 8 independent replicated for JG-98 experiments.

MTT ASSAY

The MTT assay allows to determine the treated cells viability by exploiting the reaction of reduction of the MTT (3-(4,5-dimethylthiazol-2-yl)-2,5-diphenyltetrazolium bromide) molecules in formazan, which occurs by means of the mitochondrial reductases present in living cells. MTT analysis was performed after 16h hours of treatment replacing the media of cells with 120 µL/well of culture medium without red phenol (Lonza, Swiss) containing 1.5mg/1ml of MTT powder (PanReac AppliChem, Darmstadt, Germany). Cells were incubated at 37° for 30 min with this MTT stock solution, then the stock solution was removed and 200 µl/well of 2-propanol was added to solubilize cells. Finally, the absorbance was measured at 570 nm using the spectrophotometer Enspire (PerkinElmer,

Waltham, MA, USA). To normalize the data was used a well without seeded cells, containing only the MTT stock solution. Results were expressed as the mean ± SD of 8 independent replicates.

TRANSFECTION PROCEDURE

30 pmol of HSPB8, BAG3 and non-targeting siRNA was transfected in cells using the Lipofectamine® Transfection Reagent (Invitrogen, Thermo Scientific Life Sciences Research, Waltham, MA, USA), following the manufacturer protocol.

RNA EXTRACTION AND ESXPRESSION ANALYSIS IN CELLS

RNA extraction was performed on treated and untreated cells. The culture medium of the cells was discarded while the cells were harvested using 1 ml of cold PBS and centrifuged for 5 min at 500 g at 4 °C. Cells contained in the pellet was resuspended in 300 µl of TRI Reagent (Sigma-Aldrich) and the total RNA was isolated according to the manufacturer's instructions. RNA quantification was obtained by measuring the absorbance of each sample at 260 nm using a NanoDrop 2000 (#ND-2000, ThermoFisher Scientific).

For the RNA expression analysis, 1 µg of the total RNA of each sample was treated with DNAse I (Sigma-Aldrich), and reverse transcribed into cDNA using the High-Capacity cDNA Reverse Transcription Kit (Thermo Fisher Scientific) according to the manufacturer's protocol.

The real time PCR was carried out using the CFX96 Real Time System (Bio-Rad Laboratories), in a total volume of 10 µl containing the iTaq SYBR Green Supermix (Bio-Rad Laboratories) and 500 nM of specific primers. The PCR cycling conditions set was: 94 °C for 10 minutes, 35 cycles at 94 °C for 15 seconds and 60 °C for 1 minute. Data obtained as Ct values were used for relative quantification of the target genes calculating the ΔΔCt. To exclude potential bias, data were transformed using the equation $2^{-\Delta\Delta Ct}$ to give N-fold changes in gene expression; all statistics were performed with the $2^{-\Delta\Delta Ct}$ values. Each experiment was carried out using 4 independent samples. Bag3, HspB8, Sqstm1/p62 and Map1lc3b ΔCt values for each sample were normalized with those of RplP0.

All the primers used for the real time PCR (Table 1) were designed using the Eurofins Genomics software and synthesized by Eurofins Genomics.

GENE	PRIMER	SEQUENCE
Bag3	Forward	ATGGACCTGAGCGATCTCA
	Reverse	CACGGGGATGGGGATGTA
Hspb8	Forward	ATACGTGGAAGTTTCAGGCA
	Reverse	TCTCCAAAGGGTGAGTACGG
Sqstm1/p62	Forward	AGGGAACACAGCAAGCT
	Reverse	GCCAAAGTGTCCATGTTTCA
Map1lc3b	Forward	CGTCCTGGACAAGACCAAGT
	Reverse	CCATTCACCAGGAGGAAGAA

Table 1. List of primer used for the analysis of the mRNA expression

PREPARATION OF PROTEIN EXTRACTS

The RIPA buffer (0.15 M NaCl, 0.8% Sodium Deoxycholate, 100 µM Sodium orthovanadate, 50 mM NaF, 5mM Sodium iodoacetate, 0.05M Tris HCl (pH 7.7), 10 mM EDTA (pH 8), 0.08% SDS and Triton X-100 (Sigma-Aldrich), supplemented with protease inhibitors (complete tablets, Roche Diagnostics GmbH, Mannheim, Germany) was used to extract the proteins from the NSC34 and C2C12 cells and from the EVs (for cells seeded in the 150 mm dishes, 200 µl per dish were used, for those seeded in the 6-wells multiwell were used 50 µl per well and for the EVs samples were used 15 µl).

For the total RIPA protein extract, cells ad EVs were left in RIPA buffer, in ice, for 20 min, then were slightly sonicated.

For the separation of the RIPA-soluble and RIPA-insoluble fractions, instead, 15 g of the total RIPA extract of each sample were centrifuged at 16,000 g for 20 min at 4°C. the pellet obtained was considered the insoluble fraction while the soluble was the supernatant.

For the nuclear-cytoplasmic fractionation, cells seeded in the 6-wells multiwell were collected and centrifuged at 500 g for 5 min at 4°C. The pellets obtained were lysed in lysis buffer (Tris-HCl 50 mM, pH 7.5, Triton X-100 0.5%, NaCl 137.5 mM, glycerol 10%, ethylenediaminetetraacetic acid 5 mM containing protease inhibitor cocktail) leaving them at 4°C for 15 minutes. Then, the lysed samples was centrifuged at 13’000 rpm for 15 minutes at 4°C, to extract the cytoplasmic fraction (the supernatant). The pellet obtained,

corresponding to the nuclear fraction, was washed three times with the lysis buffer and then was resuspended in lysis buffer added with 0.5 % SDS (Sigma-Aldrich), sonicated (3 hits at 10% of intensity) and centrifugated at 13'000 rpm for 15 minutes at 4°C. The supernatant containing the nuclear proteins was finally transferred into a new tube.

Proteins extracted with both the RIPA buffer and the lysis buffer for nucleus/cytoplasmic fractionation were quantified with the bicinchoninic acid assay (BCA) (#PRTD1,0500, Cyanagen, Bologna, Italy) and 15 µg for each sample (added with 4X sample buffer (0.2 M Trizma base (#T1503-1KG, Sigma-Aldrich), 5% Glycerol 60%, 4% SDS 20%, 2% beta-Mercaptoethanol) and incubated at 95°C for 5 min) were analysed in WB, except for the RIPA-insoluble fractions that were not quantified but were (after being washed with filtered PBS and centrifuged at 16,000 g at 4°C for 20 min) directly resuspended in 10 µl of 4x sample buffer, incubated at 95°C for 5 min and analysed in WB.

WESTERN BLOT ANALYSIS

Western blot is a technique that allows to evaluate the total amount of SDS-soluble protein contained in each sample, using specific antibodies. All the WB experiments were carried out using 12% acrylamide gels. The protein samples contained in the gel, after the electrophoresis, were transferred with Trans-Blot Turbo (Bio-Rad Laboratories) for 30 min at 25 V at RT on a nitrocellulose membrane with 0.45µm pores.

Nitrocellulose membranes were incubated for 1 hour in a blocking solution (1X TBST (20 mM Trizma base, 140 mM NaCl (pH 7.6) and 0.01% Tween 20 (Sigma-Aldrich)) containing 5% Nonfat dried milk powder (PanReac AppliChem), and then incubated overnight with specific primary antibody (Table 1), diluted in the same blocking solution. After the incubation with the primary antibodies, the nitrocellulose membranes were washed 3 times with 1X TBST and then incubated for 1hr with peroxidase-conjugated secondary antibodies (Table 1). After the incubation with the secondary antibody, the blots were washed 3 times with 1X TBST and 1 time with distilled water and then, chemiluminescent signals were detected, using the Westar ultra ECL Western blotting substrate (#XLS075,0100, Cyanagen Reagents for Molecular Biology) and the Chemidoc XRS System (#1708265, Bio-Rad Laboratories). Quantification analysis was performed using Image Lab Soft-ware, version 6.0.1 (Bio-Rad Laboratories).

ANTIBODY	SPECIES	DILUTION	COMPANY
Alix	Rabbit	1:1000	Abcam (ab76608)
Annexin I	Rabbit	1:1000	Thermo Fisher (ANXA1-101AP)
Anti-Mouse-HRP conjugated	Goat	1:5000 (β1-Integrin) 1:10000 (GAPDH)	Jackson ImmunoResearch Laboratories (115-035-003)
Anti-Rabbit-HRP conjugated	Goat	1:5000 (TDP C-Term, Alix, HSPB8, BAG3, SQSTM1/p62, MAP1LC3B, Annexin I, Ubiquitin, K63-linkage specific polyubiquitin) 1:10000 (Histone H3)	Jackson ImmunoResearch Laboratories (111-035-003)
BAG1	Rabbit	1:500	Santa Cruz Biotechnology (sc-939)
BAG3	Rabbit	1:1000	Abcam (ab47124)
CHIP	Rabbit	1:1000	Calbiochem (PC711)
GAPDH	Mouse	1:3000	Immunological Science (MAB-10578)
Histone H3	Rabbit	1:10000	Abcam (ab1791)
HSPB8	Rabbit	1:1000	Thermo Fisher (PA5-76780)
K63-linkage specific polyubiquitin	Rabbit	1:1000	Cell signaling (D7A11)
MAP1LC3B	Rabbit	1:1000	Sigma (L8918)
SQSTM1/p62	Rabbit	1:1000	Abcam (ab91526)
TDP C-Terminal	Rabbit	1:2000	Proteintech (12892-1-AP)
Ubiquitin	Mouse	1:1000	Santa Cruz Biotechnology (sc-8017)
β1-Integrin	Mouse	1:1000	Santa Cruz Biotechnology (sc-374429)

Table 12. List of primary and secondary antibodies used in the WB analysis

FILTER TRAP ANALYSIS

Filter trap assay (FTA) is a technique used to quantify protein aggregates bigger than 0.22µm. The FTA experiments were performed using the Bio-Dot SF Microfiltration Apparatus (Bio-Rad Laboratories) and the proteins present in each sample were detected using specific antibodies. Samples were prepared starting from the total RIPA-protein extract and for each sample were used 1,5 µg of protein extract, diluted in 100 µl of RIPA buffer. The proteins present in each sample were filtered and trapped on a cellulose acetate membrane with pores of 0.22 µm, thanks to a vacuum system. After the filtration, the proteins were fixed on the membrane using methanol (20%). The membrane was incubated for 1 hour at room temperature in blocking solution (the same used for the WB

analysis) and then was incubated overnight with the antibody directed against the C-terminal domain of TDP-43 diluted 1:2000 in the blocking solution. The day after, the primary antibody was removed, and the membrane was washed thrice with 1X TBST for 5 min. Then, the membrane was incubated for 1 hour with the Anti-Rabbit-HRP Conjugated secondary antibody diluted 1:5000 in 1X TBST. After this hour the membrane was washed three times with 1X TBST and 1 time with distilled water and then the signal was revealed using the Westar ultra ECL Western blotting substrate and the Chemidoc XRS System. As for the WB, results were analysed using Image Lab Soft-ware, version 6.0.1.

VESICULAR miRNA EXTRACTION AND ANALYSIS

RNA was extracted from treated (with MG132 or NH_4Cl) and untreated NSC34-derived LEVs and SEVs using Qiagen miRNeasy Mini kit (Qiagen, Hilden, Germany) according to the manufacturer's instructions. miRNA libraries were generated using Small RNA-Seq Library Prep Kit (Lexogen) the manufacturer's instructions and sequenced on a NextSeq 500/550 (Illumina). Interaction prediction was carried out on TargetScan and TarBase databases.

STATISTICAL ANALYSIS

Data are presented as mean ± standard deviation (SD) of n = 3 biological samples. To perform the statistical analysis was used the PRISM (version 5) software (GraphPad Software, LaJolla, CA, USA).

For WB Student's t-test was used. For NTA Welch's t-test was per-formed. Was considered statistically significant the P value < 0.05.

CHAPTER 1: THE INTERPLAY BETWEEN EVs AND THE PQC SYSTEM FOR THE DISPOSAL OF TDP SPECIES

AIMS

ALS and FTD share several pathological hallmarks. Two of the shared mechanisms are: i) the progressive neurodegeneration that arises in specific neurons and spreads to more extended area, and ii) the abnormal formation of intracellular inclusions containing the insoluble forms of TDP-43 and its CTFs TDP-35 and TDP-25. These inclusions alter the cellular homeostasis causing cells death (Berning & Walker, 2019; Jo et al., 2020; McAlary et al., 2019; Scotter et al., 2014). These two aspects are directly related, since TDP-43 and its highly aggregation prone CTFs can be transmitted from one cell to another, where they can trigger the formation of new aggregates, therefore contributing to the spreading of the disease (Laferrière et al., 2019; Nonaka & Hasegawa, 2018; Sun & Chakrabartty, 2017). A relevant role in this context is played by the EVs, that can be uptaken by other cells transporting their cargo to them. In fact, despite, the insoluble TDP species are mainly degraded by the PQC system (composed by chaperone and co-chaperone proteins, the UPS and the autophagy), their presence has been observed also in EVs obtained from ALS and FTD patients and cell models (Iguchi et al., 2016; Sproviero et al., 2018).

Despite this negative role exerted by EVs on recipient cells, the EVs release of misfolded proteins can be also viewed as a protective mechanism for the secreting cell. In this context, EVs could assist (or be part of) the intracellular PQC system in proteostasis surveillance (Cicardi et al., 2018; Huang et al., 2014; Scotter et al., 2014; Théry et al., 2018). Indeed, several PQC system components, such as the HSP70, are typically found in EVs (Théry et al., 2018).

Due to this possible dual role of EVs on the releasing or the acceptor cells, understanding the crosstalk between EVs and PQC in misfolded proteins disposal is crucial for these NDs.

Since most studies focused only on SEVs, without considering LEVs in TDP-43 trafficking (Iguchi et al., 2016), in the first part of my study I investigated the TDP secretion from neurons/motoneurons evaluating both LEVs and SEVs derived from immortalized neuronal cells, and from plasma of FTD patients and healthy volunteers. I evaluated which TDP species are mainly secreted in LEVs and SEVs and their solubility status (soluble vs insoluble). Moreover, I mimicked the disease-associated PQC impairment (using two PQC inhibitors: MG132 for the proteasome and NH_4Cl for the autophagy) and I studied the effect

on TDP-43 secretion. I also analyzed the possible role of HSP70 and its partners on this process, with a focus on the CASA-complex proteins.

Then, since in ALS also muscle cells are affected and could have a role in the onset of the pathology and knowing that also in these cells the PQC system has a relevant role in the disposal of TDP species, using a myoblast cell line, I evaluated whether also muscle cells were able to secrete TDP species in LEVs and SEVs. Finally, also in this case I evaluated the effects of PQC impairment on TDP secretion.

RESULTS

NSC34 CELLS-SECRETED LEVs AND SEVs ARE ENRICHED IN INSOLUBLE TDP SPECIES

To study the physiological secretion of TDP-43 and its CTFs from motoneurons/neurons (cells primarily affected by ALS and FTD) I used EVs released by an immortalized neuronal cell line, the NSC34 cell line. NSC34 cells are characterized by a marked neuronal phenotype achieved by spontaneous differentiation and are routinely used in my laboratory as "*bona fide*" model to evaluate the activity of the PQC system and the formation and aggregation of the TDP-43 CTFs (Cicardi et al., 2018; Crippa, Cicardi, et al., 2016). Moreover, NSC34 cells have been already used as reliable model for EVs isolation and analysis (Grad et al., 2014; Pinto et al., 2017).

The NSC34 cells, LEVs and SEVs were isolated from the culture medium of the cells through the differential ultracentrifugation method.

Before analysing the TDP content, LEVs and SEVs were characterized accordingly to the minimal information for studies of extracellular vesicles 2018 (MISEV-2018) guidelines: in particular NTA and TEM were used for size characterization and WB analysis for the identification of specific LEVs and SEVs markers (Integrin β1 (Int. β1) for the LEVs, Alix and Histone H3 for the SEVs and HSP70 for both EVs (Théry et al., 2018).

NTA showed a different dimensional profile between LEVs and SEVs, with LEVs that were significantly larger than SEVs (Fig. 40 A-C). This difference was confirmed also by the analysis of EVs with TEM (Fig. 40 D and E). WB analysis (Fig. 40 F) showed that LEVs were enriched in Int. β1 while SEVs were enriched in Alix and Histone H3. Moreover, LEVs were negative for Histone H3 but were positive, as like as the SEVs, for the cytosolic marker HSP70 (Fig. 40 F). A faint immunoreactivity for Alix and Int. β1 was also detected in LEVs and SEVs, respectively; therefore, it is possible that intermediate size vesicles were present in both populations.

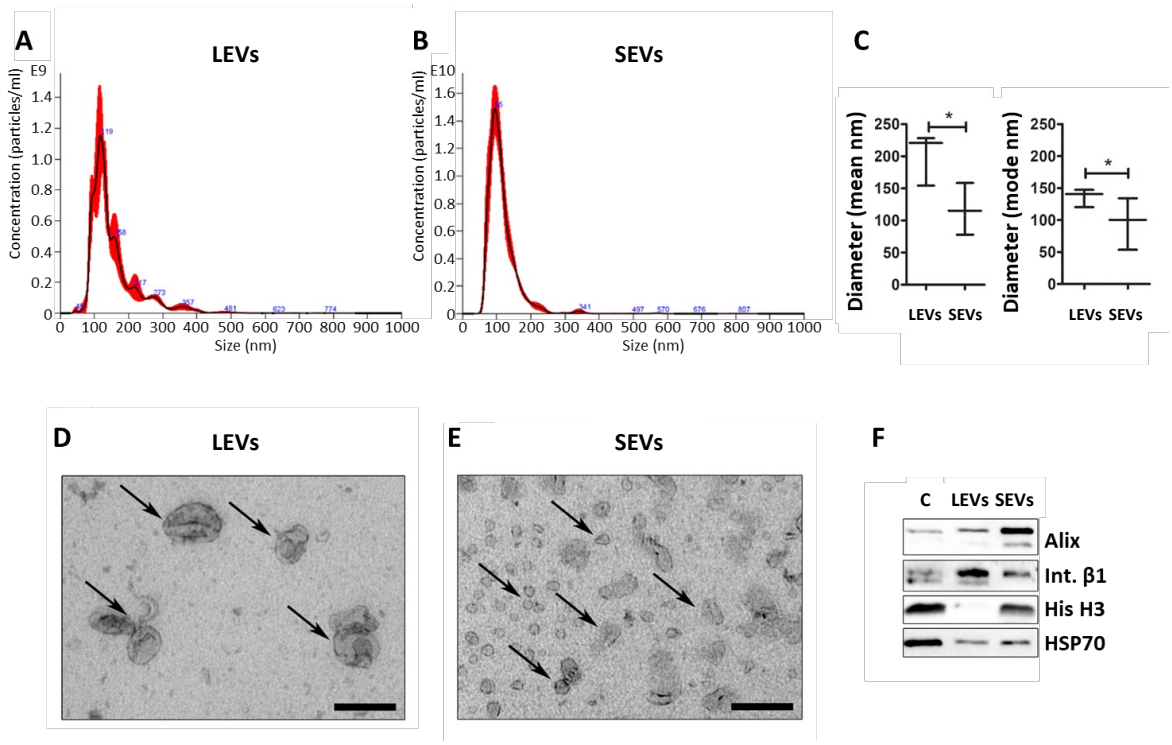

*Figure 40. Characterization of EVs obtained from NSC34 cells. Representative Nanoparticle-Tracking Analysis (NTA) distribution profile of LEVs (A) and SEVs (B). x-axis = vesicles size expressed in nm; y-axis = vesicles concentration, expressed as number of particles/ml. (C) graphs representing the mean (left bar graph) and the mode (right bar graph) diameter ± SD of LEVs (200.9 ± 40.7 nm; 136.1 ± 14.1 nm, respectively) and SEVs (117.2 ± 40.3 nm; 96.0 ± 40.5 nm, respectively) of n = 3 biological replicates analyzed by NTA (*p < 0.05, unpaired one-tailed t test). (D-E) Representative transmission electron microscopy (TEM) of LEVs (D) and SEVs (E) (scale bar: 200 nm). (F) WB analysis for characterization markers of LEVs (Int. β1) and SEVs (Alix and histone H3) (Casarotto et al., 2022)*

LEVs and SEVs were analyzed for their specific TDP-43, TDP-35 and TDP-25 content in relation to their levels in the original cell extract (Fig 41 A-D). Cells, LEVs and SEVs protein samples were extracted with the RIPA buffer and the total protein extract (i.e. soluble + insoluble protein fractions) were analyzed by WB (Fig. 41 A).

The relative abundance of the different TDP-43 species was analyzed in each sample (cells (C), LEVs and SEVs). Notably, TDP content could not be compared between different samples but only within a single sample, since the protein extract used in the WB analysis corresponded to approximately 0.1% of the entire cell protein extract, while LEVs and SEVs protein extract accounted respectively for 40% and 50% of their total extracted proteins. Data obtained showed that in cells TDP-43 immunoreactivity was mainly associated to the full length TDP-43, while the CTFs TDP-35 and TDP-25 were respectively poorly represented and almost undetectable. On the contrary, in LEVs and SEVs data showed a high immunoreactivity of TDP-35, but a faint immunoreactivity of TDP-43 and TDP-25. Relative abundance quantification of the TDP species within each sample confirmed this observation: in fact, in cells TDP-43 accounted for about 80% of the total TDP species in the sample, while TDP-35 and TDP-25 accounted for about 20% and less than 1%, respectively (Fig. 41 B). On the contrary, both in LEVs (Fig. 41 C) and SEVs (Fig. 41 D) TDP-35 was the most abundant species, representing 65% and 93% of total TDP species, respectively.

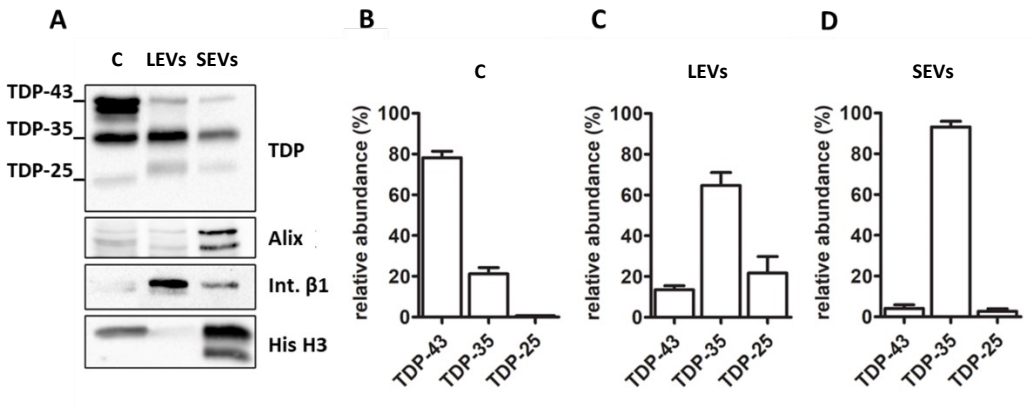

*Figure 41. WB analysis of TDP-43, TDP-35 and TDP-25 (A) and relative quantifications for each sample (cells (C), LEVs and SEVs) (B-D). In the bar graphs the relative abundance of TDP-43, TDP-35 and TDP-25 in cells (B), LEVs (C) and SEVs (D), is expressed as mean [(optical density of a single TDP species/optical densities of all the immunoreactive TDP species) *100] ± SD of n = 3 biological replicates (Casarotto et al., 2022)*

To assess whether the relative abundance of TDP species observed in cells, LEVs and SEVs was related to soluble or insoluble forms, the soluble and insoluble fractions of the RIPA-extracted protein samples were analysed by WB. WB analyses of RIPA soluble and insoluble fractions showed that in cells (Fig. 42 B) the TDP species were largely soluble, while the secreted forms were almost completely insoluble (Fig. 42 C and D).

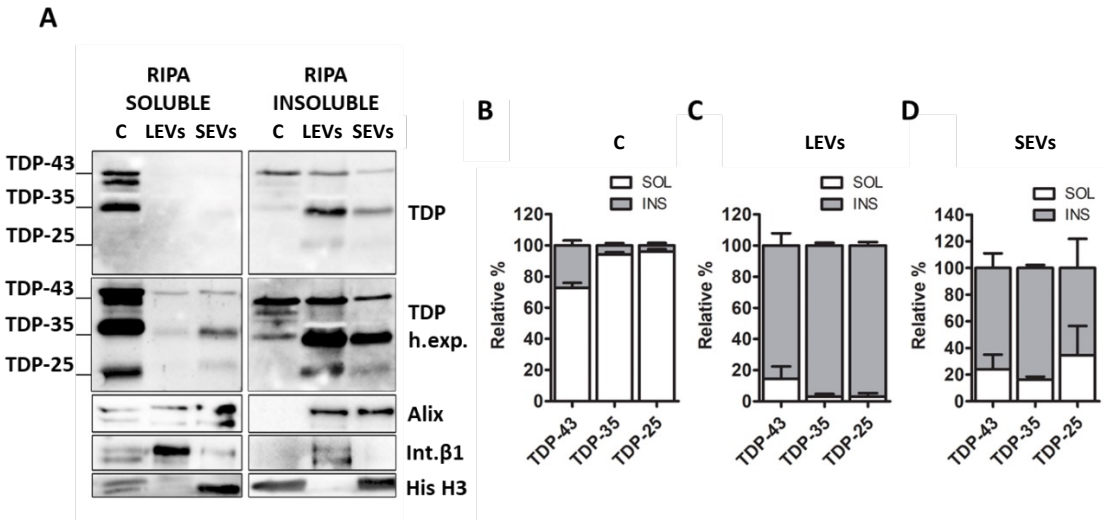

*Figure 42. WB analyses of RIPA-soluble and RIPA-insoluble fractions of cells(C), LEVs and SEVs and relative quantifications (A-D). The bar graphs represent the relative abundance of each TDP species in the soluble or insoluble fraction of cells (B), LEVs (C) and SEVs (D), expressed as [(optical density of soluble or insoluble/optical densities of soluble + insoluble TDP) *100] ± SD of n = 3 biological replicates. In cells: TDP-43, 72.8 ± 5.4 % soluble; TDP-35, 94.3 ± 2.4% soluble; TDP-25, 96.0 ± 2.7% soluble (B). In LEVs: TDP-43, 85.6 ± 13.8% insoluble; TDP-35, 96.9 ± 3.0% insoluble; TDP-25, 96.9 ± 3.8% insoluble (C). In SEVs: TDP-43, 76.0 ± 19.1% insoluble; TDP-35, 83.7 ± 3.8% insoluble; TDP-25, 65.4 ± 7.8% insoluble (D) (Casarotto et al., 2022)*

EVs CONTAIN PQC COMPONENTS INVOLVED IN THE INTRACELLULAR CLEARANCE OF INSOLUBLE TDP SPECIES

It is known that misfolded and insoluble TDP species are mainly degraded via UPS and autophagy by means of HSP70 assisted by its co-chaperone BAG1 or BAG3, respectively (Cicardi et al., 2018; Huang et al., 2014; Scotter et al., 2014). Since both LEVs and SEVs contained HSP70 and insoluble TDP species, it has been evaluated whether HSP70 co-chaperones and also other members of the PQC system (in particular chaperone and co-chaperone proteins of the CASA-complex) were present in EVs. To this purpose, the total RIPA-extracted proteins for each sample (cells, LEVs and SEVs) were analysed by WB (Fig. 43).

The results confirmed that all EVs contained HSP70 and showed that only cells contained the co-chaperone BAG1 (in particular, its 50 kDa isoform, that probably corresponds to the nuclear BAG1 isoform BAG-1L). On the contrary, all samples (cells, LEVs and SEVs) were immunoreactive for BAG3. Moreover, data showed that both LEVs and SEVs were positive for CHIP, HSPB8, SQSTM1/p62 and MAP1LC3 (both lipidated (LC3-II) and not-lipidated (LC3-I) forms) that, together with HSP70 and BAG3 are involved in the CASA-complex formation and in the degradation of insoluble TDP species via autophagy (Cicardi et al., 2018; Crippa, Cicardi, et al., 2016). Interestingly, all EVs were positive for the MAP1LC3B-I form but were mainly enriched in the MAP1LC3B-II form, differently from cells that contained high levels of the precursor MAP1LC3B-I protein and very low levels of the lipidated MAP1LC3B-II protein.

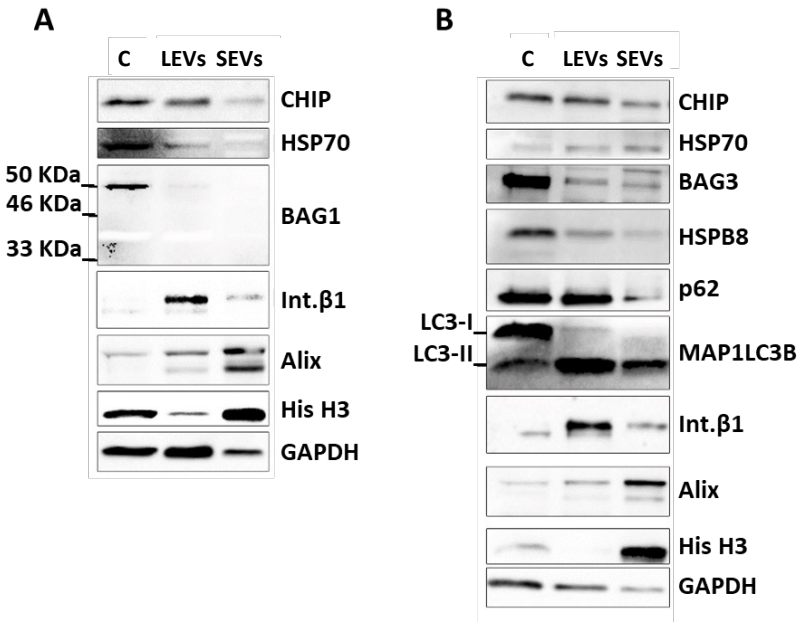

Figure 43. Representative WB analyses showing the presence of chaperone and HSP70 co-chaperone proteins members of the PQC system in cells (C), LEVs and SEVs. CHIP, HSP70, BAG1 (in particular, its 50, 46 and 33 kDa isoforms) (A), BAG3, HSPB8, SQSTM1/p62 and MAP1LC3 (both in its lapidated or not form) (B) were analysed. Int. β1 was used as LEVs marker, Alix and Histone H3 as SEVs marker and GAPDH as housekeeping protein for the cells.

THE PQC INHIBITION AFFECTS THE NUMBER AND THE CARGO OF LEVs AND SEVs

Given that EVs released by NSC34 cells contained chaperones and HSP70 co-chaperones, known to be involved in the degradation of TDP species via proteasome and autophagy (Cicardi et al., 2018; Crippa, Cicardi, et al., 2016; Huang et al., 2014), it was interesting to evaluate whether PQC and EVs could cooperate in the disposal of TDP insoluble species from cells. For this purpose, I selectively inhibited UPS, autophagy or both systems together, in NSC34 cells, and analyzed the effects on cells and EVs release and protein content. MG132 compound and NH_4Cl were used to selectively block UPS or autophagy, respectively.

First of all, UPS and autophagy inhibition in cells was assessed by RT Q-PCR ad WB analyses, by evaluating both mRNA and protein levels of BAG3, HSPB8, SQSTM1/p62 and MAP1LC3B, whose modulations under blocking conditions of the two degradative systems are well known (Crippa et al., 2010; Minoia et al., 2014). Real-time Q-PCR analysis showed that proteasome inhibition with MG132 caused a significant increase in the expression level of genes encoding for BAG3, HSPB8 and SQSTM1/p62 proteins (Fig. 44 A-C), but no changes were observed in the expression level of the gene encoding for MAP1LC3B (Fig. 44 D). Autophagy inhibition with NH_4Cl caused a significant increase in expression levels of *Sqstm1/p62* and *Map1lc3b* (Fig. 44 C and D) but not in *Bag3* and *Hspb8* mRNAs (Fig. 44 A and B). Finally, the blockage of both degradative systems caused a statistically significant increase in *Bag3, Hspb8* and *Sqsmt1/p62* expression level (Fig. 44 A-C) but not in *Map1lc3b* (Fig. 44 D).

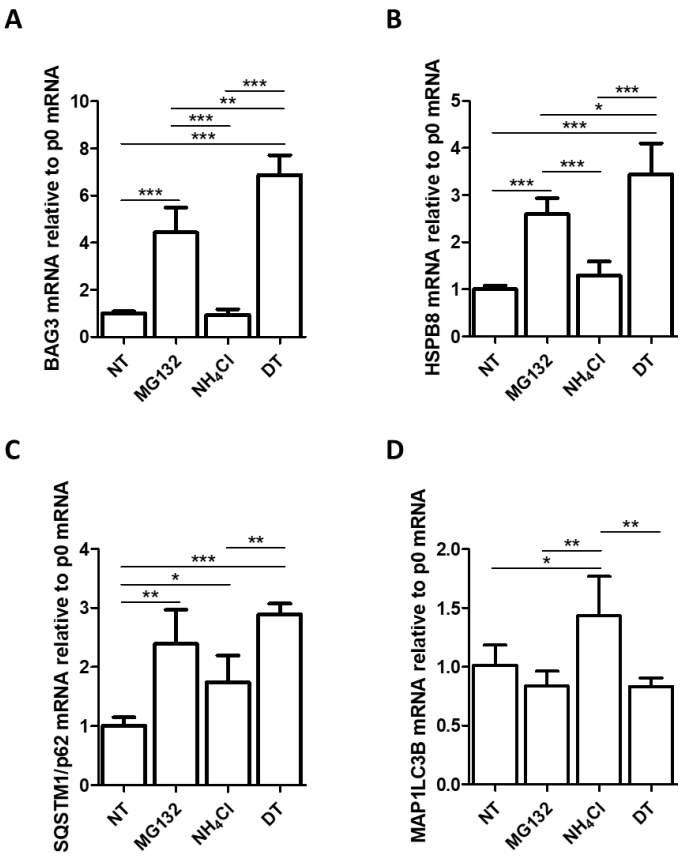

*Figure 44. mRNA expression levels of Bag3 (A), Hspb8 (B), Sqstm1/p62 (C) and Map1lc3b (D) in condition of proteasome (10 µM MG132) and autophagy (20 mM NH_4Cl) blockade together (double-treatment (DT)) or alone, compared to untreated (NT) cells. Bar graphs represent the relative fold induction of Bag3, HspB8, Sqstm1/p62 and Map1lc3B genes normalized with Rplp0 mRNA levels. Data are means ± SD of 4 independent samples (*p < 0.05, ** p < 0.01, *** p < 0,001), Oneway Anova, Bonferroni's Multiple Comparison Test) (Casarotto et al., 2022)*

mRNA expression changes were paralleled by changes in their corresponding protein. In fact, the WB analysis showed that proteasome blockage significantly increased HSPB8, SQSTM1/p62 and MAP1LC3B-II (Fig. 45 C,D,F) protein levels, while the block of the autophagy caused a statistically significant increase of SQSTM1/p62 and MAP1LC3B-II (Fig. 45 D and F). The simultaneous blockage of proteasome and autophagy resulted in a statistically significant increase of HSPB8, SQSTM1/p62 and MAP1LC3B-II (Fig. 45 C,D,F).

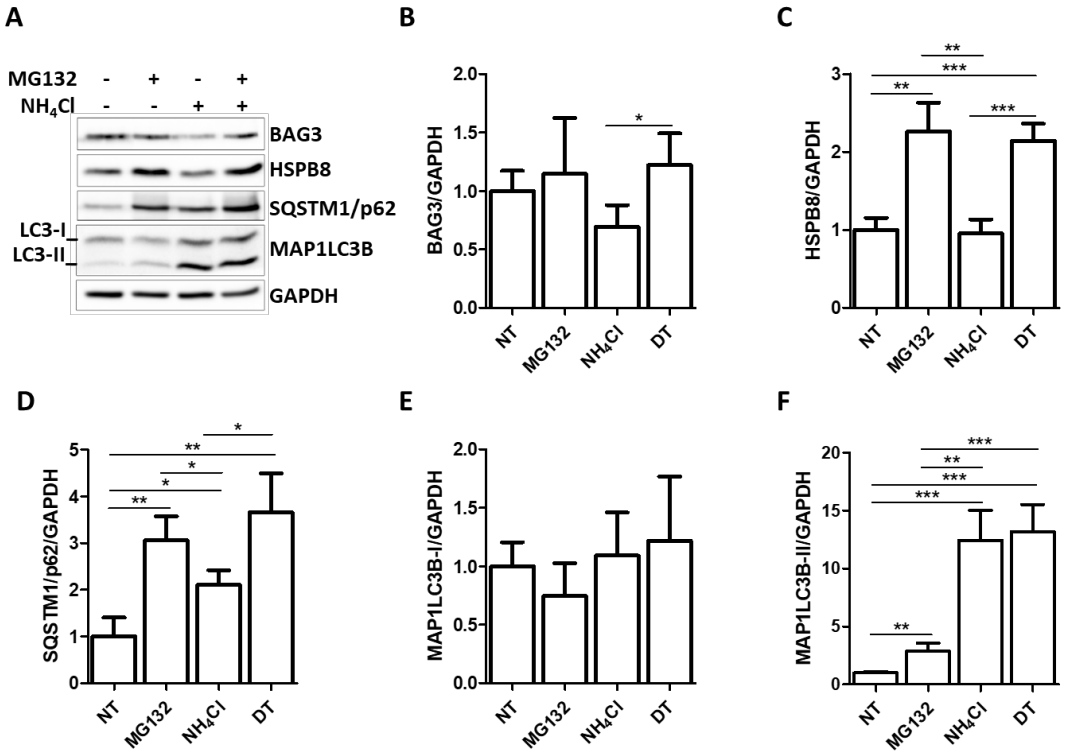

*Figure 45. Representative WB analysis of the total RIPA protein extracts of cells treated with 10 µM MG132, 20 mM NH_4Cl and both the compounds together. BAG3, HSPB8, SQSTM1/p62 and MAP1LC3B (I and II) have been analysed. Bar graphs represent the mean optical density ± SD of ta protein normalized on the optical density of GAPDH (used as housekeeping protein) and relative to untreated samples. n=3. (*p < 0.05, ** p < 0.01, *** p < 0.001, One-way Anova, Bonferroni's Multiple Comparison Test) (Casarotto et al., 2022)*

After confirming the effectiveness of the two treatments in cells, their possible effects on EVs release were assessed by NTA (for number and dimension) and WB (for protein crago) analyses.

NTA analysis showed that the UPS blockage with MG132 caused a significant increase of specific subpopulations of LEVs secreted by treated cells compared to control untreated cells (Fig. 46 A). In particular, it was statistically increased the number of the 170-190, 270-290, 350-370, 510-530 and 710-730 nm in diameter vesicles. On the contrary, data showed a decrease in the number of SEVs released by treated cells compared to the untreated cells, with 90, 190 and 250-270 nm in diameter vesicles that were significantly less (Fig. 46 B).

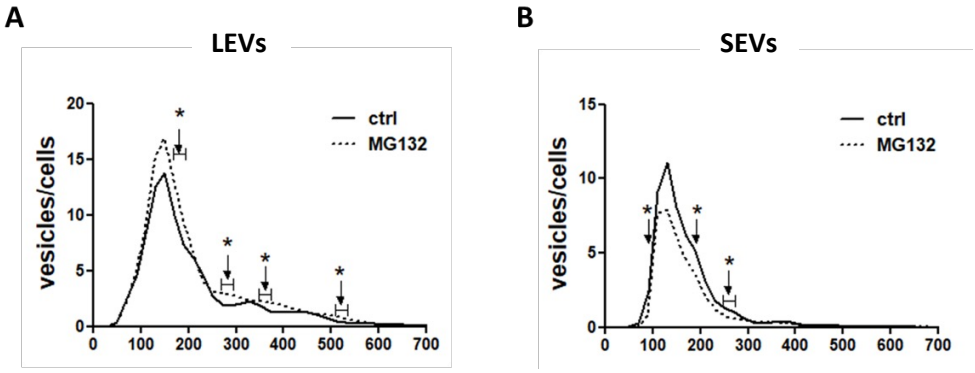

*Figure 46. Effect of UPS inhibition (10 µM MG132) on the release of LEVs (A) and SEVs (B). Graphs represent the mean of n = 3 biological replicates; x-axis = vesicles size, expressed in nm; y-axis = vesicles concentration, expressed as vesicles secreted per cell. (*p < 0.05, Welch's t-test) (Casarotto et al., 2022)*

The NTA analysis of the number of LEVs and SEVs released by cells treated with NH_4Cl compared to those released by untreated control cells showed that autophagy inhibition slightly affected LEVs release (Fig. 47 A) and caused an overall increase in the number of SEVs (Fig. 47 B). In particular, data showed a statistically significant increase of SEVs of about 110 nm in diameter in NH_4Cl sample (Fig. 47 B).

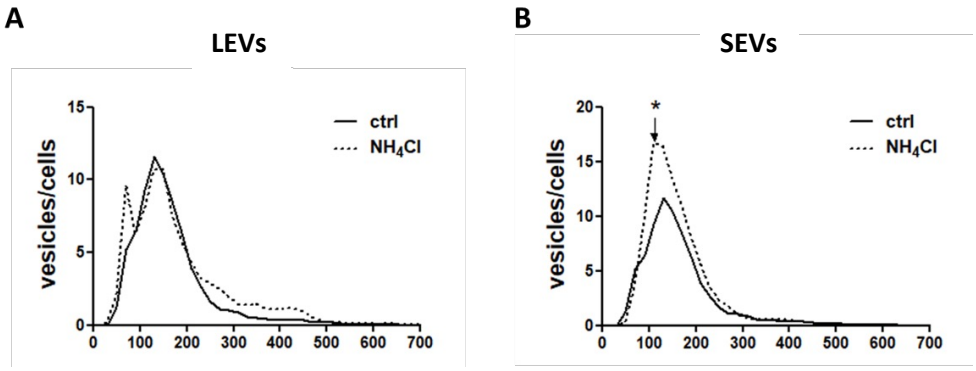

*Figure 47. Effect of autophagy inhibition (20 Mm NH_4Cl) on the number of LEVs (A) and SEVs (B) secreted. Graphs represent the mean of n = 3 biological replicates; x-axis = vesicles size, expressed in nm; y-axis = vesicles concentration, expressed as vesicles secreted per cell. (*p < 0.05, Welch's t-test) (Casarotto et al., 2022)*

Finally, the NTA analysis of the number of LEVs and SEVs released by the cells treated with both MG132 and NH_4Cl respect to those released by untreated cells showed an increased in both types of EVs (Fig. 48 A and B). However, this increase reached the statistical significance only for the LEVs, in particular, for those characterized by a diameter between 190-230 and 270-310 nm (Fig. 48 A).

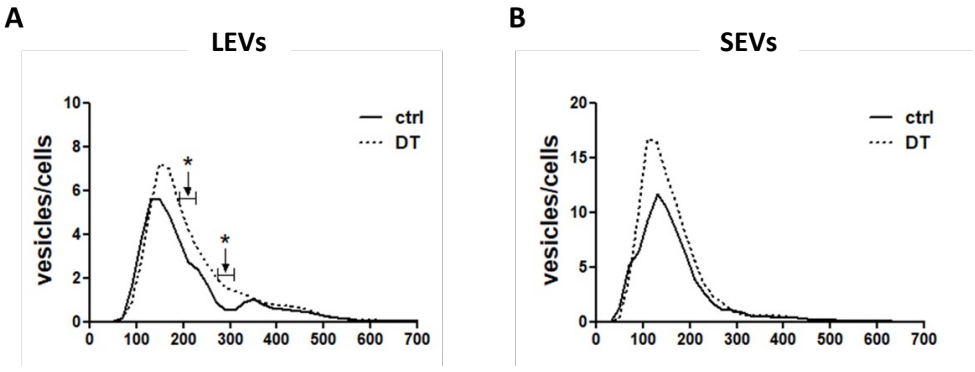

*Figure 48. Effect of autophagy and proteasome inhibition (DT = double treatment) (10 µM MG132 + 20 mM NH_4Cl) on the number of LEVs (A) and SEVs (B) secreted. Graphs represent the mean of n = 3 biological replicates; x-axis = vesicles size, expressed in nm; y-axis = vesicles concentration, expressed as vesicles secreted per cell. (*p < 0.05, Welch's t-test) (Casarotto et al., 2022)*

The effect of PQC blockage on EVs protein cargo was then characterized by WB analyses. First of all, the levels of TDP-43, TDP-35 and TDP-25 have been analysed in LEVs and SEVs released by treated cells and compared with those of untreated cells.

Data obtained from MG132-treated cells (Fig. 49) showed that, in cells, UPS blockage caused a significant increase of the full length TDP-43, but a significant decrease of TDP-35. TDP-25 fragment was not affected (Fig. 49 B). Considering LEVs secreted upon UPS inhibition, there was an enrichment in all TDP species, with a threefold increase of full length TDP-43 and a twofold increase of TDP-35, although not significant (Fig. 49 C). No difference was observed between the SEVs obtained from MG132-treated cells and those obtained from untreated cells (Fig. 49 D).

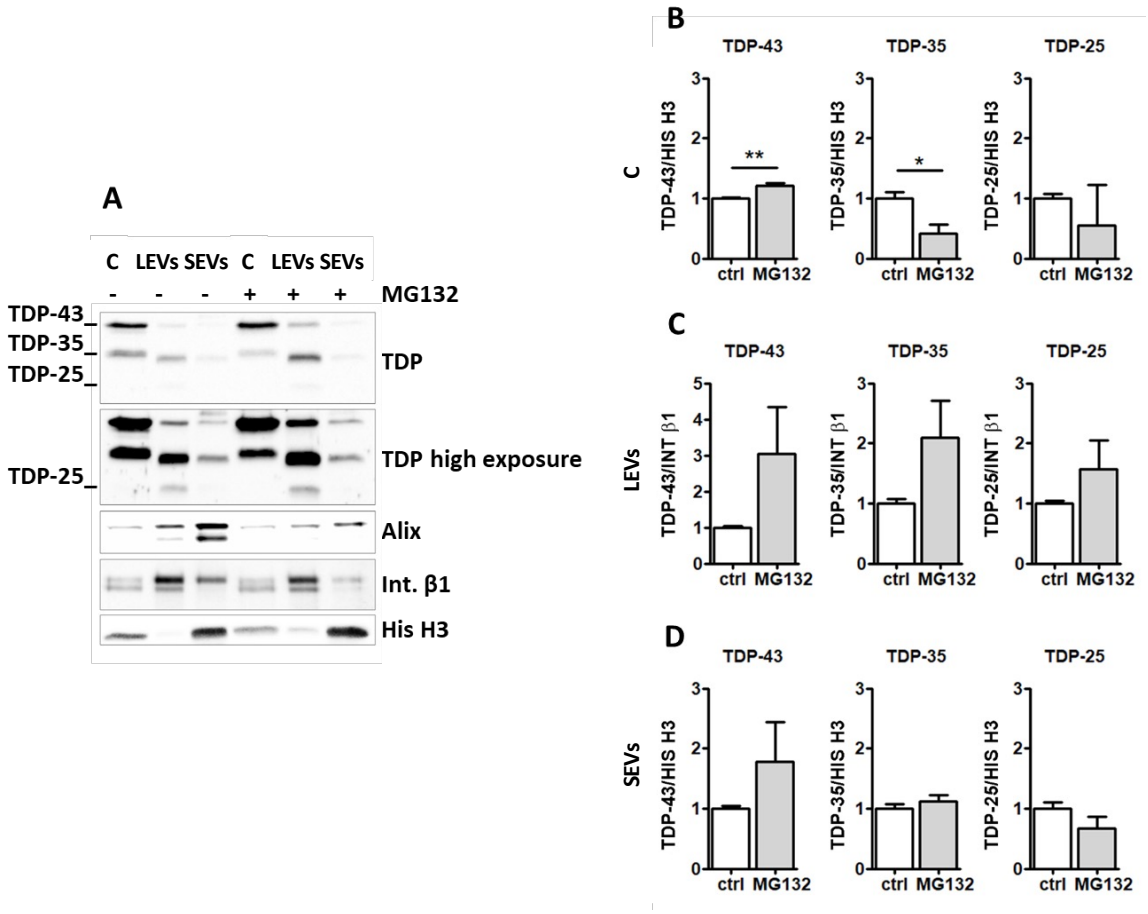

*Figure 49. The effect of UPS inhibition on the TDPs content of both cells (B), LEVs (C) and SEVs (D). WB analysis (A) and relative quantifications (B-D) of total RIPA protein extract of cells, LEVs and SEVs, untreated or treated o/n with 10 μM MG132. Bar graphs represent the mean optical density ± SD of protein in analysis normalized on the optical density of the internal housekeeping protein (HIS H3 for cells and SEVs; Int. β1 for LEVs) and expressed as relative to the corresponding untreated sample (ctrl) of 3 biological replicates (*p < 0.05, ** p < 0.01, unpaired one-tailed t test) (Casarotto et al., 2022)*

Autophagy blockade did not alter TDPs content neither in cells nor in EVs, (Fig. 50). Indeed, no differences were observed between control and NH_4Cl-treated samples in the overall protein levels of TDP-43, TDP-35 and TDP-25.

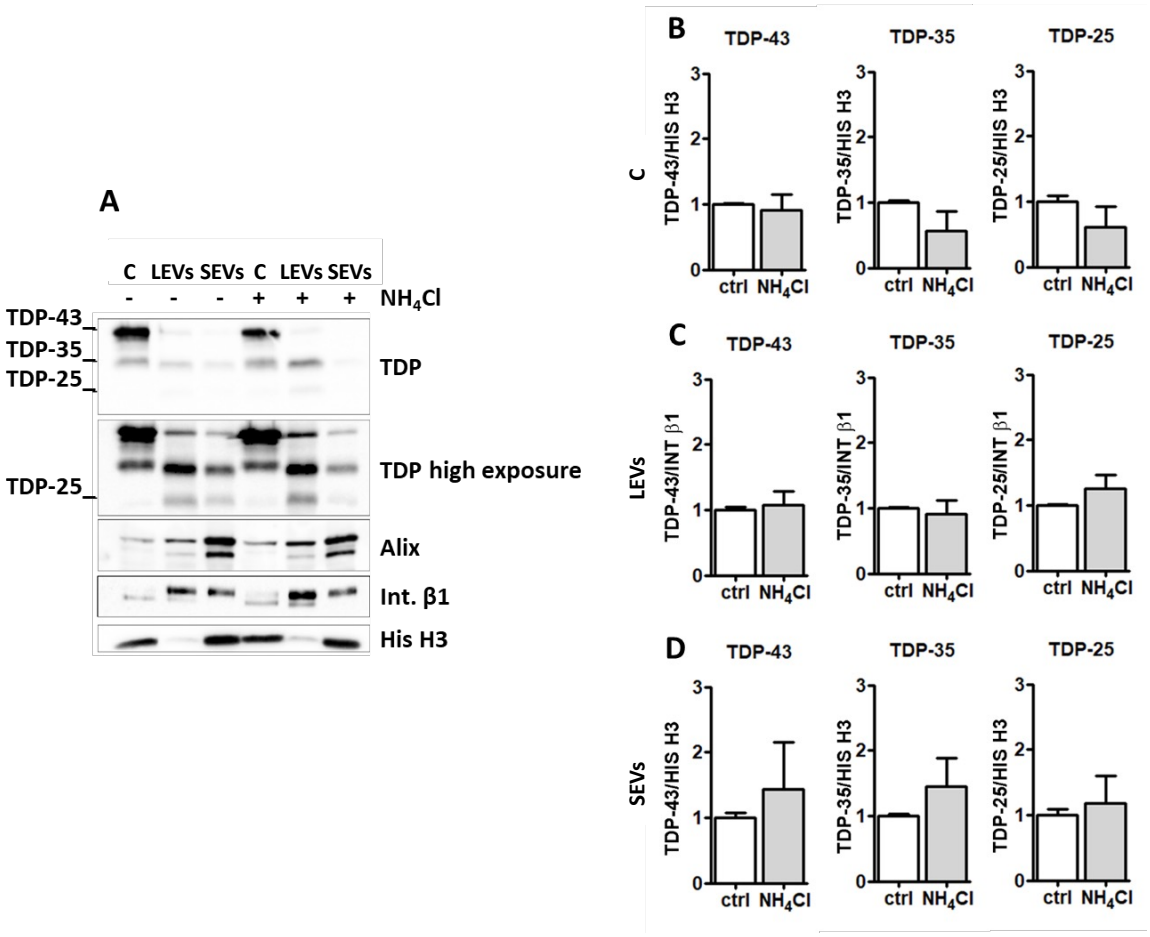

Figure 50. The effect of the autophagy inhibition on the TDP content of both cells (B), LEVs (C) and SEVs (D). WB analysis (A) and relative quantifications (B-D) of total RIPA protein extract of cells (B), LEVs (C) and SEVs (D), untreated or treated o/n with 20 mM NH_4Cl. Bar graphs represent the mean optical density ± SD of protein in analysis normalized on the optical density of the internal housekeeping protein (HIS H3 for cells and SEVs; Int. β1 for LEVs) and expressed as relative to the corresponding untreated sample (ctrl) of 3 biological replicates (unpaired one-tailed t test) (Casarotto et al., 2022)

Finally, the simultaneous blockage of UPS and autophagy (double treatment (DT); Fig. 51) caused a slight increase of the intracellular full length TDP-43 and a significant reduction of both TDP-35 and TDP-25 fragments, compared to control condition (Fig. 51 B). At the same time, data showed almost a doubling of TDP-35 and TDP-25 levels in LEVs obtained from treated compared to those obtained from untreated cells (Fig. 51 C). For the SEVs, data showed a decrease of their TDP-25 content and no difference in the level of both the full length TDP-43 and the TDP-35 fragment (Fig. 51 D).

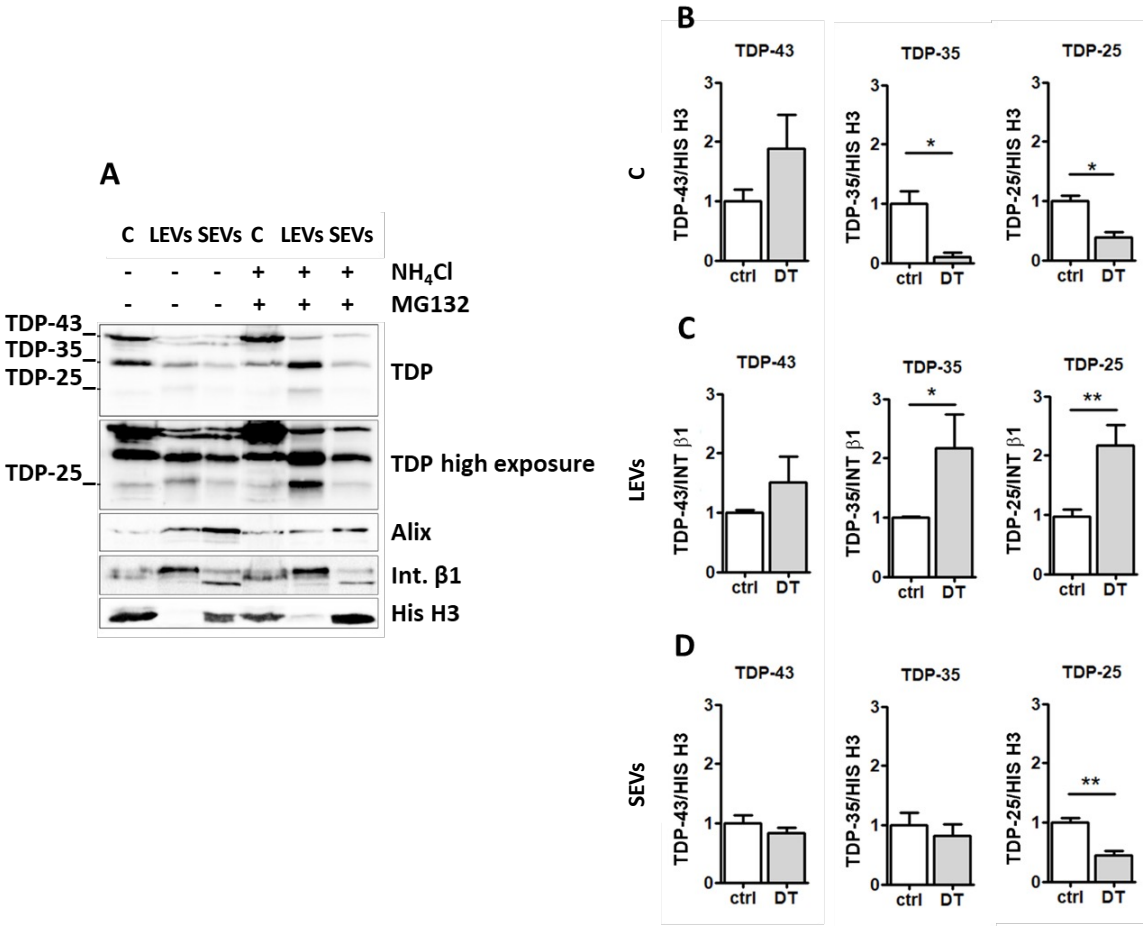

*Figure 51. The effect of the simultaneous blockage of UPS and autophagy on the TDP content of both cells (B), LEVs (C) and SEVs (D). WB analysis (A) and relative quantifications (B-D) of total RIPA protein extract of cells (B), LEVs (C) and SEVs (D), untreated or treated o/n with 10 μM MG132 and 20 mM NH_4Cl. Bar graphs represent the mean optical density ± SD of protein in analysis normalized on the optical density of the internal housekeeping protein (HIS H3 for cells and SEVs; Int. β1 for LEVs) and expressed as relative to the corresponding untreated sample (ctrl) of 3 biological replicates (*p < 0.05, ** p < 0.01, unpaired one-tailed t test) (Casarotto et al., 2022)*

At this point, given that the previous observations showed: i) the presence within the vesicles of the chaperone protein HSP70 and other PQC members, such as CHIP, BAG3, HSPB8, SQSTM1/p62 and MAP1LC3B, ii) the ability of proteasome and autophagy inhibitors to alter the intracellular expression of these chaperones and iii) the increase in the secretion of TDP species following PQC inhibition, I evaluated whether PQC inhibition could also alter the vesicular content of the above mentioned PQC members.

First, I analysed the effects of the proteasome inhibition (Fig. 52). WB analysis confirmed an increase of BAG3, HSPB8 and SQSTM1/p62 protein levels in MG132-treated cells compared to untreated condition (Fig. 52 C and F; Fig. 45). Interestingly, HSPB8 levels increased also in LEVs and SEVs obtained from treated cells compared to those obtained from the untreated cells (Fig. 52 D and E); while, differently from cells, a slight decrease in SQSTM1/p62 levels was detected both in LEVs and SEVs (Fig. 52 G and H).

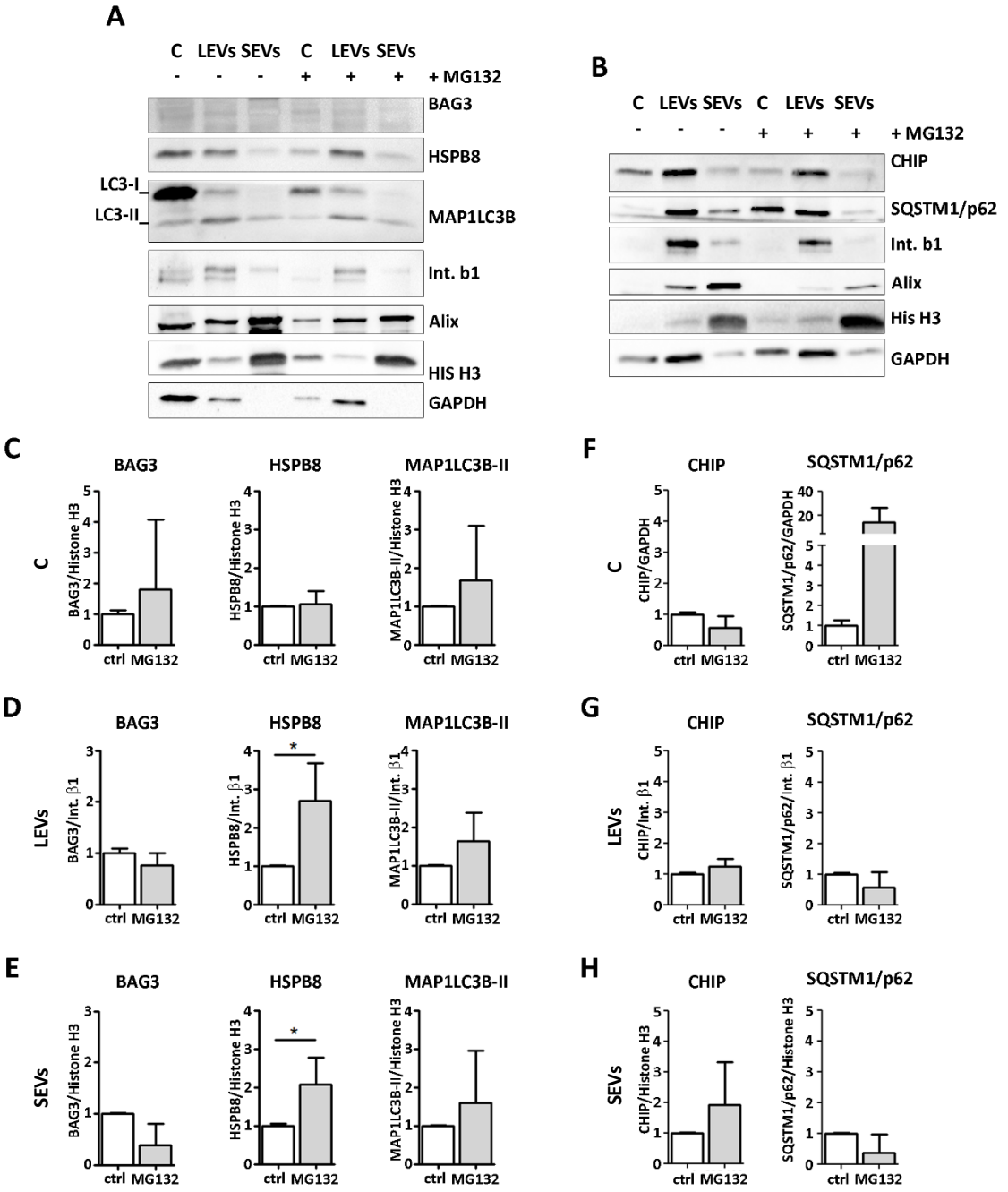

*Figure 52. The effect of the proteasome inhibition on BAG3, HSPB8, MAP1LC3B-II, CHIP and SQSTM1/p62, content of both cells (C and F), LEVs (D and G) and SEVs (E and H). Representative WB analyses (A and B) and relative quantifications (C-H) of total RIPA protein extract of cells (C and F), LEVs (D and G) and SEVs (E and H), untreated or treated o/n with 10 μM MG132. Bar graphs represent the mean optical density ± SD of protein in analysis normalized on the optical density of the internal housekeeping protein (HIS H3 (C) and GAPDH (F) for cells, Int. β1 for LEVs (D-G) and HIS H3 for SEVs (E and H)) and expressed as relative to the corresponding untreated sample (ctrl) of 3 biological replicates (*p < 0.05, unpaired one-tailed t test). WB (A) and relative quantifications (C-E) have been already published in Casarotto et al., 2022.*

Data obtained after the NH_4Cl-treatment (Fig. 53) confirmed an increase of MAP1LC3-II (Fig. 53 C) and SQSTM1/p62 (Fig. 53 F) protein levels in treated cells compared to untreated cells and also showed an increase of CHIP (Fig. 53 F), although not significant; while no change was observed in the protein levels of BAG3 and HSPB8 (Fig. 53 C). In LEVs and SEVs obtained from NH_4Cl-treated cells compared to those obtained from untreated cells, instead, data showed no changes in BAG3 and HSPB8 (Fig. 53 D and E) but an increase in SQSTM1/p62 (Fig. 53 G and H). An increase of MAP1LC3B-II was observed only in the SEVs (Fig. 53 E).

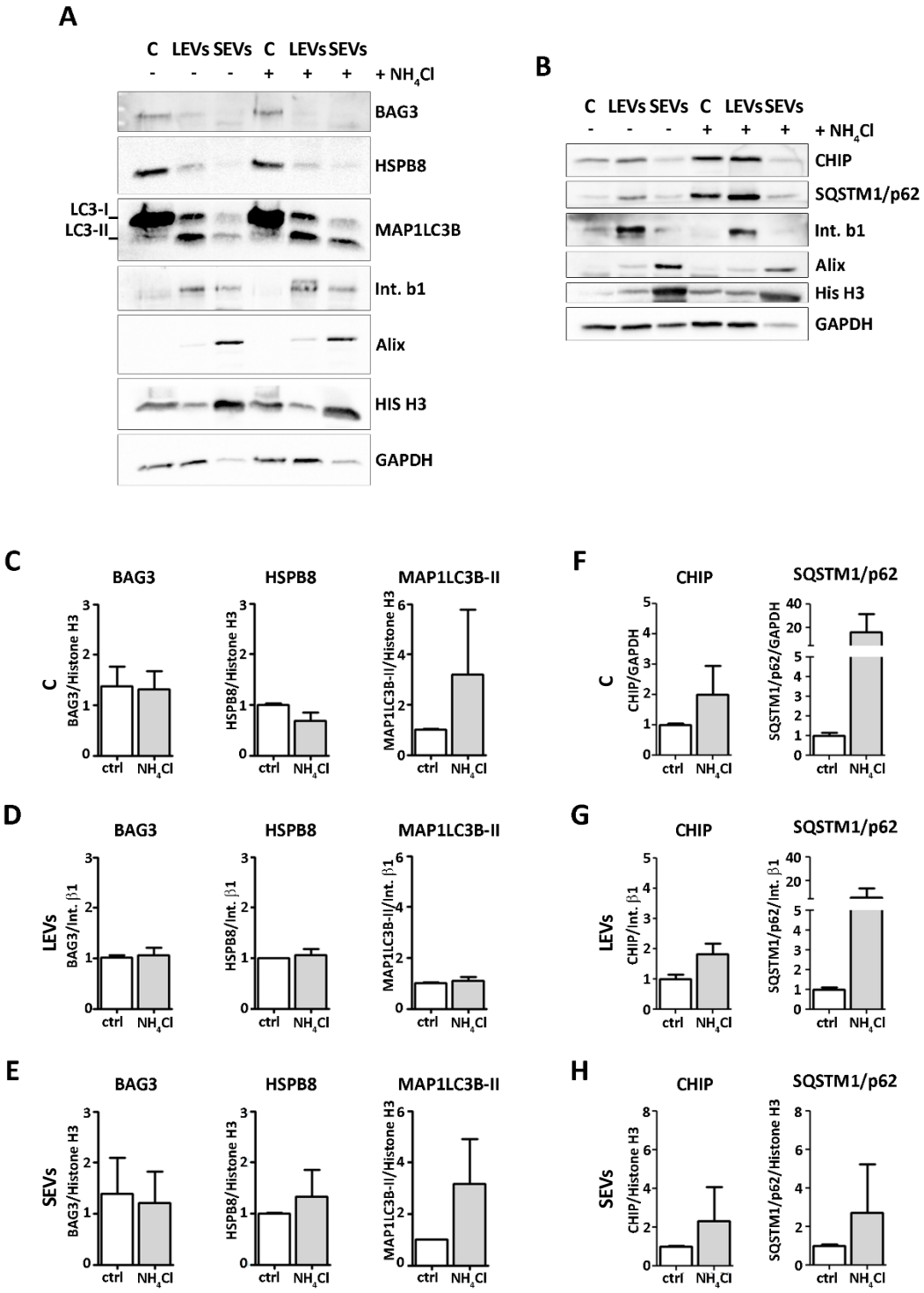

Figure 53. The effect of the autophagy inhibition on BAG3, HSPB8, MAP1LC3B-II, CHIP and SQSTM1/p62 content of both cells (C and F), LEVs (D and G) and SEVs (E and H). WB analyses (A and B) and relative quantifications (C-H) of total RIPA protein extracts of cells (C and F), LEVs (D and G) and SEVs (E and H), untreated or treated o/n with 20mM NH_4Cl. Bar graphs represent the mean optical density ± SD of the protein in analysis normalized on the optical density of the internal housekeeping protein (HIS H3 (C) and GAPDH (F) for cells, Int. β1 for LEVs (D and G) and HIS H3 for SEVs (E and H), and expressed as relative to the corresponding untreated sample (ctrl) of 3 biological replicates. WB (A) and relative quantifications (C-E) have been already published in Casarotto et al., 2022.

Finally, the effects of the proteasome and autophagy inhibition together have been analysed (Fig. 54). WB analysis of cells showed an increase of BAG3, HSPB8, MAP1LC3B-II (Fig. 54 C) and SQSTM1/p62 (Fig. 54 F) protein levels in treated samples, similarly to what was observed for the block of the proteasome alone (Fig. 52 C and F). Both LEVs and SEVs released from treated cells were enriched in BAG3, HSPB8 and MAP1LC3B-II (Fig. 54 D and E). Moreover, SEVs obtained from treated cells compared to those obtained from the untreated cells showed a decrease in SQSTM1/p62 protein levels (Fig. 54 H).

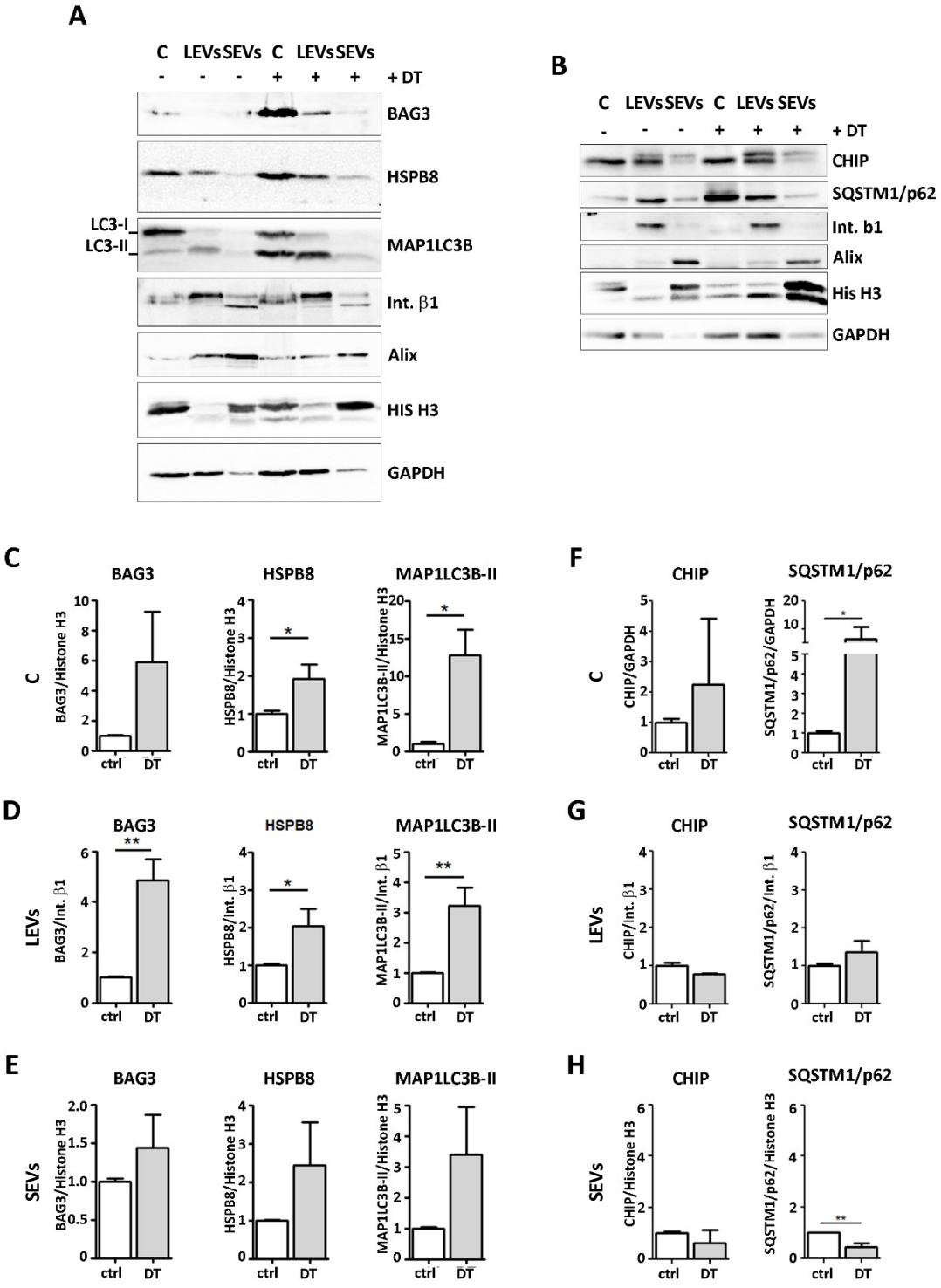

*Figure 54. The effect of the simultaneous blockade of autophagy and proteasome on BAG3, HSPB8, MAP1LC3B-II, CHIP and SQSTM1/p62 content of both cells (C and F), LEVs (D and G) and SEVs (E and H). Representative WB analyses (A and B) and relative quantifications (C-H) of total RIPA protein extract of cells (C and F), LEVs (D and G) and SEVs (E and H), untreated or treated o/n with 10μM MG132 + 20 mM NH_4Cl. Bar graphs represent the mean optical density ± SD of protein in analysis normalized on the optical density of the internal housekeeping protein (HIS H3 (C) and GAPDH (F) for cells, Int. β1 for LEVs (D and G) and HIS H3 for SEVs (E and H)) and expressed as relative to the corresponding untreated sample (ctrl) of 3 biological replicates (*p < 0.05, ** p < 0.01, unpaired one-tailed t test). WB (A) and relative quantifications (C-E) have been already published in Casarotto et al., 2022.*

Taken together, the results showed that PQC inhibition, particularly that of the UPS, enhanced the extracellular release of disease-associated TDP species and of some PQC components (HSPB8, BAG3 and MAP1LC3B-II) known for their ability to promote TDP species removal via autophagy. This suggests that PQC and EVs may cooperate in TDP disposal from cells.

Since I observed that EVs obtained from DT-derived EVs were enriched in pathological TDP species, I evaluated whether these EVs may exert toxic effect on recipient cells. For this reason, I isolated EVs from untreated and DT-cells and then I treated NSC34 cells with LEVs and SEVs together for 3, 6 and 24 hours. Cytotoxicity of EVs was evaluated through the LDH assay and the results obtained showed a slight increase (less than 5%) in toxicity in cells treated with DT-derived EVs (at all times analysed) compared to both untreated cells and cells treated with EVs derived from untreated cells (Fig. 55).

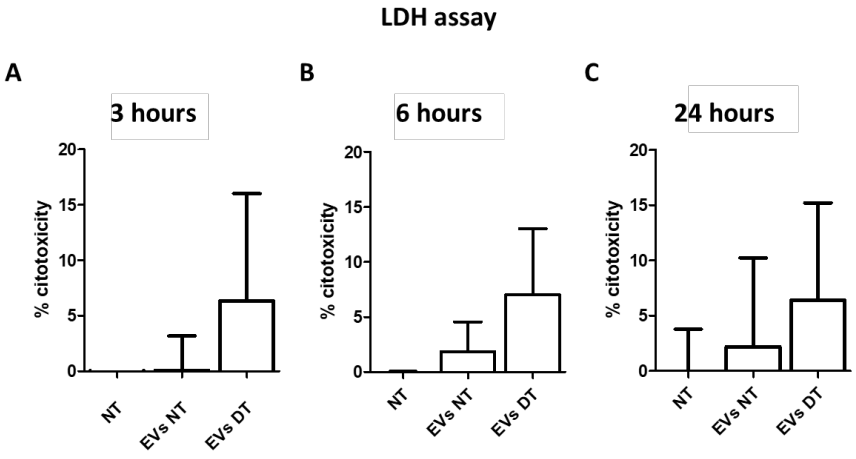

Figure 55. LDH assay on NSC34 cells treated for 3, 6 and 24 hours with EVs obtained from untreated and DT-treated (MG132 10μM and NH_4Cl 20mM for 16 h) cells. Bar graphs represent the mean percentage of cytotoxicity (n = 3).

To better understand the interplay between PQC and EVs, I analysed EVs also for their ubiquitin content, by evaluating whether the blockade of the proteasome and autophagy together or alone might affect it. Indeed, proteins that need to be degraded both by proteasome and autophagy are ubiquitinated. In particular, I used two different antibodies: one able to recognize all the types of ubiquitination that a protein can undergo, and another specifically directed against the K63 linkage, that binds together two ubiquitin

molecules contained in a polyubiquitin chain (thus able to specifically recognize the K63-polyubiquitinated proteins directed to autophagy for degradation).

The WB analysis in figure 56 showed that, both LEVs and SEVs released in physiological conditions contained several ubiquitinated species, some of which positive for K63 antibody. Interestingly, SEVs seemed to be enriched in K63-polyubiquitinated proteins. The treatment of cells with the proteasome inhibitor alone or in combination with the autophagy inhibitor caused an intracellular increase of all the ubiquitinated species (Fig. 56 A and C). Interestingly, no changes were observed in the EVs content, neither in total nor in K63 ubiquitinated proteins (Fig. 56 A and C). For the treatment with NH_4Cl instead, the results showed that the block of the autophagy did not alter the ubiquitinated and K63-polyubiquitinated proteins content of both the cells and the LEVs (Fig. 56 B). However, this treatment resulted in a slight increase of ubiquitinated proteins in SEVs obtained from treated cells compared to those obtained from untreated cells (Fig. 56 B).

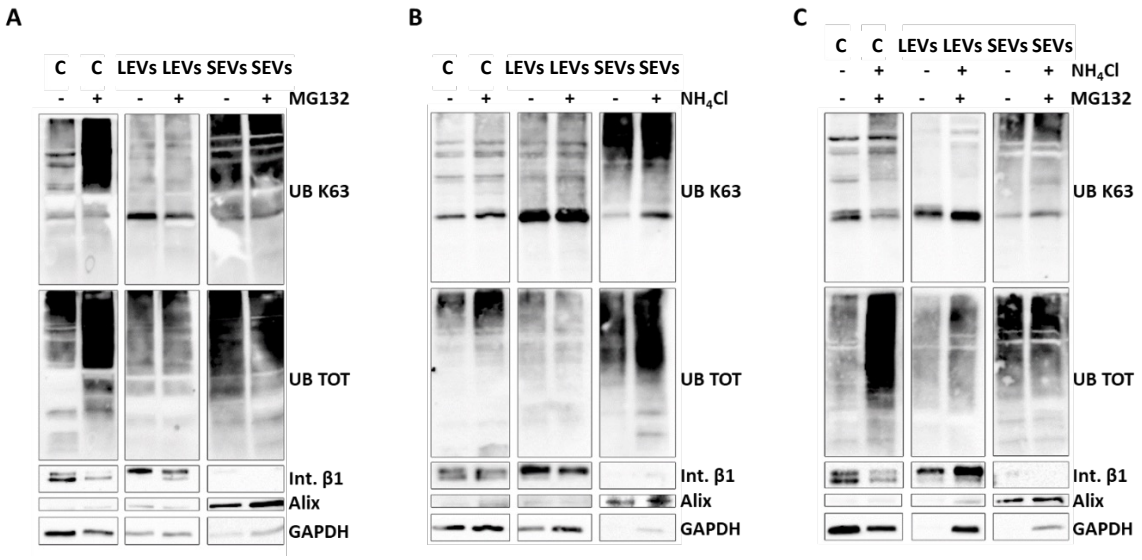

Figure 56. Representative WB analyses of the ubiquitinated and K63-polyubiquitinated proteins present in cells, LEVs and SEVs in physiological conditions and after the treatment with MG132 (A), NH_4Cl (B) and MG132 + NH_4Cl (DT) (C).

CIRCULATING EVs OBTAINED FROM FTD PATIENTS ARE ENRICHED IN PATHOLOGICAL TDP-35 AND CONTAIN THE CASA COMPLEX COMPONENTS HSPB8 AND BAG3

To validate the physiopathological relevance of the observations obtained in NSC34 cells, I isolated and analyzed circulating EVs (both LEVs and SEVs) obtained from plasma of FTD patients compared to EVs obtained from plasma of healthy donors (controls, ctrl).

EVs were first characterized for their size through NTA and TEM analyses (Fig. 57). NTA and TEM analyses showed that LEVs and SEVs were different in size, as previously demonstrated (Sproviero et al., 2018). In particular, the NTA analysis showed that the mean size in diameter for the LEVs was of 180.2 ± 3.9 nm, while for the SEVs was of 154.1 ± 1.7 nm.

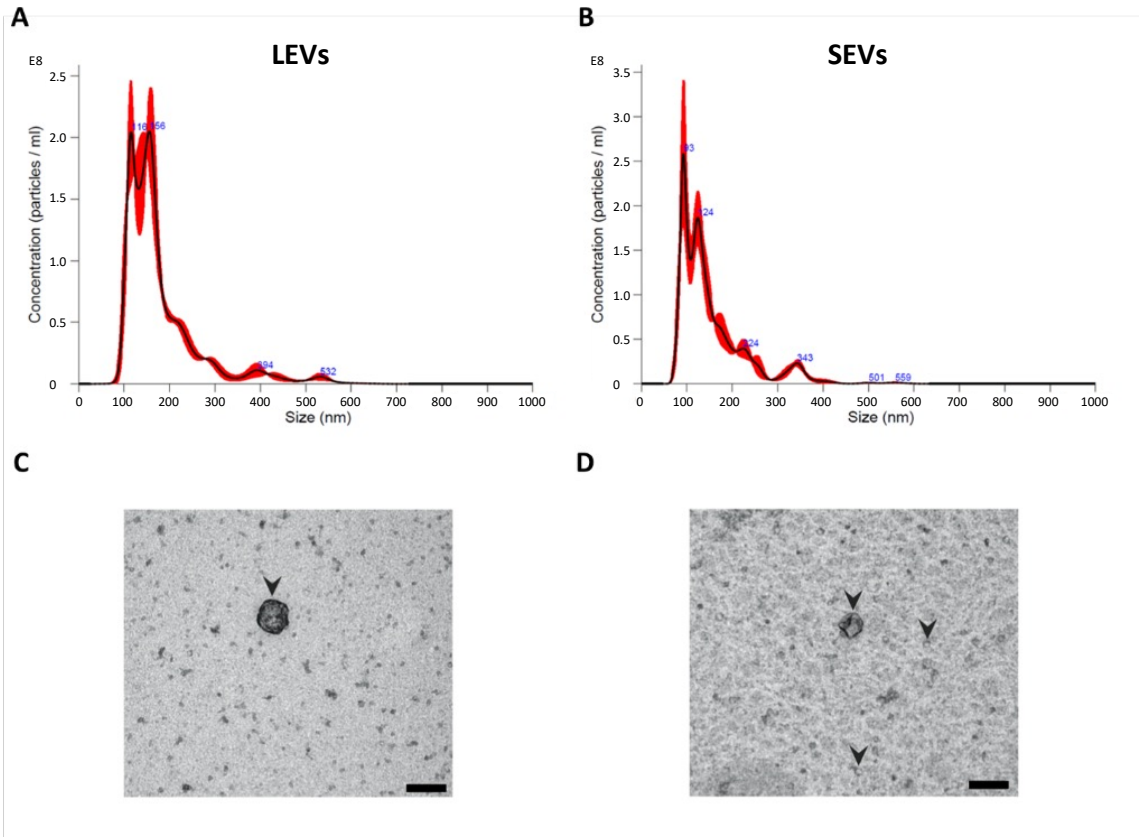

Figure 57. Plasma-derived EVs from FTD patients and healthy donors. Representative NTA analyses of LEVs (A) and SEVs (B) isolated from the plasma of a healthy control. x-axis = vesicles size, expressed in nm; y-axis = vesicles concentration, expressed as number of particles/ml. Representative TEM images of LEVs (one LV of about 200 nm) and SEVs (three SEVs of about 100-150 nm) from plasma of a healthy control (scale bar: 500 nm) (Casarotto et al., 2022)

EVs were then analysed for their protein cargo through WB analysis. Alix was used as SEVs marker, while Annexin I (considered a good LEVs marker by MISEV guidelines) was selected for LEVs, since LEVs isolated from human plasma are not enriched in Int. β, as those isolated from the NSC34 cells. WB analysis showed that both LEVs and SEVs isolated from plasma of both FTD patients and healthy controls were immunoreactive for the full length TDP-43 species, but only EVs obtained from the FTD patients were immunoreactive for the TDP-35 fragment (Fig. 58 C and D). Moreover, I found that HSPB8, BAG3 and HSP70 were present also in plasma derived EVs. However, in this case no significant difference in the content of BAG3 and HSPB8 was observed between FTD-derived EVs and EVs from healthy donors (Fig. 58 C and D). Interestingly, data showed a significant increase of HSP70 protein levels in LEVs obtained from FTD patients compared to that obtained from the control donors (Fig. 58 C).

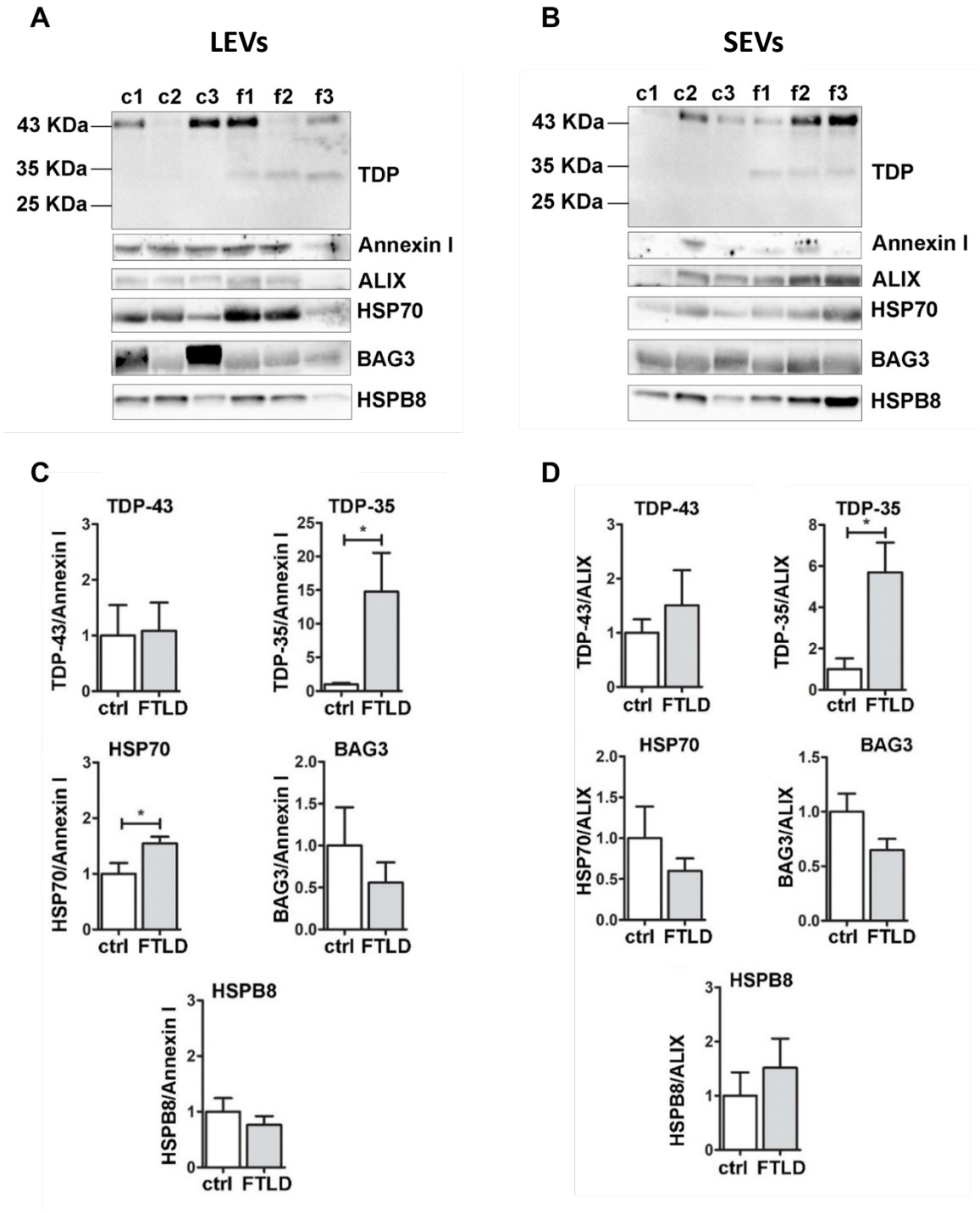

*Figure 58. Plasma-derived EVs from FTD patients and healthy controls and their TDP species and CASA-complex members content. WB (A and B) and relative quantifications of LEVs (C) and SEVs (D) samples from plasma of 3 healthy controls (c1-c2-c3) and 3 FTD (f1-f2-f3) patients. Bar graphs represent the mean optical density ± SD of the protein in analysis normalized on the optical density of the internal housekeeping protein (Annexin I for LEVs and Alix for SEVs) and reported as relative to ctrl group, for 3 biological replicates. (*p < 0.05, unpaired one-tailed t test) (Casarotto et al., 2022)*

IN PHYSIOLOGICAL CONDITIONS MUSCLE CELLS SECRETE TDP SPECIES AND SOME PQC SYSTEM MEMBERS BOTH MAINLY IN THE LEVs

Given the previously described “dying back” hypothesis, that suggests a possible role of the muscle cells in the pathogenesis of ALS, I evaluated whether also these cells were able to secrete the TDP species TDP-43, TDP-35 and TDP-25 in EVs, and how/if PQC inhibition could affect EVs cargo also in these cells.

To this purpose, I used the immortalized mouse myoblast cell line C2C12. I isolated from the culture medium of these cells both the LEVs and SEVs and, as I did for both the NSC34 cells derived EVs and for the plasma derived EVs, I characterized them through the NTA analysis (Fig. 59 A and B) and the WB analysis (Fig. 59 C).

Data showed that also for the C2C12-derived EVs the differential ultracentrifugation method allowed to separate the EVs into two populations: the first one obtained after centrifugation at 20.000 g (LEVs) and the second one collected at 100.000 g (SEVs). These two populations are characterized by a slight difference in size and protein markers. Indeed, data showed that LEVs and SEVs obtained from these cells overlapped for their size (LEVs were characterized by a mode and mean diameter of about 128,2 nm and 182,7 nm respectively; while SEVs of about 133,1 nm and 170,9 nm), and therefore suggested that C2C12 cells secreted EVs smaller than those secreted by NSC34 and not too different in size from each other. Despite this overlap in size and the presence of Alix and Int. β1 in both populations, LEVs were negative for His H3 marker. This could be explained by assuming that some LEVs of small dimension sedimented with SEVs.

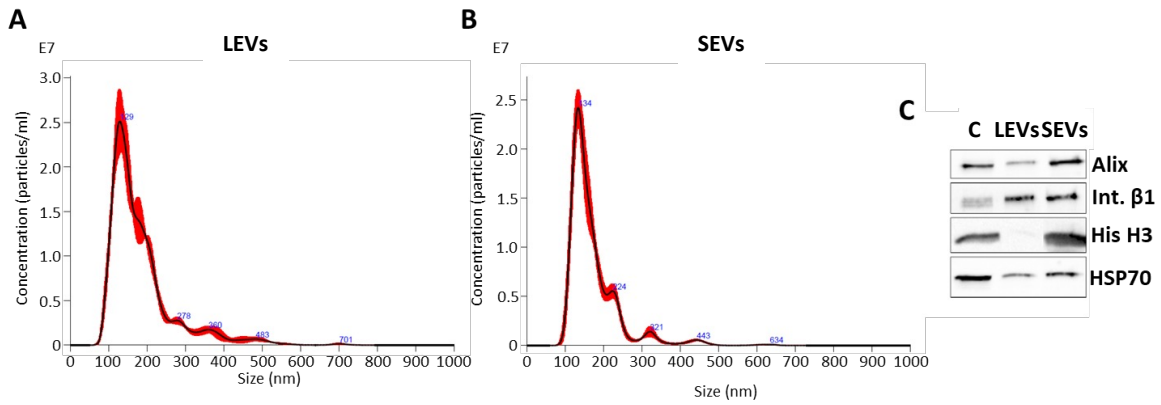

Figure 59. Characterization of EVs obtained from C2C12 cells. Representative NTA distribution profile of LEVs (A) and SEVs (B). x-axis = vesicles size expressed in nm; y-axis = vesicles concentration, expressed as number of particles/ml. WB analysis for characterization markers of LEVs (Int. ß1) and SEVs (Alix and histone H3) (C).

LEVs and SEVs were then analysed for their TDP species content and PQC components. As shown in Figure 60, in physiological conditions, C2C12 cells are able to secrete TDP-43, TDP-35 and TDP-25 both in LEVs and in SEVs. Moreover, they are enriched in the TDP-35 fragment, as observed for NSC34-derived EVs.

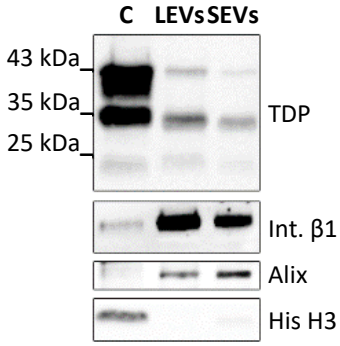

Figure 60. Representative WB analysis of TDP-43, TDP-35 and TDP-25 species in C2C12 cells and relative LEVs and SEVs.

Regarding PQC components, both LEVs and SEVs derived from C2C12 cells contained CHIP, HSP70 and the lipidated MAP1LC3B-II (Fig 61). Interestingly, C2C12-derived LEVs also contained BAG3, HSPB8, SQSTM1/p62 and MAP1LC3B-I, while all these proteins were absent in SEVs. Moreover, LEVs were also positive for the 33 kDa isoform of the co-chaperone BAG1, differently from NSC34-derived LEVs.

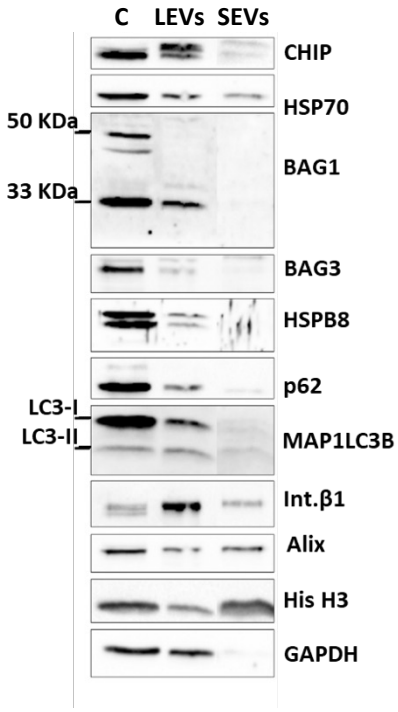

Figure 61. Representative WB analysis showing the presence of chaperone and co-chaperone proteins members of the PQC system in C2C12 cells (C) and relative LEVs and SEVs. CHIP, HSP70, BAG1 (in particular, its 50 and 33 kDa isoforms), BAG3, HSPB8, SQSTM1/p62 and MAP1LC3 (both in its lipidated or not form) are the proteins whose presence has been analysed. Int. β1 was used as LEVs marker, Alix and Histone H3 as SEVs marker and GAPDH as housekeeping protein for the cells.

THE PQC INHIBITION AFFECTS THE CARGO OF SEVs

To validate the effect of proteasome and autophagy inhibitors on C2C12, I evaluated the expression level of *Bag3, Hspb8*, *Sqstm1/p62* and *Map1lc3b* genes, trough the analysis of their mRNA levels in real-time PCR (Fig. 62) and protein levels in WB analysis (Fig. 63), as previously done in NSC34 cells.

The results showed that also in C2C12 cells MG132-treatment caused a significant increase in the expression levels of *Bag3* (Fig. 62 A), *Hspb8* (Fig. 62 B) and *Sqstm1/p62* (Fig. 62 C) mRNA. Moreover, in these cells, proteasome blockade also caused an increase in the expression level of *Map1lc3b* gene (Fig. 62 D). For the autophagy blockade, data showed a significant increase in the expression levels of *Sqstm1/p62* (Fig. 62 C) and *Map1lc3b* (Fig. 62 D) mRNA. Data also showed that for *Sqstm1/p62* (Fig. 62 C) this increase was lower than that caused by proteasome blockade.

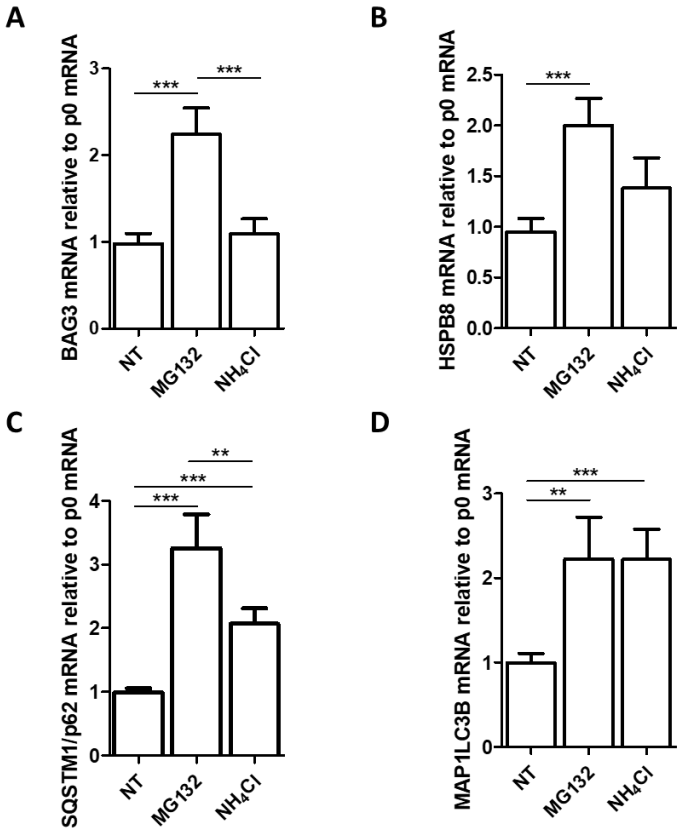

*Figure 62. mRNA expression levels of Bag3 (A), Hspb8 (B), Sqstm1/p62 (C) and Map1lc3b (D) in condition of proteasome and autophagy blockade. Bar graphs represent the relative fold induction of Bag3, HspB8, Sqstm1/p62 and Map1lc3B genes normalized with the Rplp0 mRNA levels. Data are means ± SD of 4 independent samples (** p < 0.01, *** p < 0,001 One-way Anova, Bonferroni's Multiple Comparison Test).*

WB analysis showed: a significant increase of HSPB8 (Fig. 63 C), SQSTM1/p62 (Fig. 63 D) and MAP1LC3B-II (Fig. 63 F) and a significant decrease of BAG3 (Fig. 63 B) and MAP1LC3B-I (Fig. 63 E) immunoreactivities in cells treated with MG132; a significant increase of BAG3 (Fig. 63 B), SQSTM1/p62 (Fig. 63 D), MAP1LC3B-I (Fig. 63 E) and -II (Fig. 63 F) and a significant decrease of HSPB8 (Fig. 63 C) immunoreactivities in cells treated with NH_4Cl.

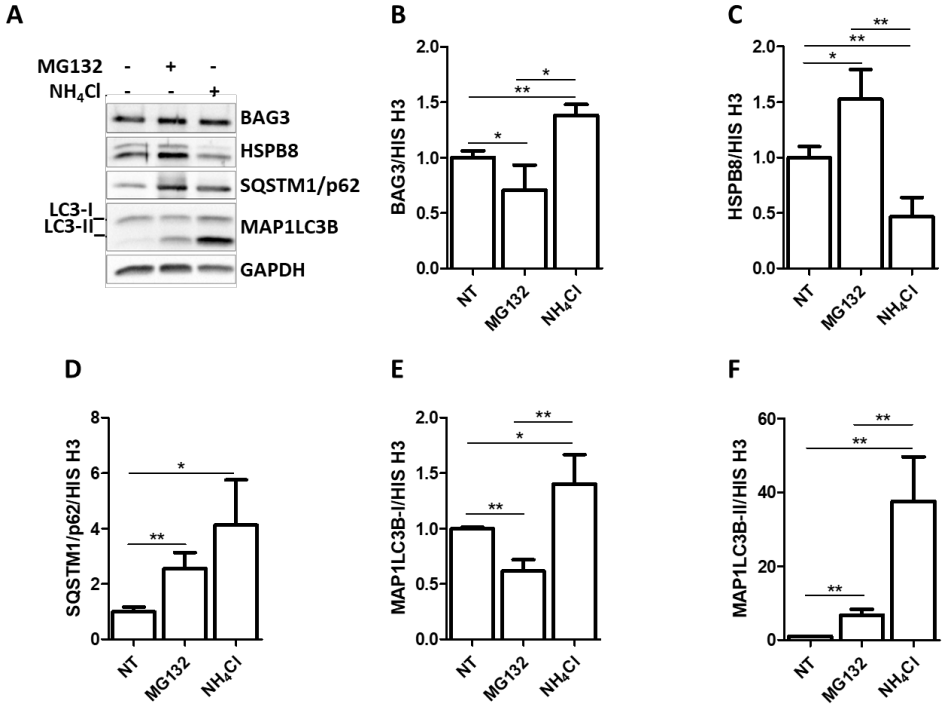

*Figure 63. Representative WB analysis of the total RIPA proteins extract of C2C12 cells treated with MG132 2,5 µ and NH_4Cl 20 mM together or alone. BAG3, HSPB8, SQSTM1/p62 and MAP1LC3B have been analysed. Bar graphs represent the mean optical density ± SD of the protein in analysis normalized on the optical density of Histone H3 used as housekeeping protein and reported in comparison to untreated samples. n=3. (*p < 0.05, ** p < 0.01, One-way Anova, Bonferroni's Multiple Comparison Test).*

These data confirmed that the selected treatments were effective also in muscle cells and therefore, I evaluated whether the block of the autophagy and the proteasome could affect the protein content of LEVs and SEVs isolated from C2C12 treated-cells (Fig. 64 and 65).

Proteasome blockade (Fig. 64) increased intracellular protein levels of the TDP-35 fragment and of the PQC system members BAG3, HSPB8 and SQSTM1/p62. However, only a slight increase in HSP70 and HSPB8 levels were observed in LEVs and no alterations were detected in SEVs.

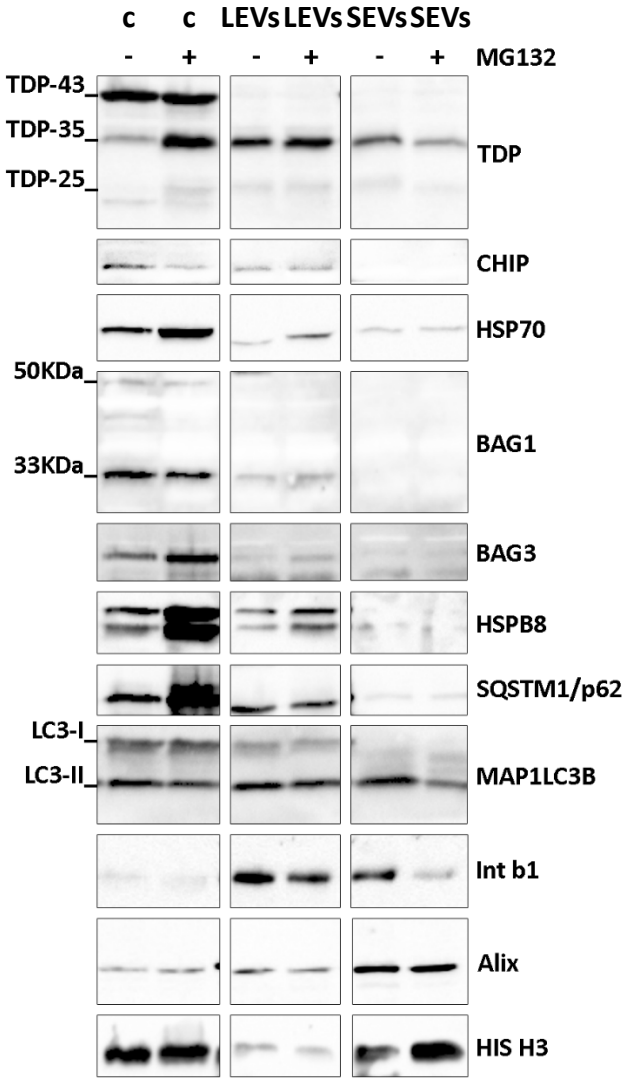

Figure 64. Representative WB analysis that shows the effect of the proteasome inhibition (MG132 2,5 µM) on TDP species, CHIP, HSP70, BAG1, BAG3, HSPB8, SQSTM1/p62, MAP1LC3B-I and MAP1LC3B-II content of the C2C12 cells and of their relative LEVs and SEVs.

For the block of the autophagy, instead, the WB analysis of the total RIPA protein extract of cells, LEVs and SEVs (Fig. 65) showed that the treatment of cells with NH_4Cl caused a decrease of the intracellular level of the TDP-35 fragments together with an increase of MAP1LC3B-II. Moreover, data showed that the LEVs obtained from the treated cells compared to those obtained from the untreated cells were enriched in MAP1LC3B-II. Interestingly, the block of the autophagy increased the secretion of the TDP-35 fragment, of the chaperone proteins HSP70 and HSPB8, and of MAP1LC3B-II in SEVs.

The results obtained in NSC34 and C2C12 cells showed that both these cell models use the secretory pathway to eliminate TDP-35, however the blockade of proteasome and autophagy appears to have an opposite effect in them.

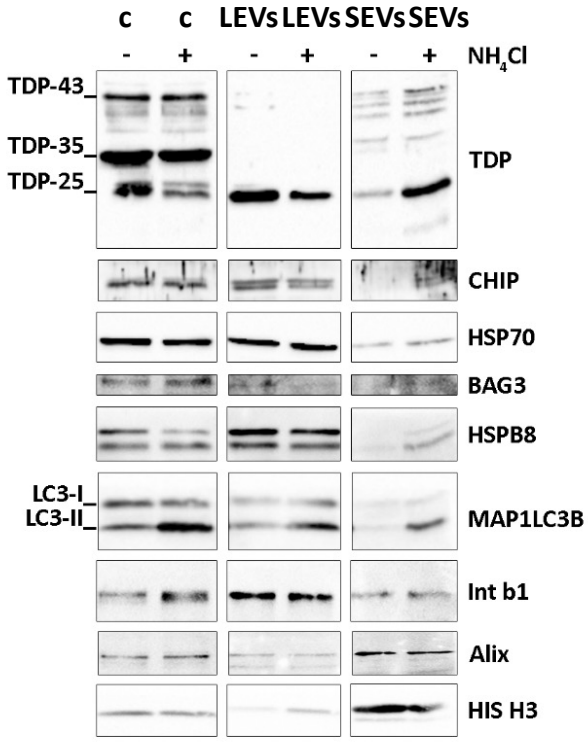

Figure 65. Representative WB analysis that shows the effect of the autophagy inhibition (NH_4Cl 20 mM) on TDP species, CHIP, HSP70, BAG3, HSPB8, MAP1LC3B-I and MAP1LC3B-II content of the C2C12 cells and of their relative LEVs and SEVs.

THE SECRETION OF THE TDP SPECIES IN EVs IS INDEPENDENT FROM THE CASA-COMPLEX BUT IT COULD BE MEDIATED BY THE HSPB8 CHAPERONE ALONE

Since the data described above showed that the blockade of the PQC system boosted the secretion of TDP species from cells and caused, at the same time, an increase in the secretion of the CASA-complex members HSPB8 and BAG3, I decided to evaluate whether these proteins could have a direct role in routing TDP species to EVs.

First of all, I silenced the expression of HSPB8 or BAG3 in NSC34 cells and analysed their effects both in untreated cells or in cells treated with MG132 and NH_4Cl together (a condition that boosts the secretion of TDP species, as above demonstrated). Total RIPA intracellular protein extracts were analysed through WB analysis and results shown in Fig. 66 and 67.

In untreated cells, HSPB8 silencing (Fig. 66) almost completely abolished its expression (Fig 66 C) and reduced BAG3 protein levels (Fig. 66 D). Moreover, HSPB8-silencing caused a significant increase of the TDP-35 fragment in cells (Fig. 66 H), indicating that HSPB8 has a relevant role in the degradation of the TDP-35 fragment. In treated-cells, HSPB8 silencing was not complete and BAG3 levels was not reduced (Fig. 66 B and D), probably because the stimulatory effect of treatments on HSPB8 and BAG3 expression prevails.

When both degradative pathways were inhibited and HSPB8 is expressed, the intracellular levels of TDP-35 fragment decreased (Fig. 66 H), as already observed in previously experiments (Fig. 51 B). When HSPB8 is silenced and PQC inhibited, TDP-35 levels did not change (Fig. 66 H). Since PQC inhibition overcomes the HSPB8 silencing, it can be assumed that in these conditions, the remaining HSPB8 is sufficient to drive TDP-35 secretion into EVs.

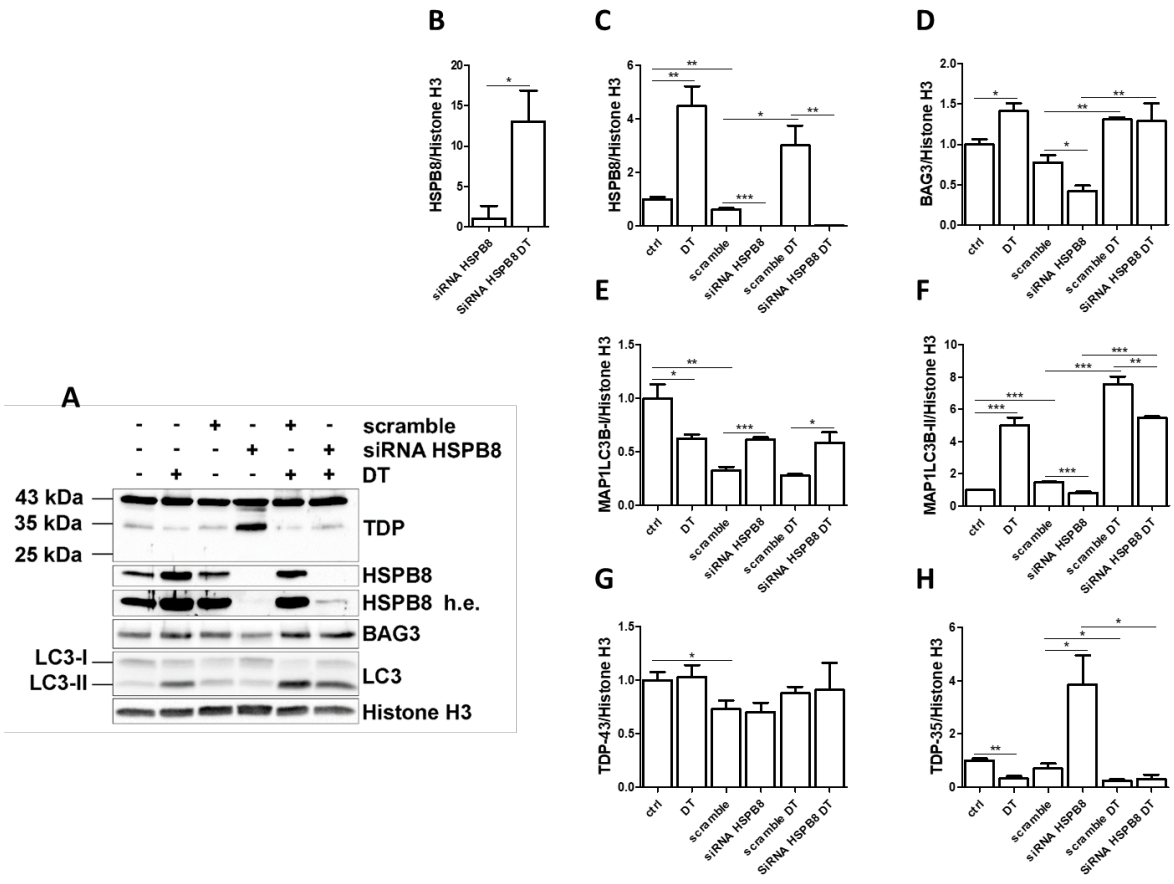

*Figure 66. The role of HSPB8 in the disposal of the TDP species in physiological ad pathological conditions. Representative WB analysis of the total RIPA proteins extract of NSC34 cells transfected with scramble or siRNA-HSPB8 and treated with MG132 (10 µM) and NH_4Cl (20 mM) together for 16 hours. HSPB8, BAG3, MAP1LC3B (I and II), TDP-43 and TDP-35 have been analysed. Bar graphs represent the mean optical density ± SD of the protein in analysis normalized on the optical density of Histone H3 used as housekeeping protein and expressed as relative to the corresponding untreated samples (C-H). The bar graph B represents the mean optical density ± SD of the protein HSPB8 acquired at high exposure (h.e.) normalized on the optical density of Histone H3 used as housekeeping protein and expressed as relative to untreated siRNA-HSPB8 transfected samples n=3 (*p < 0.05, ** p < 0.01, *** p < 0,001 unpaired one-tailed t test)*

BAG3 silencing (Fig. 67) caused a significant decrease of HSPB8 and of MAP1LC3B-II in untreated cells. Despite BAG3 reduction and HSPB8 reduction, no changes were observed in TDP-35 levels, probably because the levels of the two chaperones though low are sufficient to drive TDP-35 disposal. Treatment of BAG3-silenced cells with MG132 and NH_4Cl caused an increase of HSPB8 and MAP1LC3B-II. Indeed, no variation was detected in TDP-35 protein level.

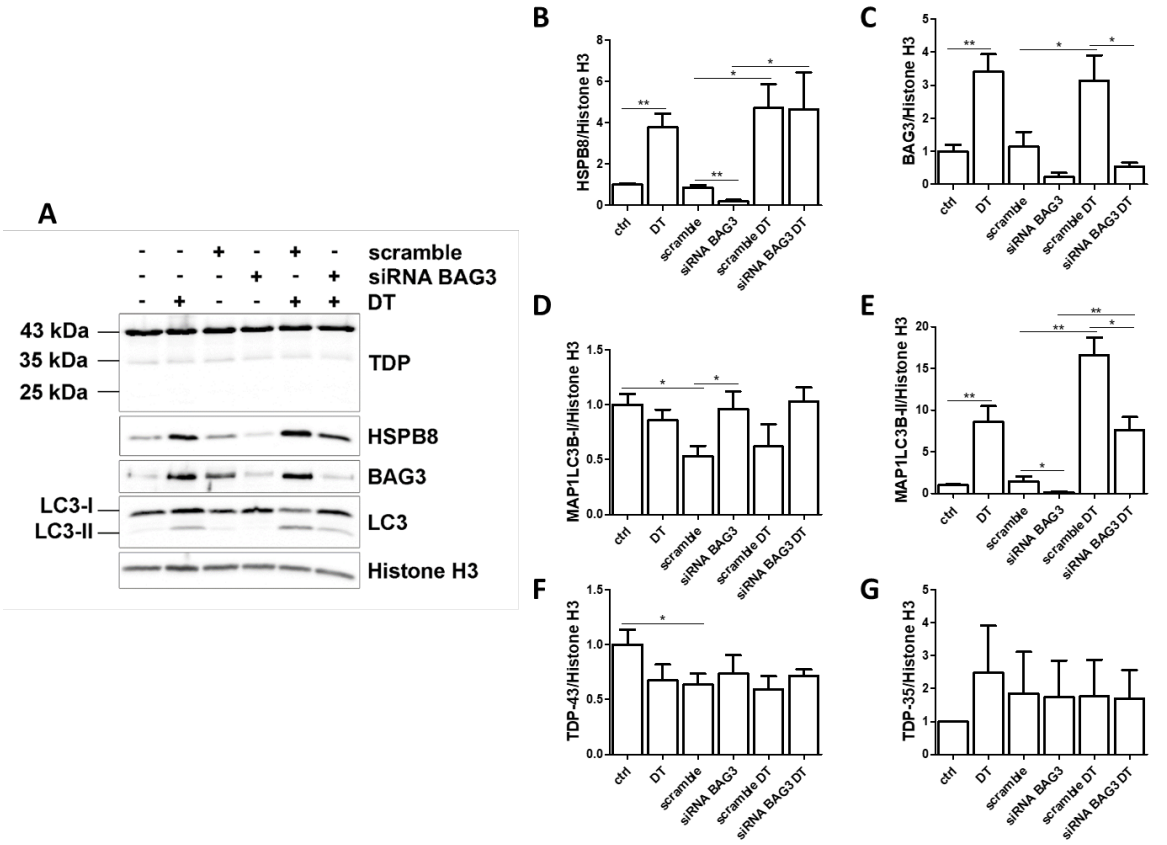

*Figure 67. The role of BAG3 in the disposal of the TDP species in physiological ad pathological conditions. Representative WB analysis of the total RIPA protein extract of NSC34 cells transfected with scramble or siRNA-BAG3 and treated with MG132 (10 μM) and NH_4Cl (20 mM) together. HSPB8, BAG3, MAP1LC3B (I and II), TDP-43 and TDP-35 have been analysed. Bar graphs represent the mean optical density ± SD of the protein in analysis normalized on the optical density of Histone H3 used as housekeeping protein and expressed as relative to the corresponding untreated sample. n=3. (*p < 0.05, ** p < 0.01, unpaired one-tailed t test)*

Unfortunately, due to the high cost of transfection reagents and the large number of cells needed for EVs analysis, it was not possible to analyze the EVs protein content in siRNA experiments. Therefore, to overcome cost limitation and to better understand the role of the HSPB8-BAG3 complex in the secretion of TDP species in EVs, I took advantage of the compound JG-98, an allosteric inhibitor of HSP70, able to inhibit the interaction of HSP70 with BAG3 and thus the assembly of the CASA-complex.

First of all, I performed MTT, LDH and WB assayes to find the optimal dose of JG-98 compound to be used in NSC34 cells (Fig. 68). For this purpose, NSC34 cells were treated with increasing doses of JG-98 (0,5 µM, 1 µM, 2 µM, 3 µM, 4 µM and 5 µM), and then analysed (Fig. 69 and 70). Doses were selected based on the literature (Martin et al., 2022).

LDH assay showed that 4 and 5 µM treatments statistically increased the cell mortality, up to a maximum of 7.5% for 5 µM treatment (Fig. 68 A). MTT assay, instead, showed that all the treatments statistically affected cells viability/division (Fig. 68 B).

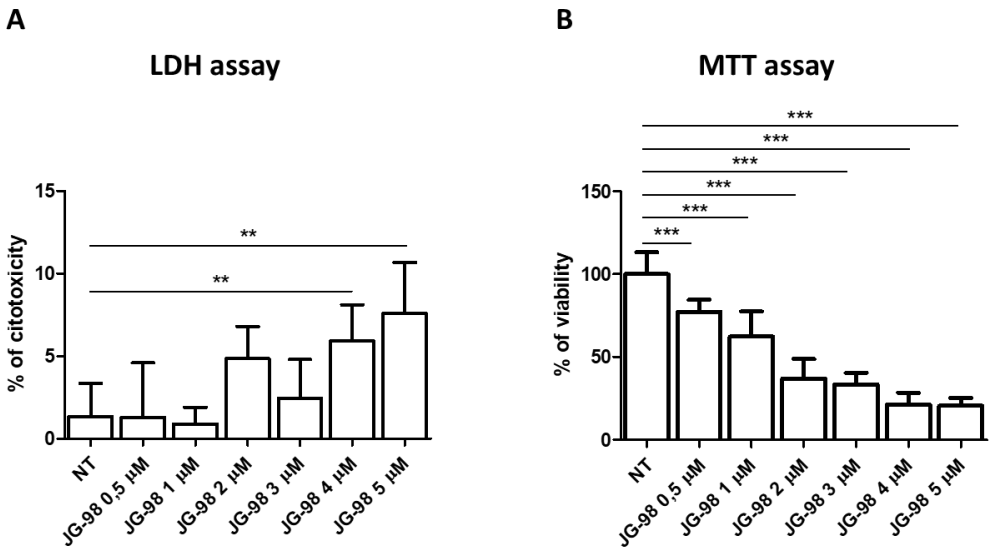

*Figure 68. LDH and MTT assays performed on NSC34 cells treated with increasing doses of JG-98 (from 0.5 µM up to 5 µM) for 16 hours. Bar graphs represent the mean percentage of cytotoxicity and viability (n = 8) (** p <0.01; *** p <0.001; unpaired one-tailed t test)*

WB analysis (Fig. 69) showed a significant decrease of the intracellular HSP70 levels in all the treated cells, except for those treated with JG-98 1 µM (Fig. 69 C), a significant decrease of BAG3 in all the cells treated with a dose of JG-98 greater than 0.5 µM (Fig. 69 E), and a significant decrease of HSPB8 for all the doses (Fig. 69 B), compared to untreated cells. These results suggested that HSP70-BAG3 interaction inhibition affects their stability, and indirectly affects that of HSPB8. In parallel to the decrease of the monomer form of the HSP70 and BAG3 proteins, an increase in high weight immunoreactive species was observed (Fig. 69 D and F).

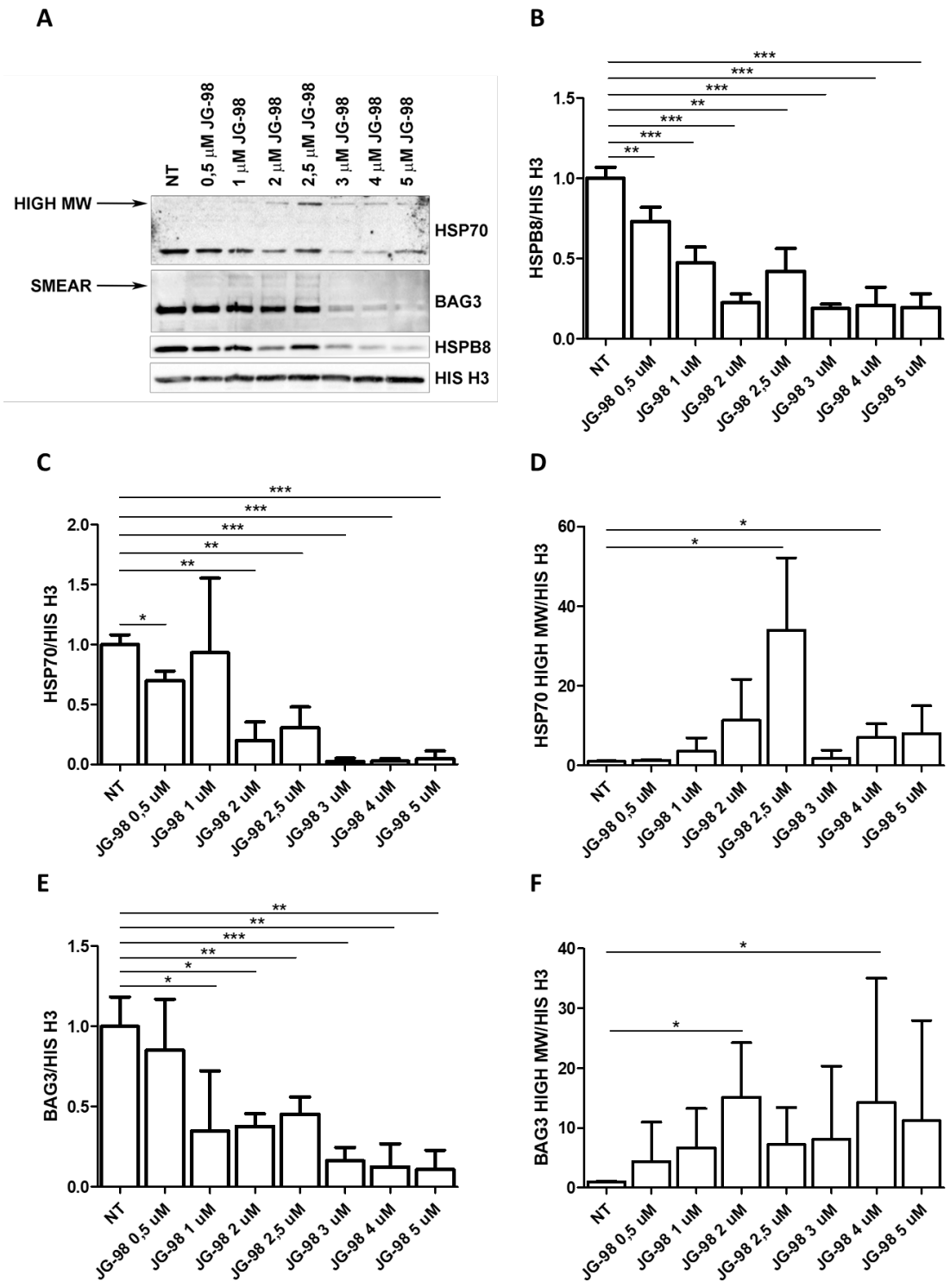

Figure 69. Representative WB analysis (A) and relative quantifications (B-F) for the NSC-34 cells treated with increasing doses of JG-98 (0,5 μM, 1 μM, 2 μM, 2,5 μM, 3 μM, 4 μM and 5 μM) for 16 hours. Bar graphs represent the mean optical density ± SD of the protein in analysis normalized on the optical density of Histone H3 used as housekeeping protein and expressed as relative to the corresponding untreated sample. n=3. (p <0,05, ** p <0,01; *** p <0,001, unpaired one-tailed t test)*

Based on these data, the 2 µM dose was selected as the best one to inhibit CASA-complex formation and study its effect on TDPs species disposal in NSC34 cells.

For this purpose, cells were treated with the 2 µmM dose of JG-98 for different hours (2, 6 and 24 hours) and RIPA protein extracts were analysed by WB (Fig. 70).

Interestingly, as observed before for HSP70 and BAG3, oligomeric TDP forms appeared in all treated-cells (Fig. 70 B), with a parallel decrease of the full length TDP-43 and TDP-35 (Fig. 70 C and D). These effects were time-dependent.

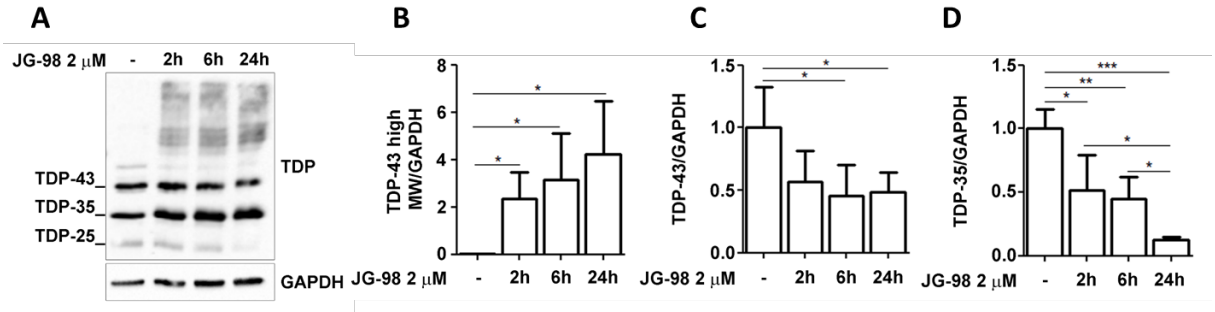

Figure 70. Representative WB analysis (A) and relative quantifications (B-D) of NSC34 cells treated for 2, 6 and 24 hours with JG-98 2 µM. Bar graphs represent the mean optical density ± SD of the protein in analysis normalized on the optical density of GAPDH used as housekeeping protein and expressed as relative to the corresponding untreated samples. (n=3). (p <0,05, ** p <0,01; *** p <0,001, unpaired one-tailed t test)*

To understand whether TDPs high molecular weight forms observed in JG-98-treated cells corresponded to aggregated forms, I evaluated their solubility in the RIPA buffer through the FTA (a technique that allows to quantify the levels of RIPA-insoluble species characterized by a size bigger than 0.22 µm) and through the WB analysis in which I analysed both the RIPA-soluble and insoluble fractions of the cells protein extract (Fig. 71 and 72).

FTA analysis (Fig. 71) demonstrated that TDP species in JG-98-treated cells were retained on the cellulose acetate membrane, suggesting that they were in an aggregated/oligomeric conformation.

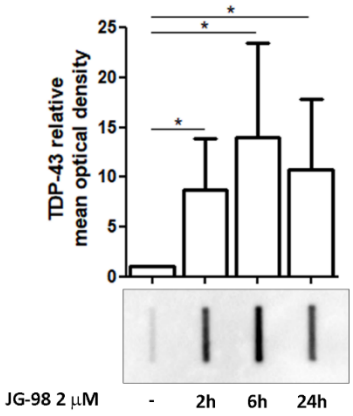

Figure 71. Representative FTA analysis of the total RIPA protein extract of cells treated with JG-98 2 µM for 2, 6 and 24 hours and relative optical quantification. (n=3) (p <0,05, unpaired one-tailed t test)*

These data were also confirmed by WB analysis in Fig. 72. Indeed, JG-98 treatment induced an increase in oligomeric but still soluble TDP species and the appearance of insoluble high molecular weight species. Moreover, treatment induced an accumulation of the insoluble TDP-43 monomer and a reduction of soluble TDP-35 fragment.

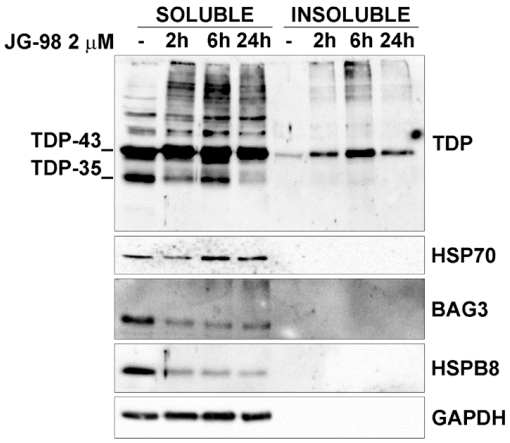

Figure 72. Representative WB analysis of RIPA soluble and insoluble fractions of the total RIPA protein extract of the cells treated with JG-98 2 μM for 2, 6 and 24 hours.

Knowing that TDP-43 is usually located in the nucleus, but aberrantly mislocalizes in the cytoplasm in disease condition, I evaluated whether JG-98 treatment induced an aggregation of TDP-43 at the nuclear level or at the cytoplasmic level.

To do this, the nuclear and the cytoplasmic fractions of treated and untreated cells were separated and protein extracts were analysed through WB analysis using antibodies directed against TDP-43 and the CASA-complex members HSP70, BAG3 and HSPB8 (Fig. 73).

The results showed in all treated samples, compared to untreated control, an increase of TDP-43 high molecular weight forms in the nucleus and in the cytosol, already after 2 hours of treatment but with a peak at 6 hours of treatment (Fig. 73 B and E). These species were different in the two compartments. Moreover, in treated cells there was a significant decrease of the full length TDP-43 in both fractions (Fig. 73 C and F), and a significant decrease of the TDP-35 fragment in the cytosol at 24 hours of treatment (Fig. 73 G).

Regarding CASA-complex members HSP70, BAG3 and HSPB8, they were detected only in the cytosolic fraction. A significant decrease in HSPB8 immunoreactivity was observed after 24 hours of treatment (Fig. 73 I), instead, JG-98 treatment caused the formation of high molecular weight forms of both HSP70 and BAG3.

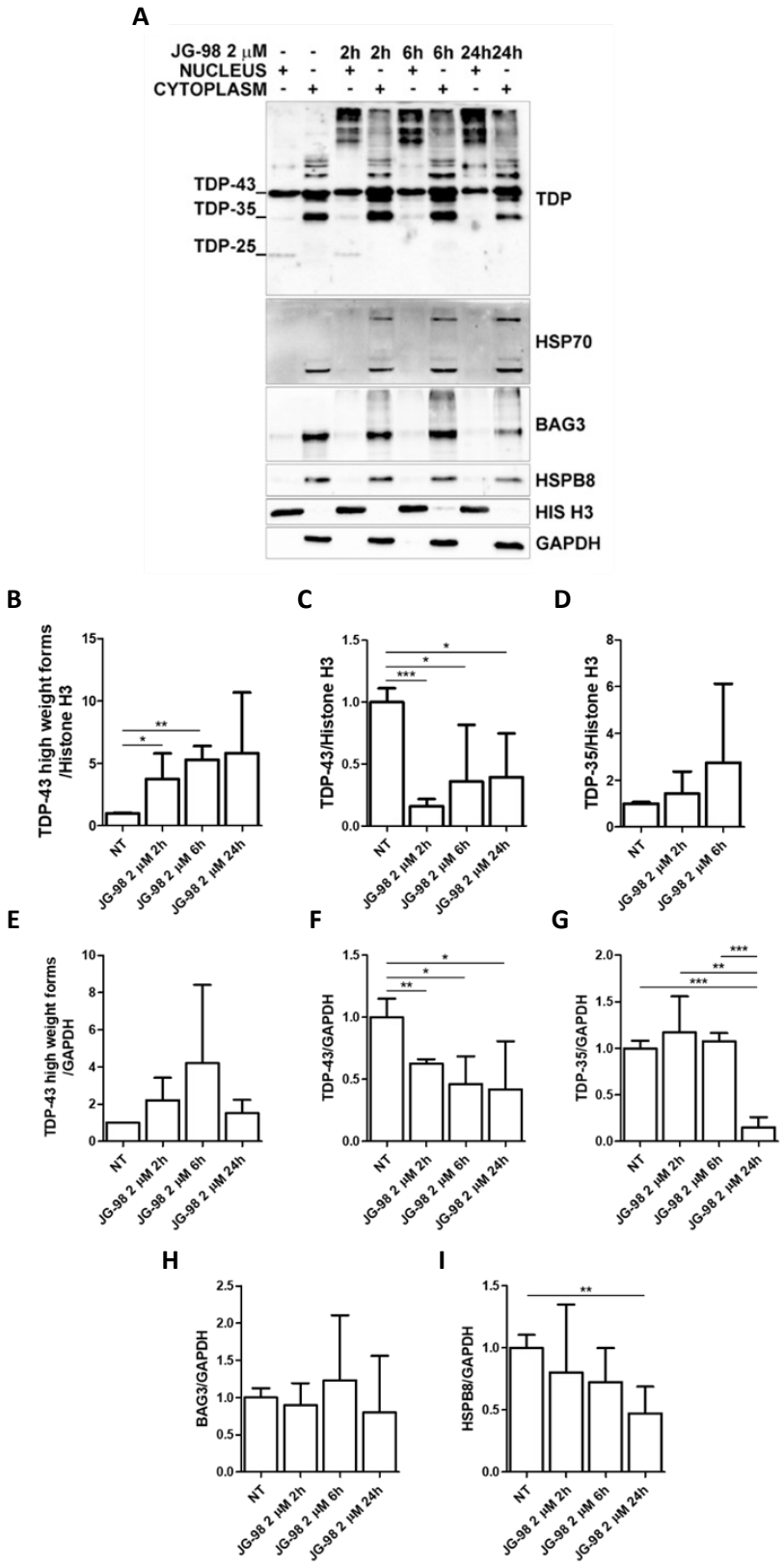

Figure 73. Representative WB analysis (A) and relative quantifications of the nuclear (B-D) and cytoplasmic (E-I) extracts of cells treated or not with JG-98 2μM for 2, 6 and 24 hours. GAPDH and histone H3 were used as loading controls for cytoplasmic and nuclear fractions, respectively. Bar graphs represent the mean optical density ± SD of the protein in analysis normalized on the optical density of the housekeeping protein and expressed as relative to the corresponding untreated samples. (n=3). (p <0,05, ** p <0,01; *** p <0,001, unpaired one-tailed t test)*

Finally, I evaluated the effect of CASA-complex blockage to the secretion of TDP species in EVs. To this purpose, LEVs and SEVs were isolated from NSC34 cells treated or not with JG-98 compound for 24 hrs and RIPA protein extracts analysed by WB (Fig. 74).

Interestingly, JG-98 treatment caused an increase in the secretion of all monomeric TDP species (TDP-43, TDP-35 and TDP-25), both in LEVs, but particularly in SEVs. Moreover, vesicles released by treated cells were also enriched in HSPB8, and, on the contrary, showed lower levels of BAG3 and HSP70, compared to vesicles of untreated cells. These data suggest that the secretion of TDP species in EVs could be mediated by the chaperone HSPB8 but independently from the CASA-complex.

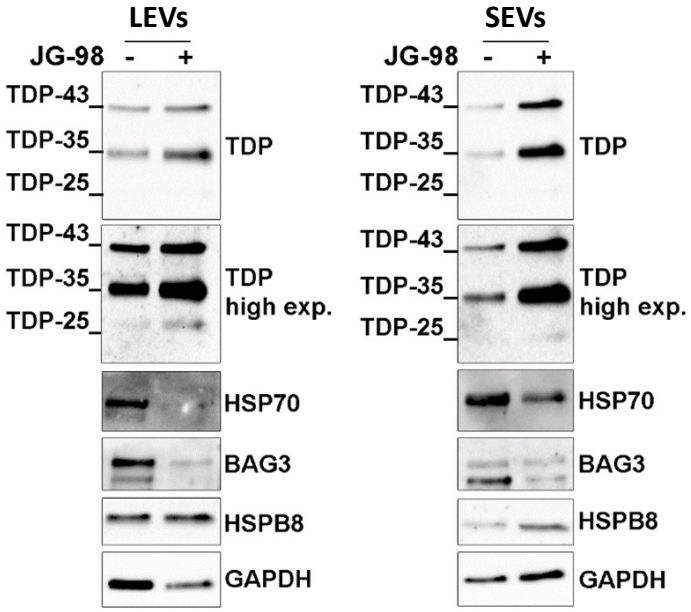

Figure 74. Representative WB analysis of LEVs and SEVs total RIPA protein extract analysed for TDP, HSP70, BAG3 and HSPB8

DISCUSSION

ALS ad FTD are two NDs characterized by an overlapping clinical spectrum and shared neuropathological features. The main common pathological hallmark is the presence of toxic cytoplasmic aggregates containing insoluble aggregated forms of TDP-43 and its CTFs TDP-35 and TDP-25, in affected cells.

Several studies have shown that the formation of TDP-43-positive cytoplasmic aggregates is mediated by aberrant PTMs, in particular TDP-43 cleavage, that results in the formation of aggregation-prone TDP-35 and TDP-25 fragments. Notably, the accumulation of these fragments increases following PQC blockade, that is a common condition observed in these diseases (Huang et al., 2014). Under physiological conditions, in fact, through the action of different chaperone and co-chaperone proteins, cells prevent aggregates formation by directing TDP-43 and its CTFs to the degradation via proteasome and autophagy (Huang et al., 2014; Scotter et al., 2014; X. Wang et al., 2010). An important role in this context is played by the chaperone protein HSP70, its partner CHIP and its co-chaperones BAG1 and BAG3. Indeed, HSP70, together with its partner CHIP can interact with BAG1 inducing the degradation of TDP species via proteasome, or with BAG3/HSPB8 forming the CASA complex, involved in protein degradation via autophagy (Cicardi et al., 2018; Crippa, Cicardi, et al., 2016). When misfolded proteins accumulate and proteasome is overwhelmed, CASA complex is triggered as a compensatory mechanism to drive substrates to autophagy for degradation (Crippa et al., 2010). Interestingly, HSP70 is also normally secreted by cells into EVs (Théry et al., 2018) and BAG3 has been found involved in the recognition and loading of EVs cargo (Diaz-Hidalgo et al., 2016), suggesting a possible role of these proteins also in the disposal of misfolded proteins via the secretory pathway. Indeed, the EVs release of misfolded proteins has been observed for several NDs-related proteins, including TDP-43 and its CTFs (Iguchi et al., 2016; Sproviero et al., 2018), and it may represent another mechanism for proteostasis surveillance, that works together with the intracellular PQC system.

Therefore, during my PhD I investigated the role of EVs in the secretion of TDP-43 and its neurotoxic CTFs, the interplay between EVs and PQC, and the possible role of the CASA complex in this process. I analysed both SEVs for which TDP-43 secretion has already been

described (Iguchi et al) and LEVs, since their involvement in TDP-43 trafficking has been little considered so far. For these purposes, I analysed EVs released by immortalized motor neuronal (NSC34) and myoblast (C2C12) cells and FTD and control plasma-derived LEVs and SEVs.

The results obtained showed that LEVs and SEVs isolated from the culture medium of the NSC34 cells through differential ultracentrifugation method are two distinct vesicular populations characterized by different sizes (the large ones are larger than the small) and enriched in different vesicular markers. The results also showed that in physiological conditions EVs contain mainly the insoluble forms of both TDP-43 and its CTFs, which, on the contrary, are almost absent in the secreting cells, suggesting that the secretory pathway plays a relevant role in the disposal of the insoluble TDP-43 species normally formed in cells in basal conditions (Casarotto et al., 2022).

Further analyses demonstrated the presence of several PQC members, including HSP70, CHIP, BAG3, HSPB8, SQSTM1/p62 and MAP1LC3B (I and II), within both LEVs and SEVs released by NSC34 cells (Casarotto et al., 2022). The presence of all CASA proteins in EVs suggests that the CASA-complex may play a role in addressing TDP species within both LEVs and SEVs. The insertion into SEVs might be associated with MAP1LC3B-II anchored to the MVBs membrane, which specifically recognizes cargoes to be secreted via the LDELS selective type of secretion (Delorme-Axford & Klionsky, 2020; Leidal et al., 2020). In the case of LEVs, the secretion might be driven by HSPB8, which can bind the inner leaflet of the plasma membrane (Chowdary et al., 2007).

Following these observations, I investigated the possible crosstalk between the PQC system and EVs in the secretion of TDP-43 and its CTFs, by selectively inhibiting UPS, autophagy or both degradative systems in NSC34 cells and analysing the effects on EVs. First of all, I confirmed that the proteasome has an important role in the disposal of the full length TDP-43 and its blockade, through MG132 treatment, causes an increase in the intracellular expression of HSPB8/BAG3. This suggests that the CASA-complex is mainly activated as a compensatory mechanism for the disposal of the insoluble TDP species (Cicardi et al., 2018; Crippa et al., 2010). Moreover, the data obtained by analysing the protein content of MG132 treated cells and their relative EVs (both LEVs and SEVs) showed that the proteasome inhibition also causes a reduction in the intracellular protein levels of the TDP-

35 and TDP-25 fragments that, on the contrary increase in the LEVs together with the proteins HSPB8, BAG3 and MAP1LC3B-I (Casarotto et al., 2022). These results indicate that, when the proteasome is blocked, the CASA-complex could target TDP insoluble toxic species not only to autophagy but also to the EVs. The autophagy blockade, instead, showed no changes in the TDP content of neither cells nor EVs, confirming that TDP species, when the proteasome works properly, are mainly degraded by it. In these conditions, only an increase in p62 in LEVs and SEVs and MAP1LC3-II in SEVs was observed, probably due to their intracellular accumulation, caused by the inhibition of the autophagosome-lysosome fusion by the treatment with NH4Cl (Casarotto et al., 2022). Taken together these results suggest that LEVs cooperate with autophagy to reduce the cytoplasmic accumulation of the insoluble TDP species caused by the proteasome blockade.

Moreover, the analysis of the EVs protein content obtained following the overall blockade of the PQC system (the inhibition of proteasome and autophagy together) showed the decrease in TDP-35 and TDP-25 fragments in cells and their increase in LEVs, together with the CASA-complex members HSPB8-BAG3 and also MAP1LC3B-II, demonstrating that in motor neuronal cells LEVs can compensate not only the proteasome system but also the autophagy in the disposal of TDP species (Casarotto et al., 2022). Indeed, CASA-complex has been proven to have a relevant role in the disposal of the TDP-25 fragment when the UPS is blocked (Cicardi et al., 2018; Crippa, Cicardi, et al., 2016). Therefore, the increased secretion of the TDP-25 fragment in LEVs, when also autophagy in blocked, suggests that CASA-complex may re-route substrates to LEVs to compensate the autophagy inhibition.

Parallel to the increase in the content of TDP-35, TDP-25, HSPB8 and BAG3, the NTA analysis of LEVs obtained from MG132-treated cells and from cells in which the proteasome and autophagy were blocked together showed that, in these conditions, cells not only secrete a larger amount of disease-associated proteins, but also a larger number of LEVs. However, since the treatment with MG132 could induce apoptosis and since it has been observed that the LEVs have sizes that could partially overlap those of the apoptotic bodies (50-5000 nm in diameter) (Kakarla et al., 2020), the increase in the number of secreted LEVs could also be attribute to an increased number of similarly sized apoptotic bodies secreted by cells in these conditions.

The interplay between PQC and EVs in the disposal of misfolded species in NSC34 cells was further confirmed by the presence within EVs of the co-chaperone protein CHIP (an E3 ubiquitin ligase protein involved in client substrate ubiquitylation and degradation by the proteasome), the protein p62 (a selective autophagy receptor involved in sorting ubiquitinated substrates for lysosome-mediated degradation), and ubiquitinated-proteins. Indeed, EVs released by NSC34, in particular SEVs, under physiological conditions, contain several poly- and K63-ubiquitinated proteins (Huebner et al., 2016). This result is in line with proteomics analysis conducted by Huebner and colleagues that showed that 15% of the over 6000 proteins identified in SEVs are ubiquitinated, both with K63-linkage (51.2%) and to a lesser extent with K48-linkage (Huebner et al., 2016). The slight increase of K63-ubiquitinated proteins in SEVs observed following autophagy blockade conditions in NSC-34 cells, suggests that the protein sorting to SEVs could be controlled by K63-linked chains. However, since no differences was observed in K63-ubiquitinated proteins released in EVs under proteasome blockade (the condition that most affected EVs protein cargo in NSC34 cells), it cannot be excluded that other types of ubiquitination, not yet analysed, may be involved in EVs protein sorting.

The analysis of the EVs obtained from plasma of FTD patients supported the hypothetical compensatory mechanism between PQC and EVs. Indeed, the presence of the toxic fragment TDP-35 was observed only in EVs obtained from FTD patients, also suggesting that TDP-35 might represent a good biomarker for FTD. Moreover, the full length TDP-43 and the CASA-complex members HSP70, BAG3 and HSPB8 were found within both LEVs and SEVs of both FTD-derived EVs and those of healthy volunteers, with no significant difference for BAG3 and HSPB8. Instead, HSP70 level were higher in FTD-derived LEVs compared to the controls (Casarotto et al., 2022), supporting previous observation showing that HSP70 secretion increased in EVs derived from AD and FTD patients during disease progression (Chanteloup et al., 2019).

Following these observations, since ALS is a disease that involves several types of cells, including muscle cells, I evaluated TDP secretion and the interplay between EVs and PQC in C2C12 myoblasts.

The data showed that muscle cells are also able to secrete the TDP species and in particular the TDP-35 fragment inside the EVs, both LEVs and SEVs. However, unlike neuronal cells, in

muscle cells the contribution of autophagy and in particular of CASA-complex in the degradation of TDP species seems more relevant (Arndt et al., 2010; Cicardi et al., 2018; Galbiati et al., 2014). Indeed, data showed that the proteasome blockade, in these cells, did not cause an increase in the secretion of TDP species, neither in LEVs nor in SEVs. This probably because autophagy alone can counteract the accumulation of TDP-43 species deriving from proteasome inhibition. In contrast, inhibition of autophagy was associated with an increased secretion of TDP species and CASA complex components primarily within SEVs. This effect is probably due to the inhibition of the MVBs-autophagosome-lysosome fusion and the consequent increased fusion of MVBs with the plasma membrane. The presence of the CASA-complex members in these vesicles also showed that the possible CASA-complex-mediated TDP secretion is not only an NSC34 cells-specific mechanism but that it is also shared by other cell types.

Finally, the silencing of HSPB8 or BAG3 in NSC34 cells, showed that HSPB8 but not BAG3 is critical for the removal of TDP-35 fragments from cells. Indeed, the results showed that the silencing of HSPB8 but not BAG3 causes the increase of the TDP-35 fragment in cells. This accumulation is not observed when PQC system is inhibited. These results suggested that HSPB8, but not BAG3 is necessary for directing toxic TDP species in EVs, in pathological conditions. HSPB8, in fact, whose expression resulted increase after the inhibition of the PQC system also in HSPB8 knockout cells, but not BAG3, was able to revert the intracellular protein levels of TDP-35 to the basal condition, even if the autophagy was blocked, suggesting that HSPB8 can effectively promote the disposal of the TDP-35 fragment within EVs.

This hypothesis was confirmed by blocking the assembly of the CASA-complex, with the HSP70 allosteric inhibitor JG-98. Indeed, JG-98 treatment causes an intracellular increase of the insoluble and high molecular weight forms of TDP-43, parallel to that observed in several studies following HP70 inhibition (Arosio et al., 2020; Kitamura et al., 2018), but a decrease in the TDP-35 and TDP-25 fragments. The treatment also causes a decrease of the monomeric forms of HSPB8, HSP70 and BAG3, and a formation of high molecular weight forms of both HSP70 and BAG3, but not HSPB8. Notably, both LEVs and SEVs obtained from JG-98 treated cells compared to those obtained from the untreated ones, are enriched in TDP-35 and TDP-25 fragments and HSPB8 but decreased in HSP70 and BAG3. Taken

together these data indicate that the insertion of TDPs into EVs may occur independently from the formation of the CASA-complex but may be mediated by HSPB8 alone. In this context, HSPB8, after recognizing and binding misfolded TDPs, could directly mediate their insertion into EVs thanks to its ability to bind to lipid membranes (Chowdary et al., 2007).

In conclusions, data support the hypothesis that HSPB8 can also act alone in the secretion of TDP species through EVs, representing an additional protective mechanism, which can be potentiated by the block and/or the improper function of HSP70 and BAG3.

CHAPTER 2: PQC INHIBITION AND ITS EFFECT ON EVs miRNAs CARGO

AIMS

TDP-43 is an RNA binding protein that plays several roles in the RNA metabolism (Buratti & Baralle, 2010). In particular, it facilitates miRNA biogenesis interacting with both Drosha and Dicer complexes in the nucleus and in the cytoplasm, respectively (Buratti & Baralle, 2010; Kawahara & Mieda-Sato, 2012). However, in ALS and FTD TDP-43 mislocalizes from the nucleus to the cytoplasm and aberrantly accumulates within insoluble cytoplasmic aggregates (Afroz et al., 2019; François-Moutal et al., 2019). This prevents it from interacting with Drosha and Dicer complexes thus causing an altered production of those miRNAs whose biogenesis is regulated by it (Buratti & Baralle, 2010; Butti & Patten, 2019; Hawley et al., 2020). For this reason, the abnormal miRNAs metabolism is considered a distinctive feature of ALS and FTD (Emde et al., 2015).

However, the alteration of miRNAs production also causes an alteration in miRNAs secreted by the affected cells. In fact, the deregulation of specific circulating miRNAs has been recently proposed to represent an effective biomarker of disease (Cloutier et al., 2015; Magen et al., 2021; Ravnik-Glavač & Glavač, 2020; Tasca et al., 2016).

As like as the proteins, miRNAs can be secreted into the plasma as free miRNAs or within the EVs (both LEVs and SEVs) and can be picked up by recipient cells by altering specific intracellular pathways, thus contributing to the spreading of the disease.

Interestingly, the secretion of miRNAs within EVs could be mediated also by several RNA binding proteins, including TDP-43 (Fabbiano et al., 2020; Groot & Lee, 2020). Therefore, since I observed in the previous chapter that EVs contain TDP-43 species and that the PQC inhibition alters their secretion, using EVs obtained from the same immortalized neuronal cell line, first I evaluated which miRNAs are physiologically secreted in LEVs and SEVs and which are the pathways targeted by them. Then, I evaluated whether the inhibition of proteasome through MG132 and autophagy through NH_4Cl could also cause a deregulation in their miRNAs content and which are the most enriched pathways targeted by miRNAs deregulated in these conditions.

RESULTS

LEVs AND SEVs VESICLES HAVE A DIFFERENT miRNAs PROFILE

The aberrant RNA metabolism is a common condition observed in many NDs, including ALS and FTD, and it has been observed that the miRNA profiles of LEVs and SEVs obtained from patients affected by different NDs are different (Sproviero et al., 2021). miRNAs are targeted to the EVs by means of RNA binding proteins, like TDP-43. As shown before, I observed that PQC inhibition, a common ALS and FTD feature, causes an increase in the secretion of the TDP species within the EVs. Therefore, it was interesting to understand whether PQC modulation could also influence EVs miRNAs content.

For this purpose, EVs have been isolated from the culture medium of NSC34 treated or not with proteasome (MG132) or autophagy (NH_4Cl) inhibitors and characterized through NTA, TEM and WB analysis. Then, to evaluate possible changes in the gene expression and pathways involvement, miRNAs have been extracted from LEVs and SEVs and analysed in collaboration with the Mondino Foundation of Pavia and the Sacco hospital of Milan. A bulk RNA-Seq was performed by comparing the transcriptome profiles of LEVs and SEVs obtained from untreated NSC34 cells or from cells treated with NH_4Cl and MG132. To investigate the gene expression and pathway involvement, differential expression analysis for miRNAs was performed using R package DESeq2 (Love et al., 2014). miRNAs were considered as differentially expressed and retained for further analysis with $|\log_2 FC| \geq 1$ and False Discovery Rate (FDR) ≤ 0.1. miRNAs pathways analysis was performed on DIANA-mirPath v3.0 (https://dianalab.e-ce.uth.gr/html/mirpathv3/index.php?r=mirpath) (Vlachos et al., 2015). miRNA-targets TarBase and TargetScan, and the KEGG pathways targeted by the most deregulated miRNAs observed in the different conditions have been analysed.

The characterization analysis of LEVs and SEVs obtained from the untreated NSC34 cells, confirmed the separation of the two populations of EVs. Indeed, as we can observed in the representative NTA, TEM and WB analysis showed in the Fig. 75, LEVs were bigger than the SEVs and enriched in Int. β1, while SEVs were smaller and enriched in Alix and Histone H3.

The RNA-Seq analysis highlighted 90 differentially expressed miRNAs (Table 3) (77 out of 90 resulted upregulated while 13 out of 90 downregulated) in SEVs compared to LEVs obtained from untreated NSC34 cells used as controls in the assay. The principal component analysis (PCA) of differentially expressed miRNAs in the two conditions showed a clear separation between the two groups as shown in panels D and E of Figure 75. They formed two well-separated clusters. This is confirmed also observing the expression profiles reported in the Heatmap showed in the figure 75 E.

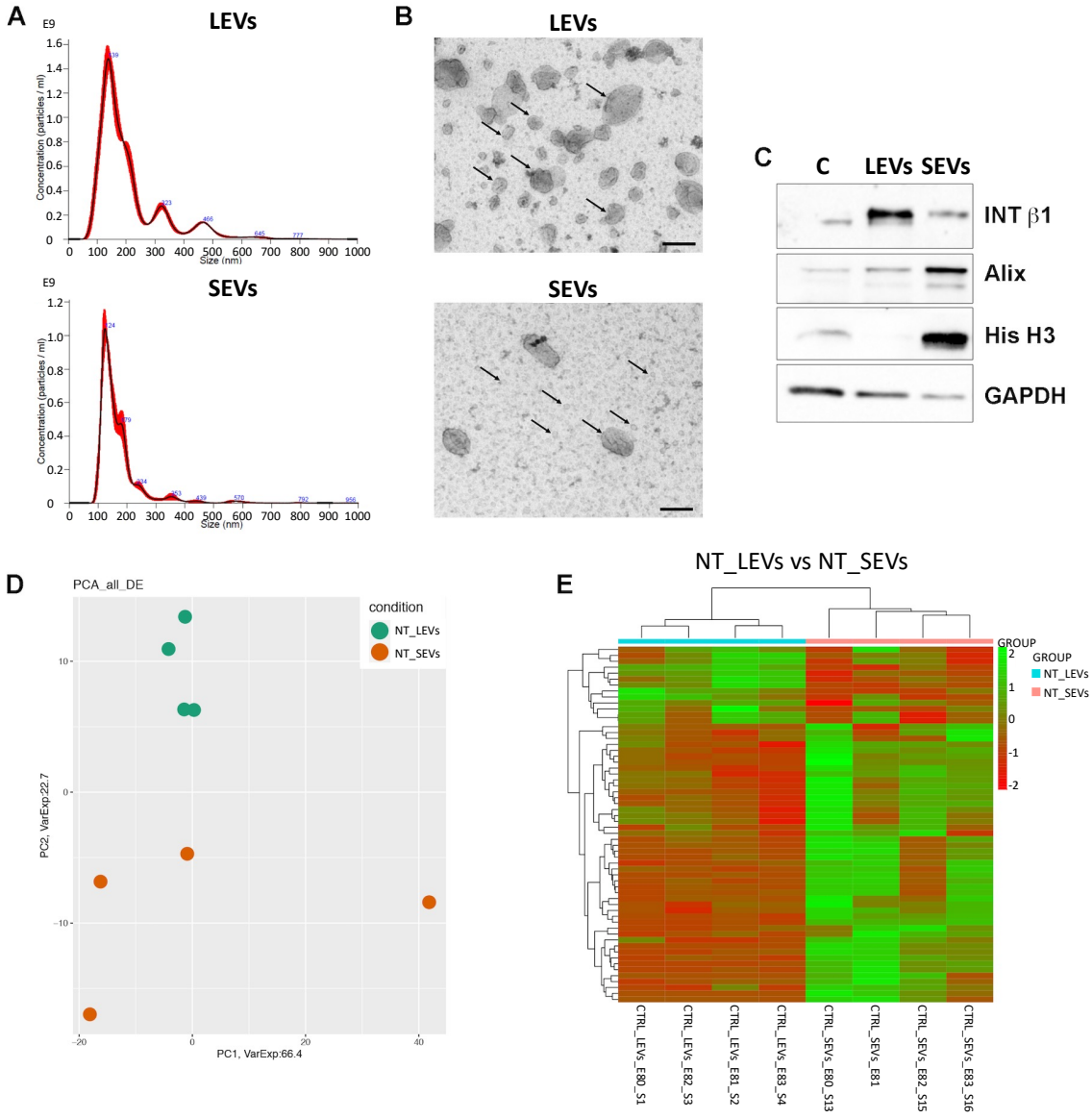

Figure 75. NSC34-derived LEVs and SEVs are enriched in different miRNA profiles. Representative NTA analysis (x-axis = vesicles size expressed in nm; y-axis = vesicles concentration, expressed as number of particles/ml) (A), TEM (scale bar: 200 nm) (B) and WB (Int. β1 used as LEVs marker, Alix and His H3 used as SEVs markers) analysis (C) of NSC34-derived LEVs and SEVs. Principal component analysis (PCA) (D) and Heatmap (E) of the miRNAs differentially expressed in LEVs vs SEVs.

Moreover, the KEGG pathways analysis (Table 4 and 5) of gene targeted by the differentially expressed miRNAs in LEVs vs SEVs highlighted an alteration in several pathways but especially “Fatty acid metabolism”, “Prion diseases”, “Proteoglycans in cancer”, “FoxO signaling pathway”, “Thyroid hormone signaling pathway”, “Adherens junction”, “Fatty acid degradation”, “Valine, leucine and isoleucine degradation”, “GABAergic synapse2, “Morphine addiction”, “Nicotine addiction”, “Mucin type O-Glycan biosynthesis”, “Biosyntesis of unsatuerd fatty acids”, “Long-term depression”, “Glycosphingolipid biosynthesis – ganglio series”, (Table 4-5 and Figure 76).

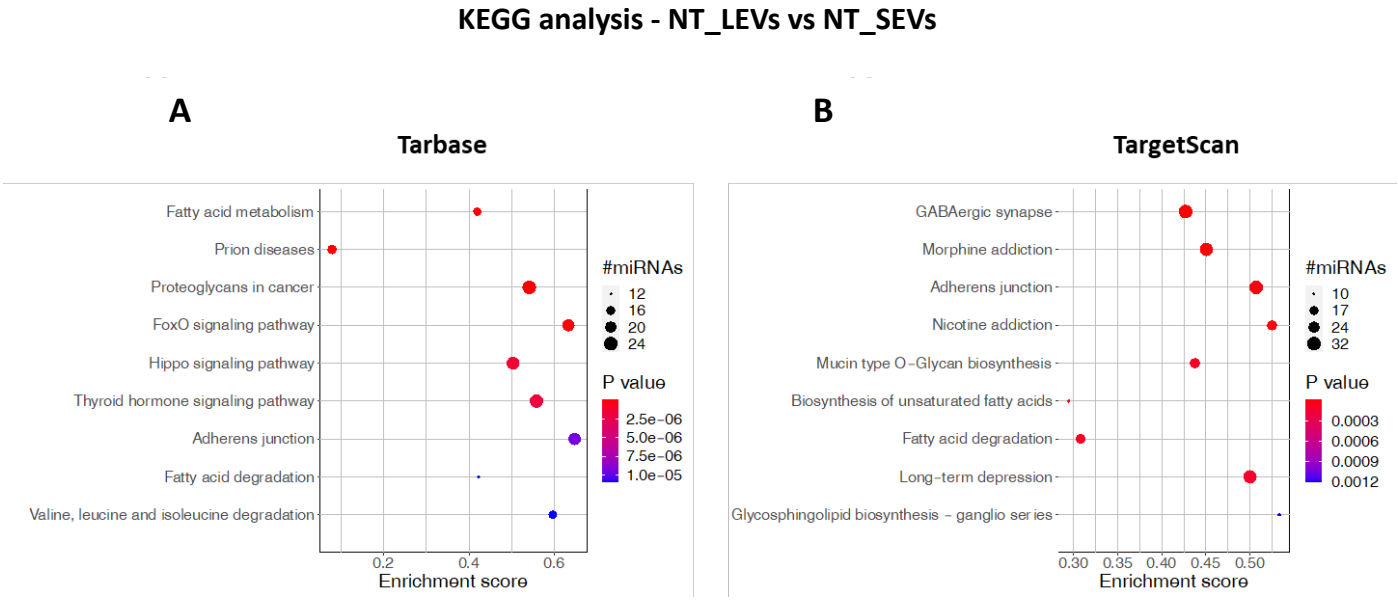

Figure 76. KEGG pathways analysis for deregulated miRNA in LEVs compared to SEVs. In the dot plots, y-axis represents the name of the pathway, the x-axis represents the Rich factor, dot size represents the number of miRNAs and the color indicates the adjusted p-value.

EVs OBTAINED FROM TREATED CELLS CONTAIN DIFFERENTIALLY EXPRESSED miRNAs

After the characterization of the miRNA content of the EVs released by NSC34 cells in physiologic conditions, the same analysis was performed on EVs (both LEVs and SEVs) obtained from the NSC34 cells treated with MG132 or NH_4Cl.

As shown in the figure 77, the untreated and MG132-treated-derived LEVs and SEVs were different in size (with a peak at 140 and 120 nm in diameter respectively) and showed the enrichment of different specific vesicular markers (Int. β1 for the LEVs and Alix and Histone H3 for the SEVs); while the NH_4Cl-derived LEVs and SEVs, despite the enrichment of Int. β1 for the LEVs and Alix and Histone H3 for the SEVs, were characterized by an almost overlapping dimensional profile with vesicles of less than 114 nm in diameter in the LEVs sample and more SEVs in the range of 150-300 nm in diameter.

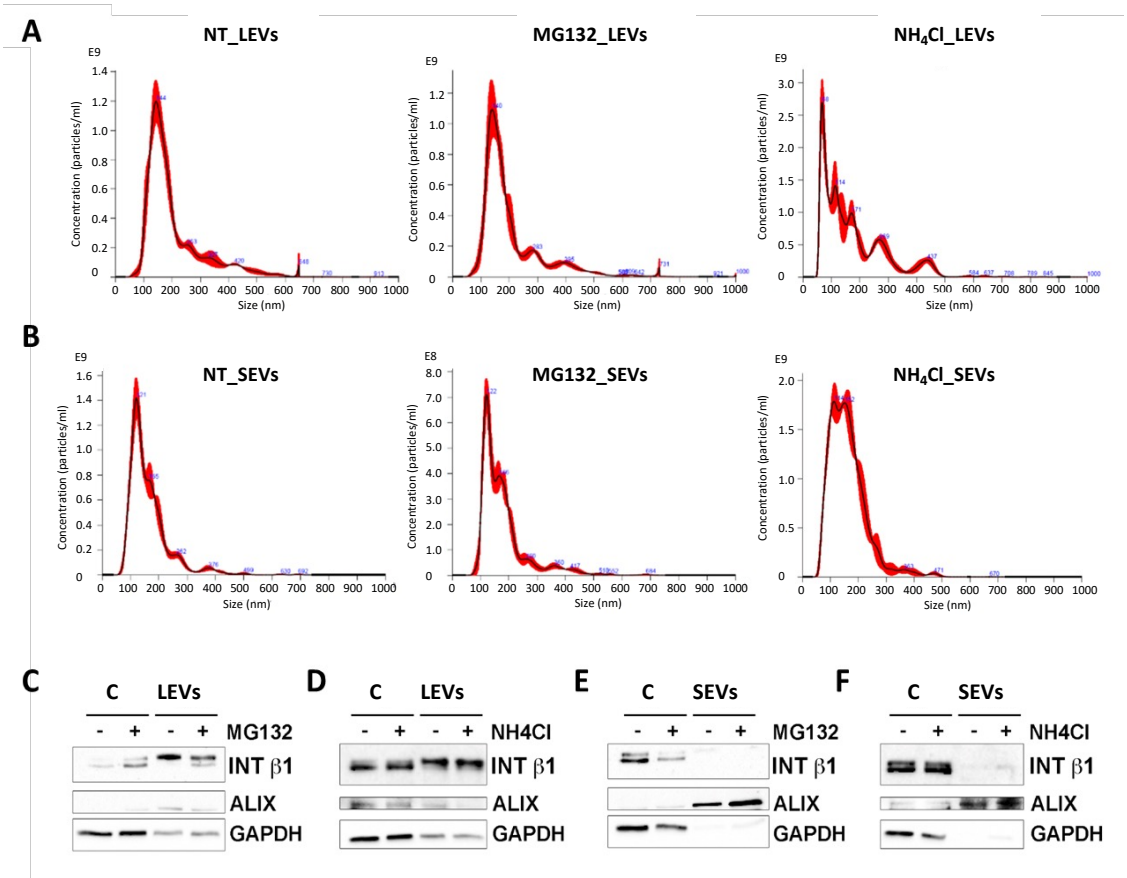

Figure 77. Characterization of LEVs (A,C,D) and SEVs (B,E,F) obtained from untreated and MG132 (10 μM)- or NH_4Cl (20 mM)-treated NSC34 cells. Representative NTA analyses (A,B) (x-axis = vesicles size expressed in nm; y-axis = vesicles concentration, expressed as number of particles/ml) and WB analysis (C,D,E,F) (Int. β1 used as LEVs marker, Alix and His H3 used as SEVs markers) of LEVs and SEVs obtained from untreated and treated (MG132 or NH_4Cl) NSC34 cells.

miRNAs content of LEVs and SEVs was then analysed through RNA-Seq analysis. First, the miRNAs content of LEVs obtained from the NSC34 cells treated with MG132 (MG132_LEVs) or NH_4Cl (NH_4Cl_LV) was compared to that of LEVs released by untreated cells (NT_LEVs). PCA analysis (Fig. 78 A) showed that only the MG132_LEVs clustered differentially from the NT_LEVs. In particular, the miRNAs differential expression analysis for the LEVs (Table 6) (NT_LEVs, MG132_LEVs), highlighted 7 differentially expressed miRNAs (3 upregulated and 4 downregulated), when considering MG132_LEVs compared to NT_LEVs, while no differentially expressed miRNAs in NH_4Cl_LEVs compared to NT_LEVs were observed.

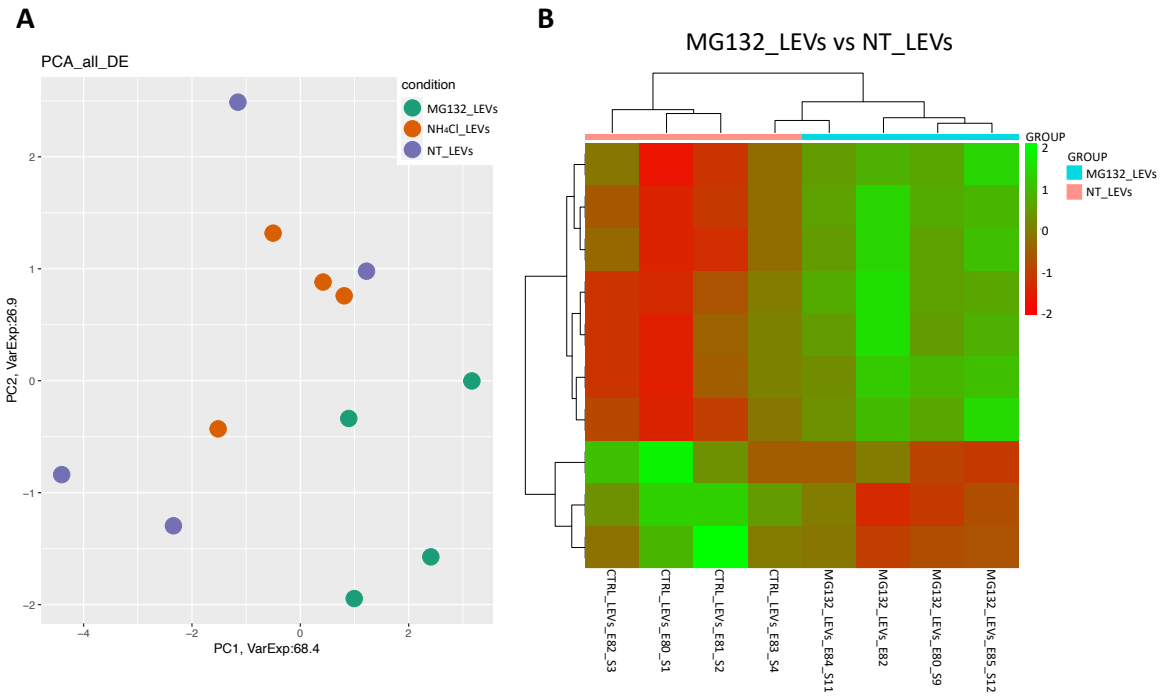

Figure 78. PCA of differentially expressed miRNAs present in NT_LEVs, MG132_LEVs and NH_4Cl_LEVs and heatmap of the miRNA differentially expressed in MG132_LEVs vs NT_LEVs. It was considered as differentially expressed only miRNA showing |log2(disease sample/healthy donor)| ≥ 1 and a False Discovery Rate ≤ 0.1). in the PCA, NT_LEVs was represented with purple dots, MG132_LEVs with green dots and NH_4Cl_LEVs with orange dots

Given these observations, I analysed which pathways was mainly targeted by the miRNAs differentially expressed in MG132_LEVs compared to the NT_LEVs. The results obtained by the analysis of the KEGG pathways on gene targets, analysed through Tarbase (Table 7) and TargetScan (Table 8), showed that the most top 8 up and down-regulated pathways targeted by these deregulated miRNAs were “Lysine degradation”, “Proteoglycans in cancer”, “HIF-1 signaling pathway”, “Renal cell carcinoma”, “Adherens junction”, “Central carbon metabolism in cancer”, “Thyroid hormone signaling pathway”, “Endocytosis”, “Focal adhesion” and “Pathways in cancer”, “Fatty acid degradation”; “Mucin type O-glycan biosynthesis”, “Glycosphingolipids biosynthesis – lacto and neolacto series”, “Propanoate metabolism” “Fatty acid metabolism”, “Valine, leucine and isoleucine degradation”, “Metabolic pathways”, “Valine, Leucine and isoleucine biosynthesis”, (Fig. 79).

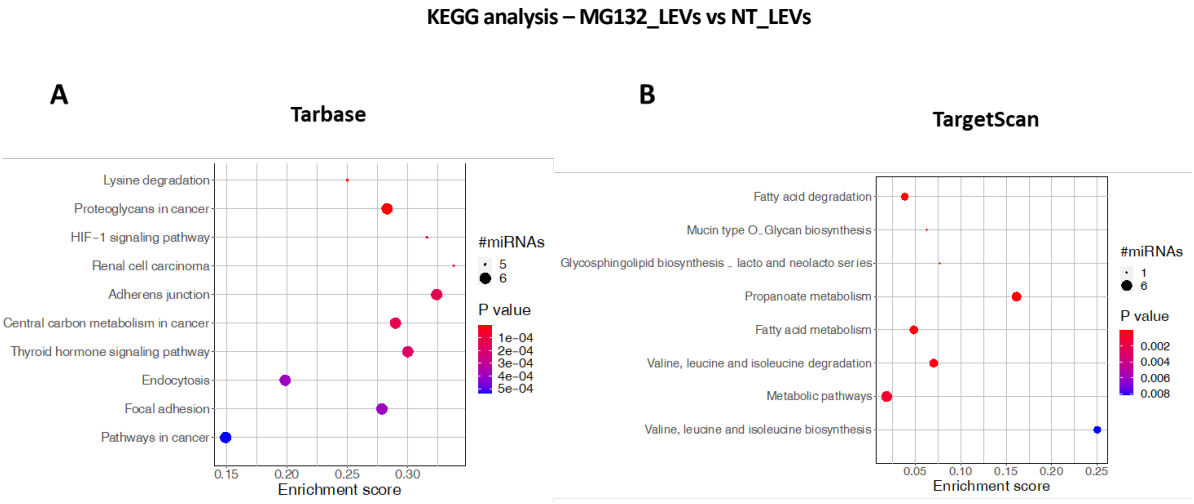

Figure 79. KEGG pathways analysis for deregulated miRNA present il MG132_LEVs compared to NT_LEVs. In the dot plots, y-axis represents the name of the pathway, the x-axis represents the Rich factor, dot size represents the number of miRNAs and the color indicates the adjusted p-value.

Then I performed the same analysis also for the SEVs obtained from the NSC34 cells untreated (NT_SEVs) and treated with MG132 (MG132_SEVs) or NH_4Cl (NH_4Cl_SEVs). In this case, as we can observe from the PCA showed in the figure 80, the miRNAs content of both the MG132_SEVs and the NH_4Cl_SEVs was different from that of the NT_SEVs. Indeed, by analysing the miRNAs present in SEVs obtained from both treated and untreated cells, I observed that 82 (23 upregulated and 59 downregulated) were differentially expressed in MG132_SEVs compared to NT_SEVs (Table 9) and 66 (17 upregulated and 49 downregulated) were differentially expressed in NH_4Cl_SEVs compared to NT_SEVs (Table 10).

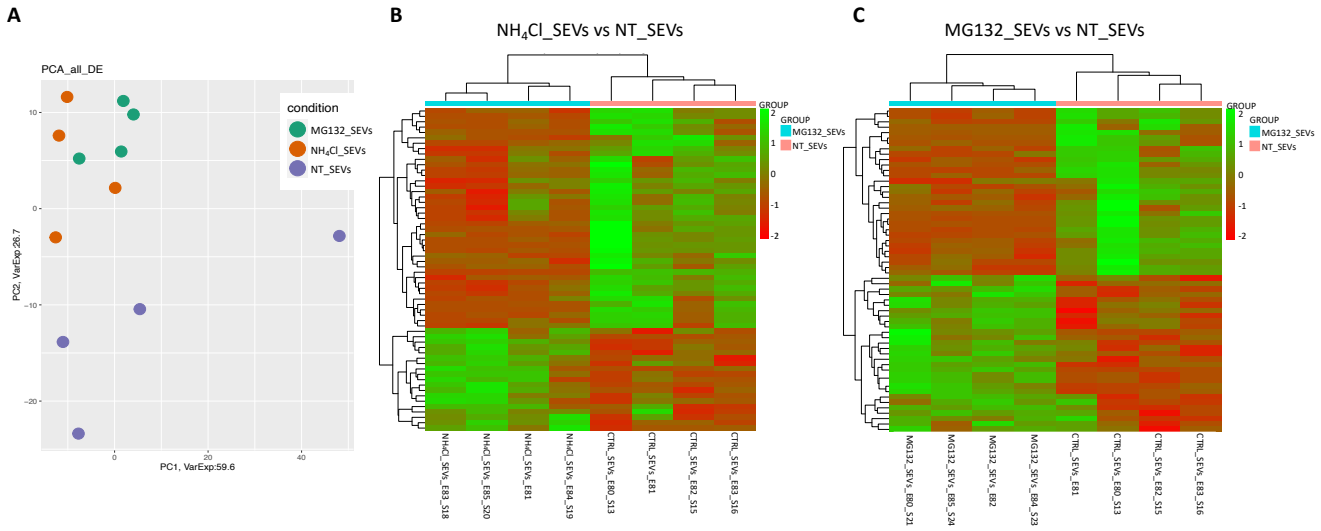

Figure 80. PCA of differentially expressed miRNAs present in NT_SEVs, MG132_SEVs and NH_4Cl_SEVs (A) and heatmaps of the miRNA differentially expressed in NH_4Cl_SEVs vs NT_SEVs (B) and of those differentially expressed in MG132_SEVs vs NT_SEVs (C). It was considered as differentially expressed only miRNA showing $|log2(disease\ sample/healthy\ donor)| \geq 1$ and a False Discovery Rate ≤ 0.1). In the PCA, NT_SEVs are represented with purple dots, MG132_SEVs with green dots and NH_4Cl_SEVs with orange dots

I analysed the KEGG pathways targeted by deregulated miRNAs (always using the database Tarbase and TargetScan) (Table 11-13 and 12-14) and I observed that among the top 10 up and down-regulated pathways targeted by miRNAs differentially expressed in the NH_4Cl_SEVs compared to the NT_SEVs there were “Prion disease”, “Proteoglycans in cancer”, “Thyroid hormone signaling pathway”, “Renal cell carcinoma”, “FoxO signaling pathway”, “N Glycan biosynthesis”, “Protein processing in endoplasmic reticulum”, “Hippo sugnaling pathway”, “Glioma”, “Endocytosis”, “Mucin type O-Glycan biosynthesis”, “GABAergic synapse”, “Other types of O-glycan biosynthesis”, “Nicotine addiction”, “Biosynthesis of unsatured fatty acids”, “Cell adhesion molecules (CAMs)”, “Pathways in cancer”, “Rap1 signaling pathway”, “Fatty acid degradation” (Fig. 81 A, Table 11-12); while among the top up and down-regulated pathways targeted by the miRNAs differentially expressed in the MG132_SEVs compared to the NT_SEVs (Fig. 81 B, Table 13-14) there were “Fatty acid metabolism”, “prion disease”, “FoxO signaling pathway”, “Proteoglicans in cancer”, “Protein processing in endoplasmic reticulum”, “Hippo signaling pathway”, “Renal cell carcinoma”, “Cell cycle”, “Thyroid hormone signaling pathway”, “Fatty acid degradation”, “Fatty acid biosynthesis”, “ECM-receptor interaction”, “Biosynthesis of unsatured fatty acids”, “Fatty acid metabolism”, “Nicotin addiction”, “Proteoglycans in cancer”, “Mucin type O-Glycan biosynthesis”, “GABAergic synapse”, “Axon guidance”.

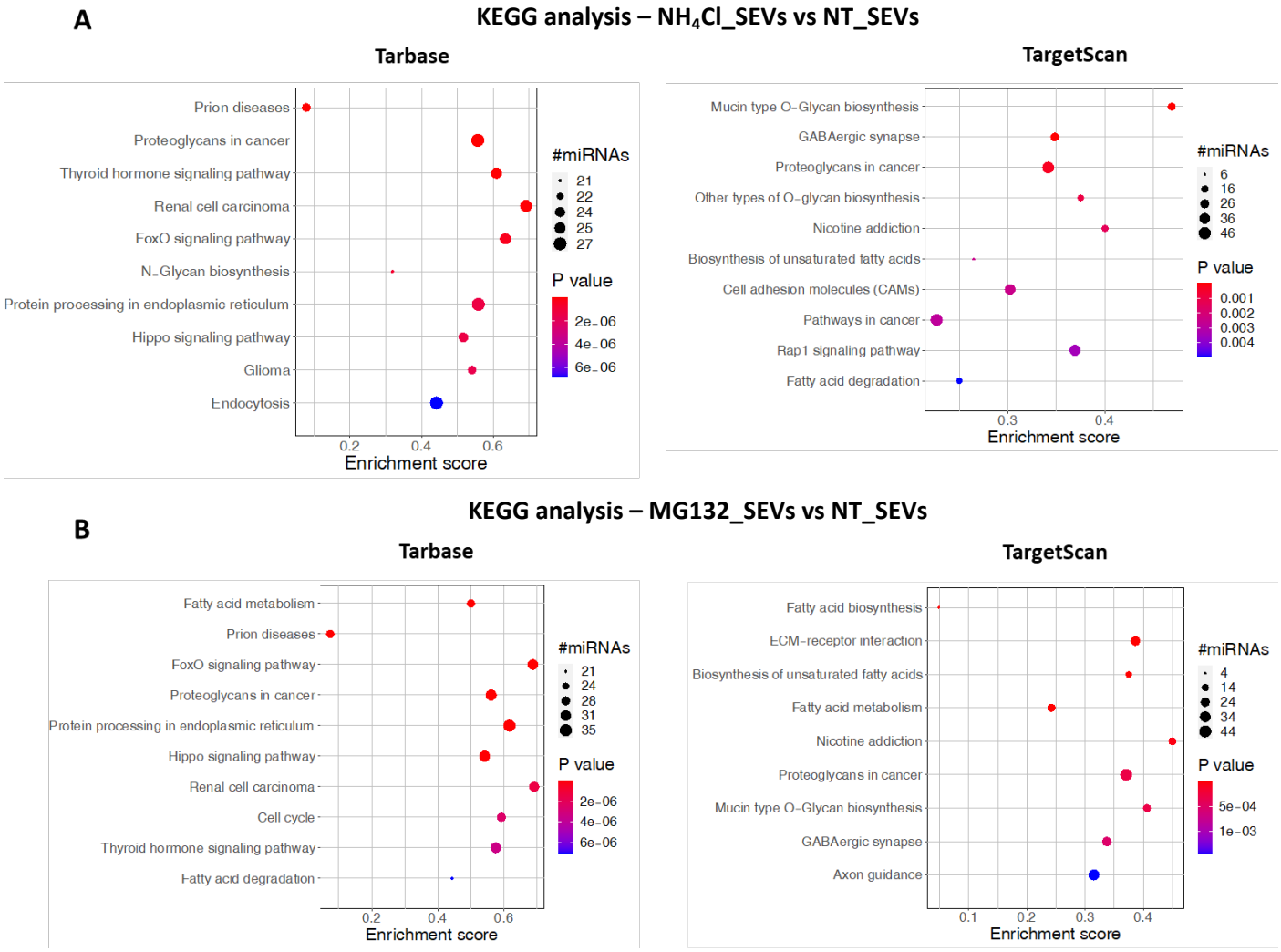

Figure 81. KEGG pathways analysis for deregulated miRNA present in NH_4Cl_SEVs compared to NT_SEVs (A) and MG132_SEVs compared to NT_SEVs (B). In the dot plots, y-axis represents the name of the pathway, the x-axis represents the Rich factor, dot size represents the number of miRNAs, and the color indicates the adjusted p-value.

The comparison between miRNAs differentially expressed in MG132_LEVs, MG132_SEVs and NH_4Cl_SEVs showed that only the miRNA mmu-miR-669c-5p were in common and upregulated both in MG132_LEVs and MG132_SEVs, while 43 were in common and deregulated in the same direction (35 out of the 43 downregulated and 8 upregulated) in MG132_SEVs and NH_4Cl_SEVs (Fig. 82 and Table 15).

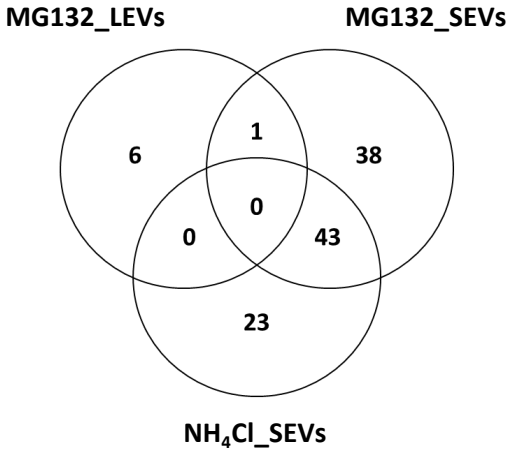

Figure 82. Common packaging of deregulated miRNAs in MG132_LEVs, MG132_SEVs and NH_4Cl_SEVs.

TREATMENTS ALTER THE PROFILE OF miRNAs TARGETING THE PRION DISEASE PATHWAY WITHIN THE SEVs

Interestingly, one of the most enriched pathways targeted by miRNAs found deregulated in SEVs released after both proteasome and autophagy inhibition was the “prion disease” pathway, with 26 miRNAs found deregulated in MG132_SEVs and 23 in NH_4Cl_ SEVs (Fig. 83 B). Several data in the literature showed that both FTD and ALS can propagate by a prion-like mechanism and EVs could be part of this mechanism. Therefore, I decided to better investigate this pathway.

As we can see in Figure 83 A and Table 16, of the total 35 miRNAs deregulated and associated to the prion disease pathway, 12 were specifically deregulated in the MG132_SEVs (8 upregulated and 3 downregulated), 9 in the NH_4Cl_ SEVs (7 upregulated and 2 downregulated) and 14 were in common between MG132_SEVs and NH_4Cl_SEVs.

Interestingly, the 14 miRNAs in common between the two treatments were deregulated in the same direction (6 upregulated and 8 downregulated).

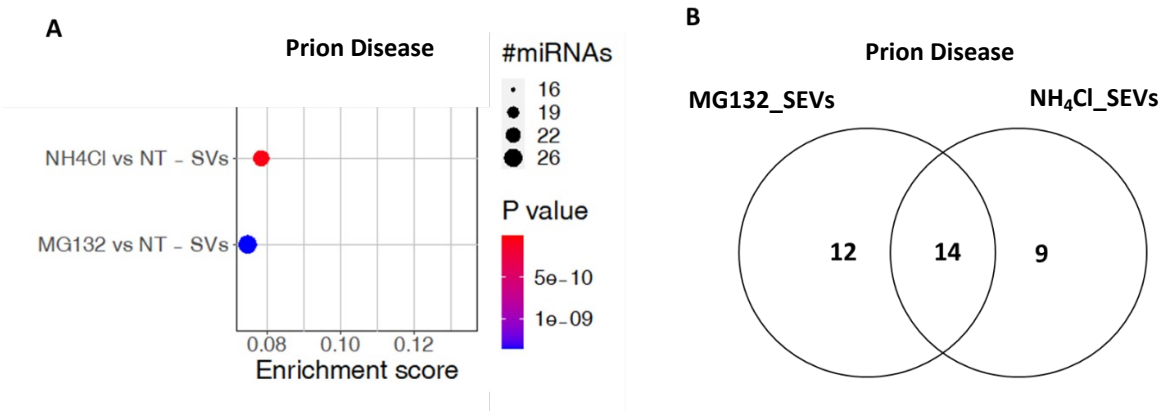

Figure 83. miRNAs that are in common between MG132_SEVs and NH_4Cl_SEVs and that have as target the prion disease pathway. Dot plot representing the enrichment score (x-axis), the number of deregulated miRNAs (dot size), and the adjusted p-value (color) for the prion disease pathway for each condition considered (A). Common packaging of deregulated miRNAs in NH_4Cl_SEVs and MG132_SEVs (B).

For these miRNAs observed deregulated in MG132_SEVs and NH_4Cl_SEVs a PubMed research was also performed to evaluate whether some of them had already been detected deregulated in NDs or as a result of alterations in the proteasome and autophagy pathway. miR-181a-5p (Ludwig et al., 2016), miR-181c-5p (Hawley et al., 2020; Siedlecki-Wullich et al., 2019; Yan et al., 2020), miR-18b-5p (K. Y. Kim et al., 2020), miR-23b-3p (Lugli et al., 2015), miR-301a-3p (Kumar et al., 2013), miR-30b-5p (Brennan et al., 2019; Dong et al., 2021; H. Guo et al., 2021; Liguori et al., 2018; Raheja et al., 2018) were already observed deregulated in NDs while others, such as miR-181c-5p (T.-H. Li et al., 2022; T. Xu et al., 2021), miR-466i-5p, miR-466k (Liao et al., 2020), miR-218-5p (M. Chen et al., 2021), miR-23b-3p (Zhou et al., 2019) were associated to alteration in the autophagic pathway or in muscle cells (table 17).

Table 3. miRNAs differentially expressed in NT_SEVs compared to NT_LEVs. Upregulated miRNAs in are represented in green, deregulated miRNAs in red.

Significantly differentially expressed miRNAs in NT_SEVs vs NT_LEVs						
	baseMean	**log2FoldChange**	**lfcSE**	**stat**	**pvalue**	**padj**
mmu-let-7a-1-3p	48,96571448	-1,469093473	0,513137925	-2,862960234	0,004197032	0,054079478
mmu-let-7c-2-3p	48,96571448	-1,469093473	0,513137925	-2,862960234	0,004197032	0,054079478
mmu-miR-101b-5p	2,365752115	3,644140846	1,41601191	2,57352415	0,010066862	0,09518919
mmu-miR-1191a	4,144666114	4,052038395	1,127394129	3,594163114	0,000325436	0,009003727
mmu-miR-1194	102,5928153	4,772743627	0,660014175	7,231274434	0,000325436	0,009003727
mmu-miR-126a-5p	17,3752834	-1,537789107	0,608130909	-2,528713939	0,011448129	0,097987017
mmu-miR-1291	500,5404653	-2,102249768	0,677969186	-3,100804303	0,001929958	0,031340839
mmu-miR-146a-5p	4,49226948	5,251808918	1,805086579	2,909449873	0,003620654	0,051030733
mmu-miR-16-5p	944,5437051	-1,117580825	0,330697309	-3,379467548	0,000726264	0,015508282
mmu-miR-1843a-3p	38,8656346	2,420748429	0,859315004	2,817067568	0,004846433	0,055696698
mmu-miR-1843b-3p	50,57815367	2,718474684	0,916349209	2,966636145	0,00301077	0,045898886
mmu-miR-1843b-5p	77,56791608	2,242899841	0,647714018	3,462793424	0,000534599	0,012882103
mmu-miR-18b-5p	5,494638237	5,012983417	1,350205435	3,712756065	0,000205014	0,006125832
mmu-miR-192-3p	1,470442275	4,344735125	1,699009113	2,557217081	0,010551335	0,097987017
mmu-miR-1930-3p	0,94821003	6,430214267	2,36561449	2,718200406	0,006563807	0,070045196
mmu-miR-1954	80,35234393	5,920650675	1,041145649	5,68666899	1,30E-08	1,94E-06
mmu-miR-1967	3,448320501	4,623199726	1,751813391	2,639093725	0,0083128	0,082795483
mmu-miR-1970	16,58757441	7,364508359	1,557272675	4,72910652	2,26E-06	0,000168456
mmu-miR-2137	1684,955103888 34	2,616468405	0,932495863	2,805876689	0,005017989	0,055946834
mmu-miR-22-3p	436,3137674	-1,330994722	0,510955332	-2,60491405	0,009189731	0,089920943
mmu-miR-27a-5p	1,475452105	3,299969708	1,268257508	2,601971356	0,009268959	0,089920943

mmu-miR-27b-3p	1400,3608459981	-1,510960583	0,538212875	-2,807366106	0,004994844	0,055946834
mmu-miR-297a-5p	10,12007466	3,68945982	0,878067907	4,201793266	0,009268959	0,089920943
mmu-miR-297c-5p	3,244348307	6,01571248	1,893526155	3,176989377	0,001488125	0,026467364
mmu-miR-3060-5p	502,3162783	3,084329027	1,138878474	2,708216106	0,006764596	0,071171171
mmu-miR-3098-3p	2,502231879	6,601796771	2,049317876	3,221460589	0,00127539	0,023817909
mmu-miR-3098-5p	2,904569642	4,583879954	1,614191193	2,839737929	0,004515061	0,055696698
mmu-miR-30b-3p	2,807136575	3,017425978	1,184769684	2,546846039	0,010870138	0,097987017
mmu-miR-30e-5p	217,6664953	-1,423340046	0,493200304	-2,885926946	0,003902627	0,053004775
mmu-miR-3103-3p	5,663940029	2,44477971	0,970310615	2,519584627	0,011749339	0,097987017
mmu-miR-320-5p	849,7690016	2,440860256	0,904946259	2,697243325	0,006991616	0,072488799
mmu-miR-3470a	711,5328743	5,074281024	0,872685613	5,814557901	6,07943405532284E-09	1,13533430983154E-06
mmu-miR-3470b	10499,1685189561	5,610035847	1,01915046	5,504619847	3,69965712767988E-08	3,94806267768124E-06
mmu-miR-3471	872,9799982	5,767983466	1,515214256	3,806711455	0,000140827	0,004573812
mmu-miR-3473c	8,283621645	3,156017113	0,793737809	3,976145623	7,00412449585236E-05	0,002906712
mmu-miR-3544-5p	9,037552568	2,288670765	0,634198114	3,608763122	0,00030766	0,008839319
mmu-miR-363-5p	14,17823444	8,877355716	1,603757143	5,535349135	3,10608995834862E-08	3,86708199814404E-06
mmu-miR-3960	464,9797455	4,136272824	0,996433591	4,151077264	3,30914021366681E-05	0,001765663
mmu-miR-423-5p	113,1248249	-1,744528471	0,450334771	-3,873848041	0,00010713	0,00380773
mmu-miR-451a	87,01643751	1,886639454	0,700604536	2,692873594	0,007083912	0,072488799
mmu-miR-463-5p	111,9949626	-1,177836999	0,393829584	-2,99072758	0,002783137	0,043312563
mmu-miR-465a-5p	57,28958517	-1,232906588	0,483406315	-2,550456108	0,010758207	0,097987017

mmu-miR-466h-3p	11,20977924	1,564969502	0,620994107	2,520103629	0,011732029	0,097987017
mmu-miR-466i-3p	1,61006536	6,545239177	1,940179049	3,373523274	0,000742128	0,015508282
mmu-miR-466i-5p	352,0329576	3,659345509	0,696366457	5,254913517	1,48094045033779E-07	1,22918057378036E-05
mmu-miR-466j	4,339383762	6,187399138	1,835163837	3,371578609	0,000747387	0,015508282
mmu-miR-466k	8,048696631	4,082606124	0,933146797	4,375095258	1,21379461200729E-05	0,000755587
mmu-miR-466q	1,656218433	5,34993596	1,872918804	2,856469778	0,004283808	0,054237364
mmu-miR-467g	10,14972866	6,204190609	1,551736913	3,998223253	6,38197422556445E-05	0,002906712
mmu-miR-467h	2,848128857	6,584717813	1,704694282	3,86269719	0,000112142	0,00380773
mmu-miR-5098	91,62445796	5,612793555	0,903945934	6,20921379	5,32503380669654E-10	1,32593341786744E-07
mmu-miR-5099	48058,3917299731	1,450234581	0,496655289	2,92000229	0,003500288	0,050282985
mmu-miR-5106	3771,96091609134	3,857582349	1,099327663	3,509037821	0,000449731	0,011584449
mmu-miR-5108	201,1339935	3,679159443	1,180595535	3,116358934	0,001830993	0,030394477
mmu-miR-511-3p	0,955165038	5,453102668	2,143732718	2,543741868	0,01096721	0,097987017
mmu-miR-5110	196,6212122	3,879135866	1,044675693	3,713244114	0,000204619	0,006125832
mmu-miR-5119	40,6956915	3,749325814	1,189353162	3,152407489	0,001619301	0,028130652
mmu-miR-532-3p	1,297192971	4,298917749	1,699609537	2,529356099	0,011427202	0,097987017
mmu-miR-542-3p	78,22973482	3,049130374	0,761830365	4,00237443	6,27099517294893E-05	0,002906712
mmu-miR-6236	35311,8873298085	4,075519765	1,022755453	3,984842862	6,75247950273803E-05	0,002906712
mmu-miR-6238	635,4680207	2,101949307	0,541801126	3,879558764	0,000104646	0,00380773
mmu-miR-6240	25196,8662224569	2,047545972	0,677268046	3,023243139	0,002500812	0,039746953
mmu-miR-6244	3,149948288	5,725105985	1,638399305	3,494328866	0,000475255	0,011833854
mmu-miR-6363	9,127777749	4,883119882	1,440181256	3,390628688	0,000697325	0,015508282
mmu-miR-6418-3p	2,696235948	4,264534578	1,489629248	2,862816089	0,004198942	0,054079478
mmu-miR-680	7,010172079	4,404487905	1,559711711	2,823911544	0,004744148	0,055696698
mmu-miR-6931-3p	4,293691563	7,200089596	1,833592199	3,926767141	8,60952596115408E-05	0,003384903

mmu-miR-6937-5p	170,2404128	5,930807862	1,089769717	5,442257908	5,26094317609032E-08	4,91240569067433E-06
mmu-miR-6948-3p	2,788445826	5,091490631	1,806846162	2,817888284	0,004834063	0,055696698
mmu-miR-6964-5p	5,090869887	4,037108114	1,391849292	2,90053538	0,003725258	0,051532733
mmu-miR-6990-5p	4,147422834	3,367999437	1,04428778	3,225164079	0,001259005	0,023817909
mmu-miR-6993-5p	2,450487399	3,6129859	1,402982533	2,575218019	0,010017692	0,09518919
mmu-miR-7007-5p	5,357550572	4,087970941	1,265116489	3,231300023	0,001232285	0,023817909
mmu-miR-7019-5p	1,153824857	6,231537995	2,474894401	2,517900558	0,011805665	0,097987017
mmu-miR-7023-3p	2,472727231	5,922694108	2,337221554	2,534074742	0,011274468	0,097987017
mmu-miR-703	198,6272633	-1,664297801	0,589298362	-2,824202319	0,004739845	0,055696698
mmu-miR-7061-5p	45,1793247	3,605445151	0,513745745	7,017956233	2,25137038591083E-12	8,40886839137694E-10
mmu-miR-7088-3p	1,009999282	5,275526791	1,901183198	2,77486504	0,005522462	0,060665869
mmu-miR-7117-5p	47,00691416	5,247858053	1,680593873	3,122621198	0,001792483	0,030394477
mmu-miR-7118-3p	2,09226141	6,304291213	2,488496147	2,53337391	0,011297038	0,097987017
mmu-miR-7211-3p	3,504886238	5,12031957	1,450791663	3,529327954	0,000416616	0,011114733
mmu-miR-743b-3p	466,2398993	-1,435559922	0,433702277	-3,310012418	0,000932918	0,018834865
mmu-miR-7652-3p	2,750815542	5,999454213	2,196555301	2,731301238	0,006308478	0,068296132
mmu-miR-7667-5p	1,334720094	4,626152243	1,736991552	2,663313036	0,00773754	0,078107326
mmu-miR-7684-5p	5,021225397	5,100298043	1,728246614	2,951140192	0,003166032	0,046373054
mmu-miR-8099	7,639882878	4,501565824	1,311109417	3,433402098	0,000596057	0,013914215
mmu-miR-8115	6,501512115	3,731477637	1,26241114	2,955833896	0,00311825	0,046373054
mmu-miR-8117	140,4835963	5,537171747	1,187941513	4,661148452	3,14449804844084E-06	0,00021354
mmu-miR-99a-5p	2,884080116	4,974839624	1,759413466	2,827555728	0,004690485	0,055696698

rco-miR396	6,256112181	5,200196246	1,618829079	3,212319518	0,001316678	0,02398924

Table 4. List of the KEGG pathways obtained with Tarbase targeted by the deregulated miRNAs present in NT_SEVs vs NT_LEVs.

KEGG pathway Tarbase	**p-value**	**#genes**	**#miRNAs**
Fatty acid metabolism	3.10561261799e-12	26	15
Prion diseases	3.10561261799e-12	21	16
Proteoglycans in cancer	1.06377235772e-10	111	24
FoxO signaling pathway	1.11390749552e-07	83	21
Hippo signaling pathway	1.50976974886e-06	79	22
Thyroid hormone signaling pathway	1.83847401176e-06	67	23
Adherens junction	9.59305961159e-06	46	21
Fatty acid degradation	1.10579974683e-05	22	12
Valine, leucine and isoleucine degradation	1.10579974683e-05	34	15
Protein processing in endoplasmic reticulum	1.10579974683e-05	93	22
Citrate cycle (TCA cycle)	1.32110576478e-05	23	15
Endocytosis	1.48700846956e-05	119	25
Axon guidance	1.55622754017e-05	71	23
Renal cell carcinoma	2.03733684583e-05	42	22
N-Glycan biosynthesis	2.08650660495e-05	25	13
Fatty acid biosynthesis	2.92454137957e-05	6	9
Colorectal cancer	0.000169420015463	38	16
Cell cycle	0.00027901242138	68	16
Inositol phosphate metabolism	0.000400181991432	34	14
T cell receptor signaling pathway	0.000573005924948	59	20
Pathways in cancer	0.000883878904726	175	25
Regulation of actin cytoskeleton	0.00134911896208	107	24
Pancreatic cancer	0.00173904974236	38	20
p53 signaling pathway	0.00214805588179	38	13
Acute myeloid leukemia	0.00281219571539	33	13
mTOR signaling pathway	0.00281219571539	36	17
Lysine degradation	0.00295733345495	28	18
Hepatitis B	0.00330211702581	68	20
Long-term depression	0.00347249937898	31	15
Neurotrophin signaling pathway	0.00394166586497	62	21
Glycosaminoglycan biosynthesis - heparan sulfate / heparin	0.00482504247594	12	11
Phosphatidylinositol signaling system	0.00553274738463	44	13
Glioma	0.00553274738463	33	18
Prostate cancer	0.00604722896777	49	22
Chronic myeloid leukemia	0.00620580487202	40	17
Ubiquitin mediated proteolysis	0.00726186333236	76	20
TGF-beta signaling pathway	0.00872066254068	38	17
Fc gamma R-mediated phagocytosis	0.00872066254068	46	21
MAPK signaling pathway	0.00872066254068	113	26
HTLV-I infection	0.00872227334007	124	23
Steroid biosynthesis	0.00879460358034	10	13

Arrhythmogenic right ventricular cardiomyopathy (ARVC)	0.00985886067731	31	16
Insulin signaling pathway	0.0098831883762	70	22
Non-small cell lung cancer	0.0110740491266	30	15
Wnt signaling pathway	0.0175484266736	65	20
Sphingolipid signaling pathway	0.0187903942122	61	19
Bacterial invasion of epithelial cells	0.0187903942122	39	20
AMPK signaling pathway	0.0187903942122	64	23
Thyroid cancer	0.0196624202739	16	10
Focal adhesion	0.0235262028829	95	25
ErbB signaling pathway	0.0270216160777	44	23
Thyroid hormone synthesis	0.0286164523895	33	19
Notch signaling pathway	0.0306943777024	27	14
Long-term potentiation	0.0306943777024	35	16
Endometrial cancer	0.0333224558886	29	16
Primary bile acid biosynthesis	0.0343374715797	9	6
Propanoate metabolism	0.0491951662999	14	10

Table 5. List of the KEGG pathways obtained with TargetScan targeted by the deregulated miRNAs present in NT_SEVs vs NT_LEVs.

KEGG pathway - TargetScan	**p-value**	**#genes**	**#miRNAs**
GABAergic synapse	1.16656058166e-10	38	32
Morphine addiction	7.436702284e-06	41	30
Adherens junction	3.08233070942e-05	36	32
Nicotine addiction	3.4129156524e-05	21	20
Mucin type O-Glycan biosynthesis	8.72440297537e-05	14	20
Biosynthesis of unsaturated fatty acids	0.000102112312015	10	10
Fatty acid degradation	0.000102112312015	16	19
Long-term depression	0.0001164926052	30	30
Glycosphingolipid biosynthesis - ganglio series	0.00120620264443	8	10
Hippo signaling pathway	0.00166569381767	60	39
Phosphatidylinositol signaling system	0.00174895310244	37	35
Regulation of actin cytoskeleton	0.00174895310244	92	49
Axon guidance	0.00211754918844	59	44
Fatty acid metabolism	0.00221676725917	15	15
Calcium signaling pathway	0.00721043476696	77	43
Rap1 signaling pathway	0.0122597529493	88	51
Pathways in cancer	0.0122597529493	148	56
Proteoglycans in cancer	0.013452650979	85	50
Serotonergic synapse	0.0172941121628	52	37
Vascular smooth muscle contraction	0.0172941121628	52	41
Nicotinate and nicotinamide metabolism	0.0178163626344	14	10
Endocytosis	0.0178163626344	89	40
TGF-beta signaling pathway	0.0323708500188	32	31
Thyroid hormone signaling pathway	0.0328218971848	47	36
Vitamin B6 metabolism	0.0364686391598	5	5
Type II diabetes mellitus	0.0427709487026	23	25

Sphingolipid metabolism	0.0445444789064	24	22
Glycosaminoglycan biosynthesis - heparan sulfate / heparin	0.0476723331539	11	15

Table 6. miRNAs differentially expressed in MG132_LEVs compared to NT_LEVs. Upregulated miRNAs are represented in green, deregulated miRNAs in red.

Significantly differentially expressed miRNAs in MG132_LEVs vs NT_LEVs						
	baseMean	**log2FoldChange**	**lfcSE**	**stat**	**pvalue**	**padj**
mmu-let-7a-5p	1842,635374	1,24858648	0,311828865	4,004076016	6,23E-05	0,010646519
mmu-let-7f-5p	658,7840022	1,216955425	0,409161322	2,974267999	0,002936884	0,068282507
mmu-let-7g-5p	451,0100402	1,327779296	0,404378721	3,283504365	0,001025251	0,043829462
mmu-miR-1195	96,13110499	-1,435538446	0,426197676	-3,368245596	0,000756482	0,04311946
mmu-miR-125-5p	474,6811025	-1,272692179	0,442305742	-2,877403697	0,004009623	0,076182832
mmu-miR-669c-5p	1019,715505	1,153082316	0,372221379	3,097840104	0,001949366	0,060984011
mmu-miR-703	198,6272633	-1,990539794	0,545179542	-3,651163776	0,000261055	0,022320176

Table 7. List of the KEGG pathways obtained with Tarbase targeted by the deregulated miRNAs present in MG132_LEVs vs NT_LEVs.

KEGG pathway - Tarbase	**p-value**	**#genes**	**#miRNAs**
Lysine degradation	8,96E-07	16	5
Proteoglycans in cancer	8,96E-07	58	6
HIF-1 signaling pathway	0,0001356	36	5
Renal cell carcinoma	0,0001356	23	5
Adherens junction	0,0001356	23	6
Central carbon metabolism in cancer	0,0001356	20	6
Thyroid hormone signaling pathway	0,00018758	36	6
Endocytosis	0,00039786	54	6
Focal adhesion	0,00039786	56	6
Pathways in cancer	0,00054249	81	6
Protein processing in endoplasmic reticulum	0,00068846	44	5
Regulation of actin cytoskeleton	0,00074566	55	6
Glioma	0,00150695	19	5
PI3K-Akt signaling pathway	0,0035149	78	6
Glycosaminoglycan biosynthesis - heparan sulfate / heparin	0,00487029	8	4
Hepatitis B	0,00498471	34	5
Arrhythmogenic right ventricular cardiomyopathy (ARVC)	0,00498471	15	5
Caffeine metabolism	0,00570974	2	1
Prostate cancer	0,00661056	27	5
Hippo signaling pathway	0,00661056	35	6
Pancreatic cancer	0,00661056	20	6
Adipocytokine signaling pathway	0,00704842	21	4
MAPK signaling pathway	0,00865707	54	6
Apoptosis	0,01305495	23	5

TNF signaling pathway	0,01305495	29	5
HTLV-I infection	0,01305495	57	5
Colorectal cancer	0,01535443	17	5
Fc gamma R-mediated phagocytosis	0,01535443	25	6
ErbB signaling pathway	0,02149496	25	5
AMPK signaling pathway	0,02822552	34	5
T cell receptor signaling pathway	0,02822552	27	5
Circadian rhythm	0,02822552	10	5
Rap1 signaling pathway	0,02822552	46	6
Other glycan degradation	0,03021846	5	3
Osteoclast differentiation	0,03515191	30	5
Acute myeloid leukemia	0,03936999	17	4
Axon guidance	0,03936999	29	5
Bacterial invasion of epithelial cells	0,03936999	19	6
Glycosphingolipid biosynthesis - ganglio series	0,04151831	5	3
Prolactin signaling pathway	0,04151831	18	5
Choline metabolism in cancer	0,04151831	25	5

Table 8. List of the KEGG pathways obtained with TargetScan targeted by the deregulated miRNAs present in MG132_LEVs vs NT_LEVs.

KEGG pathway - TargetScan	**p-value**	**#genes**	**#miRNAs**
Fatty acid degradation	1,37E-07	2	3
Mucin type O-Glycan biosynthesis	2,77E-07	2	1
Glycosphingolipid biosynthesis - lacto and neolacto series	9,02E-07	2	1
Propanoate metabolism	1,03E-05	5	5
Fatty acid metabolism	9,56E-05	3	4
Valine, leucine and isoleucine degradation	0,000171198	4	4
Metabolic pathways	0,000940018	30	6
Valine, leucine and isoleucine biosynthesis	0,008139274	1	3

Table 9. miRNAs differentially expressed in MG132_SEVs compared to NT_SEVs. Upregulated miRNAs in are represented in green, deregulated miRNAs in red.

Significantly differentially expressed miRNAs in MG132_SEVs vs NT_SEVs						
	baseMean	**log2FoldChange**	**lfcSE**	**stat**	**pvalue**	**padj**
mmu-let-7e-5p	777,4918476	1,213096183	0,277638577	4,369335839	1,25E-05	0,000547617
mmu-miR-1194	102,5928153	-5,142365384	0,669647097	-7,679217023	1,60E-14	5,98E-12
mmu-miR-1224-3p	276,626891	-2,935389596	1,087339231	-2,699607915	0,006942124	0,068233769
mmu-miR-125b-1-3p	46,0607818	1,748418512	0,571924852	3,057077353	0,002235066	0,030356259
mmu-miR-128-3p	61,6137733	1,199940914	0,395685272	3,032564008	0,002424857	0,031778385
mmu-miR-140-3p	188,5054593	-1,123724318	0,33630085	-3,341425743	0,000833493	0,014710465
mmu-miR-142a-3p	1,697686122	-5,456852453	1,84636081	-2,955463755	0,003121994	0,03761499

mmu-miR-143-3p	1521,055523	-1,884430355	0,623983064	-3,020002408	0,002527727	0,032003591
mmu-miR-155-5p	32,74705895	1,196251548	0,471033253	2,539632903	0,011096888	0,095280172
mmu-miR-181a-5p	3703,686042	1,301818295	0,241265818	5,395784233	6,82E-08	6,37E-06
mmu-miR-181c-5p	544,3753369	1,325648346	0,398169678	3,329355347	0,000870473	0,014710465
mmu-miR-18b-5p	5,494638237	-7,164373665	1,595720913	-4,489741035	7,13E-06	0,000332928
mmu-miR-1946a	411,9621023	-2,096153916	0,828191165	-2,531002508	0,011373704	0,096547233
mmu-miR-1954	80,35234393	-6,344872797	1,059094766	-5,9908452	2,09E-09	3,12E-07
mmu-miR-1970	16,58757441	-9,370848601	1,714037464	-5,467120059	4,57E-08	4,88E-06
mmu-miR-218-5p	431,0767063	1,544772379	0,532171667	2,902770807	0,003698772	0,040043229
mmu-miR-23a-3p	49,41585866	1,293361776	0,491893466	2,629353438	0,00855474	0,078583494
mmu-miR-23b-3p	190,427071	1,210397697	0,453398482	2,669611271	0,007593911	0,071805713
mmu-miR-26b-5p	375,1004585	1,424674009	0,487972426	2,919578919	0,003505046	0,039516927
mmu-miR-297a-5p	10,12007466	-3,538842662	0,889099896	-3,980253149	6,88E-05	0,001977881
mmu-miR-297c-5p	3,244348307	-6,498535813	1,954128683	-3,325541388	0,00088247	0,014710465
mmu-miR-29c-3p	2,546250554	-5,356944344	1,543670006	-3,470265227	0,000519945	0,010497261
mmu-miR-301a-3p	116,351123	1,975544825	0,568264743	3,476451512	0,000508096	0,010497261
mmu-miR-301b-5p	1,636984937	-4,660197656	1,729451448	-2,694610284	0,0070471	0,068366023
mmu-miR-3060-5p	502,3162783	-4,097387753	1,140016685	-3,594147179	0,000325456	0,00759736
mmu-miR-3066-5p	3,821547518	-3,336654277	1,182143601	-2,822545649	0,004764404	0,048753557
mmu-miR-3091-3p	7,461581345	-3,622070742	1,198792047	-3,021433744	0,002515807	0,032003591
mmu-miR-3091-5p	7,492354003	-2,78588713	1,047363419	-2,659904937	0,007816271	0,07298443
mmu-miR-3098-5p	2,904569642	-4,229432416	1,62102603	-2,609108267	0,009077852	0,079778296
mmu-miR-30b-5p	347,2284594	1,990955218	0,614885334	3,237929265	0,001204007	0,018354957
mmu-miR-30c-5p	448,4622809	1,362764532	0,440654818	3,092589652	0,001984183	0,027965748
mmu-miR-3103-3p	5,663940029	-3,197791189	1,024249058	-3,122083603	0,001795759	0,025796774
mmu-miR-320-3p	667,553653	1,226144613	0,387989582	3,160251379	0,001576331	0,023088609
mmu-miR-322-3p	78,38310497	1,204656365	0,404052124	2,981438023	0,002868981	0,035718815
mmu-miR-335-3p	630,2000246	1,094375409	0,416663701	2,626519677	0,0086263	0,078583494
mmu-miR-3470a	711,5328743	-7,054535584	0,880999884	-8,007419423	1,17E-15	8,75E-13
mmu-miR-3470b	10499,16852	-7,253677061	1,019681218	-7,113671342	1,13E-12	2,81E-10
mmu-miR-3471	872,9799982	-9,124417329	1,533716945	-5,949218569	2,69E-09	3,35E-07
mmu-miR-3473c	8,283621645	-2,591595069	0,788643311	-3,286143474	0,001015693	0,015806716

mmu-miR-363-5p	14,17823444	-5,525594386	1,342828598	-4,1148918	3,87E-05	0,001258081
mmu-miR-3960	464,9797455	-2,866959172	0,99544152	-2,880087995	0,003975642	0,042425779
mmu-miR-423-3p	100,8468349	-1,536924963	0,47667883	-3,224235829	0,001263093	0,018870615
mmu-miR-423-5p	113,1248249	1,862337598	0,450969763	4,129628528	3,63E-05	0,001233738
mmu-miR-463-5p	111,9949626	1,585663	0,393790643	4,026665004	5,66E-05	0,001690417
mmu-miR-466f	3,686241429	-4,305960561	1,466539643	-2,93613649	0,003323281	0,039404613
mmu-miR-466f-5p	3,147762723	-4,213177893	1,425529785	-2,955517265	0,003121452	0,03761499
mmu-miR-466i-3p	1,61006536	-4,882023312	1,913736962	-2,551041971	0,010740139	0,093289348
mmu-miR-466i-5p	352,0329576	-2,436485904	0,695136659	-3,505045909	0,000456529	0,010030201
mmu-miR-466k	8,048696631	-3,097251032	0,909381559	-3,405887224	0,000659494	0,01263185
mmu-miR-466q	1,656218433	-5,618961788	1,919243469	-2,927696188	0,003414835	0,039516927
mmu-miR-467g	10,14972866	-8,804130869	1,757935814	-5,008220892	5,49E-07	3,93E-05
mmu-miR-5098	91,62445796	-6,435971755	0,928952245	-6,928205179	4,26E-12	7,96E-10
mmu-miR-5101	3,047618413	-4,9446481	1,735723623	-2,848753128	0,004389092	0,045536833
mmu-miR-5126	182,2384438	-3,436400414	0,897402212	-3,829275621	0,000128521	0,003428757
mmu-miR-542-3p	78,22973482	-3,083496906	0,764600346	-4,032821749	5,51E-05	0,001690417
mmu-miR-574-5p	170,0441401	1,307163666	0,395996248	3,300949621	0,000963582	0,015623303
mmu-miR-615-5p	23,57224926	-3,551190133	0,775810804	-4,577391956	4,71E-06	0,000234463
mmu-miR-6236	35311,88733	-5,101565025	1,022787711	-4,987902151	6,10E-07	3,93E-05
mmu-miR-6240	25196,86622	-2,268579098	0,677276304	-3,349562187	0,000809394	0,014710465
mmu-miR-6244	3,149948288	-5,60085295	1,684784238	-3,324374021	0,000886173	0,014710465
mmu-miR-6363	9,127777749	-8,538405642	1,71409209	-4,98129925	6,32E-07	3,93E-05
mmu-miR-6418-3p	2,696235948	-5,769765643	1,668822343	-3,457387581	0,00054544	0,010722197
mmu-miR-6538	145,2543708	-4,082732002	0,815746337	-5,004903872	5,59E-07	3,93E-05
mmu-miR-669a-5p	202,2077115	1,294723978	0,443991456	2,916101108	0,003544356	0,039516927
mmu-miR-669c-5p	1019,715505	1,704070468	0,399743584	4,262908864	2,02E-05	0,000793325
mmu-miR-669p-5p	202,2077115	1,294723978	0,443991456	2,916101108	0,003544356	0,039516927
mmu-miR-676-3p	121,0604624	-1,72696629	0,56180117	-3,073981297	0,002112227	0,029219137
mmu-miR-680	7,010172079	-4,878087169	1,601237372	-3,046448487	0,002315622	0,030888737
mmu-miR-682	25,76312187	-2,904255759	0,833630814	-3,483863251	0,000494232	0,010497261
mmu-miR-690	1287,724203	-2,362514742	0,481497121	-4,906602011	9,27E-07	5,32E-05
mmu-miR-6937-5p	170,2404128	-4,503765005	1,083334758	-4,157316077	3,22E-05	0,00114543
mmu-miR-6967-3p	2,048593869	-5,716976438	2,035970012	-2,807986563	0,004985231	0,050323883
mmu-miR-7012-3p	16,53918067	-5,682124788	1,326842614	-4,282440681	1,85E-05	0,000767146
mmu-miR-7012-5p	16,07144442	-5,384451924	1,289335409	-4,176145234	2,96E-05	0,001107392
mmu-miR-712-3p	41,74727909	-4,014340983	0,833649162	-4,815384176	1,47E-06	7,84E-05
mmu-miR-712-5p	75,69045739	-3,001905657	0,763621065	-3,931145689	8,45E-05	0,002338996
mmu-miR-7211-3p	3,504886238	-5,099464201	1,507779536	-3,382102011	0,000719334	0,013433567

mmu-miR-7684-5p	5,021225397	-5,118188876	1,759545743	-2,908812627	0,003628042	0,039855112
mmu-miR-8112	6,011191056	-3,753336398	1,138979656	-3,295349816	0,000982992	0,015623303
mmu-miR-8115	6,501512115	-4,67258045	1,328579412	-3,516974905	0,000436495	0,009880661
mmu-miR-8117	140,4835963	-4,31236924	1,182961938	-3,645399824	0,000266976	0,006572327
mmu-miR-871-5p	283,2346425	1,265842055	0,335224759	3,776099529	0,000159303	0,004103435

Table 10. miRNAs differentially expressed in NH_4Cl_SEVs compared to NT_SEVs. Upregulated miRNAs in are represented in green, deregulated miRNAs in red.

Significantly differentially expressed miRNAs in NH_4Cl_SEVs vs NT_SEVs						
	baseMean	**log2FoldChange**	**lfcSE**	**stat**	**pvalue**	**padj**
mmu-miR-1194	102,5928153	-4,322520984	0,653594962	-6,613455178	3,75E-11	1,40E-08
mmu-miR-16-5p	944,5437051	1,068597853	0,33056612	3,232629687	0,001226564	0,025451213
mmu-miR-181a-5p	3703,686042	1,036186106	0,241197492	4,296006974	1,74E-05	0,001082541
mmu-miR-181c-5p	544,3753369	1,497329737	0,3976871	3,765095059	0,000166486	0,005407167
mmu-miR-18b-5p	5,494638237	-6,496104541	1,434774092	-4,527614889	5,97E-06	0,000445609
mmu-miR-1930-3p	0,94821003	-6,205531617	2,362433468	-2,626754023	0,008620362	0,096110607
mmu-miR-1943-5p	11,06631819	-2,500790377	0,783812415	-3,190547036	0,001420037	0,027914943
mmu-miR-1954	80,35234393	-4,898919211	1,025939069	-4,775058635	1,80E-06	0,00022367
mmu-miR-1970	16,58757441	-5,225625171	1,410959727	-3,703596261	0,000212564	0,006616069
mmu-miR-19a-3p	25,26184563	2,358919368	0,861716387	2,737466067	0,006191451	0,078390062
mmu-miR-19b-3p	121,8914052	2,007767923	0,703379189	2,854460234	0,004311003	0,06197746
mmu-miR-218-5p	431,0767063	1,488813307	0,531855531	2,799281421	0,005121648	0,069114668
mmu-miR-222-3p	2,223219986	-5,548878638	1,612288731	-3,441615965	0,000578251	0,014398439
mmu-miR-23b-3p	190,427071	1,291180373	0,452377043	2,854212859	0,004314361	0,06197746
mmu-miR-297a-5p	10,12007466	-3,332957961	0,854737714	-3,899392652	9,64E-05	0,003551099
mmu-miR-301a-3p	116,351123	1,869234292	0,567351302	3,294668196	0,00098538	0,021649368
mmu-miR-3060-5p	502,3162783	-3,27408841	1,138767968	-2,875114599	0,004038809	0,060339803
mmu-miR-3091-3p	7,461581345	-3,386000754	1,100535152	-3,076685689	0,002093159	0,03636255
mmu-miR-3091-5p	7,492354003	-3,789437649	1,051151784	-3,605033741	0,000312112	0,008635109
mmu-miR-30a-5p	898,547558	1,409048971	0,444707764	3,16848296	0,001532367	0,02810443
mmu-miR-30b-5p	347,2284594	2,043631181	0,614542304	3,3254524	0,000882752	0,019982289
mmu-miR-30d-5p	2679,61245	1,014905126	0,249452765	4,068526257	4,73E-05	0,002208852
mmu-miR-30e-5p	217,6664953	1,797527127	0,492471192	3,650014777	0,000262225	0,00783529
mmu-miR-3470a	711,5328743	-5,926286287	0,873360405	-6,785613653	1,16E-11	8,63E-09

mmu-miR-3470b	10499,16852	-6,368994528	1,019192592	-6,249058892	4,13E-10	1,03E-07
mmu-miR-3471	872,9799982	-7,774275253	1,518182473	-5,120777899	3,04E-07	4,55E-05
mmu-miR-3473c	8,283621645	-3,197790021	0,77859847	-4,107110591	4,01E-05	0,002067831
mmu-miR-34c-5p	588,6439549	1,515009484	0,476899743	3,176788217	0,001489157	0,02810443
mmu-miR-363-5p	14,17823444	-6,307271792	1,336076671	-4,720740906	2,35E-06	0,000243933
mmu-miR-421-5p	2,377739385	-6,481030992	2,249925936	-2,880553039	0,003969782	0,060339803
mmu-miR-423-5p	113,1248249	1,496593139	0,449958094	3,326072271	0,000880791	0,019982289
mmu-miR-463-5p	111,9949626	1,230914989	0,392581209	3,135440416	0,001715963	0,030519625
mmu-miR-466i-3p	1,61006536	-5,163510658	1,844872086	-2,798844808	0,005128578	0,069114668
mmu-miR-466i-5p	352,0329576	-2,702832018	0,694636058	-3,891004484	9,98E-05	0,003551099
mmu-miR-466k	8,048696631	-4,333871509	0,922266134	-4,699154992	2,61E-06	0,000243933
mmu-miR-467g	10,14972866	-5,945431064	1,506750717	-3,945862441	7,95E-05	0,003126126
mmu-miR-467h	2,848128857	-4,157828425	1,463811382	-2,840412689	0,00450552	0,063502336
mmu-miR-5098	91,62445796	-5,203583672	0,895348099	-5,811799541	6,18E-09	1,15E-06
mmu-miR-5101	3,047618413	-4,949372007	1,6448826	-3,008951524	0,002621509	0,04450608
mmu-miR-5124a	1230,857664	-3,535443127	1,214717749	-2,910505861	0,003608442	0,057351195
mmu-miR-5126	182,2384438	-2,385046209	0,893441698	-2,669504025	0,007596336	0,090030795
mmu-miR-6236	35311,88733	-3,664015926	1,022744478	-3,58253308	0,000340279	0,009078145
mmu-miR-6240	25196,86622	-2,41780969	0,677266798	-3,5699516	0,000357047	0,009197043
mmu-miR-6244	3,149948288	-3,909846625	1,467461482	-2,664360648	0,007713482	0,090030795
mmu-miR-6363	9,127777749	-5,463854692	1,445015937	-3,781172618	0,000156091	0,005300012
mmu-miR-6418-3p	2,696235948	-3,933560161	1,42561897	-2,759194599	0,005794402	0,0746279
mmu-miR-6538	145,2543708	-2,410025696	0,807201706	-2,985654858	0,002829718	0,046973322
mmu-miR-680	7,010172079	-7,730939705	1,754019403	-4,407556549	1,05E-05	0,000709944
mmu-miR-6937-5p	170,2404128	-3,416050349	1,078789754	-3,16655802	0,001542546	0,02810443
mmu-miR-6993-5p	2,450487399	-3,774161545	1,383734478	-2,727518613	0,006381266	0,079446758
mmu-miR-7012-3p	16,53918067	-3,259519957	0,955481476	-3,411390007	0,000646326	0,015574365
mmu-miR-7012-5p	16,07144442	-3,969239409	0,981661746	-4,043388087	5,27E-05	0,002315011
mmu-miR-712-3p	41,74727909	-3,365107314	0,799181443	-4,210692505	2,55E-05	0,001462908
mmu-miR-712-5p	75,69045739	-1,992623834	0,749475173	-2,65869225	0,007844458	0,090150926
mmu-miR-714	86,54577762	-3,137788964	0,784759086	-3,998410492	6,38E-05	0,002646425
mmu-miR-7652-3p	2,750815542	-5,595946601	2,129237284	-2,628146071	0,008585164	0,096110607
mmu-miR-7653-3p	2,098413922	-4,727693377	1,607590313	-2,940857095	0,003273055	0,053151566
mmu-miR-7667-5p	1,334720094	-6,461521111	1,784607659	-3,620695606	0,000293812	0,008441445
mmu-miR-7684-3p	3,118016014	-8,438253041	2,918970529	-2,890831873	0,003842236	0,059794799
mmu-miR-7684-5p	5,021225397	-8,863506603	1,926037305	-4,601939215	4,19E-06	0,000347418
mmu-miR-7687-5p	1,546878355	-4,918098122	1,759265012	-2,79554137	0,005181287	0,069114668
mmu-miR-8112	6,011191056	-3,459770718	1,078179758	-3,208899716	0,00133244	0,026900875

mmu-miR-8115	6,501512115	-5,391126718	1,315281295	-4,098839341	4,15E-05	0,002067831
mmu-miR-878-5p	408,071809	1,476850351	0,533263286	2,769458148	0,005614962	0,073585551
mmu-miR-883b-5p	14,45461641	1,56579053	0,579173259	2,703492446	0,006861501	0,084025263
mmu-miR-98-3p	1,053171459	-6,929427405	2,114425219	-3,277215644	0,001048363	0,022375055

Table 11. List of the KEGG pathways obtained with Tarbase targeted by the deregulated miRNAs present in NH_4Cl_SEVs vs NT_SEVs.

KEGG pathway - Tarbase	**p-value**	**#genes**	**#miRNAs**
Prion diseases	5,19423E-11	21	23
Proteoglycans in cancer	2,21377E-10	114	27
Thyroid hormone signaling pathway	6,90939E-09	73	25
Renal cell carcinoma	2,98082E-08	47	26
FoxO signaling pathway	3,89437E-07	83	25
N-Glycan biosynthesis	7,97697E-07	28	21
Protein processing in endoplasmic reticulum	1,37199E-06	96	27
Hippo signaling pathway	1,41086E-06	81	24
Glioma	1,59758E-06	40	23
Endocytosis	6,83722E-06	120	27
Fatty acid metabolism	7,26088E-06	24	23
Chronic myeloid leukemia	3,83775E-05	45	25
Central carbon metabolism in cancer	5,79965E-05	36	23
Fatty acid biosynthesis	0,000107193	6	13
HIF-1 signaling pathway	0,000159681	65	22
Insulin signaling pathway	0,00040074	79	26
Citrate cycle (TCA cycle)	0,000430269	22	22
Pancreatic cancer	0,000465552	41	22
Cell cycle	0,000465552	71	24
T cell receptor signaling pathway	0,000465552	59	25
AMPK signaling pathway	0,000465552	73	26
Adherens junction	0,00054378	43	24
Ubiquitin mediated proteolysis	0,000799159	82	28
Pathways in cancer	0,000815708	184	28
Hepatitis B	0,0011317	70	26
Prostate cancer	0,0011317	51	26
MAPK signaling pathway	0,0011317	123	30
Long-term depression	0,001291768	33	23
ErbB signaling pathway	0,001291768	48	27
Sphingolipid signaling pathway	0,001306482	69	26
Axon guidance	0,001376217	67	27
Fc gamma R-mediated phagocytosis	0,001529788	50	24
Phosphatidylinositol signaling system	0,00162534	47	20
Chagas disease (American trypanosomiasis)	0,00162534	53	22
Inositol phosphate metabolism	0,001772431	34	20
Colorectal cancer	0,001785212	37	21
Lysine degradation	0,001838279	29	23

Neurotrophin signaling pathway	0,001838279	65	25
Thyroid cancer	0,001916813	18	20
mTOR signaling pathway	0,001916813	37	23
Non-small cell lung cancer	0,002645334	34	22
TNF signaling pathway	0,002726851	54	23
Gap junction	0,002747955	46	23
Regulation of actin cytoskeleton	0,002963677	105	28
Estrogen signaling pathway	0,004247695	50	24
Wnt signaling pathway	0,005920599	70	26
Prolactin signaling pathway	0,006509112	40	24
Circadian rhythm	0,008520374	19	19
Adrenergic signaling in cardiomyocytes	0,008739253	69	25
Acute myeloid leukemia	0,008895178	32	20
Dorso-ventral axis formation	0,012519859	17	21
Glycosaminoglycan biosynthesis - keratan sulfate	0,01286614	8	13
Melanogenesis	0,016608321	50	23
Fatty acid degradation	0,020998329	20	20
HTLV-I infection	0,026276281	124	27
Progesterone-mediated oocyte maturation	0,028133963	46	21
Endometrial cancer	0,030548076	29	23
Long-term potentiation	0,030923871	36	22
Steroid biosynthesis	0,031212644	9	16
Propanoate metabolism	0,031787292	15	16
Sulfur relay system	0,032327668	5	10
Osteoclast differentiation	0,033722833	61	25
Choline metabolism in cancer	0,033722833	51	25
p53 signaling pathway	0,041657523	34	19
Oxytocin signaling pathway	0,045081041	74	26
Transcriptional misregulation in cancer	0,045081041	78	27
Notch signaling pathway	0,046567358	27	22

Table 12. List of the KEGG pathways obtained with TargetScan targeted by the deregulated miRNAs present in NH_4Cl_SEVs vs NT_SEVs.

KEGG pathway - TrgetScan	**p-value**	**#genes**	**#miRNAs**
Mucin type O-Glycan biosynthesis	2,29567E-13	15	19
GABAergic synapse	9,65985E-07	31	23
Proteoglycans in cancer	0,000341394	70	42
Other types of O-glycan biosynthesis	0,000971085	12	13
Nicotine addiction	0,001387195	16	15
Biosynthesis of unsaturated fatty acids	0,002465109	9	6
Cell adhesion molecules (CAMs)	0,002465109	55	35
Pathways in cancer	0,002836038	123	46
Rap1 signaling pathway	0,003494424	79	38
Fatty acid degradation	0,004930019	13	12
Nicotinate and nicotinamide metabolism	0,005752231	13	11
Hippo signaling pathway	0,008199222	60	40

Morphine addiction	0,00941446	32	23
Calcium signaling pathway	0,00941446	64	31
Axon guidance	0,00941446	50	31
Endocytosis	0,009987889	80	34
Adherens junction	0,014226251	28	19
Glycosphingolipid biosynthesis - ganglio series	0,019646345	6	5
Ras signaling pathway	0,019646345	75	34
Sulfur relay system	0,03166086	5	7
Gap junction	0,03556992	28	25
Long-term depression	0,041526154	21	19
Regulation of actin cytoskeleton	0,0467054	71	34

Table 13. List of the KEGG pathways obtained with Tarbase targeted by the deregulated miRNAs present in MG132_SEVs vs NT_SEVs.

KEGG pathway - Tarbase	**p-value**	**#genes**	**#miRNAs**
Fatty acid metabolism	1.35860754236e-09	26	26
Prion diseases	1.35860754236e-09	20	26
FoxO signaling pathway	2.11686874683e-09	90	31
Proteoglycans in cancer	6.8000867728e-09	115	32
Protein processing in endoplasmic reticulum	1.09456546276e-08	106	35
Hippo signaling pathway	2.11465640647e-08	85	32
Renal cell carcinoma	1.45166521198e-06	47	30
Cell cycle	2.55472114867e-06	74	28
Thyroid hormone signaling pathway	3.47761993967e-06	69	31
Fatty acid degradation	7.1475851151e-06	23	21
AMPK signaling pathway	1.03016956407e-05	79	37
Adherens junction	1.3286500069e-05	46	28
TNF signaling pathway	2.01596638438e-05	63	27
Insulin signaling pathway	2.85656938236e-05	85	32
Pathways in cancer	3.84123272566e-05	199	37
Citrate cycle (TCA cycle)	8.07991716921e-05	23	27
N-Glycan biosynthesis	8.92442092154e-05	27	23
Endocytosis	0.000101841969848	117	34
T cell receptor signaling pathway	0.000190514430313	63	32
Colorectal cancer	0.000240402325019	40	26
Pancreatic cancer	0.000252787503371	43	27
Propanoate metabolism	0.000421117020785	19	19
Chagas disease (American trypanosomiasis)	0.000492965925629	57	27
HIF-1 signaling pathway	0.000492965925629	65	28
Ubiquitin mediated proteolysis	0.00056449901801	85	33
Glioma	0.000573165150518	37	26
Hepatitis B	0.000621523683316	74	30
Neurotrophin signaling pathway	0.000718886949973	69	29
Prostate cancer	0.000718886949973	53	31
TGF-beta signaling pathway	0.000945166085499	45	32
mTOR signaling pathway	0.000986986358626	39	29

Valine, leucine and isoleucine degradation	0.00101616167954	32	27
Fatty acid biosynthesis	0.00134702009959	4	12
Lysine degradation	0.00173039434799	30	27
Chronic myeloid leukemia	0.00221979307766	44	27
Acute myeloid leukemia	0.00224412542249	34	28
Axon guidance	0.00330032258656	68	32
MAPK signaling pathway	0.00382689535866	123	37
Steroid biosynthesis	0.00386633276792	11	19
Thyroid cancer	0.00402605800305	18	23
Adipocytokine signaling pathway	0.00432919490502	40	28
Estrogen signaling pathway	0.00438220902328	52	28
Regulation of actin cytoskeleton	0.00493442883098	108	35
Bacterial invasion of epithelial cells	0.00645763046429	42	29
Fc gamma R-mediated phagocytosis	0.00723983112494	49	30
Glyoxylate and dicarboxylate metabolism	0.00868221091395	16	20
GnRH signaling pathway	0.00964421617575	49	24
Osteoclast differentiation	0.0101658962527	66	31
Circadian rhythm	0.0158860035058	19	21
Pyruvate metabolism	0.0158860035058	23	23
Inositol phosphate metabolism	0.0158860035058	31	26
ErbB signaling pathway	0.0178949352292	49	34
Transcriptional misregulation in cancer	0.0178949352292	82	34
Peroxisome	0.0180728766541	45	28
Rap1 signaling pathway	0.0180728766541	102	31
HTLV-I infection	0.0180908823442	129	34
Terpenoid backbone biosynthesis	0.0186463777552	14	22
Wnt signaling pathway	0.0186463777552	69	29
Choline metabolism in cancer	0.0186463777552	54	31
Central carbon metabolism in cancer	0.0198538901597	34	27
Sphingolipid signaling pathway	0.023541750381	64	30
Oocyte meiosis	0.0251638084234	56	32
Phosphatidylinositol signaling system	0.0311427990971	44	27
Butanoate metabolism	0.031619440516	17	21
Progesterone-mediated oocyte maturation	0.0330683995744	47	27
p53 signaling pathway	0.0474081251664	37	23
Arrhythmogenic right ventricular cardiomyopathy (ARVC)	0.0475181752353	31	24
Fc epsilon RI signaling pathway	0.0475181752353	39	27
Signaling pathways regulating pluripotency of stem cells	0.0475181752353	66	33
Endometrial cancer	0.0493788822577	30	28
NF-kappa B signaling pathway	0.0495040019221	44	27

Table 14. List of the KEGG pathways obtained with TargetScan targeted by the deregulated miRNAs present in MG132_SEVs vs NT_SEVs.

KEGG pathway - TargetScan	**p-value**	**#genes**	**#miRNAs**
Fatty acid biosynthesis	3.55607120863e-11	3	4
ECM-receptor interaction	2.70648568564e-08	34	26

Biosynthesis of unsaturated fatty acids	8.18978120115e-08	12	11
Fatty acid metabolism	1.08406569755e-07	15	18
Nicotine addiction	4.39966214511e-05	18	16
Proteoglycans in cancer	0.000306990411567	76	44
Mucin type O-Glycan biosynthesis	0.000310065297477	13	17
GABAergic synapse	0.00052218294323	30	26
Axon guidance	0.00145662004485	57	36
Thyroid hormone signaling pathway	0.0015219593959	45	31
Phosphatidylinositol signaling system	0.00191616867027	36	30
Regulation of actin cytoskeleton	0.00191616867027	84	48
Pathways in cancer	0.00191616867027	135	53
Amoebiasis	0.00363505412607	44	26
Cell adhesion molecules (CAMs)	0.00363505412607	55	35
Adherens junction	0.00370739627517	31	25
Signaling pathways regulating pluripotency of stem cells	0.00602837076991	53	34
Other types of O-glycan biosynthesis	0.00923446073401	13	13
Morphine addiction	0.0103488631082	37	32
Platelet activation	0.0119528912543	51	33
Bacterial invasion of epithelial cells	0.0129374060631	32	22
Synaptic vesicle cycle	0.0129683448857	29	28
Rap1 signaling pathway	0.014446648054	80	48
Long-term depression	0.0146148318588	25	23
Sphingolipid signaling pathway	0.0345984651404	47	31
Taurine and hypotaurine metabolism	0.0437737882191	7	12
Hippo signaling pathway	0.0455459303718	62	44
Basal cell carcinoma	0.0497963261835	25	20
Focal adhesion	0.0497963261835	74	39

Table 15. miRNAs commonly deregulated in MG132_LEVs, MG132_SEVs and NH_4Cl_SEVs. In green = upregulated (1 in common between MG132_LEVs and MG132_SEVs and 8 in common between MG132_SEVs and NH_4Cl_SEVs), in red = downregulated (35 in common between MG132_SEVs and NH_4Cl_SEVs).

MG132_LEVs and MG132_SEVs	**MG132_SEVs and NH_4Cl_SEVs**
mmu-miR-669c-5p	mmu-miR-181a-5p
	mmu-miR-181c-5p
	mmu-miR-218-5p
	mmu-miR-23b-3p
	mmu-miR-301a-3p
	mmu-miR-30b-5p
	mmu-miR-423-5p
	mmu-miR-463-5p
	mmu-miR-1194
	mmu-miR-18b-5p
	mmu-miR-1954
	mmu-miR-1970
	mmu-miR-297a-5p

	mmu-miR-3060-5p
	mmu-miR-3091-3p
	mmu-miR-3091-5p
	mmu-miR-3470a
	mmu-miR-3470b
	mmu-miR-3471
	mmu-miR-3473c
	mmu-miR-363-5p
	mmu-miR-466i-3p
	mmu-miR-466i-5p
	mmu-miR-466k
	mmu-miR-467g
	mmu-miR-5098
	mmu-miR-5101
	mmu-miR-5126
	mmu-miR-6236
	mmu-miR-6240
	mmu-miR-6244
	mmu-miR-6363
	mmu-miR-6418-3p
	mmu-miR-6538
	mmu-miR-680
	mmu-miR-6937-5p
	mmu-miR-7012-3p
	mmu-miR-7012-5p
	mmu-miR-712-3p
	mmu-miR-712-5p
	mmu-miR-7684-5p
	mmu-miR-8112
	mmu-miR-8115

Table 16. miRNAs deregulated in MG132_SEVs and NH_4Cl_SEVs targeting the prion pathway. In green = upregulated (14 in MG132_SEVs and 13 in NH_4Cl_SEVs), in red = downregulated (12 in MG132_SEVs and 10 in NH_4Cl_SEVs), in bold = miRNAs in common between MG132_SEVs and NH_4Cl_SEVs (6 upregulated and 8 downregulated).

MG132_SEVs	**NH4Cl_SEVs**
mmu-let-7e-5p	mmu-miR-16-5p
mmu-miR-128-3p	**mmu-miR-181a-5p**
mmu-miR-155-5p	**mmu-miR-181c-5p**
mmu-miR-181a-5p	mmu-miR-19a-3p
mmu-miR-181c-5p	mmu-miR-19b-3p
mmu-miR-218-5p	**mmu-miR-218-5p**
mmu-miR-23a-3p	**mmu-miR-23b-3p**
mmu-miR-23b-3p	**mmu-miR-301a-3p**
mmu-miR-26b-5p	mmu-miR-30a-5p
mmu-miR-301a-3p	**mmu-miR-30b-5p**
mmu-miR-30b-5p	mmu-miR-30d-5p
mmu-miR-30c-5p	mmu-miR-30e-5p
mmu-miR-574-5p	mmu-miR-34c-5p
mmu-miR-669c-5p	**mmu-miR-18b-5p**
mmu-miR-143-3p	**mmu-miR-1954**
mmu-miR-18b-5p	mmu-miR-222-3p
mmu-miR-1954	**mmu-miR-466i-5p**
mmu-miR-29c-3p	**mmu-miR-466k**
mmu-miR-3470b	**mmu-miR-467g**
mmu-miR-466i-5p	mmu-miR-467h
mmu-miR-466k	**mmu-miR-5098**
mmu-miR-466q	**mmu-miR-712-5p**
mmu-miR-467g	**mmu-miR-3470b**
mmu-miR-5098	
mmu-miR-690	
mmu-miR-712-5p	

Table 17. miRNAs deregulated in NT_SEVs, MG132_SEVs and NH_4Cl_SEVs already associated to other conditions.

miRNA	sample	Regulation in NT_SEVs, MG132_SEVs and NH_4Cl_SEVs	reference	Regulation in reference
miR-181a-5p	MG132_SEVs NH_4Cl_SEVs	Upregulated Upregulated	miR-181a-5p is the ninth most abundant miRNA in laser capture micro-dissected human motor neurons of ALS patients and is also abundant in the CNS (Ludwig et al., 2016)	Upregulated
miR-181c-5p	MG132_SEVs NH_4Cl_SEVs	Upregulated Upregulated	miR-181c-5p expression was significantly increased as a result of 3-MA autophagy inhibitor treatment; miR-181c-5p reduced the LC3II/LC3I ratio and promoted p62 expression and suppress ATG5 expression (Xu et al., 2021)	Upregulated
			miR-181c-5p bound to autophagy-related gene ATG7 and inhibited its expression (Li et al., 2022)	Upregulated
			TDP-43 is in a regulatory negative feedback network with miR-181c-5p and miR-27b-3p that is dependent on its nuclear localization within HEK293T cells. Cellular stress which induces a redistribution of TDP-43 from the nucleus to the cytoplasm correlates	Downregulated

			with the reduced production of miR-27b-3p and miR-181c-5p (Hawley et al., 2020)	
			MAPT (encoding the tau protein) and TTBK1 (encoding a tau kinase) were identified as direct target genes of miR-181c-5p (Yan et al., 2020)	Upregulated
			Significant upregulation of miR-92a-3p, miR-181c-5p and miR-210-3p was found in the plasma of both MCI and AD subjects (Siedlecki-Wullich et al., 2019)	Upregulated
miR-18b-5p	MG132_SEVs NH_4Cl_SEVs	Downregulated Downregulated	downregulated in SOD1 G93A mice (Kim et al., 2020)	Downregulated
miR-466i-5p and **miR-466k**	MG132_SEVs NH_4Cl_SEVs	Downregulated Downregulated	suppression of miR-466k and miR-466i-5p enhanced cell injury in hypoxia-induced cardiomyocytes (Liao et al., 2020)	Downregulated
miR-218-5p	MG132_SEVs NH_4Cl_SEVs	Upregulated Upregulated	Mechanism of miR-218-5p in autophagy, apoptosis and oxidative stress in rheumatoid arthritis synovial fibroblasts is mediated by KLF9 and JAK/STAT3 pathways (Chen et al., 2021)	Downregulated miR-218-5p promotes autophagy
miR-23b-3p	MG132_SEVs NH_4Cl_SEVs	Upregulated Upregulated	Plasma Exosomal miRNAs in Persons with and without Alzheimer Disease: Altered Expression and Prospects for Biomarkers (Lugli et al., 2015)	Downregulated in AD exosomes
			miR-23b-3p regulates apoptosis and autophagy via suppressing SIRT1 in lens epithelial cells (Zhou et al., 2019)	Upregulated
miR-301a-3p	MG132_SEVs NH_4Cl_SEVs	Upregulated Upregulated	Circulating miRNA biomarkers for Alzheimer's disease (Kumar et al., 2013)	Upregulated in AD/MCI patients but downregulated for the validation through TaqMan analysis
miR-30b-5p	MG132_SEVs NH_4Cl_SEVs	Upregulated Upregulated	Panoramic Visualization of Circulating MicroRNAs Across Neurodegenerative Diseases in Humans (Brennan et al., 2019)	Downregulated in AD, PD and ALS patients
			Dysregulation of MicroRNAs and Target Genes Networks in Peripheral Blood of Patients with Sporadic Amyotrophic Lateral Sclerosis (Liguori et al., 2019)	Downregulated in sALS patients
			Correlating serum MicroRNAs and clinical parameters in amyotrophic lateral sclerosis (Raheja et al., 2018)	Downregulated
			Profiling of Serum Exosome MiRNA Reveals the Potential of a MiRNA Panel as Diagnostic Biomarker for Alzheimer's Disease (Dong et al., 2021)	Downregulated in AD patients
			Nuclear miR-30b-5p suppresses TFEB-mediated lysosomal biogenesis and autophagy (miR-30b-5p) has a role in autophagy) (Guo et al., 2021)	Upregulated

DISCUSSION

EVs secretion was initially considered a mechanism through which cells eliminate unnecessary proteins. However, now it is known that it could serve an intercellular communication purpose. A strong support for this concept was obtained by the observation that EVs also contain mRNAs and microRNAs that, when transferred to recipient cells, remain functional and may affect cellular behaviour (Mathieu et al., 2019).

In the last years, several studies observed the presence of deregulated miRNAs also in LEVs ad SEVs obtained from patients affected by many NDs (including ALS and FTD), suggesting that miRNAs contained in EVs can also have a role in the pathogenesis and progression of these diseases (Sproviero et al., 2021).

Neither the reason nor the mechanism by which miRNAs are targeted to LEVs and SEVs are yet known. However, it has been observed that the two vesicular populations often contain different miRNAs which secretion seems to be differentially deregulated in different NDs (Sproviero et al., 2021).

One of the possible mechanisms involved in targeting miRNAs in EVs is the RNA-binding protein mediated transport of miRNAs (Groot & Lee, 2020).

Since in the first part of my work I analysed the secretion of TDP species in NSC34 cells both in physiological and pathological conditions (autophagy and proteasome blockade) and I observed that the secretion of TDP species increases considerably following the blockade of the proteasome, knowing that TDP is an RNA binding protein, I considered interesting to evaluate whether the alterations affecting the PQC system could also alter the physiological secretion of miRNAs in LEVs and SEVs.

To this purpose, I first analyzed the miRNAs content of LEVs and SEVs obtained from cells in physiological conditions and I observed that the two different types of EVs produced by the NSC34 cells differ not only in size and enrichment in specific vesicular markers, but also in their content of miRNAs. In fact, they are characterized by two different miRNAs profile, with 90 miRNAs that are differentially expressed between LEVs and SEVs. This suggests that LEVs and SEVs may differentially affect genes expression profile of recipient cells. Interestingly, the KEGG pathway analyses of these miRNAs showed that they target several

intracellular pathways including “GABAergic synapse”, “Fatty acid metabolism”, “Fatty acids degradation” “Glycosphingolipids metabolism” and “prion disease”, that play important role in neurons and whose alteration has been observed to be associated to NDs, including ALS. Therefore, the secretion of these miRNAs in physiological conditions may contribute to regulate in the recipient cells neuronal excitability (the primary role of the GABAergic synapses) that is fundamental in the central nervous system (Roth & Draguhn, 2012), and the expression of genes encoding for proteins involved in the maintenance of lipid homeostasis, that is particularly important in the central nervous system since lipids modulate membrane fluidity, electric signal transduction, and synaptic stabilization (Falabella et al., 2021).

Moreover, the secretion of miRNAs able to regulate the expression of genes involved in the prion pathway suggests that their secretion within LEVs and SEVs may also contribute to modulate protein aggregation in the recipient cells.

Then, the data obtained by evaluating the miRNA profile of LEVs and SEVs arising from cells treated with MG132 and NH_4Cl respect to those obtained from untreated cells demonstrated that the inhibition of proteasome and autophagy can alter the miRNA profile of LEVs and SEVs respect to the control condition. In particular, data showed that proteasome inhibition causes an alteration in miRNAs expression in both LEVs and SEVs, with a greater number of miRNAs differentially expressed in MG132_SEVs respect to NT_SEVs, than those differentially expressed in MG132_LEVs respect to NT_LEVs. While, inhibition of autophagy causes an alteration only in the expression of miRNAs in SEVs. Moreover, most of miRNAs deregulated in SEVs resulted in common between the two treatments and mainly downregulated in both conditions. This seems to be in contrast with data observed for TDP species in the previous chapter that, mainly following the UPS inhibition are more secreted. This opposite control of the miRNAs and TDP species secretion in NSC34-treated derived SEVs suggests that the miRNAs found downregulated in EVs are not co-transported by TDP-43. However, since I observed that the most secreted TDP species are the CTFs, TDP-25 and TDP-35, the reduced secretion of miRNA could be related to the loss or partial loss of the RRM1, necessary to TDP-43 to bind RNA (H.-J. Chen et al., 2019; Takagi et al., 2013). In addition, since both proteasome and autophagy impairment cause an increase of the TDP-43 aggregation in the cytoplasm reducing its

activity (Cicardi et al., 2018; Huang et al., 2014), the rate of miRNAs whose biogenesis is mediated by TDP-43 could be reduced and consequently also their secretion in EVs.

On the other side, the upregulation of a subset of miRNAs secreted in LEVs after the proteasome blockade, confirms that the increased secretion of TDP-43 may cause a consequent increase of secreted miRNAs.

The analysis of KEGG pathways targeted by miRNAs deregulated in SEVs, after the treatment of cells with MG132 and NH_4Cl, showed that among the most enriched pathways there is the prion disease. The presence in EVs of miRNAs targeting the prion disease pathway has shown that EVs contain potentially harmful miRNAs that if up or downregulated with respect to the control condition may contribute to the pathogenesis and progression of neurodegenerative diseases, including ALS and FTD. In addition, the deregulation of miRNAs targeting the prion disease pathway, especially in MG132_SEVs and NH_4Cl_SEVs but not in NT_SEVs, suggested that blockade of both the proteasome and autophagy can affect the secretion of these potentially harmful miRNAs in SEVs. Interestingly, it has been observed that the two treatments can specifically deregulate some miRNAs, but the majority of deregulated miRNAs were the same for both treatment; moreover, these commonly deregulated miRNA were moving in the same direction (up or down) in the two treatments. These results suggest that proteasome and autophagy blockage, common conditions observed during disease progression in NDs, can activate specific but also common responses, that may similarly contribute to the progression of these diseases.

Interestingly, some of these miRNAs targeting the prion disease pathway and deregulated in both treated SEVs, such as miR-181a-5p (Ludwig et al., 2016), miR-181c-5p (Hawley et al., 2020; T.-H. Li et al., 2022; Siedlecki-Wullich et al., 2019; T. Xu et al., 2021; Yan et al., 2020), miR-18b-5p (K. Y. Kim et al., 2020), miR-466i-5p, miR-466k (Liao et al., 2020), miR-218-5p (M. Chen et al., 2021), miR-23b-3p (Lugli et al., 2015; Zhou et al., 2019), miR-301a-3p (Kumar et al., 2013), miR-30b-5p (Brennan et al., 2019; Dong et al., 2021; H. Guo et al., 2021; Liguori et al., 2018; Raheja et al., 2018) have been already observed deregulated in NDs conditions and as a result of alterations in the proteasome and autophagy pathway in other studies, suggesting that their deregulation is effectively mediated by the PQC inhibition and may have a role in the spreading of the disease.

In particular, in parallel with data obtained in my study that showed an upregulation of miR-181a-5p in both MG132_SEVs and NH_4Cl_SEVs, miR-181a-5p was observed to be the ninth most present miRNA in laser capture micro-dissected of ALS patients motor neurons and also abundant in cells of the central nervous system (Ludwig et al., 2016). This suggests that its increased secretion could be related to the impairment of the PQC system (a common condition observed in ALS patients).

For miR-181c-5p, the observation of its upregulation in NH_4Cl_SEVs are in accordance with the results obtained by Xu and colleagues (T. Xu et al., 2021) and Li and colleagues (T.-H. Li et al., 2022) that observed its increased expression in cells as a result of 3-MA autophagy inhibitor treatment. This miRNA is able to target ATG7 (a protein essential for the formation and closure of autophagosomes) and to promote autophagy inhibition. Therefore, inhibition of autophagy through NH_4Cl may cause an increased expression of this miRNA in cells and consequently its secretion in SEVs. The increased secretion of miR-181c-5p in NH_4Cl_SEVs could be explained by the fact that NH_4Cl by neutralizing lysosomal pH, inhibits the degradation of MVBs into lysosome and favours their fusion with the plasma membrane, with a consequent higher SEVs secretion. However, the increased secretion of miR-181c-5p also in MG132_SEVs may represent a protective mechanism that cells use to reduce the intracellular level of this miRNA in order to prevent the autophagy inhibition caused by the interaction of miR-181c-5p with ATG7 and increase, on the contrary, the autophagic activity.

Other two studies also confirmed the involvement of miR-181c-5p in Alzheimer's disease (AD) which, as like as in ALS/FTD, is characterized by a prion-like mechanism of propagation and an alteration of the PQC system (Siedlecki-Wullich et al., 2019; Yan et al., 2020). In particular, Siedlecki-Wullich and colleagues, showed a significant upregulation of this miRNA in the plasma of AD subjects suggesting that its secretion could be potentiated in pathological conditions, and its uptake could contribute to the spreading of the disease modulating the expression of specific genes involved in the prion disease pathway, like MAPT (encoding the tau protein) and TTBK1 (encoding a tau kinase). Moreover, a study conducted by Hawley ad colleagues showed that miR-181c-5p is also involved in a regulatory negative feedback network with TDP-43 (Hawley et al., 2020). In particular, the authors observed that the translocation of TDP-43 from the nucleus to the cytoplasm

following cellular stress results in a reduced production of this miRNA. However, since data obtained in MG132_SEVs and NH_4Cl_SEVs show that PQC inhibition increases the secretion of miR-181c-5p in SEVs respect to the control conditions, it is possible to hypothesize that, under stress conditions (such as proteasome or autophagy blockade), the translocation of TDP-43 from the nucleus to the cytoplasm, not only causes a decrease in the biogenesis of miR-181c-5p but increases its secretion in SEVs. The secretion of this miRNA in the extracellular space and its subsequent uptake by another healthy or affected cell, however, could cause in the latter an intracellular increase of this miRNA and therefore an alteration of its negative feedback network with TDP-43, thus affecting TDP-43 behaviour.

For the miRNA miR-18b-5p, that I observed downregulated both in MG132_SEVs and in NH_4Cl_SEVs, Kim and colleagues observed its downregulation in NSC34 cells expressing the mutated form G93A of the protein SOD1, associated to fALS (K. Y. Kim et al., 2020). G93A mutation results in the formation of SOD1 aggregates in affected neurons. As like as the TDP-43 aggregation, the aggregation of SOD1 is associated to an impairment of the PQC system, for this reason, the decreased expression of miR-18b-5p in NSC34 cells expressing SOD1 G93A suggests that the inhibition of the PQC system could effectively alter the expression of this miRNA and consequently its secretion.

The downregulation of miR-466i-5p and miR-466k, that I observed downregulated in MG132_SEVs and NH_4Cl_SEVs, was observed to promote cell injury in hypoxia-induced cardiomyocytes (Liao et al., 2020). Therefore, these miRNAs seem to exert protective function in cells and their reduced levels in SEVs could result in a less protection for the recipient cells. This in turn can contribute to the spreading of the disease.

For the miRNA miR-218-5p, Chen and colleagues observed that its downregulation promotes the autophagy (M. Chen et al., 2021). Therefore, it might be assumed that an inhibition of autophagy has the opposite effect, as I observed. Also miR-23b-3p was observed to promotes autophagy however, this miRNAs promotes also apoptosis, suggesting that its increased secretion (that I observed in MG132_SEVs and NH_4Cl_SEVs) could be harmful for the recipient cells (Zhou et al., 2019). This miRNA resulted secreted also in SEVs obtained from plasma of AD patients (Lugli et al., 2015), however, in this condition, in contrast to the results obtained in MG132_SEVs and NH_4Cl_SEVs, it resulted

downregulated, suggesting that the expression of miR-23b-3p and its secretion can be modulated by different factors, not only the impairment of the PQC system.

The results obtained in the study conducted by Kumar and colleagues on the circulating miRNAs enriched in AD patients, showed an enrichment of the miR-301a-3p in plasma of this patients (Kumar et al., 2013). I also observed the upregulation of this miRNA in treated-EVs, supporting the hypothesis that its secretion is associated to NDs conditions and could have a role in the propagation of the disease.

Finally, the results obtained for miR-30b-5p are in contrast with data showing a downregulation of this miRNAs in ALS blood (Brennan et al., 2019; Liguori et al., 2018; Raheja et al., 2018) and in plasma of AD patients (Dong et al., 2021). However, it should be considered that data obtained in NSC34 are the result of acute stress, whereas the data obtained in patients reflect the result of a chronic disease condition. On the other hand, the observation of Guo et al. that the overexpression of miR-30b-5p decreases the lysosomal biogenesis is in line with my results obtained in EVs isolated from NSC34 cells in which UPS and autophagy were impaired (H. Guo et al., 2021). This, in fact, allows to assume that the pathological conditions (mimicked inhibiting autophagy and proteasome) can increase the secretion in SEVs of miR-30b-5p that, whether internalized by the recipient cells can alter in them the lysosomal biogenesis. The lysosomes are fundamental for the autophagy degradation of protein aggregated in NDs, therefore, problems in its biogenesis can contribute to increase the protein aggregation and consequently also the spreading of the disease.

In conclusions, it seems that the inhibition of proteasome and autophagy can effectively modulate the secretion of miRNAs that are harmful for the recipient cells and can contribute to the propagation of the disease through a prion-like mechanism.

To confirm these hypotheses, the validation of miRNAs associated to the prion diseases and deregulated in SEVs is in progress, in collaboration with the Mondino Foundation of Pavia and the Sacco Hospital of Milan. All these data are included in a manuscript in preparation.

CONCLUSIONS

EVs play a central role in ALS and FTD since they may spread the pathology or contribute to the intracellular PQC system for the clearance of TDP-43 and its aggregation-prone CTFs TDP-35 and TDP-25. During my PhD period, I focused my attention on i) the crosstalk between EVs, both LEVs and SEVs, and the PQC system in the disposal of TDP species, both in neurons and myoblasts, ii) the contribution of the CASA-complex members in targeting TDP species to EVs, iii) the effect of EVs exposure on recipient cells, iv) the miRNAs content of LEVs and SEVs both in physiological and in pathological (UPS or autophagy blockade) and v) the pathways targeted by miRNAs contained in EVs and their possible role in the spreading of the disease.

From the results obtained in the first part of my study, mainly focused on EVs protein content and the interplay between EVs and PQC system for the disposal of disease-associated proteins, I can assume that TDP-43 species (mainly as TDP-35 and TDP-25 fragments in their insoluble form) are physiologically secreted within both LEVs and SEVs, together with the PQC system members HSP70, CHIP, BAG3, HSPB8, MAP1LC3B (I and II) and SQSTM1/p62. I can also assume that, in neurons, proteasome is the main mechanism used by cells to remove TDP species and that autophagy and secretion within EVs, assisted by the CASA-complex members HSPB8 and BAG3, represent two compensatory mechanisms able to favour the disposal of TDP species when the proteasome is impaired. Indeed, when proteasome is pharmacologically blocked, the secretion of TDP species and the CASA-complex members HSPB8 and BAG3 is boosted.

The increased secretion of TDP species in EVs when the PQC is blocked can favour the spreading of the disease, indeed the treatment of cells with EVs released by cells after PQC impairment is more toxic than the treatment with EVs released by untreated cells.

Moreover, I observed that also muscle cells secrete TDP species and CASA-complex members within EVs, but in these cells autophagy may have a more relevant role in the disposal of TDP species, indeed the secretion is increased mainly in SEVs when the autophagy is impaired.

Finally, I demonstrated that the inhibition of the CASA-complex formation increases the secretion in EVs of TDP species and HSPB8 but not HSP70 and BAG3, suggesting that HSPB8 may direct TDP species to EVs also independently from binding BAG3 and the other CASA-complex proteins, by means of its ability to bind membrane lipids.

On the other hand, the results obtained in the second part of my study, focused on the miRNA content of LEVs and SEVs and on the effect of the PQC inhibition (a typical feature observed in ALS and FTD affected cells during disease progression) to their secretion, allow to assume that LEVs and SEVs are characterized by two different miRNA profile and that the inhibition of proteasome and autophagy can modulate the levels of several miRNAs. Among the miRNAs commonly deregulated by both treatments, a number targets genes involved in the prion disease pathway (potentially harmful whether picked up by the recipient cells), especially in SEVs.

In conclusion, the increased EVs secretion of insoluble TDP-43 species and potentially harmful miRNAs could have a double role in pathological conditions: it could help cells to reduce the amount of TDP species that accumulate in their cytoplasm because of PQC impairment, and miRNAs targeting the prion disease pathway, probably more expressed in cells in pathological conditions, however it could also favour the spreading of the disease following the uptake of these EVs by neighbouring or more distant healthy cells.

BIBLIOGRAPHY

ADAMS, J. (2003). The proteasome: structure, function, and role in the cell. *Cancer Treatment Reviews*, *29*, 3–9. https://doi.org/10.1016/S0305-7372(03)00081-1

Afroz, T., Hock, E.-M., Ernst, P., Foglieni, C., Jambeau, M., Gilhespy, L. A. B., Laferriere, F., Maniecka, Z., Plückthun, A., Mittl, P., Paganetti, P., Allain, F. H. T., & Polymenidou, M. (2017). Functional and dynamic polymerization of the ALS-linked protein TDP-43 antagonizes its pathologic aggregation. *Nature Communications*, *8*(1), 45. https://doi.org/10.1038/s41467-017-00062-0

Afroz, T., Pérez-Berlanga, M., & Polymenidou, M. (2019). Structural Transition, Function and Dysfunction of TDP-43 in Neurodegenerative Diseases. *CHIMIA*, *73*(5), 380. https://doi.org/10.2533/chimia.2019.380

Al-Chalabi, A., & Hardiman, O. (2013). The epidemiology of ALS: a conspiracy of genes, environment and time. *Nature Reviews Neurology*, *9*(11), 617–628. https://doi.org/10.1038/nrneurol.2013.203

Altinok, S., Sanchez-Hodge, R., Stewart, M., Smith, K., & Schisler, J. C. (2021). With or without You: Co-Chaperones Mediate Health and Disease by Modifying Chaperone Function and Protein Triage. *Cells*, *10*(11), 3121. https://doi.org/10.3390/cells10113121

Alvarez-Erviti, L., Seow, Y., Schapira, A. H., Gardiner, C., Sargent, I. L., Wood, M. J. A., & Cooper, J. M. (2011). Lysosomal dysfunction increases exosome-mediated alpha-synuclein release and transmission. *Neurobiology of Disease*, *42*(3), 360–367. https://doi.org/10.1016/j.nbd.2011.01.029

Alvira, S., Cuéllar, J., Röhl, A., Yamamoto, S., Itoh, H., Alfonso, C., Rivas, G., Buchner, J., & Valpuesta, J. M. (2014). Structural characterization of the substrate transfer mechanism in Hsp70/Hsp90 folding machinery mediated by Hop. *Nature Communications*, *5*(1), 5484. https://doi.org/10.1038/ncomms6484

Amin, A., Perera, N. D., Beart, P. M., Turner, B. J., & Shabanpoor, F. (2020). Amyotrophic Lateral Sclerosis and Autophagy: Dysfunction and Therapeutic Targeting. *Cells*, *9*(11), 2413. https://doi.org/10.3390/cells9112413

Anckar, J., & Sistonen, L. (2011). Regulation of H <scp>SF</scp> 1 Function in the Heat Stress Response: Implications in Aging and Disease. *Annual Review of Biochemistry*, *80*(1), 1089–1115. https://doi.org/10.1146/annurev-biochem-060809-095203

Annunziata, C. M., Kleinberg, L., Davidson, B., Berner, A., Gius, D., Tchabo, N., Steinberg, S. M., & Kohn, E. C. (2007). BAG-4/SODD and Associated Antiapoptotic Proteins Are Linked to Aggressiveness of Epithelial Ovarian Cancer. *Clinical Cancer Research*, *13*(22), 6585–6592. https://doi.org/10.1158/1078-0432.CCR-07-0327

Aragonès Pedrola, J., & Rüdiger, S. G. D. (2021). Double J-domain piloting of an Hsp70 substrate. *Journal of Biological Chemistry*, *296*, 100717. https://doi.org/10.1016/j.jbc.2021.100717

Arai, T., Hasegawa, M., Akiyama, H., Ikeda, K., Nonaka, T., Mori, H., Mann, D., Tsuchiya, K., Yoshida, M., Hashizume, Y., & Oda, T. (2006). TDP-43 is a component of ubiquitin-positive tau-negative inclusions in frontotemporal lobar degeneration and amyotrophic lateral sclerosis.

Biochemical and Biophysical Research Communications, *351*(3), 602–611. https://doi.org/10.1016/j.bbrc.2006.10.093

Ardley, H. C., Hung, C.-C., & Robinson, P. A. (2005). The aggravating role of the ubiquitin-proteasome system in neurodegeneration. *FEBS Letters*, *579*(3), 571–576. https://doi.org/10.1016/j.febslet.2004.12.058

Arndt, V., Daniel, C., Nastainczyk, W., Alberti, S., & Höhfeld, J. (2005). BAG-2 Acts as an Inhibitor of the Chaperone-associated Ubiquitin Ligase CHIP. *Molecular Biology of the Cell*, *16*(12), 5891–5900. https://doi.org/10.1091/mbc.e05-07-0660

Arndt, V., Dick, N., Tawo, R., Dreiseidler, M., Wenzel, D., Hesse, M., Fürst, D. O., Saftig, P., Saint, R., Fleischmann, B. K., Hoch, M., & Höhfeld, J. (2010). Chaperone-Assisted Selective Autophagy Is Essential for Muscle Maintenance. *Current Biology*, *20*(2), 143–148. https://doi.org/10.1016/j.cub.2009.11.022

Arosio, A., Cristofani, R., Pansarasa, O., Crippa, V., Riva, C., Sirtori, R., Rodriguez-Menendez, V., Riva, N., Gerardi, F., Lunetta, C., Cereda, C., Poletti, A., Ferrarese, C., Tremolizzo, L., & Sala, G. (2020). HSC70 expression is reduced in lymphomonocytes of sporadic ALS patients and contributes to TDP-43 accumulation. *Amyotrophic Lateral Sclerosis and Frontotemporal Degeneration*, *21*(1–2), 51–62. https://doi.org/10.1080/21678421.2019.1672749

Ayala, Y. M., de Conti, L., Avendaño-Vázquez, S. E., Dhir, A., Romano, M., D'Ambrogio, A., Tollervey, J., Ule, J., Baralle, M., Buratti, E., & Baralle, F. E. (2011). TDP-43 regulates its mRNA levels through a negative feedback loop. *The EMBO Journal*, *30*(2), 277–288. https://doi.org/10.1038/emboj.2010.310

Ayala, Y. M., Pantano, S., D'Ambrogio, A., Buratti, E., Brindisi, A., Marchetti, C., Romano, M., & Baralle, F. E. (2005). Human, Drosophila, and C.elegans TDP43: Nucleic Acid Binding Properties and Splicing Regulatory Function. *Journal of Molecular Biology*, *348*(3), 575–588. https://doi.org/10.1016/j.jmb.2005.02.038

Ayala, Y. M., Zago, P., D'Ambrogio, A., Xu, Y.-F., Petrucelli, L., Buratti, E., & Baralle, F. E. (2008). Structural determinants of the cellular localization and shuttling of TDP-43. *Journal of Cell Science*, *121*(22), 3778–3785. https://doi.org/10.1242/jcs.038950

Bannwarth, S., Ait-El-Mkadem, S., Chaussenot, A., Genin, E. C., Lacas-Gervais, S., Fragaki, K., Berg-Alonso, L., Kageyama, Y., Serre, V., Moore, D. G., Verschueren, A., Rouzier, C., le Ber, I., Augé, G., Cochaud, C., Lespinasse, F., N'Guyen, K., de Septenville, A., Brice, A., … Paquis-Flucklinger, V. (2014). A mitochondrial origin for frontotemporal dementia and amyotrophic lateral sclerosis through CHCHD10 involvement. *Brain*, *137*(8), 2329–2345. https://doi.org/10.1093/brain/awu138

Bayer, T. A. (2015). Proteinopathies, a core concept for understanding and ultimately treating degenerative disorders? *European Neuropsychopharmacology*, *25*(5), 713–724. https://doi.org/10.1016/j.euroneuro.2013.03.007

Behl, C. (2016). Breaking BAG: The Co-Chaperone BAG3 in Health and Disease. *Trends in Pharmacological Sciences*, *37*(8), 672–688. https://doi.org/10.1016/j.tips.2016.04.007

Benajiba, L., le Ber, I., Camuzat, A., Lacoste, M., Thomas-Anterion, C., Couratier, P., Legallic, S., Salachas, F., Hannequin, D., Decousus, M., Lacomblez, L., Guedj, E., Golfier, V., Camu, W., Dubois, B., Campion, D., Meininger, V., & Brice, A. (2009). *TARDBP* mutations in motoneuron

disease with frontotemporal lobar degeneration. *Annals of Neurology*, *65*(4), 470–473. https://doi.org/10.1002/ana.21612

Bendotti, C., Marino, M., Cheroni, C., Fontana, E., Crippa, V., Poletti, A., & de Biasi, S. (2012). Dysfunction of constitutive and inducible ubiquitin-proteasome system in amyotrophic lateral sclerosis: Implication for protein aggregation and immune response. *Progress in Neurobiology*, *97*(2), 101–126. https://doi.org/10.1016/j.pneurobio.2011.10.001

Berning, B. A., & Walker, A. K. (2019). The Pathobiology of TDP-43 C-Terminal Fragments in ALS and FTLD. *Frontiers in Neuroscience*, *13*. https://doi.org/10.3389/fnins.2019.00335

Birgisdottir, Å. B., Lamark, T., & Johansen, T. (2013). The LIR motif – crucial for selective autophagy. *Journal of Cell Science*, *126*(15), 3237–3247. https://doi.org/10.1242/jcs.126128

Bjørkøy, G., Lamark, T., Brech, A., Outzen, H., Perander, M., Øvervatn, A., Stenmark, H., & Johansen, T. (2005). p62/SQSTM1 forms protein aggregates degraded by autophagy and has a protective effect on huntingtin-induced cell death. *Journal of Cell Biology*, *171*(4), 603–614. https://doi.org/10.1083/jcb.200507002

Borroni, B., Bonvicini, C., Alberici, A., Buratti, E., Agosti, C., Archetti, S., Papetti, A., Stuani, C., di Luca, M., Gennarelli, M., & Padovani, A. (2009). Mutation within *TARDBP* leads to Frontotemporal Dementia without motor neuron disease. *Human Mutation*, *30*(11), E974–E983. https://doi.org/10.1002/humu.21100

Bose, J. K., Huang, C.-C., & Shen, C.-K. J. (2011). Regulation of Autophagy by Neuropathological Protein TDP-43. *Journal of Biological Chemistry*, *286*(52), 44441–44448. https://doi.org/10.1074/jbc.M111.237115

Boukouris, S., & Mathivanan, S. (2015). Exosomes in bodily fluids are a highly stable resource of disease biomarkers. *PROTEOMICS - Clinical Applications*, *9*(3–4), 358–367. https://doi.org/10.1002/prca.201400114

Boylan, K. (2015). Familial Amyotrophic Lateral Sclerosis. *Neurologic Clinics*, *33*(4), 807–830. https://doi.org/10.1016/j.ncl.2015.07.001

Brennan, S., Keon, M., Liu, B., Su, Z., & Saksena, N. K. (2019). Panoramic Visualization of Circulating MicroRNAs Across Neurodegenerative Diseases in Humans. *Molecular Neurobiology*, *56*(11), 7380–7407. https://doi.org/10.1007/s12035-019-1615-1

Brown, R. H., & Al-Chalabi, A. (2017). Amyotrophic Lateral Sclerosis. *New England Journal of Medicine*, *377*(2), 162–172. https://doi.org/10.1056/NEJMra1603471

Buratti, E. (2015). *Functional Significance of TDP-43 Mutations in Disease* (pp. 1–53). https://doi.org/10.1016/bs.adgen.2015.07.001

Buratti, E. (2018). TDP-43 post-translational modifications in health and disease. *Expert Opinion on Therapeutic Targets*, *22*(3), 279–293. https://doi.org/10.1080/14728222.2018.1439923

Buratti, E., & Baralle, F. E. (2001). Characterization and Functional Implications of the RNA Binding Properties of Nuclear Factor TDP-43, a Novel Splicing Regulator ofCFTR Exon 9. *Journal of Biological Chemistry*, *276*(39), 36337–36343. https://doi.org/10.1074/jbc.M104236200

Buratti, E., & Baralle, F. E. (2010). The multiple roles of TDP-43 in pre-mRNA processing and gene expression regulation. *RNA Biology*, *7*(4), 420–429. https://doi.org/10.4161/rna.7.4.12205

Bustamante, H. A., González, A. E., Cerda-Troncoso, C., Shaughnessy, R., Otth, C., Soza, A., & Burgos, P. v. (2018). Interplay Between the Autophagy-Lysosomal Pathway and the Ubiquitin-Proteasome System: A Target for Therapeutic Development in Alzheimer's Disease. *Frontiers in Cellular Neuroscience*, *12*. https://doi.org/10.3389/fncel.2018.00126

Butti, Z., & Patten, S. A. (2019). RNA Dysregulation in Amyotrophic Lateral Sclerosis. *Frontiers in Genetics*, *9*. https://doi.org/10.3389/fgene.2018.00712

Candelise, N., Scaricamazza, S., Salvatori, I., Ferri, A., Valle, C., Manganelli, V., Garofalo, T., Sorice, M., & Misasi, R. (2021). Protein Aggregation Landscape in Neurodegenerative Diseases: Clinical Relevance and Future Applications. *International Journal of Molecular Sciences*, *22*(11), 6016. https://doi.org/10.3390/ijms22116016

Carey, J. L., & Guo, L. (2022). Liquid-Liquid Phase Separation of TDP-43 and FUS in Physiology and Pathology of Neurodegenerative Diseases. *Frontiers in Molecular Biosciences*, *9*. https://doi.org/10.3389/fmolb.2022.826719

Carlos, A. F., & Josephs, K. A. (2022). Frontotemporal lobar degeneration with TAR DNA-binding protein 43 (TDP-43): its journey of more than 100 years. *Journal of Neurology*, *269*(8), 4030–4054. https://doi.org/10.1007/s00415-022-11073-3

Carra, S., Crippa, V., Rusmini, P., Boncoraglio, A., Minoia, M., Giorgetti, E., Kampinga, H. H., & Poletti, A. (2012). Alteration of protein folding and degradation in motor neuron diseases: Implications and protective functions of small heat shock proteins. *Progress in Neurobiology*, *97*(2), 83–100. https://doi.org/10.1016/j.pneurobio.2011.09.009

Carra, S., Seguin, S. J., & Landry, J. (2008). HspB8 and Bag3: A new chaperone complex targeting misfolded proteins to macroautophagy. *Autophagy*, *4*(2), 237–239. https://doi.org/10.4161/auto.5407

Casarotto, E., Sproviero, D., Corridori, E., Gagliani, M. C., Cozzi, M., Chierichetti, M., Cristofani, R., Ferrari, V., Galbiati, M., Mina, F., Piccolella, M., Rusmini, P., Tedesco, B., Gagliardi, S., Cortese, K., Cereda, C., Poletti, A., & Crippa, V. (2022). Neurodegenerative Disease-Associated TDP-43 Fragments Are Extracellularly Secreted with CASA Complex Proteins. *Cells*, *11*(3), 516. https://doi.org/10.3390/cells11030516

Cascella, R., Fani, G., Bigi, A., Chiti, F., & Cecchi, C. (2019). Partial Failure of Proteostasis Systems Counteracting TDP-43 Aggregates in Neurodegenerative Diseases. *International Journal of Molecular Sciences*, *20*(15), 3685. https://doi.org/10.3390/ijms20153685

Cascella, R., Fani, G., Capitini, C., Rusmini, P., Poletti, A., Cecchi, C., & Chiti, F. (2017). Quantitative assessment of the degradation of aggregated TDP-43 mediated by the ubiquitin proteasome system and macroautophagy. *The FASEB Journal*, *31*(12), 5609–5624. https://doi.org/10.1096/fj.201700292RR

Celen, A. B., & Sahin, U. (2020). Sumoylation on its 25th anniversary: mechanisms, pathology, and emerging concepts. *The FEBS Journal*, *287*(15), 3110–3140. https://doi.org/10.1111/febs.15319

Chanteloup, G., Cordonnier, M., Moreno-Ramos, T., Pytel, V., Matías-Guiu, J., Gobbo, J., Cabrera-Martín, M. N., Gómez-Pinedo, U., Garrido, C., & Matías-Guiu, J. A. (2019). Exosomal HSP70 for Monitoring of Frontotemporal Dementia and Alzheimer's Disease: Clinical and FDG-PET

Correlation. *Journal of Alzheimer's Disease*, *71*(4), 1263–1269. https://doi.org/10.3233/JAD-190545

Chen, H.-J., Topp, S. D., Hui, H. S., Zacco, E., Katarya, M., McLoughlin, C., King, A., Smith, B. N., Troakes, C., Pastore, A., & Shaw, C. E. (2019). RRM adjacent TARDBP mutations disrupt RNA binding and enhance TDP-43 proteinopathy. *Brain*, *142*(12), 3753–3770. https://doi.org/10.1093/brain/awz313

Chen, M., Li, M., Zhang, N., Sun, W., Wang, H., & Wei, W. (2021). Mechanism of miR-218-5p in autophagy, apoptosis and oxidative stress in rheumatoid arthritis synovial fibroblasts is mediated by KLF9 and JAK/STAT3 pathways. *Journal of Investigative Medicine*, *69*(4), 824–832. https://doi.org/10.1136/jim-2020-001437

Chen, Q. Y., Wen, T., Wu, P., Jia, R., Zhang, R., & Dang, J. (2021). Exosomal Proteins and miRNAs as Mediators of Amyotrophic Lateral Sclerosis. *Frontiers in Cell and Developmental Biology*, *9*. https://doi.org/10.3389/fcell.2021.718803

Chi, H., Chang, H.-Y., & Sang, T.-K. (2018). Neuronal Cell Death Mechanisms in Major Neurodegenerative Diseases. *International Journal of Molecular Sciences*, *19*(10), 3082. https://doi.org/10.3390/ijms19103082

Chiti, F., & Dobson, C. M. (2017). Protein Misfolding, Amyloid Formation, and Human Disease: A Summary of Progress Over the Last Decade. *Annual Review of Biochemistry*, *86*(1), 27–68. https://doi.org/10.1146/annurev-biochem-061516-045115

Chopra, G., Shabir, S., Yousuf, S., Kauts, S., Bhat, S. A., Mir, A. H., & Singh, M. P. (2022). Proteinopathies: Deciphering Physiology and Mechanisms to Develop Effective Therapies for Neurodegenerative Diseases. *Molecular Neurobiology*, *59*(12), 7513–7540. https://doi.org/10.1007/s12035-022-03042-8

Chowdary, T. K., Raman, B., Ramakrishna, T., & Rao, Ch. M. (2007). Interaction of mammalian Hsp22 with lipid membranes. *Biochemical Journal*, *401*(2), 437–445. https://doi.org/10.1042/BJ20061046

Cicardi, M. E., Cristofani, R., Rusmini, P., Meroni, M., Ferrari, V., Vezzoli, G., Tedesco, B., Piccolella, M., Messi, E., Galbiati, M., Boncoraglio, A., Carra, S., Crippa, V., & Poletti, A. (2018). Tdp-25 Routing to Autophagy and Proteasome Ameliorates its Aggregation in Amyotrophic Lateral Sclerosis Target Cells. *Scientific Reports*, *8*(1), 12390. https://doi.org/10.1038/s41598-018-29658-2

Cicardi, M. E., Marrone, L., Azzouz, M., & Trotti, D. (2021). Proteostatic imbalance and protein spreading in amyotrophic lateral sclerosis. *The EMBO Journal*, *40*(10). https://doi.org/10.15252/embj.2020106389

Ciechanover, A., & Kwon, Y. T. (2017). Protein Quality Control by Molecular Chaperones in Neurodegeneration. *Frontiers in Neuroscience*, *11*. https://doi.org/10.3389/fnins.2017.00185

Ciechanover, A., & Stanhill, A. (2014). The complexity of recognition of ubiquitinated substrates by the 26S proteasome. *Biochimica et Biophysica Acta (BBA) - Molecular Cell Research*, *1843*(1), 86–96. https://doi.org/10.1016/j.bbamcr.2013.07.007

Cloutier, F., Marrero, A., O'Connell, C., & Morin, P. J. (2015). MicroRNAs as Potential Circulating Biomarkers for Amyotrophic Lateral Sclerosis. *Journal of Molecular Neuroscience*, *56*(1), 102–112. https://doi.org/10.1007/s12031-014-0471-8

Cohen, T. J., Hwang, A. W., Restrepo, C. R., Yuan, C.-X., Trojanowski, J. Q., & Lee, V. M. Y. (2015). An acetylation switch controls TDP-43 function and aggregation propensity. *Nature Communications*, *6*(1), 5845. https://doi.org/10.1038/ncomms6845

Coleman, M. P. (2022). Axon Biology in ALS: Mechanisms of Axon Degeneration and Prospects for Therapy. *Neurotherapeutics*, *19*(4), 1133–1144. https://doi.org/10.1007/s13311-022-01297-6

Colombrita, C., Onesto, E., Megiorni, F., Pizzuti, A., Baralle, F. E., Buratti, E., Silani, V., & Ratti, A. (2012). TDP-43 and FUS RNA-binding Proteins Bind Distinct Sets of Cytoplasmic Messenger RNAs and Differently Regulate Their Post-transcriptional Fate in Motoneuron-like Cells. *Journal of Biological Chemistry*, *287*(19), 15635–15647. https://doi.org/10.1074/jbc.M111.333450

Coyne, A. N., Siddegowda, B. B., Estes, P. S., Johannesmeyer, J., Kovalik, T., Daniel, S. G., Pearson, A., Bowser, R., & Zarnescu, D. C. (2014). Futsch/MAP1B mRNA Is a Translational Target of TDP-43 and Is Neuroprotective in a Drosophila Model of Amyotrophic Lateral Sclerosis. *Journal of Neuroscience*, *34*(48), 15962–15974. https://doi.org/10.1523/JNEUROSCI.2526-14.2014

Crippa, V., Boncoraglio, A., Galbiati, M., Aggarwal, T., Rusmini, P., Giorgetti, E., Cristofani, R., Carra, S., Pennuto, M., & Poletti, A. (2013). Differential autophagy power in the spinal cord and muscle of transgenic ALS mice. *Frontiers in Cellular Neuroscience*, *7*. https://doi.org/10.3389/fncel.2013.00234

Crippa, V., Cicardi, M. E., Ramesh, N., Seguin, S. J., Ganassi, M., Bigi, I., Diacci, C., Zelotti, E., Baratashvili, M., Gregory, J. M., Dobson, C. M., Cereda, C., Pandey, U. B., Poletti, A., & Carra, S. (2016). The chaperone HSPB8 reduces the accumulation of truncated TDP-43 species in cells and protects against TDP-43-mediated toxicity. *Human Molecular Genetics*, *25*(18), 3908–3924. https://doi.org/10.1093/hmg/ddw232

Crippa, V., D'Agostino, V. G., Cristofani, R., Rusmini, P., Cicardi, M. E., Messi, E., Loffredo, R., Pancher, M., Piccolella, M., Galbiati, M., Meroni, M., Cereda, C., Carra, S., Provenzani, A., & Poletti, A. (2016). Transcriptional induction of the heat shock protein B8 mediates the clearance of misfolded proteins responsible for motor neuron diseases. *Scientific Reports*, *6*(1), 22827. https://doi.org/10.1038/srep22827

Crippa, V., Sau, D., Rusmini, P., Boncoraglio, A., Onesto, E., Bolzoni, E., Galbiati, M., Fontana, E., Marino, M., Carra, S., Bendotti, C., de Biasi, S., & Poletti, A. (2010). The small heat shock protein B8 (HspB8) promotes autophagic removal of misfolded proteins involved in amyotrophic lateral sclerosis (ALS). *Human Molecular Genetics*, *19*(17), 3440–3456. https://doi.org/10.1093/hmg/ddq257

D'Ambrogio, A., Buratti, E., Stuani, C., Guarnaccia, C., Romano, M., Ayala, Y. M., & Baralle, F. E. (2009). Functional mapping of the interaction between TDP-43 and hnRNP A2 in vivo. *Nucleic Acids Research*, *37*(12), 4116–4126. https://doi.org/10.1093/nar/gkp342

D'Anca, M., Fenoglio, C., Serpente, M., Arosio, B., Cesari, M., Scarpini, E. A., & Galimberti, D. (2019). Exosome Determinants of Physiological Aging and Age-Related Neurodegenerative Diseases. *Frontiers in Aging Neuroscience*, *11*. https://doi.org/10.3389/fnagi.2019.00232

de Boer, E. M. J., Orie, V. K., Williams, T., Baker, M. R., de Oliveira, H. M., Polvikoski, T., Silsby, M., Menon, P., van den Bos, M., Halliday, G. M., van den Berg, L. H., van den Bosch, L., van Damme, P., Kiernan, M. C., van Es, M. A., & Vucic, S. (2021). TDP-43 proteinopathies: a new wave of neurodegenerative diseases. *Journal of Neurology, Neurosurgery & Psychiatry*, *92*(1), 86–95. https://doi.org/10.1136/jnnp-2020-322983

DeJesus-Hernandez, M., Mackenzie, I. R., Boeve, B. F., Boxer, A. L., Baker, M., Rutherford, N. J., Nicholson, A. M., Finch, N. A., Flynn, H., Adamson, J., Kouri, N., Wojtas, A., Sengdy, P., Hsiung, G.-Y. R., Karydas, A., Seeley, W. W., Josephs, K. A., Coppola, G., Geschwind, D. H., … Rademakers, R. (2011). Expanded GGGGCC Hexanucleotide Repeat in Noncoding Region of C9ORF72 Causes Chromosome 9p-Linked FTD and ALS. *Neuron*, *72*(2), 245–256. https://doi.org/10.1016/j.neuron.2011.09.011

Delorme-Axford, E., & Klionsky, D. J. (2020). The LC3-conjugation machinery specifies cargo loading and secretion of extracellular vesicles. *Autophagy*, *16*(7), 1169–1171. https://doi.org/10.1080/15548627.2020.1760057

Deng, H.-X., Chen, W., Hong, S.-T., Boycott, K. M., Gorrie, G. H., Siddique, N., Yang, Y., Fecto, F., Shi, Y., Zhai, H., Jiang, H., Hirano, M., Rampersaud, E., Jansen, G. H., Donkervoort, S., Bigio, E. H., Brooks, B. R., Ajroud, K., Sufit, R. L., … Siddique, T. (2011). Mutations in UBQLN2 cause dominant X-linked juvenile and adult-onset ALS and ALS/dementia. *Nature*, *477*(7363), 211–215. https://doi.org/10.1038/nature10353

Dewey, C. M., Cenik, B., Sephton, C. F., Johnson, B. A., Herz, J., & Yu, G. (2012). TDP-43 aggregation in neurodegeneration: Are stress granules the key? *Brain Research*, *1462*, 16–25. https://doi.org/10.1016/j.brainres.2012.02.032

Diaz-Hidalgo, L., Altuntas, S., Rossin, F., D'Eletto, M., Marsella, C., Farrace, M. G., Falasca, L., Antonioli, M., Fimia, G. M., & Piacentini, M. (2016). Transglutaminase type 2-dependent selective recruitment of proteins into exosomes under stressful cellular conditions. *Biochimica et Biophysica Acta (BBA) - Molecular Cell Research*, *1863*(8), 2084–2092. https://doi.org/10.1016/j.bbamcr.2016.05.005

Ding, X., Xiang, Z., Qin, C., Chen, Y., Tian, H., Meng, L., Xia, D., Liu, H., Song, J., Fu, J., Ma, M., & Wang, X. (2021). Spreading of TDP-43 pathology via pyramidal tract induces ALS-like phenotypes in TDP-43 transgenic mice. *Acta Neuropathologica Communications*, *9*(1), 15. https://doi.org/10.1186/s40478-020-01112-3

Doll, S. G., Meshkin, H., Bryer, A. J., Li, F., Ko, Y.-H., Lokareddy, R. K., Gillilan, R. E., Gupta, K., Perilla, J. R., & Cingolani, G. (2022). Recognition of the TDP-43 nuclear localization signal by importin α1/β. *Cell Reports*, *39*(13), 111007. https://doi.org/10.1016/j.celrep.2022.111007

Dong, Z., Gu, H., Guo, Q., Liang, S., Xue, J., Yao, F., Liu, X., Li, F., Liu, H., Sun, L., & Zhao, K. (2021). Profiling of Serum Exosome MiRNA Reveals the Potential of a MiRNA Panel as Diagnostic Biomarker for Alzheimer's Disease. *Molecular Neurobiology*, *58*(7), 3084–3094. https://doi.org/10.1007/s12035-021-02323-y

Dormann, D., Capell, A., Carlson, A. M., Shankaran, S. S., Rodde, R., Neumann, M., Kremmer, E., Matsuwaki, T., Yamanouchi, K., Nishihara, M., & Haass, C. (2009). Proteolytic processing of TAR DNA binding protein-43 by caspases produces C-terminal fragments with disease defining properties independent of progranulin. *Journal of Neurochemistry*, *110*(3), 1082–1094. https://doi.org/10.1111/j.1471-4159.2009.06211.x

Dugger, B. N., & Dickson, D. W. (2017). Pathology of Neurodegenerative Diseases. *Cold Spring Harbor Perspectives in Biology*, *9*(7), a028035. https://doi.org/10.1101/cshperspect.a028035

Eck, R. J., Kraemer, B. C., & Liachko, N. F. (2021). Regulation of TDP-43 phosphorylation in aging and disease. *GeroScience*, *43*(4), 1605–1614. https://doi.org/10.1007/s11357-021-00383-5

Eitan, E., Suire, C., Zhang, S., & Mattson, M. P. (2016). Impact of lysosome status on extracellular vesicle content and release. *Ageing Research Reviews*, *32*, 65–74. https://doi.org/10.1016/j.arr.2016.05.001

Emde, A., Eitan, C., Liou, L., Libby, R. T., Rivkin, N., Magen, I., Reichenstein, I., Oppenheim, H., Eilam, R., Silvestroni, A., Alajajian, B., Ben-Dov, I. Z., Aebischer, J., Savidor, A., Levin, Y., Sons, R., Hammond, S. M., Ravits, J. M., Möller, T., & Hornstein, E. (2015). Dysregulated mi <scp>RNA</scp> biogenesis downstream of cellular stress and <scp>ALS</scp> -causing mutations: a new mechanism for <scp>ALS</scp>. *The EMBO Journal*, *34*(21), 2633–2651. https://doi.org/10.15252/embj.201490493

Fabbiano, F., Corsi, J., Gurrieri, E., Trevisan, C., Notarangelo, M., & D'Agostino, V. G. (2020). RNA packaging into extracellular vesicles: An orchestra of RNA-binding proteins? *Journal of Extracellular Vesicles*, *10*(2). https://doi.org/10.1002/jev2.12043

Falabella, M., Vernon, H. J., Hanna, M. G., Claypool, S. M., & Pitceathly, R. D. S. (2021). Cardiolipin, Mitochondria, and Neurological Disease. *Trends in Endocrinology & Metabolism*, *32*(4), 224–237. https://doi.org/10.1016/j.tem.2021.01.006

Farrawell, N. E., McAlary, L., Lum, J. S., Chisholm, C. G., Warraich, S. T., Blair, I. P., Vine, K. L., Saunders, D. N., & Yerbury, J. J. (2020). Ubiquitin Homeostasis Is Disrupted in TDP-43 and FUS Cell Models of ALS. *IScience*, *23*(11), 101700. https://doi.org/10.1016/j.isci.2020.101700

Feiler, M. S., Strobel, B., Freischmidt, A., Helferich, A. M., Kappel, J., Brewer, B. M., Li, D., Thal, D. R., Walther, P., Ludolph, A. C., Danzer, K. M., & Weishaupt, J. H. (2015). TDP-43 is intercellularly transmitted across axon terminals. *Journal of Cell Biology*, *211*(4), 897–911. https://doi.org/10.1083/jcb.201504057

Feneberg, E., Gray, E., Ansorge, O., Talbot, K., & Turner, M. R. (2018). Towards a TDP-43-Based Biomarker for ALS and FTLD. *Molecular Neurobiology*, *55*(10), 7789–7801. https://doi.org/10.1007/s12035-018-0947-6

Feng, S., Che, C., Feng, S., Liu, C., Li, L., Li, Y., Huang, H., & Zou, Z. (2019). Novel mutation in optineurin causing aggressive ALS+/−frontotemporal dementia. *Annals of Clinical and Translational Neurology*, *6*(12), 2377–2383. https://doi.org/10.1002/acn3.50928

Ferri, A., Nencini, M., Battistini, S., Giannini, F., Siciliano, G., Casali, C., Damiano, M. G., Ceroni, M., Chio, A., Rotilio, G., & Carri, M. T. (2004). Activity of protein phosphatase calcineurin is decreased in sporadic and familial amyotrophic lateral sclerosispatients. *Journal of Neurochemistry*, *90*(5), 1237–1242. https://doi.org/10.1111/j.1471-4159.2004.02588.x

Fevrier, B., Vilette, D., Archer, F., Loew, D., Faigle, W., Vidal, M., Laude, H., & Raposo, G. (2004). Cells release prions in association with exosomes. *Proceedings of the National Academy of Sciences*, *101*(26), 9683–9688. https://doi.org/10.1073/pnas.0308413101

Fontaine, S. N., Zheng, D., Sabbagh, J. J., Martin, M. D., Chaput, D., Darling, A., Trotter, J. H., Stothert, A. R., Nordhues, B. A., Lussier, A., Baker, J., Shelton, L., Kahn, M., Blair, L. J., Stevens, S. M., & Dickey, C. A. (2016). DnaJ/Hsc70 chaperone complexes control the extracellular release of neurodegenerative-associated proteins. *The EMBO Journal*, *35*(14), 1537–1549. https://doi.org/10.15252/embj.201593489

François-Moutal, L., Perez-Miller, S., Scott, D. D., Miranda, V. G., Mollasalehi, N., & Khanna, M. (2019). Structural Insights Into TDP-43 and Effects of Post-translational Modifications. *Frontiers in Molecular Neuroscience*, *12*. https://doi.org/10.3389/fnmol.2019.00301

Fred Dice, J. (1990). Peptide sequences that target cytosolic proteins for lysosomal proteolysis. *Trends in Biochemical Sciences*, *15*(8), 305–309. https://doi.org/10.1016/0968-0004(90)90019-8

Freibaum, B. D., Chitta, R. K., High, A. A., & Taylor, J. P. (2010). Global Analysis of TDP-43 Interacting Proteins Reveals Strong Association with RNA Splicing and Translation Machinery. *Journal of Proteome Research*, *9*(2), 1104–1120. https://doi.org/10.1021/pr901076y

Freischmidt, A., Wieland, T., Richter, B., Ruf, W., Schaeffer, V., Müller, K., Marroquin, N., Nordin, F., Hübers, A., Weydt, P., Pinto, S., Press, R., Millecamps, S., Molko, N., Bernard, E., Desnuelle, C., Soriani, M.-H., Dorst, J., Graf, E., … Weishaupt, J. H. (2015). Haploinsufficiency of TBK1 causes familial ALS and fronto-temporal dementia. *Nature Neuroscience*, *18*(5), 631–636. https://doi.org/10.1038/nn.4000

Galbiati, M., Crippa, V., Rusmini, P., Cristofani, R., Cicardi, M. E., Giorgetti, E., Onesto, E., Messi, E., & Poletti, A. (2014). ALS-related misfolded protein management in motor neurons and muscle cells. *Neurochemistry International*, *79*, 70–78. https://doi.org/10.1016/j.neuint.2014.10.007

Galimberti, D., Dell'Osso, B., Altamura, A. C., & Scarpini, E. (2015). Psychiatric Symptoms in Frontotemporal Dementia: Epidemiology, Phenotypes, and Differential Diagnosis. *Biological Psychiatry*, *78*(10), 684–692. https://doi.org/10.1016/j.biopsych.2015.03.028

Gamerdinger, M., Carra, S., & Behl, C. (2011). Emerging roles of molecular chaperones and co-chaperones in selective autophagy: focus on BAG proteins. *Journal of Molecular Medicine*, *89*(12), 1175–1182. https://doi.org/10.1007/s00109-011-0795-6

Gao, J., Wang, L., Huntley, M. L., Perry, G., & Wang, X. (2018). Pathomechanisms of TDP-43 in neurodegeneration. *Journal of Neurochemistry*, *146*(1), 7–20. https://doi.org/10.1111/jnc.14327

Garrido, C., Gurbuxani, S., Ravagnan, L., & Kroemer, G. (2001). Heat Shock Proteins: Endogenous Modulators of Apoptotic Cell Death. *Biochemical and Biophysical Research Communications*, *286*(3), 433–442. https://doi.org/10.1006/bbrc.2001.5427

Glickman, M. H., & Ciechanover, A. (2002). The Ubiquitin-Proteasome Proteolytic Pathway: Destruction for the Sake of Construction. *Physiological Reviews*, *82*(2), 373–428. https://doi.org/10.1152/physrev.00027.2001

Glickman, M. H., Rubin, D. M., Coux, O., Wefes, I., Pfeifer, G., Cjeka, Z., Baumeister, W., Fried, V. A., & Finley, D. (1998). A Subcomplex of the Proteasome Regulatory Particle Required for Ubiquitin-Conjugate Degradation and Related to the COP9-Signalosome and eIF3. *Cell*, *94*(5), 615–623. https://doi.org/10.1016/S0092-8674(00)81603-7

Gordon, P. (2013). Amyotrophic Lateral Sclerosis: An update for 2013 Clinical Features, Pathophysiology, Management and Therapeutic Trials. *Aging and Disease*, *04*(05), 295–310. https://doi.org/10.14336/AD.2013.0400295

Gosset, P., Camu, W., Raoul, C., & Mezghrani, A. (2022). Prionoids in amyotrophic lateral sclerosis. *Brain Communications*, *4*(3). https://doi.org/10.1093/braincomms/fcac145

Goto, S., Takahashi, R., Kumiyama, A., Radák, Z., Hayashi, T., Takenouchi, M., & Abe, R. (2006). Implications of Protein Degradation in Aging. *Annals of the New York Academy of Sciences*, *928*(1), 54–64. https://doi.org/10.1111/j.1749-6632.2001.tb05635.x

Grad, L. I., Yerbury, J. J., Turner, B. J., Guest, W. C., Pokrishevsky, E., O'Neill, M. A., Yanai, A., Silverman, J. M., Zeineddine, R., Corcoran, L., Kumita, J. R., Luheshi, L. M., Yousefi, M., Coleman, B. M., Hill, A. F., Plotkin, S. S., Mackenzie, I. R., & Cashman, N. R. (2014). Intercellular propagated misfolding of wild-type Cu/Zn superoxide dismutase occurs via exosome-dependent and -independent mechanisms. *Proceedings of the National Academy of Sciences*, *111*(9), 3620–3625. https://doi.org/10.1073/pnas.1312245111

Groot, M., & Lee, H. (2020). Sorting Mechanisms for MicroRNAs into Extracellular Vesicles and Their Associated Diseases. *Cells*, *9*(4), 1044. https://doi.org/10.3390/cells9041044

Grumati, P., & Dikic, I. (2018). Ubiquitin signaling and autophagy. *Journal of Biological Chemistry*, *293*(15), 5404–5413. https://doi.org/10.1074/jbc.TM117.000117

Gu, J., Wang, W., Miao, S., Chen, F., Wu, F., Hu, W., Iqbal, K., Gong, C.-X., & Liu, F. (2018). Protein Phosphatase 1 dephosphorylates TDP-43 and suppresses its function in tau exon 10 inclusion. *FEBS Letters*, *592*(3), 402–410. https://doi.org/10.1002/1873-3468.12976

Guo, F., Jiao, F., Song, Z., Li, S., Liu, B., Yang, H., Zhou, Q., & Li, Z. (2015). Regulation of MALAT1 expression by TDP43 controls the migration and invasion of non-small cell lung cancer cells in vitro. *Biochemical and Biophysical Research Communications*, *465*(2), 293–298. https://doi.org/10.1016/j.bbrc.2015.08.027

Guo, H., Pu, M., Tai, Y., Chen, Y., Lu, H., Qiao, J., Wang, G., Chen, J., Qi, X., Huang, R., Tao, Z., & Ren, J. (2021). Nuclear miR-30b-5p suppresses TFEB-mediated lysosomal biogenesis and autophagy. *Cell Death & Differentiation*, *28*(1), 320–336. https://doi.org/10.1038/s41418-020-0602-4

Gupta, M. K., Randhawa, P. K., & Masternak, M. M. (2022). Role of BAG5 in Protein Quality Control: Double-Edged Sword? *Frontiers in Aging*, *3*. https://doi.org/10.3389/fragi.2022.844168

Hans, F., Eckert, M., von Zweydorf, F., Gloeckner, C. J., & Kahle, P. J. (2018). Identification and characterization of ubiquitinylation sites in TAR DNA-binding protein of 43 kDa (TDP-43). *Journal of Biological Chemistry*, *293*(41), 16083–16099. https://doi.org/10.1074/jbc.RA118.003440

Hans, F., Fiesel, F. C., Strong, J. C., Jäckel, S., Rasse, T. M., Geisler, S., Springer, W., Schulz, J. B., Voigt, A., & Kahle, P. J. (2014). UBE2E Ubiquitin-conjugating Enzymes and Ubiquitin Isopeptidase Y

Regulate TDP-43 Protein Ubiquitination. *Journal of Biological Chemistry*, *289*(27), 19164–19179. https://doi.org/10.1074/jbc.M114.561704

Hanson, P. I., & Cashikar, A. (2012). Multivesicular Body Morphogenesis. *Annual Review of Cell and Developmental Biology*, *28*(1), 337–362. https://doi.org/10.1146/annurev-cellbio-092910-154152

Hartl, F. U. (2017). Protein Misfolding Diseases. *Annual Review of Biochemistry*, *86*(1), 21–26. https://doi.org/10.1146/annurev-biochem-061516-044518

Hartl, F. U., Bracher, A., & Hayer-Hartl, M. (2011). Molecular chaperones in protein folding and proteostasis. *Nature*, *475*(7356), 324–332. https://doi.org/10.1038/nature10317

Hasegawa, M., Arai, T., Nonaka, T., Kametani, F., Yoshida, M., Hashizume, Y., Beach, T. G., Buratti, E., Baralle, F., Morita, M., Nakano, I., Oda, T., Tsuchiya, K., & Akiyama, H. (2008). Phosphorylated TDP-43 in frontotemporal lobar degeneration and amyotrophic lateral sclerosis. *Annals of Neurology*, *64*(1), 60–70. https://doi.org/10.1002/ana.21425

Hawley, Z. C. E., Campos-Melo, D., & Strong, M. J. (2020). Evidence of A Negative Feedback Network Between TDP-43 and miRNAs Dependent on TDP-43 Nuclear Localization. *Journal of Molecular Biology*, *432*(24), 166695. https://doi.org/10.1016/j.jmb.2020.10.029

Hebron, M. L., Lonskaya, I., Sharpe, K., Weerasinghe, P. P. K., Algarzae, N. K., Shekoyan, A. R., & Moussa, C. E.-H. (2013). Parkin Ubiquitinates Tar-DNA Binding Protein-43 (TDP-43) and Promotes Its Cytosolic Accumulation via Interaction with Histone Deacetylase 6 (HDAC6). *Journal of Biological Chemistry*, *288*(6), 4103–4115. https://doi.org/10.1074/jbc.M112.419945

Hicks, D. A., Cross, L. L., Williamson, R., & Rattray, M. (2020). Endoplasmic Reticulum Stress Signalling Induces Casein Kinase 1-Dependent Formation of Cytosolic TDP-43 Inclusions in Motor Neuron-Like Cells. *Neurochemical Research*, *45*(6), 1354–1364. https://doi.org/10.1007/s11064-019-02832-2

Hill, A. F. (2019). Extracellular Vesicles and Neurodegenerative Diseases. *The Journal of Neuroscience*, *39*(47), 9269–9273. https://doi.org/10.1523/JNEUROSCI.0147-18.2019

Hoter, A., El-Sabban, M., & Naim, H. (2018). The HSP90 Family: Structure, Regulation, Function, and Implications in Health and Disease. *International Journal of Molecular Sciences*, *19*(9), 2560. https://doi.org/10.3390/ijms19092560

Huang, C.-C., Bose, J. K., Majumder, P., Lee, K.-H., Huang, J.-T. J., Huang, J. K., & Shen, C.-K. J. (2014). Metabolism and mis-metabolism of the neuropathological signature protein TDP-43. *Journal of Cell Science*. https://doi.org/10.1242/jcs.136150

Huebner, A. R., Cheng, L., Somparn, P., Knepper, M. A., Fenton, R. A., & Pisitkun, T. (2016). Deubiquitylation of Protein Cargo Is Not an Essential Step in Exosome Formation. *Molecular & Cellular Proteomics*, *15*(5), 1556–1571. https://doi.org/10.1074/mcp.M115.054965

Iguchi, Y., Eid, L., Parent, M., Soucy, G., Bareil, C., Riku, Y., Kawai, K., Takagi, S., Yoshida, M., Katsuno, M., Sobue, G., & Julien, J.-P. (2016). Exosome secretion is a key pathway for clearance of pathological TDP-43. *Brain*, *139*(12), 3187–3201. https://doi.org/10.1093/brain/aww237

Jiang, L.-L., Xue, W., Hong, J.-Y., Zhang, J.-T., Li, M.-J., Yu, S.-N., He, J.-H., & Hu, H.-Y. (2017). The N-terminal dimerization is required for TDP-43 splicing activity. *Scientific Reports*, *7*(1), 6196. https://doi.org/10.1038/s41598-017-06263-3

Jo, M., Lee, S., Jeon, Y.-M., Kim, S., Kwon, Y., & Kim, H.-J. (2020). The role of TDP-43 propagation in neurodegenerative diseases: integrating insights from clinical and experimental studies. *Experimental & Molecular Medicine*, *52*(10), 1652–1662. https://doi.org/10.1038/s12276-020-00513-7

Kakarla, R., Hur, J., Kim, Y. J., Kim, J., & Chwae, Y.-J. (2020). Apoptotic cell-derived exosomes: messages from dying cells. *Experimental & Molecular Medicine*, *52*(1), 1–6. https://doi.org/10.1038/s12276-019-0362-8

Kalra, H., Drummen, G., & Mathivanan, S. (2016). Focus on Extracellular Vesicles: Introducing the Next Small Big Thing. *International Journal of Molecular Sciences*, *17*(2), 170. https://doi.org/10.3390/ijms17020170

Kametani, F., Nonaka, T., Suzuki, T., Arai, T., Dohmae, N., Akiyama, H., & Hasegawa, M. (2009). Identification of casein kinase-1 phosphorylation sites on TDP-43. *Biochemical and Biophysical Research Communications*, *382*(2), 405–409. https://doi.org/10.1016/j.bbrc.2009.03.038

Kampinga, H. H., & Craig, E. A. (2010). The HSP70 chaperone machinery: J proteins as drivers of functional specificity. *Nature Reviews Molecular Cell Biology*, *11*(8), 579–592. https://doi.org/10.1038/nrm2941

Karagiannis, P., & Inoue, H. (2020). ALS, a cellular whodunit on motor neuron degeneration. *Molecular and Cellular Neuroscience*, *107*, 103524. https://doi.org/10.1016/j.mcn.2020.103524

Karunanayake, C., & Page, R. C. (2021). Cytosolic protein quality control machinery: Interactions of Hsp70 with a network of co-chaperones and substrates. *Experimental Biology and Medicine*, *246*(12), 1419–1434. https://doi.org/10.1177/1535370221999812

Kawahara, Y., & Mieda-Sato, A. (2012). TDP-43 promotes microRNA biogenesis as a component of the Drosha and Dicer complexes. *Proceedings of the National Academy of Sciences*, *109*(9), 3347–3352. https://doi.org/10.1073/pnas.1112427109

Kermer, P., Köhn, A., Schnieder, M., Lingor, P., Bähr, M., Liman, J., & Dohm, C. P. (2015). BAG1 is Neuroprotective in In Vivo and In Vitro Models of Parkinson's Disease. *Journal of Molecular Neuroscience*, *55*(3), 587–595. https://doi.org/10.1007/s12031-014-0396-2

Khalfallah, Y., Kuta, R., Grasmuck, C., Prat, A., Durham, H. D., & vande Velde, C. (2018). TDP-43 regulation of stress granule dynamics in neurodegenerative disease-relevant cell types. *Scientific Reports*, *8*(1), 7551. https://doi.org/10.1038/s41598-018-25767-0

Kim, K. Y., Kim, Y. R., Choi, K. W., Lee, M., Lee, S., Im, W., Shin, J.-Y., Kim, J. Y., Hong, Y. H., Kim, M., Kim, J.-I., & Sung, J.-J. (2020). Downregulated miR-18b-5p triggers apoptosis by inhibition of calcium signaling and neuronal cell differentiation in transgenic SOD1 (G93A) mice and SOD1 (G17S and G86S) ALS patients. *Translational Neurodegeneration*, *9*(1), 23. https://doi.org/10.1186/s40035-020-00203-4

Kim, Y. E., Hipp, M. S., Bracher, A., Hayer-Hartl, M., & Ulrich Hartl, F. (2013). Molecular Chaperone Functions in Protein Folding and Proteostasis. *Annual Review of Biochemistry*, *82*(1), 323–355. https://doi.org/10.1146/annurev-biochem-060208-092442

Kitamura, A., Iwasaki, N., & Kinjo, M. (2018). Molecular chaperone HSP70 prevents formation of inclusion bodies of the 25-kDa C-terminal fragment of TDP-43 by preventing aggregate accumulation. *Cell Stress and Chaperones*, *23*(6), 1177–1183. https://doi.org/10.1007/s12192-018-0930-1

Komander, D., Clague, M. J., & Urbé, S. (2009). Breaking the chains: structure and function of the deubiquitinases. *Nature Reviews Molecular Cell Biology*, *10*(8), 550–563. https://doi.org/10.1038/nrm2731

Kovacs, G. G. (2018). *Concepts and classification of neurodegenerative diseases* (pp. 301–307). https://doi.org/10.1016/B978-0-12-802395-2.00021-3

Kovacs, G. G. (2019). Molecular pathology of neurodegenerative diseases: principles and practice. *Journal of Clinical Pathology*, *72*(11), 725–735. https://doi.org/10.1136/jclinpath-2019-205952

Kowal, J., Arras, G., Colombo, M., Jouve, M., Morath, J. P., Primdal-Bengtson, B., Dingli, F., Loew, D., Tkach, M., & Théry, C. (2016). Proteomic comparison defines novel markers to characterize heterogeneous populations of extracellular vesicle subtypes. *Proceedings of the National Academy of Sciences*, *113*(8). https://doi.org/10.1073/pnas.1521230113

Koyama, A., Sugai, A., Kato, T., Ishihara, T., Shiga, A., Toyoshima, Y., Koyama, M., Konno, T., Hirokawa, S., Yokoseki, A., Nishizawa, M., Kakita, A., Takahashi, H., & Onodera, O. (2016). Increased cytoplasmic *TARDBP* mRNA in affected spinal motor neurons in ALS caused by abnormal autoregulation of TDP-43. *Nucleic Acids Research*, *44*(12), 5820–5836. https://doi.org/10.1093/nar/gkw499

Krach, F., Batra, R., Wheeler, E. C., Vu, A. Q., Wang, R., Hutt, K., Rabin, S. J., Baughn, M. W., Libby, R. T., Diaz-Garcia, S., Stauffer, J., Pirie, E., Saberi, S., Rodriguez, M., Madrigal, A. A., Kohl, Z., Winner, B., Yeo, G. W., & Ravits, J. (2018). Transcriptome–pathology correlation identifies interplay between TDP-43 and the expression of its kinase CK1E in sporadic ALS. *Acta Neuropathologica*, *136*(3), 405–423. https://doi.org/10.1007/s00401-018-1870-7

Kulka, L. A. M., Fangmann, P.-V., Panfilova, D., & Olzscha, H. (2020). Impact of HDAC Inhibitors on Protein Quality Control Systems: Consequences for Precision Medicine in Malignant Disease. *Frontiers in Cell and Developmental Biology*, *8*. https://doi.org/10.3389/fcell.2020.00425

Kumar, P., Dezso, Z., MacKenzie, C., Oestreicher, J., Agoulnik, S., Byrne, M., Bernier, F., Yanagimachi, M., Aoshima, K., & Oda, Y. (2013). Circulating miRNA Biomarkers for Alzheimer's Disease. *PLoS ONE*, *8*(7), e69807. https://doi.org/10.1371/journal.pone.0069807

Kung, J. T. Y., Colognori, D., & Lee, J. T. (2013). Long Noncoding RNAs: Past, Present, and Future. *Genetics*, *193*(3), 651–669. https://doi.org/10.1534/genetics.112.146704

Kuo, P.-H., Chiang, C.-H., Wang, Y.-T., Doudeva, L. G., & Yuan, H. S. (2014). The crystal structure of TDP-43 RRM1-DNA complex reveals the specific recognition for UG- and TG-rich nucleic acids. *Nucleic Acids Research*, *42*(7), 4712–4722. https://doi.org/10.1093/nar/gkt1407

Kwiatkowski, T. J., Bosco, D. A., LeClerc, A. L., Tamrazian, E., Vanderburg, C. R., Russ, C., Davis, A., Gilchrist, J., Kasarskis, E. J., Munsat, T., Valdmanis, P., Rouleau, G. A., Hosler, B. A., Cortelli, P., de Jong, P. J., Yoshinaga, Y., Haines, J. L., Pericak-Vance, M. A., Yan, J., … Brown, R. H. (2009). Mutations in the *FUS/TLS* Gene on Chromosome 16 Cause Familial Amyotrophic Lateral Sclerosis. *Science*, *323*(5918), 1205–1208. https://doi.org/10.1126/science.1166066

Labbadia, J., & Morimoto, R. I. (2015). The Biology of Proteostasis in Aging and Disease. *Annual Review of Biochemistry*, *84*(1), 435–464. https://doi.org/10.1146/annurev-biochem-060614-033955

Lackie, R. E., Maciejewski, A., Ostapchenko, V. G., Marques-Lopes, J., Choy, W.-Y., Duennwald, M. L., Prado, V. F., & Prado, M. A. M. (2017). The Hsp70/Hsp90 Chaperone Machinery in Neurodegenerative Diseases. *Frontiers in Neuroscience*, *11*. https://doi.org/10.3389/fnins.2017.00254

Laferrière, F., Maniecka, Z., Pérez-Berlanga, M., Hruska-Plochan, M., Gilhespy, L., Hock, E.-M., Wagner, U., Afroz, T., Boersema, P. J., Barmettler, G., Foti, S. C., Asi, Y. T., Isaacs, A. M., Al-Amoudi, A., Lewis, A., Stahlberg, H., Ravits, J., de Giorgi, F., Ichas, F., … Polymenidou, M. (2019). TDP-43 extracted from frontotemporal lobar degeneration subject brains displays distinct aggregate assemblies and neurotoxic effects reflecting disease progression rates. *Nature Neuroscience*, *22*(1), 65–77. https://doi.org/10.1038/s41593-018-0294-y

Larburu, N., Adams, C. J., Chen, C.-S., Nowak, P. R., & Ali, M. M. U. (2020). Mechanism of Hsp70 specialized interactions in protein translocation and the unfolded protein response. *Open Biology*, *10*(8). https://doi.org/10.1098/rsob.200089

Lattante, S., Ciura, S., Rouleau, G. A., & Kabashi, E. (2015). Defining the genetic connection linking amyotrophic lateral sclerosis (ALS) with frontotemporal dementia (FTD). *Trends in Genetics*, *31*(5), 263–273. https://doi.org/10.1016/j.tig.2015.03.005

Lattante, S., Rouleau, G. A., & Kabashi, E. (2013). *TARDBP* and *FUS* Mutations Associated with Amyotrophic Lateral Sclerosis: Summary and Update. *Human Mutation*, *34*(6), 812–826. https://doi.org/10.1002/humu.22319

Law, J. A., & Jacobsen, S. E. (2010). Establishing, maintaining and modifying DNA methylation patterns in plants and animals. *Nature Reviews Genetics*, *11*(3), 204–220. https://doi.org/10.1038/nrg2719

Lee, S.-J., Desplats, P., Sigurdson, C., Tsigelny, I., & Masliah, E. (2010). Cell-to-cell transmission of non-prion protein aggregates. *Nature Reviews Neurology*, *6*(12), 702–706. https://doi.org/10.1038/nrneurol.2010.145

Lee, Y.-C., Huang, W.-C., Lin, J.-H., Kao, T.-J., Lin, H.-C., Lee, K.-H., Lin, H.-C., Shen, C.-K. J., Chang, W.-C., & Huang, C.-C. (2018). Znf179 E3 ligase-mediated TDP-43 polyubiquitination is involved in TDP-43- ubiquitinated inclusions (UBI) (+)-related neurodegenerative pathology. *Journal of Biomedical Science*, *25*(1), 76. https://doi.org/10.1186/s12929-018-0479-4

Leidal, A. M., Huang, H. H., Marsh, T., Solvik, T., Zhang, D., Ye, J., Kai, F., Goldsmith, J., Liu, J. Y., Huang, Y.-H., Monkkonen, T., Vlahakis, A., Huang, E. J., Goodarzi, H., Yu, L., Wiita, A. P., & Debnath, J. (2020). The LC3-conjugation machinery specifies the loading of RNA-binding proteins into extracellular vesicles. *Nature Cell Biology*, *22*(2), 187–199. https://doi.org/10.1038/s41556-019-0450-y

Li, B., Antonyak, M. A., Zhang, J., & Cerione, R. A. (2012). RhoA triggers a specific signaling pathway that generates transforming microvesicles in cancer cells. *Oncogene*, *31*(45), 4740–4749. https://doi.org/10.1038/onc.2011.636

Li, F., Xiao, H., Hu, Z., Zhou, F., & Yang, B. (2018). Exploring the multifaceted roles of heat shock protein B8 (HSPB8) in diseases. *European Journal of Cell Biology*, *97*(3), 216–229. https://doi.org/10.1016/j.ejcb.2018.03.003

Li, H.-R., Chiang, W.-C., Chou, P.-C., Wang, W.-J., & Huang, J. (2018). TAR DNA-binding protein 43 (TDP-43) liquid–liquid phase separation is mediated by just a few aromatic residues. *Journal of Biological Chemistry*, *293*(16), 6090–6098. https://doi.org/10.1074/jbc.AC117.001037

Li, T.-H., Sun, H.-W., Song, L.-J., Yang, B., Zhang, P., Yan, D.-M., Liu, X.-Z., & Luo, Y.-R. (2022). Long non-coding RNA MEG3 regulates autophagy after cerebral ischemia/reperfusion injury. *Neural Regeneration Research*, *17*(4), 824. https://doi.org/10.4103/1673-5374.322466

Li, W., Reeb, A. N., Lin, B., Subramanian, P., Fey, E. E., Knoverek, C. R., French, R. L., Bigio, E. H., & Ayala, Y. M. (2017). Heat Shock-induced Phosphorylation of TAR DNA-binding Protein 43 (TDP-43) by MAPK/ERK Kinase Regulates TDP-43 Function. *Journal of Biological Chemistry*, *292*(12), 5089–5100. https://doi.org/10.1074/jbc.M116.753913

Liachko, N. F., McMillan, P. J., Guthrie, C. R., Bird, T. D., Leverenz, J. B., & Kraemer, B. C. (2013). CDC7 inhibition blocks pathological TDP-43 phosphorylation and neurodegeneration. *Annals of Neurology*, *74*(1), 39–52. https://doi.org/10.1002/ana.23870

Liachko, N. F., Saxton, A. D., McMillan, P. J., Strovas, T. J., Currey, H. N., Taylor, L. M., Wheeler, J. M., Oblak, A. L., Ghetti, B., Montine, T. J., Keene, C. D., Raskind, M. A., Bird, T. D., & Kraemer, B. C. (2016). The phosphatase calcineurin regulates pathological TDP-43 phosphorylation. *Acta Neuropathologica*, *132*(4), 545–561. https://doi.org/10.1007/s00401-016-1600-y

Liao, B., Dong, S., Xu, Z., Gao, F., Zhang, S., & Liang, R. (2020). LncRNA Kcnq1ot1 renders cardiomyocytes apoptosis in acute myocardial infarction model by up-regulating Tead1. *Life Sciences*, *256*, 117811. https://doi.org/10.1016/j.lfs.2020.117811

Liguori, M., Nuzziello, N., Introna, A., Consiglio, A., Licciulli, F., D'Errico, E., Scarafino, A., Distaso, E., & Simone, I. L. (2018). Dysregulation of MicroRNAs and Target Genes Networks in Peripheral Blood of Patients With Sporadic Amyotrophic Lateral Sclerosis. *Frontiers in Molecular Neuroscience*, *11*. https://doi.org/10.3389/fnmol.2018.00288

Lim, Y.-J., & Lee, S.-J. (2017). Are exosomes the vehicle for protein aggregate propagation in neurodegenerative diseases? *Acta Neuropathologica Communications*, *5*(1), 64. https://doi.org/10.1186/s40478-017-0467-z

Ling, S.-C., Polymenidou, M., & Cleveland, D. W. (2013). Converging Mechanisms in ALS and FTD: Disrupted RNA and Protein Homeostasis. *Neuron*, *79*(3), 416–438. https://doi.org/10.1016/j.neuron.2013.07.033

Liu, X., Li, D., Zhang, W., Guo, M., & Zhan, Q. (2012). Long non-coding RNA *gadd7* interacts with TDP-43 and regulates *Cdk6* mRNA decay. *The EMBO Journal*, *31*(23), 4415–4427. https://doi.org/10.1038/emboj.2012.292

Logroscino, G., Urso, D., & Tortelli, R. (2022). The challenge of amyotrophic lateral sclerosis descriptive epidemiology: to estimate low incidence rates across complex phenotypes in

different geographic areas. *Current Opinion in Neurology*, *35*(5), 678–685. https://doi.org/10.1097/WCO.0000000000001097

Lourenco, G. F., Janitz, M., Huang, Y., & Halliday, G. M. (2015). Long noncoding RNAs in TDP-43 and FUS/TLS-related frontotemporal lobar degeneration (FTLD). *Neurobiology of Disease*, *82*, 445–454. https://doi.org/10.1016/j.nbd.2015.07.011

Love, M. I., Huber, W., & Anders, S. (2014). Moderated estimation of fold change and dispersion for RNA-seq data with DESeq2. *Genome Biology*, *15*(12), 550. https://doi.org/10.1186/s13059-014-0550-8

Lu, S., Hu, J., Arogundade, O. A., Goginashvili, A., Vazquez-Sanchez, S., Diedrich, J. K., Gu, J., Blum, J., Oung, S., Ye, Q., Yu, H., Ravits, J., Liu, C., Yates, J. R., & Cleveland, D. W. (2022). Heat-shock chaperone HSPB1 regulates cytoplasmic TDP-43 phase separation and liquid-to-gel transition. *Nature Cell Biology*, *24*(9), 1378–1393. https://doi.org/10.1038/s41556-022-00988-8

Ludwig, N., Leidinger, P., Becker, K., Backes, C., Fehlmann, T., Pallasch, C., Rheinheimer, S., Meder, B., Stähler, C., Meese, E., & Keller, A. (2016). Distribution of miRNA expression across human tissues. *Nucleic Acids Research*, *44*(8), 3865–3877. https://doi.org/10.1093/nar/gkw116

Lugli, G., Cohen, A. M., Bennett, D. A., Shah, R. C., Fields, C. J., Hernandez, A. G., & Smalheiser, N. R. (2015). Plasma Exosomal miRNAs in Persons with and without Alzheimer Disease: Altered Expression and Prospects for Biomarkers. *PLOS ONE*, *10*(10), e0139233. https://doi.org/10.1371/journal.pone.0139233

Mackenzie, I. R., Nicholson, A. M., Sarkar, M., Messing, J., Purice, M. D., Pottier, C., Annu, K., Baker, M., Perkerson, R. B., Kurti, A., Matchett, B. J., Mittag, T., Temirov, J., Hsiung, G.-Y. R., Krieger, C., Murray, M. E., Kato, M., Fryer, J. D., Petrucelli, L., … Rademakers, R. (2017). TIA1 Mutations in Amyotrophic Lateral Sclerosis and Frontotemporal Dementia Promote Phase Separation and Alter Stress Granule Dynamics. *Neuron*, *95*(4), 808-816.e9. https://doi.org/10.1016/j.neuron.2017.07.025

Magen, I., Yacovzada, N. S., Yanowski, E., Coenen-Stass, A., Grosskreutz, J., Lu, C.-H., Greensmith, L., Malaspina, A., Fratta, P., & Hornstein, E. (2021). Circulating miR-181 is a prognostic biomarker for amyotrophic lateral sclerosis. *Nature Neuroscience*, *24*(11), 1534–1541. https://doi.org/10.1038/s41593-021-00936-z

Majumder, P., Chen, Y.-T., Bose, J. K., Wu, C.-C., Cheng, W.-C., Cheng, S.-J., Fang, Y.-H., Chen, Y.-L., Tsai, K.-J., Lien, C.-C., & Shen, C.-K. J. (2012). TDP-43 regulates the mammalian spinogenesis through translational repression of Rac1. *Acta Neuropathologica*, *124*(2), 231–245. https://doi.org/10.1007/s00401-012-1006-4

Mancuso, R., & Navarro, X. (2015). Amyotrophic lateral sclerosis: Current perspectives from basic research to the clinic. *Progress in Neurobiology*, *133*, 1–26. https://doi.org/10.1016/j.pneurobio.2015.07.004

Maniecka, Z., & Polymenidou, M. (2015). From nucleation to widespread propagation: A prion-like concept for ALS. *Virus Research*, *207*, 94–105. https://doi.org/10.1016/j.virusres.2014.12.032

Maraschi, A., Gumina, V., Dragotto, J., Colombrita, C., Mompeán, M., Buratti, E., Silani, V., Feligioni, M., & Ratti, A. (2021). SUMOylation Regulates TDP-43 Splicing Activity and Nucleocytoplasmic Distribution. *Molecular Neurobiology*, *58*(11), 5682–5702. https://doi.org/10.1007/s12035-021-02505-8

Martin, T. G., Delligatti, C. E., Muntu, N. A., Stachowski-Doll, M. J., & Kirk, J. A. (2022). Pharmacological inhibition of BAG3-HSP70 with the proposed cancer therapeutic JG-98 is toxic for cardiomyocytes. *Journal of Cellular Biochemistry*, *123*(1), 128–141. https://doi.org/10.1002/jcb.30140

Martínez-González, L., Rodríguez-Cueto, C., Cabezudo, D., Bartolomé, F., Andrés-Benito, P., Ferrer, I., Gil, C., Martín-Requero, Á., Fernández-Ruiz, J., Martínez, A., & de Lago, E. (2020). Motor neuron preservation and decrease of in vivo TDP-43 phosphorylation by protein CK-1δ kinase inhibitor treatment. *Scientific Reports*, *10*(1), 4449. https://doi.org/10.1038/s41598-020-61265-y

Mathieu, M., Martin-Jaular, L., Lavieu, G., & Théry, C. (2019). Specificities of secretion and uptake of exosomes and other extracellular vesicles for cell-to-cell communication. *Nature Cell Biology*, *21*(1), 9–17. https://doi.org/10.1038/s41556-018-0250-9

Maurel, C., Chami, A. A., Thépault, R.-A., Marouillat, S., Blasco, H., Corcia, P., Andres, C. R., & Vourc'h, P. (2020). A role for SUMOylation in the Formation and Cellular Localization of TDP-43 Aggregates in Amyotrophic Lateral Sclerosis. *Molecular Neurobiology*, *57*(3), 1361–1373. https://doi.org/10.1007/s12035-019-01810-7

McAlary, L., Plotkin, S. S., & Cashman, N. R. (2019). Emerging Developments in Targeting Proteotoxicity in Neurodegenerative Diseases. *CNS Drugs*, *33*(9), 883–904. https://doi.org/10.1007/s40263-019-00657-9

Miao, Y., Li, G., Zhang, X., Xu, H., & Abraham, S. N. (2015). A TRP Channel Senses Lysosome Neutralization by Pathogens to Trigger Their Expulsion. *Cell*, *161*(6), 1306–1319. https://doi.org/10.1016/j.cell.2015.05.009

Minoia, M., Boncoraglio, A., Vinet, J., Morelli, F. F., Brunsting, J. F., Poletti, A., Krom, S., Reits, E., Kampinga, H. H., & Carra, S. (2014). BAG3 induces the sequestration of proteasomal clients into cytoplasmic puncta. *Autophagy*, *10*(9), 1603–1621. https://doi.org/10.4161/auto.29409

Mompeán, M., Romano, V., Pantoja-Uceda, D., Stuani, C., Baralle, F. E., Buratti, E., & Laurents, D. v. (2016). The TDP-43 N-terminal domain structure at high resolution. *The FEBS Journal*, *283*(7), 1242–1260. https://doi.org/10.1111/febs.13651

Muranova, L. K., Ryzhavskaya, A. S., Sudnitsyna, M. v., Shatov, V. M., & Gusev, N. B. (2019). Small Heat Shock Proteins and Human Neurodegenerative Diseases. *Biochemistry (Moscow)*, *84*(11), 1256–1267. https://doi.org/10.1134/S000629791911004X

Nandi, D., Tahiliani, P., Kumar, A., & Chandu, D. (2006). The ubiquitin-proteasome system. *Journal of Biosciences*, *31*(1), 137–155. https://doi.org/10.1007/BF02705243

Neumann, M., Frick, P., Paron, F., Kosten, J., Buratti, E., & Mackenzie, I. R. (2021). Correction to: Antibody against TDP-43 phosphorylated at serine 369 suggests conformational differences of TDP-43 aggregates among FTLD-TDP subtypes. *Acta Neuropathologica*, *141*(1), 137–137. https://doi.org/10.1007/s00401-020-02242-7

Neumann, M., Kwong, L. K., Lee, E. B., Kremmer, E., Flatley, A., Xu, Y., Forman, M. S., Troost, D., Kretzschmar, H. A., Trojanowski, J. Q., & Lee, V. M.-Y. (2009). Phosphorylation of S409/410 of TDP-43 is a consistent feature in all sporadic and familial forms of TDP-43 proteinopathies. *Acta Neuropathologica*, *117*(2), 137–149. https://doi.org/10.1007/s00401-008-0477-9

Neumann, M., Sampathu, D. M., Kwong, L. K., Truax, A. C., Micsenyi, M. C., Chou, T. T., Bruce, J., Schuck, T., Grossman, M., Clark, C. M., McCluskey, L. F., Miller, B. L., Masliah, E., Mackenzie, I. R., Feldman, H., Feiden, W., Kretzschmar, H. A., Trojanowski, J. Q., & Lee, V. M.-Y. (2006). Ubiquitinated TDP-43 in Frontotemporal Lobar Degeneration and Amyotrophic Lateral Sclerosis. *Science*, *314*(5796), 130–133. https://doi.org/10.1126/science.1134108

Newell, K., Paron, F., Mompean, M., Murrell, J., Salis, E., Stuani, C., Pattee, G., Romano, M., Laurents, D., Ghetti, B., & Buratti, E. (2019). Dysregulation of TDP-43 intracellular localization and early onset ALS are associated with a *TARDBP* S375G variant. *Brain Pathology*, *29*(3), 397–413. https://doi.org/10.1111/bpa.12680

Nieto-Torres, J. L., Leidal, A. M., Debnath, J., & Hansen, M. (2021). Beyond Autophagy: The Expanding Roles of ATG8 Proteins. *Trends in Biochemical Sciences*, *46*(8), 673–686. https://doi.org/10.1016/j.tibs.2021.01.004

Nonaka, T., & Hasegawa, M. (2018). TDP-43 Prions. *Cold Spring Harbor Perspectives in Medicine*, *8*(3), a024463. https://doi.org/10.1101/cshperspect.a024463

Nonaka, T., Kametani, F., Arai, T., Akiyama, H., & Hasegawa, M. (2009). Truncation and pathogenic mutations facilitate the formation of intracellular aggregates of TDP-43. *Human Molecular Genetics*, *18*(18), 3353–3364. https://doi.org/10.1093/hmg/ddp275

Ojaimi, Y. al, Dangoumau, A., Alarcan, H., Hergesheimer, R., Vourc'h, P., Corcia, P., Lanznaster, D., & Blasco, H. (2022). TAR DNA-binding protein of 43 kDa (TDP-43) and amyotrophic lateral sclerosis (ALS): a promising therapeutic target. *Expert Opinion on Therapeutic Targets*, *26*(6), 575–592. https://doi.org/10.1080/14728222.2022.2083958

Olney, N. T., Spina, S., & Miller, B. L. (2017). Frontotemporal Dementia. *Neurologic Clinics*, *35*(2), 339–374. https://doi.org/10.1016/j.ncl.2017.01.008

Onyike, C. U., & Diehl-Schmid, J. (2013). The epidemiology of frontotemporal dementia. *International Review of Psychiatry*, *25*(2), 130–137. https://doi.org/10.3109/09540261.2013.776523

Pankiv, S., Clausen, T. H., Lamark, T., Brech, A., Bruun, J.-A., Outzen, H., Øvervatn, A., Bjørkøy, G., & Johansen, T. (2007). p62/SQSTM1 Binds Directly to Atg8/LC3 to Facilitate Degradation of Ubiquitinated Protein Aggregates by Autophagy. *Journal of Biological Chemistry*, *282*(33), 24131–24145. https://doi.org/10.1074/jbc.M702824200

Park, C.-W., & Ryu, K.-Y. (2014). Cellular ubiquitin pool dynamics and homeostasis. *BMB Reports*, *47*(9), 475–482. https://doi.org/10.5483/BMBRep.2014.47.9.128

Parkinson, N., Ince, P. G., Smith, M. O., Highley, R., Skibinski, G., Andersen, P. M., Morrison, K. E., Pall, H. S., Hardiman, O., Collinge, J., Shaw, P. J., & Fisher, E. C. (2006). ALS phenotypes with mutations in CHMP2B (charged multivesicular body protein 2B). *Neurology*, *67*(6), 1074–1077. https://doi.org/10.1212/01.wnl.0000231510.89311.8b

Parzych, K. R., & Klionsky, D. J. (2014). An Overview of Autophagy: Morphology, Mechanism, and Regulation. *Antioxidants & Redox Signaling*, *20*(3), 460–473. https://doi.org/10.1089/ars.2013.5371

Pikatza-Menoio, O., Elicegui, A., Bengoetxea, X., Naldaiz-Gastesi, N., López de Munain, A., Gerenu, G., Gil-Bea, F. J., & Alonso-Martín, S. (2021). The Skeletal Muscle Emerges as a New Disease

Target in Amyotrophic Lateral Sclerosis. *Journal of Personalized Medicine*, *11*(7), 671. https://doi.org/10.3390/jpm11070671

Pinarbasi, E. S., Cağatay, T., Fung, H. Y. J., Li, Y. C., Chook, Y. M., & Thomas, P. J. (2018). Active nuclear import and passive nuclear export are the primary determinants of TDP-43 localization. *Scientific Reports*, *8*(1), 7083. https://doi.org/10.1038/s41598-018-25008-4

Pinto, S., Cunha, C., Barbosa, M., Vaz, A. R., & Brites, D. (2017). Exosomes from NSC-34 Cells Transfected with hSOD1-G93A Are Enriched in miR-124 and Drive Alterations in Microglia Phenotype. *Frontiers in Neuroscience*, *11*. https://doi.org/10.3389/fnins.2017.00273

Polymenidou, M., & Cleveland, D. W. (2011). The Seeds of Neurodegeneration: Prion-like Spreading in ALS. *Cell*, *147*(3), 498–508. https://doi.org/10.1016/j.cell.2011.10.011

Pozzi, B., Bragado, L., Will, C. L., Mammi, P., Risso, G., Urlaub, H., Lührmann, R., & Srebrow, A. (2017). SUMO conjugation to spliceosomal proteins is required for efficient pre-mRNA splicing. *Nucleic Acids Research*, *45*(11), 6729–6745. https://doi.org/10.1093/nar/gkx213

Prasad, A., Bharathi, V., Sivalingam, V., Girdhar, A., & Patel, B. K. (2019). Molecular Mechanisms of TDP-43 Misfolding and Pathology in Amyotrophic Lateral Sclerosis. *Frontiers in Molecular Neuroscience*, *12*. https://doi.org/10.3389/fnmol.2019.00025

Protter, D. S. W., & Parker, R. (2016). Principles and Properties of Stress Granules. *Trends in Cell Biology*, *26*(9), 668–679. https://doi.org/10.1016/j.tcb.2016.05.004

Qin, H., Lim, L.-Z., Wei, Y., & Song, J. (2014). TDP-43 N terminus encodes a novel ubiquitin-like fold and its unfolded form in equilibrium that can be shifted by binding to ssDNA. *Proceedings of the National Academy of Sciences*, *111*(52), 18619–18624. https://doi.org/10.1073/pnas.1413994112

Raheja, R., Regev, K., Healy, B. C., Mazzola, M. A., Beynon, V., von Glehn, F., Paul, A., Diaz-Cruz, C., Gholipour, T., Glanz, B. I., Kivisakk, P., Chitnis, T., Weiner, H. L., Berry, J. D., & Gandhi, R. (2018). Correlating serum microrna and clinical parameters in amyotrophic lateral sclerosis. *Muscle & Nerve*, *58*(2), 261–269. https://doi.org/10.1002/mus.26106

Rajendran, L., Honsho, M., Zahn, T. R., Keller, P., Geiger, K. D., Verkade, P., & Simons, K. (2006). Alzheimer's disease β-amyloid peptides are released in association with exosomes. *Proceedings of the National Academy of Sciences*, *103*(30), 11172–11177. https://doi.org/10.1073/pnas.0603838103

Rao, P. P. N., Shakeri, A., Zhao, Y., & Calon, F. (2021). Strategies in the design and development of (TAR) DNA-binding protein 43 (TDP-43) binding ligands. *European Journal of Medicinal Chemistry*, *225*, 113753. https://doi.org/10.1016/j.ejmech.2021.113753

Rastogi, S., Sharma, V., Bharti, P. S., Rani, K., Modi, G. P., Nikolajeff, F., & Kumar, S. (2021). The Evolving Landscape of Exosomes in Neurodegenerative Diseases: Exosomes Characteristics and a Promising Role in Early Diagnosis. *International Journal of Molecular Sciences*, *22*(1), 440. https://doi.org/10.3390/ijms22010440

Ratti, A., & Buratti, E. (2016). Physiological functions and pathobiology of TDP-43 and FUS/TLS proteins. *Journal of Neurochemistry*, *138*, 95–111. https://doi.org/10.1111/jnc.13625

Ravnik-Glavač, M., & Glavač, D. (2020). Circulating RNAs as Potential Biomarkers in Amyotrophic Lateral Sclerosis. *International Journal of Molecular Sciences*, *21*(5), 1714. https://doi.org/10.3390/ijms21051714

Renton, A. E., Majounie, E., Waite, A., Simón-Sánchez, J., Rollinson, S., Gibbs, J. R., Schymick, J. C., Laaksovirta, H., van Swieten, J. C., Myllykangas, L., Kalimo, H., Paetau, A., Abramzon, Y., Remes, A. M., Kaganovich, A., Scholz, S. W., Duckworth, J., Ding, J., Harmer, D. W., … Traynor, B. J. (2011). A Hexanucleotide Repeat Expansion in C9ORF72 Is the Cause of Chromosome 9p21-Linked ALS-FTD. *Neuron*, *72*(2), 257–268. https://doi.org/10.1016/j.neuron.2011.09.010

Riemenschneider, H., Guo, Q., Bader, J., Frottin, F., Farny, D., Kleinberger, G., Haass, C., Mann, M., Hartl, F. U., Baumeister, W., Hipp, M. S., Meissner, F., Fernández-Busnadiego, R., & Edbauer, D. (2022). Gel-like inclusions of C-terminal fragments of TDP-43 sequester stalled proteasomes in neurons. *EMBO Reports*, *23*(6). https://doi.org/10.15252/embr.202153890

Rojas-Prats, E., Martinez-Gonzalez, L., Gonzalo-Consuegra, C., Liachko, N. F., Perez, C., Ramírez, D., Kraemer, B. C., Martin-Requero, Á., Perez, D. I., Gil, C., de Lago, E., & Martinez, A. (2021). Targeting nuclear protein TDP-43 by cell division cycle kinase 7 inhibitors: A new therapeutic approach for amyotrophic lateral sclerosis. *European Journal of Medicinal Chemistry*, *210*, 112968. https://doi.org/10.1016/j.ejmech.2020.112968

Roos-Mattjus, P., & Sistonen, L. (2004). The ubiquitin-proteasome pathway. *Annals of Medicine*, *36*(4), 285–295. https://doi.org/10.1080/07853890310016324

Roth, F. C., & Draguhn, A. (2012). GABA Metabolism and Transport: Effects on Synaptic Efficacy. *Neural Plasticity*, *2012*, 1–12. https://doi.org/10.1155/2012/805830

Rubino, E., Rainero, I., Chio, A., Rogaeva, E., Galimberti, D., Fenoglio, P., Grinberg, Y., Isaia, G., Calvo, A., Gentile, S., Bruni, A. C., st. George-Hyslop, P. H., Scarpini, E., Gallone, S., & Pinessi, L. (2012). SQSTM1 mutations in frontotemporal lobar degeneration and amyotrophic lateral sclerosis. *Neurology*, *79*(15), 1556–1562. https://doi.org/10.1212/WNL.0b013e31826e25df

Rudiger, S. (1997). Substrate specificity of the DnaK chaperone determined by screening cellulose-bound peptide libraries. *The EMBO Journal*, *16*(7), 1501–1507. https://doi.org/10.1093/emboj/16.7.1501

Rusmini, P., Cristofani, R., Galbiati, M., Cicardi, M. E., Meroni, M., Ferrari, V., Vezzoli, G., Tedesco, B., Messi, E., Piccolella, M., Carra, S., Crippa, V., & Poletti, A. (2017). The Role of the Heat Shock Protein B8 (HSPB8) in Motoneuron Diseases. *Frontiers in Molecular Neuroscience*, *10*. https://doi.org/10.3389/fnmol.2017.00176

Russo, A., Scardigli, R., la Regina, F., Murray, M. E., Romano, N., Dickson, D. W., Wolozin, B., Cattaneo, A., & Ceci, M. (2019). Corrigendum: Increased cytoplasmic TDP-43 reduces global protein synthesis by interacting with RACK1 on polyribosomes. *Human Molecular Genetics*, *28*(7), 1226–1226. https://doi.org/10.1093/hmg/ddy407

Sadowski, M., Suryadinata, R., Tan, A. R., Roesley, S. N. A., & Sarcevic, B. (2012). Protein monoubiquitination and polyubiquitination generate structural diversity to control distinct biological processes. *IUBMB Life*, *64*(2), 136–142. https://doi.org/10.1002/iub.589

Sahin, U., Ferhi, O., Jeanne, M., Benhenda, S., Berthier, C., Jollivet, F., Niwa-Kawakita, M., Faklaris, O., Setterblad, N., de Thé, H., & Lallemand-Breitenbach, V. (2014). Oxidative stress–induced

assembly of PML nuclear bodies controls sumoylation of partner proteins. *Journal of Cell Biology*, *204*(6), 931–945. https://doi.org/10.1083/jcb.201305148

Saibil, H. (2013). Chaperone machines for protein folding, unfolding and disaggregation. *Nature Reviews Molecular Cell Biology*, *14*(10), 630–642. https://doi.org/10.1038/nrm3658

Salado, I. G., Redondo, M., Bello, M. L., Perez, C., Liachko, N. F., Kraemer, B. C., Miguel, L., Lecourtois, M., Gil, C., Martinez, A., & Perez, D. I. (2014). Protein Kinase CK-1 Inhibitors As New Potential Drugs for Amyotrophic Lateral Sclerosis. *Journal of Medicinal Chemistry*, *57*(6), 2755–2772. https://doi.org/10.1021/jm500065f

Saman, S., Kim, W., Raya, M., Visnick, Y., Miro, S., Saman, S., Jackson, B., McKee, A. C., Alvarez, V. E., Lee, N. C. Y., & Hall, G. F. (2012). Exosome-associated Tau Is Secreted in Tauopathy Models and Is Selectively Phosphorylated in Cerebrospinal Fluid in Early Alzheimer Disease. *Journal of Biological Chemistry*, *287*(6), 3842–3849. https://doi.org/10.1074/jbc.M111.277061

Scarian, E., Fiamingo, G., Diamanti, L., Palmieri, I., Gagliardi, S., & Pansarasa, O. (2022). The Role of VCP Mutations in the Spectrum of Amyotrophic Lateral Sclerosis—Frontotemporal Dementia. *Frontiers in Neurology*, *13*. https://doi.org/10.3389/fneur.2022.841394

Scotter, E. L., Vance, C., Nishimura, A. L., Lee, Y.-B., Chen, H.-J., Urwin, H., Sardone, V., Mitchell, J. C., Rogelj, B., Rubinsztein, D. C., & Shaw, C. E. (2014). Differential roles of the ubiquitin proteasome system (UPS) and autophagy in the clearance of soluble and aggregated TDP-43 species. *Journal of Cell Science*. https://doi.org/10.1242/jcs.140087

Shaid, S., Brandts, C. H., Serve, H., & Dikic, I. (2013). Ubiquitination and selective autophagy. *Cell Death & Differentiation*, *20*(1), 21–30. https://doi.org/10.1038/cdd.2012.72

Sheinerman, K. S., Toledo, J. B., Tsivinsky, V. G., Irwin, D., Grossman, M., Weintraub, D., Hurtig, H. I., Chen-Plotkin, A., Wolk, D. A., McCluskey, L. F., Elman, L. B., Trojanowski, J. Q., & Umansky, S. R. (2017). Circulating brain-enriched microRNAs as novel biomarkers for detection and differentiation of neurodegenerative diseases. *Alzheimer's Research & Therapy*, *9*(1), 89. https://doi.org/10.1186/s13195-017-0316-0

Shvets, E., Fass, E., Scherz-Shouval, R., & Elazar, Z. (2008). The N-terminus and Phe52 residue of LC3 recruit p62/SQSTM1 into autophagosomes. *Journal of Cell Science*, *121*(16), 2685–2695. https://doi.org/10.1242/jcs.026005

Siedlecki-Wullich, D., Català-Solsona, J., Fábregas, C., Hernández, I., Clarimon, J., Lleó, A., Boada, M., Saura, C. A., Rodríguez-Álvarez, J., & Miñano-Molina, A. J. (2019). Altered microRNAs related to synaptic function as potential plasma biomarkers for Alzheimer's disease. *Alzheimer's Research & Therapy*, *11*(1), 46. https://doi.org/10.1186/s13195-019-0501-4

Smith, H. L., Li, W., & Cheetham, M. E. (2015). Molecular chaperones and neuronal proteostasis. *Seminars in Cell & Developmental Biology*, *40*, 142–152. https://doi.org/10.1016/j.semcdb.2015.03.003

Song, J., Durrin, L. K., Wilkinson, T. A., Krontiris, T. G., & Chen, Y. (2004). Identification of a SUMO-binding motif that recognizes SUMO-modified proteins. *Proceedings of the National Academy of Sciences*, *101*(40), 14373–14378. https://doi.org/10.1073/pnas.0403498101

Soto, C. (2001). Protein misfolding and disease; protein refolding and therapy. *FEBS Letters*, *498*(2–3), 204–207. https://doi.org/10.1016/S0014-5793(01)02486-3

Soto, C., & Pritzkow, S. (2018). Protein misfolding, aggregation, and conformational strains in neurodegenerative diseases. *Nature Neuroscience*, *21*(10), 1332–1340. https://doi.org/10.1038/s41593-018-0235-9

Sproviero, D., Gagliardi, S., Zucca, S., Arigoni, M., Giannini, M., Garofalo, M., Olivero, M., Dell'Orco, M., Pansarasa, O., Bernuzzi, S., Avenali, M., Cotta Ramusino, M., Diamanti, L., Minafra, B., Perini, G., Zangaglia, R., Costa, A., Ceroni, M., Perrone-Bizzozero, N. I., … Cereda, C. (2021). Different miRNA Profiles in Plasma Derived Small and Large Extracellular Vesicles from Patients with Neurodegenerative Diseases. *International Journal of Molecular Sciences*, *22*(5), 2737. https://doi.org/10.3390/ijms22052737

Sproviero, D., la Salvia, S., Giannini, M., Crippa, V., Gagliardi, S., Bernuzzi, S., Diamanti, L., Ceroni, M., Pansarasa, O., Poletti, A., & Cereda, C. (2018). Pathological Proteins Are Transported by Extracellular Vesicles of Sporadic Amyotrophic Lateral Sclerosis Patients. *Frontiers in Neuroscience*, *12*. https://doi.org/10.3389/fnins.2018.00487

Stavoe, A. K. H., & Holzbaur, E. L. F. (2019). Autophagy in Neurons. *Annual Review of Cell and Developmental Biology*, *35*(1), 477–500. https://doi.org/10.1146/annurev-cellbio-100818-125242

Sternburg, E. L., Gruijs da Silva, L. A., & Dormann, D. (2022). Post-translational modifications on RNA-binding proteins: accelerators, brakes, or passengers in neurodegeneration? *Trends in Biochemical Sciences*, *47*(1), 6–22. https://doi.org/10.1016/j.tibs.2021.07.004

Stürner, E., & Behl, C. (2017). The Role of the Multifunctional BAG3 Protein in Cellular Protein Quality Control and in Disease. *Frontiers in Molecular Neuroscience*, *10*. https://doi.org/10.3389/fnmol.2017.00177

Suk, T. R., & Rousseaux, M. W. C. (2020). The role of TDP-43 mislocalization in amyotrophic lateral sclerosis. *Molecular Neurodegeneration*, *15*(1), 45. https://doi.org/10.1186/s13024-020-00397-1

Sun, Y., & Chakrabartty, A. (2017). Phase to Phase with TDP-43. *Biochemistry*, *56*(6), 809–823. https://doi.org/10.1021/acs.biochem.6b01088

Swanger, S. A., & Bassell, G. J. (2011). Making and breaking synapses through local mRNA regulation. *Current Opinion in Genetics & Development*, *21*(4), 414–421. https://doi.org/10.1016/j.gde.2011.04.002

Szafranski, K. (2015). Non-coding RNA in neural function, disease, and aging. *Frontiers in Genetics*, *6*. https://doi.org/10.3389/fgene.2015.00087

Takagi, S., Iguchi, Y., Katsuno, M., Ishigaki, S., Ikenaka, K., Fujioka, Y., Honda, D., Niwa, J., Tanaka, F., Watanabe, H., Adachi, H., & Sobue, G. (2013). RNP2 of RNA Recognition Motif 1 Plays a Central Role in the Aberrant Modification of TDP-43. *PLoS ONE*, *8*(6), e66966. https://doi.org/10.1371/journal.pone.0066966

Tasca, E., Pegoraro, V., Merico, A., & Angelini, C. (2016). Circulating microRNAs as biomarkers of muscle differentiation and atrophy in ALS. *Clinical Neuropathology*, *35*(01), 22–30. https://doi.org/10.5414/NP300889

Taylor, J. P., Hardy, J., & Fischbeck, K. H. (2002). Toxic Proteins in Neurodegenerative Disease. *Science*, *296*(5575), 1991–1995. https://doi.org/10.1126/science.1067122

Taylor, L. M., McMillan, P. J., Liachko, N. F., Strovas, T. J., Ghetti, B., Bird, T. D., Keene, C. D., & Kraemer, B. C. (2018). Pathological phosphorylation of tau and TDP-43 by TTBK1 and TTBK2 drives neurodegeneration. *Molecular Neurodegeneration*, *13*(1), 7. https://doi.org/10.1186/s13024-018-0237-9

Tedesco, B., Cristofani, R., Ferrari, V., Cozzi, M., Rusmini, P., Casarotto, E., Chierichetti, M., Mina, F., Galbiati, M., Piccolella, M., Crippa, V., & Poletti, A. (2022). Insights on Human Small Heat Shock Proteins and Their Alterations in Diseases. *Frontiers in Molecular Biosciences*, *9*. https://doi.org/10.3389/fmolb.2022.842149

Tedesco, B., Ferrari, V., Cozzi, M., Chierichetti, M., Casarotto, E., Pramaggiore, P., Mina, F., Galbiati, M., Rusmini, P., Crippa, V., Cristofani, R., & Poletti, A. (2022). The Role of Small Heat Shock Proteins in Protein Misfolding Associated Motoneuron Diseases. *International Journal of Molecular Sciences*, *23*(19), 11759. https://doi.org/10.3390/ijms231911759

Théry, C., Witwer, K. W., Aikawa, E., Alcaraz, M. J., Anderson, J. D., Andriantsitohaina, R., Antoniou, A., Arab, T., Archer, F., Atkin-Smith, G. K., Ayre, D. C., Bach, J.-M., Bachurski, D., Baharvand, H., Balaj, L., Baldacchino, S., Bauer, N. N., Baxter, A. A., Bebawy, M., … Zuba-Surma, E. K. (2018). Minimal information for studies of extracellular vesicles 2018 (MISEV2018): a position statement of the International Society for Extracellular Vesicles and update of the MISEV2014 guidelines. *Journal of Extracellular Vesicles*, *7*(1), 1535750. https://doi.org/10.1080/20013078.2018.1535750

Tollervey, J. R., Curk, T., Rogelj, B., Briese, M., Cereda, M., Kayikci, M., König, J., Hortobágyi, T., Nishimura, A. L., Župunski, V., Patani, R., Chandran, S., Rot, G., Zupan, B., Shaw, C. E., & Ule, J. (2011). Characterizing the RNA targets and position-dependent splicing regulation by TDP-43. *Nature Neuroscience*, *14*(4), 452–458. https://doi.org/10.1038/nn.2778

Tracz, M., & Bialek, W. (2021). Beyond K48 and K63: non-canonical protein ubiquitination. *Cellular & Molecular Biology Letters*, *26*(1), 1. https://doi.org/10.1186/s11658-020-00245-6

Trajkovic, K., Hsu, C., Chiantia, S., Rajendran, L., Wenzel, D., Wieland, F., Schwille, P., Brügger, B., & Simons, M. (2008). Ceramide Triggers Budding of Exosome Vesicles into Multivesicular Endosomes. *Science*, *319*(5867), 1244–1247. https://doi.org/10.1126/science.1153124

Tran, N.-N., & Lee, B.-H. (2022). Functional implication of ubiquitinating and deubiquitinating mechanisms in TDP-43 proteinopathies. *Frontiers in Cell and Developmental Biology*, *10*. https://doi.org/10.3389/fcell.2022.931968

Tricarico, C., Clancy, J., & D'Souza-Schorey, C. (2017). Biology and biogenesis of shed microvesicles. *Small GTPases*, *8*(4), 220–232. https://doi.org/10.1080/21541248.2016.1215283

Tziortzouda, P., van den Bosch, L., & Hirth, F. (2021). Triad of TDP43 control in neurodegeneration: autoregulation, localization and aggregation. *Nature Reviews Neuroscience*, *22*(4), 197–208. https://doi.org/10.1038/s41583-021-00431-1

Uchida, T., Tamaki, Y., Ayaki, T., Shodai, A., Kaji, S., Morimura, T., Banno, Y., Nishitsuji, K., Sakashita, N., Maki, T., Yamashita, H., Ito, H., Takahashi, R., & Urushitani, M. (2016). CUL2-mediated clearance of misfolded TDP-43 is paradoxically affected by VHL in oligodendrocytes in ALS. *Scientific Reports*, *6*(1), 19118. https://doi.org/10.1038/srep19118

Urushitani, M., Sato, T., Bamba, H., Hisa, Y., & Tooyama, I. (2009). Synergistic effect between proteasome and autophagosome in the clearance of polyubiquitinated TDP-43. *Journal of Neuroscience Research*, NA-NA. https://doi.org/10.1002/jnr.22243

van Eersel, J., Ke, Y. D., Gladbach, A., Bi, M., Götz, J., Kril, J. J., & Ittner, L. M. (2011). Cytoplasmic Accumulation and Aggregation of TDP-43 upon Proteasome Inhibition in Cultured Neurons. *PLoS ONE*, *6*(7), e22850. https://doi.org/10.1371/journal.pone.0022850

van Niel, G., D'Angelo, G., & Raposo, G. (2018). Shedding light on the cell biology of extracellular vesicles. *Nature Reviews Molecular Cell Biology*, *19*(4), 213–228. https://doi.org/10.1038/nrm.2017.125

Vance, C., Rogelj, B., Hortobágyi, T., de Vos, K. J., Nishimura, A. L., Sreedharan, J., Hu, X., Smith, B., Ruddy, D., Wright, P., Ganesalingam, J., Williams, K. L., Tripathi, V., Al-Saraj, S., Al-Chalabi, A., Leigh, P. N., Blair, I. P., Nicholson, G., de Belleroche, J., … Shaw, C. E. (2009). Mutations in FUS, an RNA Processing Protein, Cause Familial Amyotrophic Lateral Sclerosis Type 6. *Science*, *323*(5918), 1208–1211. https://doi.org/10.1126/science.1165942

Vaquer-Alicea, J., & Diamond, M. I. (2019). Propagation of Protein Aggregation in Neurodegenerative Diseases. *Annual Review of Biochemistry*, *88*(1), 785–810. https://doi.org/10.1146/annurev-biochem-061516-045049

Verma, A. (2014). Tale of two diseases: Amyotrophic lateral sclerosis and frontotemporal dementia. *Neurology India*, *62*(4), 347. https://doi.org/10.4103/0028-3886.141174

Verma, A. (2021). Clinical Manifestation and Management of Amyotrophic Lateral Sclerosis. In *Amyotrophic Lateral Sclerosis* (pp. 1–14). Exon Publications. https://doi.org/10.36255/exonpublications.amyotrophiclateralsclerosis.management.2021

Verma, R., Aravind, L., Oania, R., McDonald, W. H., Yates, J. R., Koonin, E. v., & Deshaies, R. J. (2002). Role of Rpn11 Metalloprotease in Deubiquitination and Degradation by the 26 *S* Proteasome. *Science*, *298*(5593), 611–615. https://doi.org/10.1126/science.1075898

Versluys, L., Ervilha Pereira, P., Schuermans, N., de Paepe, B., de Bleecker, J. L., Bogaert, E., & Dermaut, B. (2022). Expanding the TDP-43 Proteinopathy Pathway From Neurons to Muscle: Physiological and Pathophysiological Functions. *Frontiers in Neuroscience*, *16*. https://doi.org/10.3389/fnins.2022.815765

Vertegaal, A. C. O. (2022). Signalling mechanisms and cellular functions of SUMO. *Nature Reviews Molecular Cell Biology*, *23*(11), 715–731. https://doi.org/10.1038/s41580-022-00500-y

Vilette, D., Courte, J., Peyrin, J. M., Coudert, L., Schaeffer, L., Andréoletti, O., & Leblanc, P. (2018). Cellular mechanisms responsible for cell-to-cell spreading of prions. *Cellular and Molecular Life Sciences*, *75*(14), 2557–2574. https://doi.org/10.1007/s00018-018-2823-y

Vishal, S. S., Wijegunawardana, D., Salaikumaran, M. R., & Gopal, P. P. (2022). Sequence Determinants of TDP-43 Ribonucleoprotein Condensate Formation and Axonal Transport in Neurons. *Frontiers in Cell and Developmental Biology*, *10*. https://doi.org/10.3389/fcell.2022.876893

Vlachos, I. S., Zagganas, K., Paraskevopoulou, M. D., Georgakilas, G., Karagkouni, D., Vergoulis, T., Dalamagas, T., & Hatzigeorgiou, A. G. (2015). DIANA-miRPath v3.0: deciphering microRNA

function with experimental support. *Nucleic Acids Research*, *43*(W1), W460–W466. https://doi.org/10.1093/nar/gkv403

Wagey, R., Krieger, C., & Shaw, C. A. (1997). Abnormal Dephosphorylation Effect on NMDA Receptor Regulation in ALS Spinal Cord. *Neurobiology of Disease*, *4*(5), 350–355. https://doi.org/10.1006/nbdi.1997.0145

Walker, A. K., Tripathy, K., Restrepo, C. R., Ge, G., Xu, Y., Kwong, L. K., Trojanowski, J. Q., & Lee, V. M.-Y. (2015). An insoluble frontotemporal lobar degeneration-associated TDP-43 C-terminal fragment causes neurodegeneration and hippocampus pathology in transgenic mice. *Human Molecular Genetics*, *24*(25), 7241–7254. https://doi.org/10.1093/hmg/ddv424

Wang, A., Conicella, A. E., Schmidt, H. B., Martin, E. W., Rhoads, S. N., Reeb, A. N., Nourse, A., Ramirez Montero, D., Ryan, V. H., Rohatgi, R., Shewmaker, F., Naik, M. T., Mittag, T., Ayala, Y. M., & Fawzi, N. L. (2018). A single N-terminal phosphomimic disrupts TDP-43 polymerization, phase separation, and RNA splicing. *The EMBO Journal*, *37*(5). https://doi.org/10.15252/embj.201797452

Wang, I.-F., Wu, L.-S., Chang, H.-Y., & Shen, C.-K. J. (2008). TDP-43, the signature protein of FTLD-U, is a neuronal activity-responsive factor. *Journal of Neurochemistry*, *105*(3), 797–806. https://doi.org/10.1111/j.1471-4159.2007.05190.x

Wang, M.-D., Little, J., Gomes, J., Cashman, N. R., & Krewski, D. (2017). Identification of risk factors associated with onset and progression of amyotrophic lateral sclerosis using systematic review and meta-analysis. *NeuroToxicology*, *61*, 101–130. https://doi.org/10.1016/j.neuro.2016.06.015

Wang, X., Fan, H., Ying, Z., Li, B., Wang, H., & Wang, G. (2010). Degradation of TDP-43 and its pathogenic form by autophagy and the ubiquitin-proteasome system. *Neuroscience Letters*, *469*(1), 112–116. https://doi.org/10.1016/j.neulet.2009.11.055

Watabe, K., Kato, Y., Sakuma, M., Murata, M., Niida-Kawaguchi, M., Takemura, T., Hanagata, N., Tada, M., Kakita, A., & Shibata, N. (2020). Praja1 <scp>RING</scp> -finger <scp>E3</scp> ubiquitin ligase suppresses neuronal cytoplasmic <scp>TDP</scp> -43 aggregate formation. *Neuropathology*, *40*(6), 570–586. https://doi.org/10.1111/neup.12694

Watts, G. D. J., Wymer, J., Kovach, M. J., Mehta, S. G., Mumm, S., Darvish, D., Pestronk, A., Whyte, M. P., & Kimonis, V. E. (2004). Inclusion body myopathy associated with Paget disease of bone and frontotemporal dementia is caused by mutant valosin-containing protein. *Nature Genetics*, *36*(4), 377–381. https://doi.org/10.1038/ng1332

Wegorzewska, I., & Baloh, R. H. (2011). TDP-43-Based Animal Models of Neurodegeneration: New Insights into ALS Pathology and Pathophysiology. *Neurodegenerative Diseases*, *8*(4), 262–274. https://doi.org/10.1159/000321547

Wijesekera, L. C., & Nigel Leigh, P. (2009). Amyotrophic lateral sclerosis. *Orphanet Journal of Rare Diseases*, *4*(1), 3. https://doi.org/10.1186/1750-1172-4-3

Williams, K. L., Topp, S., Yang, S., Smith, B., Fifita, J. A., Warraich, S. T., Zhang, K. Y., Farrawell, N., Vance, C., Hu, X., Chesi, A., Leblond, C. S., Lee, A., Rayner, S. L., Sundaramoorthy, V., Dobson-Stone, C., Molloy, M. P., van Blitterswijk, M., Dickson, D. W., … Blair, I. P. (2016). CCNF mutations in amyotrophic lateral sclerosis and frontotemporal dementia. *Nature Communications*, *7*(1), 11253. https://doi.org/10.1038/ncomms11253

Winton, M. J., Igaz, L. M., Wong, M. M., Kwong, L. K., Trojanowski, J. Q., & Lee, V. M.-Y. (2008). Disturbance of Nuclear and Cytoplasmic TAR DNA-binding Protein (TDP-43) Induces Disease-like Redistribution, Sequestration, and Aggregate Formation. *Journal of Biological Chemistry*, *283*(19), 13302–13309. https://doi.org/10.1074/jbc.M800342200

Wollert, T., Wunder, C., Lippincott-Schwartz, J., & Hurley, J. H. (2009). Membrane scission by the ESCRT-III complex. *Nature*, *458*(7235), 172–177. https://doi.org/10.1038/nature07836

Wood, A., Gurfinkel, Y., Polain, N., Lamont, W., & Lyn Rea, S. (2021). Molecular Mechanisms Underlying TDP-43 Pathology in Cellular and Animal Models of ALS and FTLD. *International Journal of Molecular Sciences*, *22*(9), 4705. https://doi.org/10.3390/ijms22094705

Xu, T., Xu, X., Chu, Y., Jiang, D., & Xu, G. (2021). Long-chain non-coding RNA *GAS5* promotes cell autophagy by modulating the miR-181c-5p/ *ATG5* and miR-1192/ *ATG12* axes. *International Journal of Molecular Medicine*, *48*(6), 209. https://doi.org/10.3892/ijmm.2021.5042

Xu, W., Ocak, U., Gao, L., Tu, S., Lenahan, C. J., Zhang, J., & Shao, A. (2021). Selective autophagy as a therapeutic target for neurological diseases. *Cellular and Molecular Life Sciences*, *78*(4), 1369–1392. https://doi.org/10.1007/s00018-020-03667-9

Xu, Z., Page, R. C., Gomes, M. M., Kohli, E., Nix, J. C., Herr, A. B., Patterson, C., & Misra, S. (2008). Structural basis of nucleotide exchange and client binding by the Hsp70 cochaperone Bag2. *Nature Structural & Molecular Biology*, *15*(12), 1309–1317. https://doi.org/10.1038/nsmb.1518

Xue, M., Zhuo, Y., & Shan, B. (2017). *MicroRNAs, Long Noncoding RNAs, and Their Functions in Human Disease* (pp. 1–25). https://doi.org/10.1007/978-1-4939-7046-9_1

Yan, Y., Yan, H., Teng, Y., Wang, Q., Yang, P., Zhang, L., Cheng, H., & Fu, S. (2020). Long non-coding RNA 00507/miRNA-181c-5p/TTBK1/MAPT axis regulates tau hyperphosphorylation in Alzheimer's disease. *The Journal of Gene Medicine*, *22*(12). https://doi.org/10.1002/jgm.3268

Yang, J.-M., & Gould, S. J. (2013). The *cis* -acting signals that target proteins to exosomes and microvesicles. *Biochemical Society Transactions*, *41*(1), 277–282. https://doi.org/10.1042/BST20120275

Yerbury, J. J. (2016). Protein aggregates stimulate macropinocytosis facilitating their propagation. *Prion*, *10*(2), 119–126. https://doi.org/10.1080/19336896.2016.1141860

Yin, Z., Pascual, C., & Klionsky, D. (2016). Autophagy: machinery and regulation. *Microbial Cell*, *3*(12), 588–596. https://doi.org/10.15698/mic2016.12.546

Yu, H., Lu, S., Gasior, K., Singh, D., Vazquez-Sanchez, S., Tapia, O., Toprani, D., Beccari, M. S., Yates, J. R., da Cruz, S., Newby, J. M., Lafarga, M., Gladfelter, A. S., Villa, E., & Cleveland, D. W. (2021). HSP70 chaperones RNA-free TDP-43 into anisotropic intranuclear liquid spherical shells. *Science*, *371*(6529). https://doi.org/10.1126/science.abb4309

Zhang, K., Pan, H., Zhao, Y., Wang, Y., Zeng, Q., Zhou, X., He, R., Zhou, X., Xiang, Y., Zhou, Z., Li, Y., Xu, Q., Sun, Q., Tan, J., Yan, X., Li, J., Guo, J., Tang, B., & Liu, Z. (2022). Genetic Analysis of HSP40/DNAJ Family Genes in Parkinson's Disease: a Large Case-Control Study. *Molecular Neurobiology*, *59*(9), 5443–5451. https://doi.org/10.1007/s12035-022-02920-5

Zhang, R., Chen, Y., Wang, X., Tian, H., Liu, H., Xiang, Z., Qi, D., Huang, J. H., Wu, E., Ding, X., & Wang, X. (2021). Spreading of pathological TDP-43 along corticospinal tract axons induces ALS-like

phenotypes in Atg5 $^{+/-}$ mice. *International Journal of Biological Sciences*, *17*(2), 390–401. https://doi.org/10.7150/ijbs.53872

Zhang, Y.-J., Caulfield, T., Xu, Y.-F., Gendron, T. F., Hubbard, J., Stetler, C., Sasaguri, H., Whitelaw, E. C., Cai, S., Lee, W. C., & Petrucelli, L. (2013). The dual functions of the extreme N-terminus of TDP-43 in regulating its biological activity and inclusion formation. *Human Molecular Genetics*, *22*(15), 3112–3122. https://doi.org/10.1093/hmg/ddt166

Zhang, Y.-J., Gendron, T. F., Xu, Y.-F., Ko, L.-W., Yen, S.-H., & Petrucelli, L. (2010). Phosphorylation regulates proteasomal-mediated degradation and solubility of TAR DNA binding protein-43 C-terminal fragments. *Molecular Neurodegeneration*, *5*(1), 33. https://doi.org/10.1186/1750-1326-5-33

Zhang, Y.-J., Xu, Y. -f., Dickey, C. A., Buratti, E., Baralle, F., Bailey, R., Pickering-Brown, S., Dickson, D., & Petrucelli, L. (2007). Progranulin Mediates Caspase-Dependent Cleavage of TAR DNA Binding Protein-43. *Journal of Neuroscience*, *27*(39), 10530–10534. https://doi.org/10.1523/JNEUROSCI.3421-07.2007

Zhang, Y.-J., Xu, Y.-F., Cook, C., Gendron, T. F., Roettges, P., Link, C. D., Lin, W.-L., Tong, J., Castanedes-Casey, M., Ash, P., Gass, J., Rangachari, V., Buratti, E., Baralle, F., Golde, T. E., Dickson, D. W., & Petrucelli, L. (2009). Aberrant cleavage of TDP-43 enhances aggregation and cellular toxicity. *Proceedings of the National Academy of Sciences*, *106*(18), 7607–7612. https://doi.org/10.1073/pnas.0900688106

Zhao, L., Yu, J., Wang, J., Li, H., Che, J., & Cao, B. (2017). Isolation and Identification of miRNAs in exosomes derived from serum of colon cancer patients. *Journal of Cancer*, *8*(7), 1145–1152. https://doi.org/10.7150/jca.18026

Zhou, W., Xu, J., Wang, C., Shi, D., & Yan, Q. (2019). miR-23b-3p regulates apoptosis and autophagy via suppressing SIRT1 in lens epithelial cells. *Journal of Cellular Biochemistry*, *120*(12), 19635–19646. https://doi.org/10.1002/jcb.29270